Electrospinning of composite biomaterials: incorporation of bioactive agents and formation of hierarchical nanostructures

Electrospinning of Composite Biomaterials: Incorporation of Bioactive Agents and Formation of Hierarchical Nanostructures

by

Wanwei Zhang

Supervisor: Dr. Elisa Mele

A Doctoral Thesis. Submitted in partial fulfilment of the requirements for the award of the degree of Doctor of Philosophy of Loughborough University.

2019

Acknowledgement

I would like to give my thanks to my dear supervisor Dr. Elisa Mele and second supervisor Dr Noreen Thomas. I could not have better guidance throughout this PhD. Thank you for giving me invaluable advice, support, and encouragement throughout this endeavour and being role models in my life.

I also would like to thank group members of Helen/Elisa Group and Dr. Leno Mascia, Mr. Chao Huang, Mr. Jiawei Zhao, Mr. Jianshen Wu, Miss Yumeng Cheng, and Miss Yicheng Dong for their generous help in my academic life. A Special thanks to Mr. Gianluca Balzamo, for being a true friend and provider of ideas.

Additional thanks is due to LMCC staffs and technicians in the Department of Materials for your guide and training in material characterisation. My PhD would not be so smooth without your help.

Lastly, I would like to thank my family. To my parents, I am blessed to be your child. Thank you for supporting me to chase my dreams. To my husband, Mr. Christian Protheroe, thank you for being my IT support, tea maker, player B, best friend, and snack supplier.

Abstract

This PhD focused on promotion of bioactivity of electrospun fibres. Two methods were used to achieve this objective: using antimicrobial agents and, creating hierarchical structures.

Antimicrobial agents, essential oils and zinc oxide nanoparticles, were encapsulated in polymer nanofibres to promote antimicrobial properties.

Tea tree and Manuka essential oils were encapsulated in poly (lactic acid) (PLA) by dissolving in their common solvent acetone and then electrospin. Plasticising effect of essential oils was observed in differential scanning calorimetry (DSC)test. Glass transition temperature of PLA fibres decreased with increasing essential oil concentration. This corresponded with mechanical results. Manuka/PLA fibres showed successful result in inhibition of *E. coli* in antimicrobial test.

Zinc oxide nanoparticles have previously been used in electrospun fibres for antimicrobial purpose. To my knowledge, previous studies have only achieved to encapsulate zinc oxide nanoparticles directly in electrospun fibres. In this thesis, for the first time, zinc oxide nanoparticles were first in-situ synthesised in polyethyleneimine (PEI) and then combined with zein to electrospin fibres. Resulting fibres showed better mechanical properties when compared to pure electrospun zein fibres.

The second method, creating hierarchical structure, was achieved by phase separation. An unique dual-porosity structure of electrospun poly(ethyl cyanoacrylate)/polycaprolactone (PECA/PCL) was demonstrated. Composition of fibres was confirmed by Fourier-transform infrared spectroscopy (FTIR). Hierarchical structures are believed to favour cell attachment and proliferation by increasing fibre surface roughness and surface-to-volume ratio.

Contents

Introduction

Objectives and motivations

Electrospinning, short for electrostatic spinning, has attracted great interest in the last decade, thanks to its capability of easily and effectively processing a huge range of polymeric materials in the form of nanofibres [1]. Compared with other nanofiber fabrication processes, such as self-assembly and phase separation [2], electrospinning has the advantages of versatility and flexibility, in terms of material selection and control over fibres' morphology and diameter [3]. Moreover, it offers the possibility to form various fibre networks, including nonwoven, aligned or patterned fibre meshes, randomly distributed three dimensional (3D) structures, sub-micron spring and convoluted fibres [1]. These characteristics, together with the extremely high surface to volume ratio, make electrospun fibres nanomaterials of election in applications ranging from sensors, energy, biomedicine and filtration [4] [5].

Various studies have demonstrated the use of electrospun fibres for tissue engineering, bone regeneration, wound dressings, drug delivery [6]. The high porosity and similarity to the extracellular matrix (ECM) make electrospun fibres excellent to promote wound healing [6]. Additionally, by loading medicines in electrospun fibres, they can also have antimicrobial, antioxidation, anti-inflammatory, and anti-cancer properties [6].

The aim of my PhD is to create electrospun bioactive composite biomaterials using two different approaches: hierarchical structure for cell adhesion and proliferation; and combining antibacterial agents for antibacterial properties. To induce the hierarchical structure, poly (ethyl cyanoacrylate)/polycaprolactone blends in a ternary solvent system via non-solvent induced phase separation; Two types of antibacterial agents, essential oils (tea tree and manuka) and zinc oxide nanoparticles, were separately loaded in electrospun fibres of poly(lactic acid) and zein to improve their antibacterial properties.

Papers published, and conference attended

Papers:

- Wanwei Zhang, Sara Ronca, Elisa Mele, “Electrospun nanofibres containing antimicrobial plant extracts”, Nanomaterials 2017, 7(2), 42.
- Wanwei Zhang, Chao Huang, Olga Kusmartseva, Noreen L. Thomas, Elisa Mele “Electrospinning of polylactic acid fibres containing tea tree and manuka oil”, Reactive and Functional Polymers 2017, 117, 106
- Wanwei Zhang, Elisa Mele “Phase separation events induce the coexistence of distinct nanofeatures in electrospun fibres of poly(ethyl cyanoacrylate) and polycaprolactone”, Materials Today Communications 2018, 16, 135
- Leno Mascia, Wanwei Zhang, Francesca Gatto, Alice Scarpellini, Pier Paolo Pompa, Elisa Mele “Electrospinning of zein fibres containing in-situ generated ZnO nanoparticles within a polyethyleneimine matrix”, accepted, ACS Applied Polymer Materials, https://pubs.acs.org/doi/abs/10.1021/acsapm.9b00276.

Conference:

Macrogroup Young Researchers Meeting (YRM) 2018, Oral presentation, “Electrospun fibres with antibacterial properties and hierarchical structure”

Chapter 1 Background on electrospinning process

In the electrospinning process, the production of fibres is driven by an electro-hydro-dynamic phenomenon for which an electric force is able to extrude and stretch thin filaments of polymer solutions or melts [7]. The main components of an electrospinning apparatus are a supply system, a collector and a high voltage power generator (Figure 1). The supply system is typically a metallic needle connected to a syringe filled with a solvent-based polymer solution (solution electrospinning) or with a molten polymer (melt electrospinning). In both cases, when a high voltage in range of 5-30 kV is applied between the needle and the grounded metallic collector, electrical charges are generated on the surface of the droplet at the tip of the needle. The droplet consequently deforms and tends to acquire a cone-like shape (known as Taylor cone). If the liquid surface tension is overcome by the electric force, a polymeric filament is extruded at the tip of the Taylor cone and it is attracted by the collector. In this phase, the filament further elongates, and the evaporation of the solvent takes place, resulting in a network of non-woven fibres on the surface of the collector [8] (Figure 2).

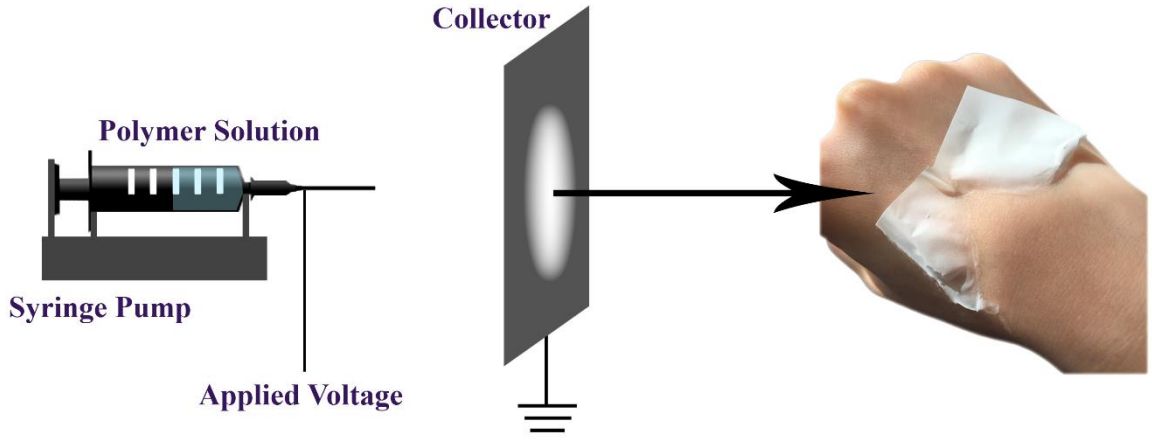

Figure 1 A basic setup of electrospinning system.

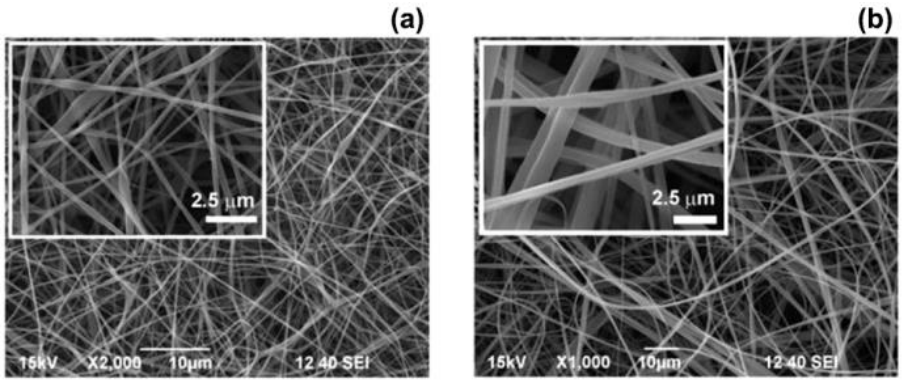

Figure 2 Scanning electron microscope images of electrospun fibres of (a) a fluoroacryl-ic copolymer and (b) cellulose acetate [8].

1.1. Parameters affecting the electrospinning process

The electrospinning of a wide range of materials has been demonstrated so far, including synthetic and natural polymers, proteins, composite and nanocomposite systems [9]. Experimental observations have proved that the size and the morphology of the electrospun fibres can be controlled by acting on the polymer viscosity, surface tension, conductivity, together with operational parameters (voltage, needle-collector distance, environmental humidity and temperature).

1.1.1. Polymer concentration

A minimum polymer concentration, also known as critical concentration, is required to form fibres by electrospinning [10]. Below this concentration, a mixture of beads and fibres is likely to be produced. If the concentration is too low (it varies for different polymer-solvent systems), only beads or beads-on-string structure can be formed. Combinations of different polymers and solvents require different minimum concentration of polymer. To give examples of polymers relevant to this PhD project, for poly (lactic acid) (PLA) dissolved in acetone/dimethyl formamide (DMF) (50/50 v/v), the minimum concentration for defect-free fibres is 12.5 w/v% [11]. For poly(ε-

caprolactone) (PCL), the minimal concentration was found at 8 w/v% in chloroform/methanol (5/1 v/v) [12] and commonly used concentration ranges from 8 w/v% to 20 w/v% [13].

However, a too high concentration may also become a problem. A study on regeneration of *Bombyx mori* silk by electrospinning by Sukigara et al. reported that continuous fibres without beads could be produced at a silk concentration higher than 12% w/w [14]. However, when the concentration was above 15% w/w, the formation of continuous fibres was prohibited due to the fact that the flow of solution at the tip of the needle could not be maintained.

Additionally, an aspect that has emerged as relevant to the formation of fibres during electrospinning is the entanglement of the polymer chains, which is associated with the polymer molecular weight and solution concentration [15], [16]. When the chain entanglement is insufficient to stabilise the liquid jet, beads or non-uniform fibres are formed. On the contrary, an appropriate level of chain entanglement promotes the generation of a jet that is stable during the solvent evaporation and leads to fibrous structures [17], [18]. For instance, for chloroform and DMF solutions of poly(methyl methacrylate) (PMMA) it has been demonstrated that elastic stretching of the polymer network and entanglement loss determine fragmentation of the electrospun jet, resulting in short nanofibres [19]. Shenoy et al. studied various polymers and their good solvent combination and found a correlation between the solution entanglement number and intermolecular interaction, which was depended on ($\phi_p M_w$) in semi-dilute solution, where ϕ_p is the volume fraction of polymer and M_w is the weight average molecular weight [15]. The experimental results of this study suggested that fibre formation could be theoretically predicted based on the entanglement molecular weight of the undiluted polymer. Wang et al. came up with an equation to describe relation between fibre diameter and entanglement based on their study on the electrospinning of poly(N-isopropylacrylamide) (PNIPAM)/DMF [20]:

$$\frac{d_f}{d_{f,e}} = \left(\frac{\phi}{\phi_e}\right)^{2.5}$$

where d_f is the diameter of the fibres, $\underline{\phi}$ is the solution concentration (volume fraction), $d_{f,e}$ is the diameter of the fibres electrospun from the solution with an entanglement concentration of ϕ_e, which was determined using specific viscosity. Since entanglement density was directly reflected on plateau modulus rather than viscosity,

the study suggested that the key role in determining the fibre diameter was the plateau modulus, the characteristic elastic modulus, of the polymer solution. The study also suggested that fibre formation was due to the high deformation rate and polymer solutions behaved like rapidly stretched ‘elastic swollen gel’. Interestingly, for some polymer solutions that cannot be electrospun, adding another polymer could improve electrospinnability by interfering with the molecule chains of the original polymer. For instance, adding polyethylene oxide (PEO) could improve the electrospinnability of sodium alginate (SA) aqueous solution [21]. Nie et al. developed a model to explain how PEO with different molecular weight interfering with SA in electrospinning process [22]. Since the chain conformation of SA is rigid, in solution SA molecule chains cannot entangle each other. When high molecular PEO100 with flexible chains was added, SA chains were enclosed on PEO100 network ‘cages’. With improved entanglement, electrospinnability was improved. On the contrary, when low molecular PEO2 with short chains was added, PEO2 itself formed short random coil, which did not interfere with SA molecules. Thus, the electrospinnability did not change.

1.1.2. Solvent

Solvent selection has a big influence on the surface tension and conductivity of the polymer solution, hence on the morphology of electrospun fibres [1]. A summary of properties and applications of commonly used solvents in electrospinning is listed in Table 1. During this PhD, acetone, acetonitrile, chloroform, and ethanol were used.

Table 1 Summary of polymers electrospun in different solvents

Solvent	Boiling point (°C)	Dielectric constant at 20 °C	Surface tension at 20 °C (dyn/cm)	Polymers
Acetic acid	118	6.2	27.4	Gelatin [23] [24] (acetic acid/ethyl acetate) [25] PCL [26](acetic acid/acetone) [24] Chitosan/PCL (formic acid/acetic acid) [27] Gelatin/PCL (acetic acid/ethyl acetate) [28] Collagen/PCL [29] Cellulose acetate [29] (DMAc/acetic acid) [30] Chitosan [29] [31] Chitosan/PEO [29] Polyvinyl alcohol (PVA)/cellulase [32] Polystyrene (PS) [33]
Acetone	56	20.6	23.3	Cellulose acetate (DMAc/acetone) [30] [34] (DCM/acetone) [35] Cellulose acetate/PVC (DMAc/acetone) [36] Chitosan/PCL (formic acid/acetone) [37] PLA [38] [39][40] [11](acetone/chloroform) [41] [42] Polysulfone (DMAc/acetone) [43] PMMA [44] (acetone/acetonitrile/chloroform) [45] (DMAc/acetone) [46] PCL (chloroform/acetone) [47] [48] PLA/PCL (chloroform/acetone) [48] Poly(ethyl cyanoacrylate) (PECA) [49]
Acetonitrile	82	37.5	29.1	PS [33] Nylon-6 [50] PEO [51] PVA [52] PECA/PCL (acetone/acetonitrile/chloro-form) [53] Polyindole [54] PMMA (acetonitrile/ethanol) [45]
Tetrahydrofuran (THF)	66	7.6	28	PLA [40] [11] PS [55] [33] (THF/DMF) [56] [57] [58] [59] Polycarbonate (PC) (THF/DMF) [60] Polyvinyl chloride (PVC) (THF/DMF) [61] PVC/polyurethane (PU) (THF/DMF) [62] PU (THF/DMF) [63] PCL [64] [64] (THF/chloroform) [65]
Dimethylformamide (DMF)	153	36.7	35	PLA [40] [11] (chloroform/DMF) [42] PCL (DMF/DCM) [48] PS [55] [33] (THF/DMF) [56] [57] [58] [59] PCL [64] [66] PLA/PCL [67] (DCM/DMF) [68] PC (THF/DMF) [60] PMMA [69] PVC (THF/DMF) [61] PVC/PU (THF/DMF) [62]

				Poly(vinylidene difluoride) (PVDF) (DMF/acetone) [70] PU (THF/DMF) [63] [71] Dextran (DMSO/DMF) [72] Polymethylsilsesquioxane [73] Hyaluronic acid (formic acid/DMF) [74] Cyclodextrin [75] Polyimide [76]
Chloroform	61	4.8	27.16	PCL/PEO [77] PCL/gelatin (chloroform/methanol) [78] PLA [40] [42] [47] [79] [80] PS [55] PCL [64] [81] [47] [64](THF/chloroform) [65] (chloroform/acetone) [12](methanol/chloroform) PCL/ Polyvinylpyrrolidone (PVP) (chloro-form/ethanol) [82] PLA/PCL [48] [68] PECA/PCL(acetone/acetonitrile/chloro-form) [53] Polymethylsilsesquioxane [73] Poly(2-octyl cyanoacrylate) [83]
Dimethylacetamide (DMAc)	166	37.8	34	Cellulose acetate [84] [85](DMAc/acetone or DMAc/acetic acid) [30] Cellulose acetate/PVC (DMAc/acetone) [36] Cellulose/Polyacrylonitrile (PAN) [86] Polysulfone (DMAc/acetone) [43] Polyurethane [87] Cellulose [88] PVP [89] PAN [90] PVDF [91] PLA [11](DMAc/DCM) [92] PMMA (DMAc/acetone) [46]
Dimethylsulphoxide (DMSO)	189	46.6	43.7	PCL [64] Cellulose [93] [94] [95] Starch [96] [97] [98] [99] [100] Poly(ethersulfone) [101] Dextran [72] Polymethylsilsesquioxane [73] PVA [83] Polyacrylonitrile [102] [103] [104]
Methanol	64	32.6	22.6	Nylon-6 [50] PCL (DCM/methanol) [105] [12](methanol/chloroform) PCL/gelatin (chloroform/methanol) [78] PLA/PCL [68] (chloroform/methanol)[48] Silk Fibroin [106] Polymethylsilsesquioxane [73]
Ethanol	78	22.4	22.3	PMMA (acetonitrile/ethanol) [45] PCL/PVP (chloroform/ethanol) [82] Gelatin (ethanol/formic acid) [107] PVP [90] Zein [108] [109] [110] [111] Zein/chitosan [112] [113] Zein/PVP/hyaluronic acid [114] Zein/PEO [115] Polymethylsilsesquioxane [73]

Formic acid	101	51.1	37.37	Silk fibroin [116] Silk fibroin/PCL (formic acid/acetic acid) [117] Silk fibroin/chitosan [118] Chitosan/PCL (formic acid/acetone) [37] (formic acid/acetic acid) [27] PCL [64] [81] [64] Gelatin [119] [23] (ethanol/formic acid) [107] Nylon-6 [120] [121] Hyaluronic acid (formic acid/DMF) [74]

Generally, a solvent with low surface tension is preferred. Electrospun fibres are resulted from a balance between electrostatic repulsive force on the surface of the solution and surface tension of the solution. Low surface tension favours the 'whipping' of jet as well as its stability, resulting in continuous fibres, while high surface tension makes the jet unstable and generates sprayed droplets [1] [58] [122] [123].
Based on the assumption of that the jet obeyed to the conservation of mass and conservation of charge, Hohman et al. developed the following equation [124]:

$$\mathrm{E}_0 = \sqrt{\gamma/(\varepsilon - \bar{\varepsilon})\mathrm{r}_0}$$

where E_0 is the electrical field strength, $\varepsilon \text{ and } \bar{\varepsilon}$ are the dielectric constants of fluids and air, respectively, γ is the fluid surface tension, r_0 is a length scale, determined by the nozzle radius. Therefore, to reach a stable jet, when γ is decreased, less electrical force was required. Fridrikh et al. later presented a model to predict the terminal diameter of the whipping jet (h_t) [122]:

$$h_t = (\gamma\varepsilon\frac{Q^2}{I^2}\frac{2}{\pi(2ln\chi - 3)})^{1/3}$$

where γ is the surface tension, ε is the dielectric constant, Q is the flow rate, I is electric current, and χ is a constant measuring instability responsible for the normal displacements. The equation was derived based on the assumption that the electrospinning jet was produced from the repulsion force of the charged surface overcoming surface tension (surface charge replusion ≥ surface tension of solution). From the equation, the study stated that the diameter of the electrospun fibres is influenced by the surface tension and conductivity of the solution, flow rate, and applied voltage.
Many studies agree that the conductivity of solvents also played an important role in electrospinning [125] [33] [30] [126] [81]. Solvents with high electrical conductivity are believed to produce higher electrostatic and Coulombic forces on the solution, resulting in better stretching. If the electrical conductivity is too low, the elongation of

a jet is insufficient which may cause beads formation [1]. For instance, Jarusuwannapoom et al. tested eighteen solvents (benzene, t-butylacetate, carbontetrachloride, chlorobenzene, chloroform, cyclohexane, decahydronaphthalene, 1,2-dichloroethane, DMF, 1,4-dioxane, ethylacetate, ethylbenzene, hexane, methylethylketone (MEK), nitrobenzene, THF, 1,2,3,4-tetrahydronaphthalene and toluene) for electrospinning polystyrene (PS) [126]. Only PS solutions in1,2-dichloroethane, DMF, ethylacetate, MEK, and THF were electrospinnable, and all these solvents exhibited high value of dipole moment and conductivity. Uyar et al. used DMF from different suppliers to electrospin PS and found that the morphology of electrospun fibres remarkable changed [125]. The study found that conductivity of DMF from different suppliers varied hugely, from highest 10.1 μS/cm (DMF1-Adrich99) to lowest 0.4 μS/cm (DMF-Fluka98). When PS concentration was low (10 w/v%), the number of beads on electrospun fibres decreased with increasing conductivity. When PS concentration increased to 20 w/v%, only DMF1-Adrich 99 was able to produce beadless free fibres. Additionally, when PS concentration raised to 30 w/v% and all solvents were able to produce beadless fibres, the average diameter of fibres decreased with increasing conductivity. The study concluded that conductivity of solvents affected the minimum polymer concentration required for beadless fibres and was more likely to produce thinner fibres. It has been reported that increasing conductivity without changing solvent is achievable via adding ionic salts, such as KH_2PO_4, NaH_2PO_4, NaCl, to the polymer solution. This has been used for PEO [127], [128], poly (acrylic acid) (PAA) [129], chitosan [29], PMMA [69], etc.. Arayanarakul et al. tested the effect of adding various salts (NaCl, LiCl, KCl, $MgCl_2$, $CaCl_2$) for electrospinning PEO aqueous solutions and found that, with the adding of salt, the minimum concentration of PEO to produce beadless fibres decreased from 5 w/v% to 4 w/v% [128]. With 2.0 w/v % salt added, the conductivity of 4 w/v % solution increased from 50 μScm^{-1} to 32-40 $mScm^{-1}$. However, NaCl was the only one that contributed to produce defined fibres. Beadless fibres started to be produced when NaCl concentration was higher than 0.5 w/v%. For rest of the salts, regardless of the concentration, only PEO films of fused fibres with salt crystals could be produced. The study discussed that the difference was caused by the comparatively low hygroscopicity of NaCl. Interestingly, Moghe et al. used pyridine, which reacted with the glacial acetic acid and became a fugitive salt, to improve electrospinning PCL [26]. Comparing with the ionic salts mentioned above, the fugitive salt of pyridine

could evaporate during electrospinning and resulting in pure polymer fibres. Lee et al. tested the influence of adding the non-solvent DMF to methylene chloride (MC) for electrospinning PCL [66]. With increasing DMF content (MC/DMF from 100/0 to 40/60) and at 13 w/v% PCL solution, the average diameter of fibres decreased from 5500 nm to <200 nm. In agreement with other studies, this was explained by the increased conductivity and decreased surface tension caused by adding DMF. Additionally, the combinations of different solvents could lead to phase separation and cause porosity, this will be discussed in detail in Chapter 3.

1.1.3. Applied electrostatic force

Electrostatic force provides the necessary charges in the solution and initiates the electrospinning process. A minimum voltage is required for fibre formation, depending on the polymer solution used. The effect of increasing applied voltage on the diameter of the nanofibres is hard to predict. Increasing the applied voltage increases the electrostatic repulsive force on the jet which can lead to greater stretching of the solution causing thinner fibres to be produced [130]. However, it also causes the solution to be removed more quickly from the capillary tip, and the solvent to evaporate faster that may lead to thicker fibres [1], [131]. Dhanalakshmi et al. tested the electrospinning of nylon 11 with different parameters and observed a slight increase in fibre diameter with increased voltage [132]. The study explained that higher voltage led to higher velocity of fibres, which reduced both stretch rate and flight time, resulting in less elongation of fibres.
The electrostatic force applied during the electrospinning process is not only responsible for fibre formation, but it has an effect also on the orientation of the polymer chains along the main fibre axis [133], [134]. A recent study on polyethylene (PE) nanofibres has demonstrated that the level of molecular orientation was dependent on the intensity of the electric field used [135]. When PE was electrospun at a voltage of 45 kV, high crystallinity was achieved, as demonstrated by micro-Raman spectroscopy. Moreover, the thermal conductivity of the fibres increases with increasing the voltage: thermal conductivity of 9.3 W m^{-1} K^{-1} was obtained at 45 kW that was 10 times higher than the thermal conductivity of PE fibres electrospun at 9 kV (0.8 W m^{-1} K^{-1}). This was clearly linked with a higher degree of orientation of the

polymer chains that allowed thermal conduction through lattice movements in an electrically insulating polymer. Kakade et al. achieved aligned electrospun PEO fibres with aligned polymer chains parallel to the fibre using two counter-charged aluminium plates [136]. In the study, positively charged fibres acquired negative charge when in touch with the collector and the charge repulsion caused 'hopping back and forth' of the fibres, resulting in the alignment. While the orientation of fibres was caused by the designed collector, the orientation of polymer chains was results of applied electrostatic force on solution. When the solution was charged, the solvent (water) molecules oriented due to their large dipole moment, which helped to oriented PEO chains whose C-O ether bonds were flexible. Kongkhlang et al. stated that electrospinning could produce extended chain crystals in polyoxymethylene (POM) [137]. The study discussed the change in molecular structure caused by shear force during the flow in the needle, and Columbic force when the electrical force was applied.

1.1.4. Flow rate

Generally, it is preferable to extrude the polymer solution at low flow rates (usually below 2ml/hr), even though this results in low efficiency [1]. When the flow rate is too high, the delivery rate of the solution is higher than the rate at which the solution is removed from the tip. Thus, the applied electric force is not enough to give sufficient stretching to the solution [138] and the polymer jet becomes unstable [131]. Additionally, the faster flow rate gives less time to the solvent to evaporate before reaching the collector [43]. Both could lead to beads formation.
Ranjith et al. electrospun Naringin encapsulated PCL fibres using two flow rates, 1ml/hr and 2 ml/hr [139]. With flow rate set at 2 ml/hr, fibre diameter increased about 18-20% comparing with fibres produced from 1ml/hr. The study also found that the cumulative release of naringin was faster for fibres produced at 2 ml/hr. Tang et al. developed a theoretical model using the conservation law based on the assumption that the rate of increase of mass within the fluid element is equal to the net rate at which mass enters the elemental volume [140]. The study developed the following equation:

$$\pi r^2 \rho^k u^k = Q^k$$

where Q^k is the volume flow rate of the k^{th} phase, r is the radius of the jet, ρ^k is the density of the k^{th} phase, and u^k is the velocity of k^{th} phase. The equation described the square of diameter of charged jet proportional to the volume of flow rate. The experiment in this study on electrospinning of PLA in DMF/chloroform supported this model. Zargham et al. studied effect of flow rate on the electrospinning of nylon (polyamide-6) fibres. The study found that, with flow rate set at 0.5 ml/hr, uniform fibres were produced. But with higher flow rate (1 ml/hr and 1.5 ml/hr), defects, such as blobs, splitting and branched fibres, were observed. Though the shape of the elongated jets under 1 ml/hr and 1.5 ml/hr were different, the results were similar: the jets broke due to the surface tension and divided into droplets, and the formation of continuous fibres was prohibited (Figure 3).

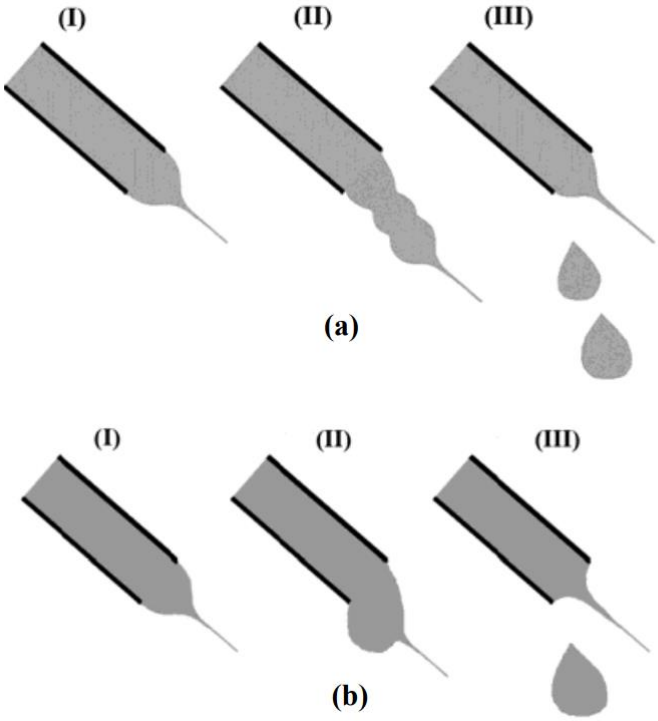

Figure 3 Schematic illustration of various charged jet modes in the electro-spinning process with flow rate of (a) 1 ml/hr and 1.5 ml/hr [138].

1.1.5. Types of collectors

The simplest collector used in a standard electrospinning apparatus is a metallic plate (aluminium or copper) which is electrically conductive to attract non-woven randomly orientated fibres. However, for some applications it is required to produce electrospun mats of aligned fibres. Unidirectionally aligned nanofibres not only have an effect on the mechanical properties of the fibrous mats but also, for biomedical uses, favour the directional growth of the cells [3]. In order to obtain aligned fibres, different types of collectors have been used, for instance, rotating drums/disks [141] [142] with different kind of modifications [143]–[146], parallel electrodes [147], parallel rings collector [148], etc.

Kim et al. tested the effect of the linear velocity of drum surface on electrospun PET nonwoven nanofibers (Figure 4) [149]. Fibres were collected on drum with 15, 30, 45 m/min velocity. The degree of alignment was quantified by frequency distribution of fibre orientation in machine direction (MD) or transverse direction (TD). Though there were always more fibre oriented in MD than TD from all three velocity values, the percentage of fibres in MD increased with increasing velocity, implying higher degree of alignment. However, for the tensile properties, highest Young's modulus, yield stress and tensile strength were shown for samples collected from 30 m/min. The decrease of tensile properties from 30 m/min to 45 m/min was explained by the decrease of fibre density. When velocity was too high, fibres 'flew into the air' rather than collected on the drum. One possible reason might be that when the drum rotating too fast, a vortex of air could be formed close to the drum. A more detailed study was done by Edwards et al. on electrospinning of aligned PCL fibres [150]. The velocity of the rotating collector was varied from 0 to 8 m/s. The optimum speed was found at 4.3 m/s with fibres exhibiting extension ratio at ~4.5 and average diameter ~7 μm (Figure 5(c)). The study found that, with the rotation velocity lower than jet velocity (in this case <2m/s), fibres were collected without significant tension, resulting in less orientation. When the velocity was within 2-6 m/s, 'hoop alignment' took place and the fibres were stretched and aligned parallel to the rotation direction. Higher velocity led to higher stretching, resulting in smaller fibre diameters. When rotation velocity was too high (> 6 m/s), less fibres were able to be collected due to breakage. The tension applied on the fibres also affected the orientation of the PCL crystals. X-ray scattering was used in the study to study the crystallinity of PCL. The highest

crystal orientation was obtained at 5 m/s velocity. Wang et al. developed aligned poly-L-lactic acid (PLLA) fibres using a rotating drum (Figure 6 (a)) [151]. Three rotation speeds were tested: 250 rpm, 500 rpm, and 1000 rpm, and better alignment was achieved with higher rotation speed (Figure 6 (b)-(g)). This was explained by the higher stretch of the fibres in the study. *In vitro* test showed that the aligned fibres favoured the attachment of rat Schwann cells and directed neurite outgrowth along the fibre direction.

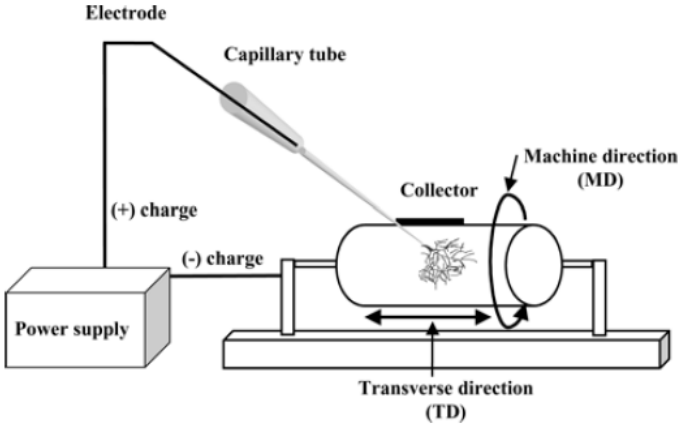

Figure 4 Schematic diagram of electrospinning device using rotating drum as collector [149].

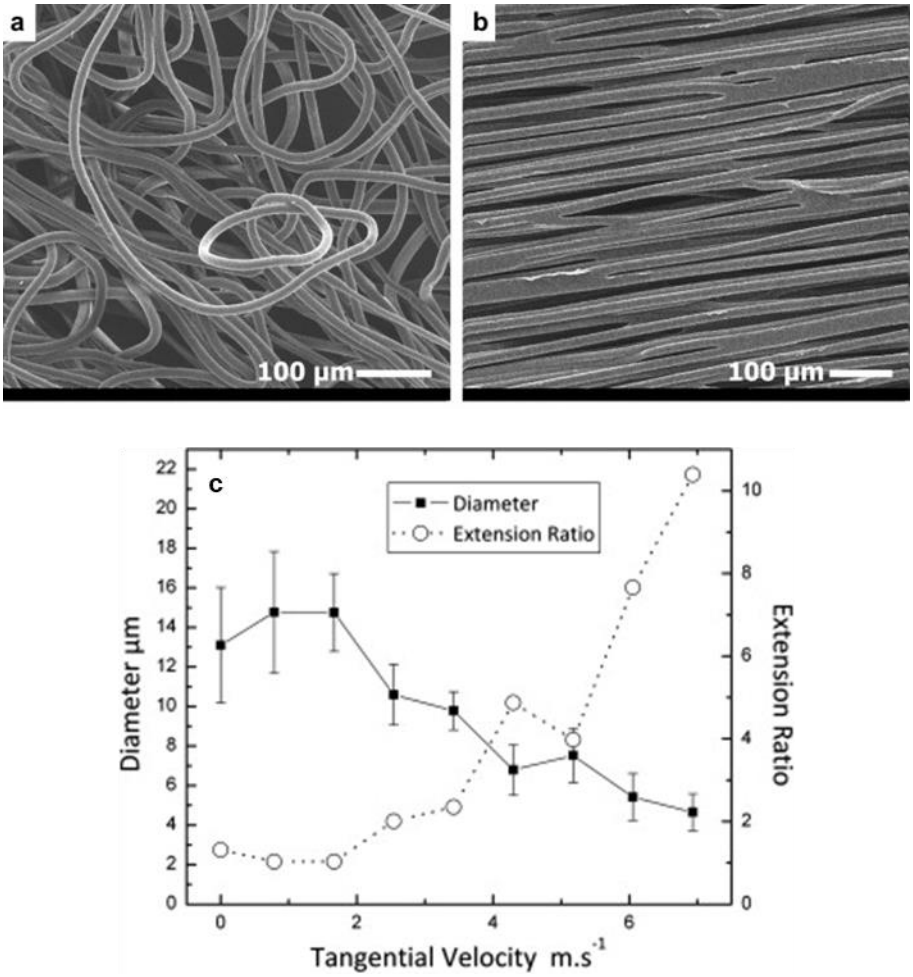

Figure 5 SEM images of PCL fibres collected from (a) static collector, (b) rotating collector with velocity of 4.3 m/s. (c) A plot of the mean fibre diameter (solid circles) against the velocity of the rotating collector (the range bars represent the width of the diameter distribution) and a plot of the extension ratio (empty circles) derived from the diameter data [150].

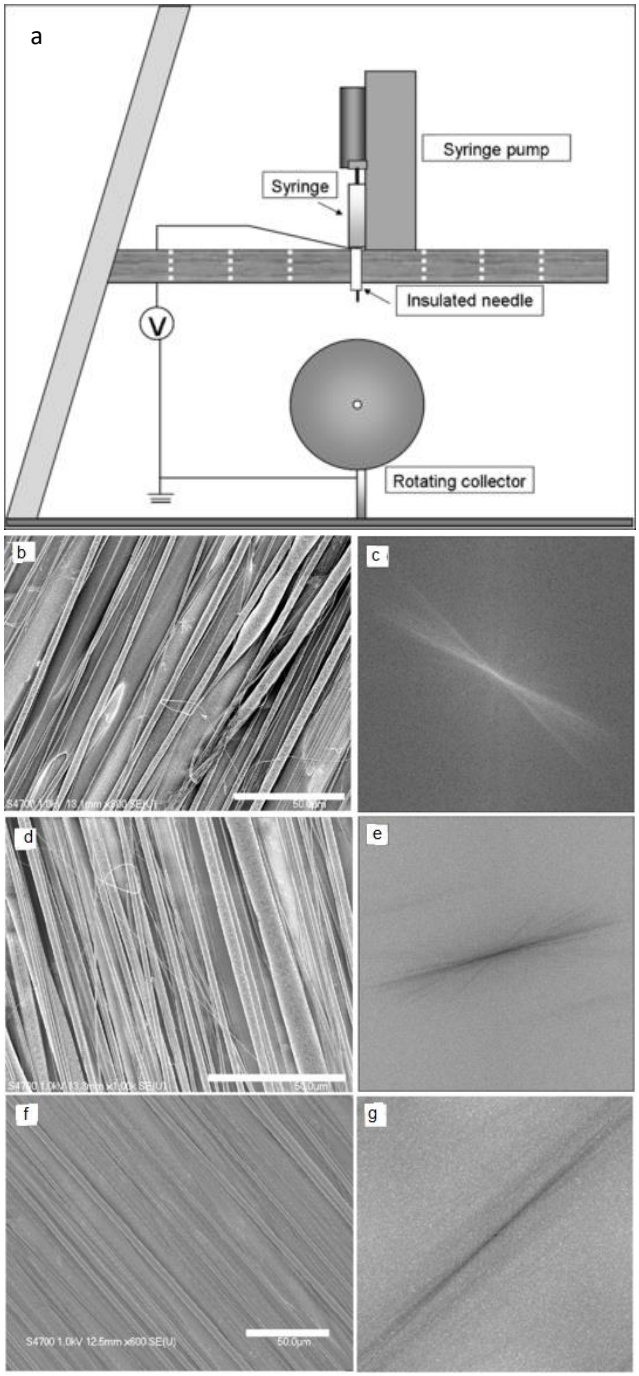

Figure 6 (a) Schematic of the setup to create aligned PLLA fibers by electro-spinning using an insulated sharp needle and a rotating disk collector. SEM images of fibres collected with rotation speed: (b) 250 rpm, (d) 500 rpm, (f) 1000 rpm, and their fast Fourier transformation images: (c), (e), (g) [151].

Xu et al. used rotating disk for collecting aligned poly(l-lactid-co-ε-caprolactone) [P(LLA-CL)] (75:25) for blood vessel engineering, (Figure 7(a)) [142]. Aligned fibres

with average diameter of 550±120 nm were collected at rotation velocity 11 m/s (Figure 7(b) and (c)). Aligned fibres and tissue culture polystyrene (TCPS) showed similar cell adhesion values (64% and 68%) in *in vitro* study using smooth muscle cells, and both were much higher than solution cast P(LLA-CL) films (44%). In cell proliferation tests, 5-fold expansion in cell numbers was seen on aligned fibres in 7 days while only 2.5-fold was seen on TCPS, indicating faster proliferation on aligned fibres than TCPS.

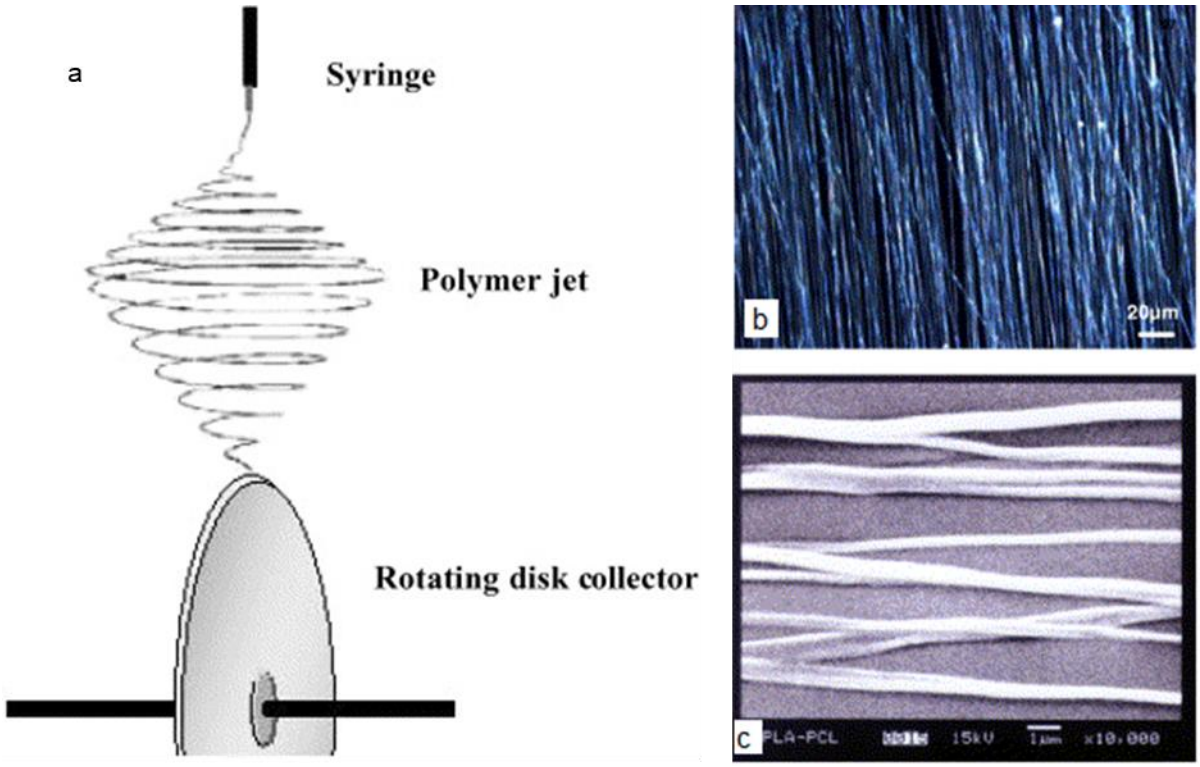

Figure 7 (a) Schematic setup to fabricate aligned nanofibrous scaffold by electrospinning with a disk collector. (b) Optical microscope and (c) SEM images of aligned P(LLA-CL) fibres [142].

Li et al. generated patterned electrospun polyvinylpyrrolidone (PVP) using conductive electrodes [147]. Researchers first discovered that uniaxial aligned fibres could be easily collected on two silicon strips with a void gap in-between (Figure 8 (a)). The gap between strips changed the electric field comparing with grouped conductive plate, which would attract fibres to the electrodes and pull them towards the edges. However, fibres collected by this method needed to have enough mechanical strength to support the weight of the fibrous mats. Thus, the method was limited to

collecting fibres with thickness of the mat over 150 nm. The study replaced silicon electrodes with gold ones and put them on three types of substrates: quartz, PS sheets and glass slides. The insulation of substrate materials was critical for the formation of aligned fibres. Randomly oriented fibres were collected on glass slides due to its low bulk resistivity (10^{11} Ωcm), while quartz and PS sheets could successfully collect aligned fibres with bulk resistivity greater than 10^{22} Ωcm. Additionally, the study also found that various patterns of fibres could be achieved by different configurations of the electrodes (Figure 8 (b) to (g)).

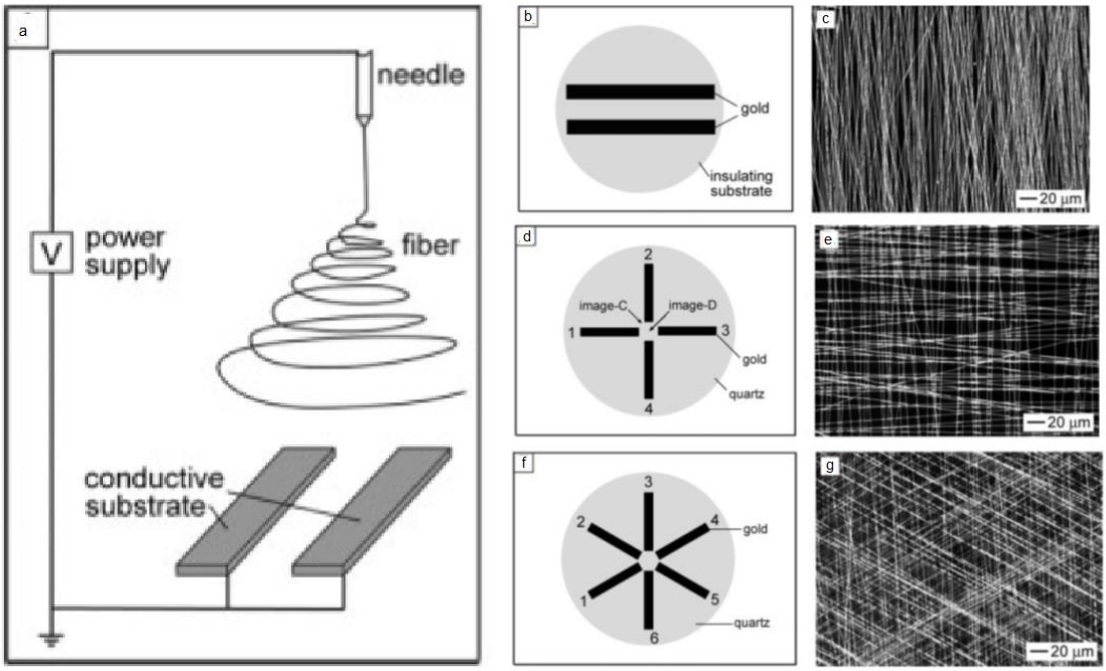

Figure 8 (a)Schematic illustration of the set-up used to electrospin nanofibres as uniaxially aligned arrays. Schematic illustration of a test pattern that comprised gold electrodes: (b) two, (d) four, and (f) six. (c), (e), (g) presents dark-field optical micrographs of PVP fibres collected on quartz wafer collected from (b), (d), (f). [147]

Dalton et al. demonstrated the formation of PCL multi-filament yarn using parallel rings collector (Figure 9(a)) [148]. Aligned PCL fibres were first collected between rings. The study found that the distance between the rings affected the distribution of the fibres. With a distance below 40 mm or above 100 mm, fibres accumulated at either top or the bottom of the collection rings. To form multi-filament yarn, a stirrer with 2500 rpm speed was applied on one of the rings until fibres twisted into a single yarn (Figure 9 (b) and (c)).

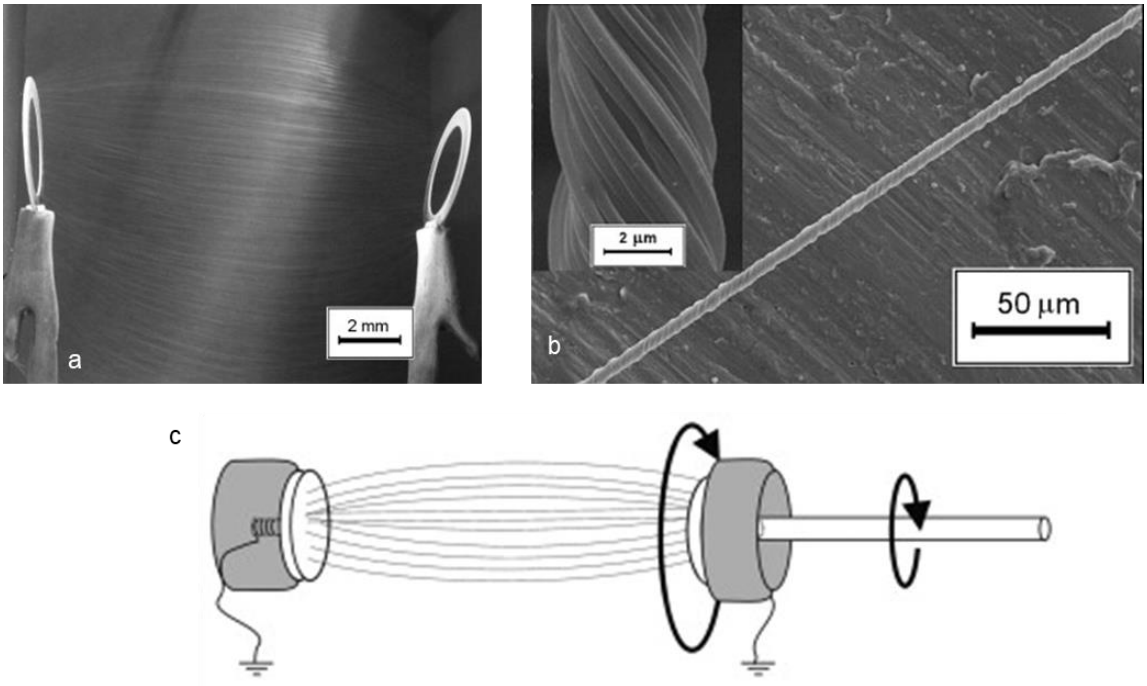

Figure 9 (a) Photograph of collection rings with an array of electrospun fibres, (b) SEM micrograph of wound PCL fibres, forming a multi-filament yarn. The insert shows a larger magnification of the yarn, (c) Schematic of electrospinning collection system for fabricating a yarn of electrospun fibres [148].

The collector is usually a solid material, but researchers have found that liquid collections can also be used. For instance, Smit et al. collected continuous yarn composed of electrospun poly(vinyl acetate) (PVAc), poly(vinylidene difluoride) (PVDF) and PAN [152]**.** The setup of electrospinning system is shown in Figure 10. In this process, a fibre web was firstly formed on the surface of water bath and then drawn out. During the drawing, the fibre web was elongated, and the alignment of fibres took place. The surface tension of the remaining water on the web pulled the fibres together into a three-dimensional round yarn structure (Figure 10(a) and (b))**.** Liquid

bath can also be used for coagulation purpose [109], [153]–[156]. For instance, Wang et al. developed ‘wet-electrospinning’ for producing poly(ethyleneimine) (PEI) fibres with the aid of adding PVA for fibre forming [156]. The fibres were crosslinked and collected in a glutaraldehyde (GA)/DMF (1/20 v/v) coagulation bath. With conventional electrospinning, PEI/PVA fibres could be produced with up to 61.5 w % PEI content [157]. Fibres with higher PEI content were likely to merge together due to the slow evaporation of the solvent, causing by strong hydrogen bond between PEI and solvent. In this study, fibres were successfully produced with a PEI content up to 90 w % (Figure 11). The crosslinking of PEI in the bath prevented the fibres from sticking to each other.

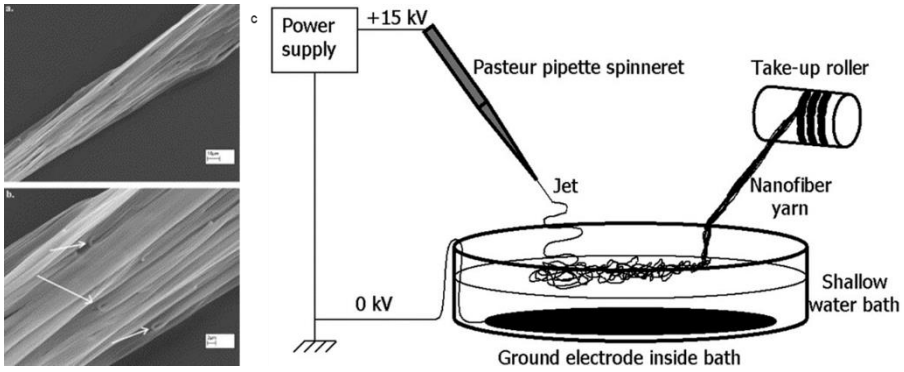

Figure 10 (a) and (b): SEM images of electrospun fibrous yarn of PVAc, (c) schematic diagram of the electro-wet spinning apparatus [152].

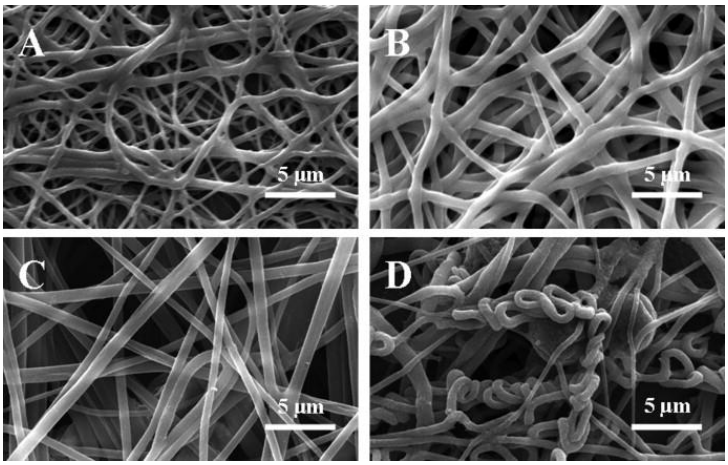

Figure 11 The SEM images of PVA doped PEI nanofibrous membranes fabricated by wet-electrospinning with different PEI/PVA weight ratios: A: 20/80; B: 50/50; C: 90/10; D: 95/5 [148].

1.1.6. Tip-to-collector distance

The effect of the distance between the tip and the collector is arguably not as significant as other parameters above. Though most studies agreed that a minimum distance is required to give the fibres sufficient time to dry before reaching the collector and to prevent beads forming [1], only a few studies actually electrospun fibres using different tip-to-collector distances to test the influence. Hekmati et al. electrospun polyamide-6 with four different tip-to-collector distances (5 cm, 10cm, 15 cm, 20 cm) [158]. The study found that with decrease of tip-to-collector distance, the area of collected non-woven mat decreased but the average fibre diameter increased. Notably, the increase between average diameter of fibres produced from 10 cm and 5 cm was minor. The study suggested that, after the jet left the needle, it went through bending and whipping before hitting the collector. The decrease in tip-to-collector distance caused shorter bending and whipping time, which led to less stretching of fibres. Buchko et al. electrospun Silk-Like Polymer with Fibronectin functionality (SLPF) using 0.5-4.0 cm tip-to-collector distance [159]. The minimum tip-to-collector distance was found at 2 cm below which wet fibres or beads were produced (Figure 12). At 0.5 cm, bonded ribbon shaped fibres were produced due to the wet-coating effect. Solvent left in the fibres caused the collapse and bonding of fibres. Homayoni et al. found that decreasing tip-to-collector distance showed similar effect with increasing applied voltage since both reduced jet flight and solvent evaporation time [31]. Agreeing with other studies, the study observed the decrease of tip-to-collector distance resulted in increase of fibre diameter.

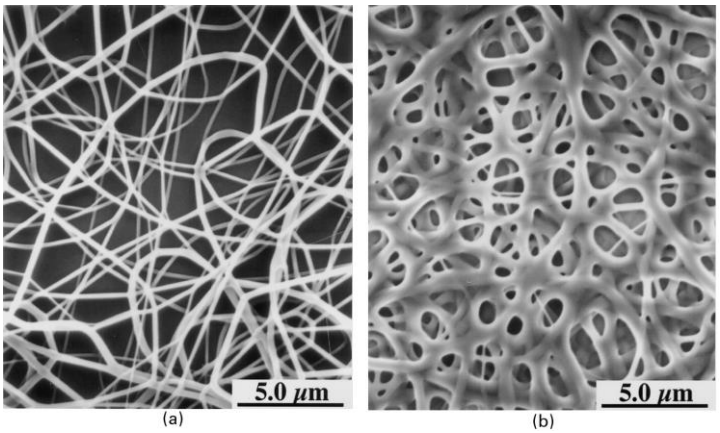

Figure 12 SEM images showing that deposition distance controls morphology: (a) deposited at 2.0 cm, resulting in round fibres, (b) deposited at 0.5 cm, resulting in flat fibres [159].

1.1.7. Electrospinning setup for this PhD

In electrospinning, the first step is always optimising the parameters (polymer concentration, solvents, applied voltage, flow rate, tip-to-collector-distance, and types of collectors) to obtain fibres with the desired properties. Here, all the parameters are explained in detail for a better knowledge. For this thesis, horizontal set up electrospinning with grounded metal plate as collector was used. The solvents were chosen depending on their conductivity, volatility and ability to solubilise the polymers of interest. For each experimental work, various combinations of polymer concentration, applied voltage, flow rate and tip-to-collector distance were tested in preliminary studies to reach the optimum.

Chapter 2 Electrospinning of polylactic acid fibres containing tea tree and manuka essential oils

2.1. Introduction

This introduction is modified on published papers: *Reactive and Functional Polymers* [40] , and *Nanomaterials* [160]. Recently, the growing demand for naturally derived compounds that are able to replace synthetic ones in cosmetics, medicine and food industry has influenced the electrospinning research [9] [160]. In fact, the last ten years have seen an increased number of publications on fibres produced by electrospinning a variety of plant extracts (Figure 13 (a)). Plants are sources of many chemical compounds with, among others, anti-oxidation, anti-inflammatory and antimicrobial activity [161] [162]. Therefore, composite electrospun fibres containing plant extracts have been developed for applications that mainly include medicine, agriculture and food industry (Figure 21(b)). The current total number of articles on this topic is low if compared with the number of papers published every year on electrospinning, but it is expected to further rise in the coming years.

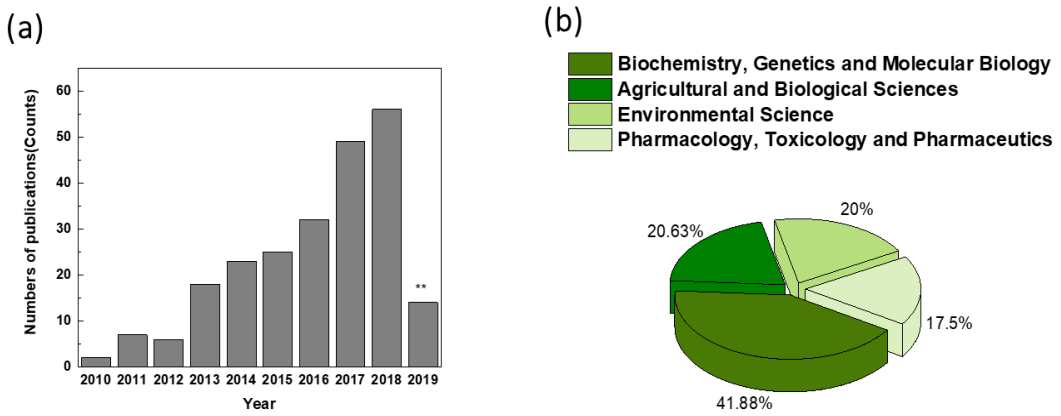

Figure 13 (a) Number of publications per year on electrospun nanofibres containing plant extracts. ** This count considers only the first four months of 2019. (b) Analysis of the results by subject area. Scopus database was used to determine the total number of publications, searching for "electrospinning" plus "plant extract" or "essential oil". This figure is modified based on published paper [160].

Nanostructured systems containing essential oils (EOs), mainly produced by electrospinning, have so far been proposed for wound management and food packaging applications [83] [163] [164] [165] [166] [167] [168]. Literatures on electrospun fibres containing plant extracts and their applications is reviewed in detail in 2.2. This review has been published [160].

In this chapter, electrospinning composite fibres of PLA and essential oils derived from *Melaleuca alternifolia* (Australian tea tree oil) and *Leptospermum scoparium* (New Zealand manuka oil) were demonstrated and their properties were analysed. The EOs extracted from these two different species of *Myrtaceae* are typically used in aromatherapy and for the treatment of microbial infections. It is shown that tea tree oil and manuka oil are highly miscible with PLA, resulting in fibres with a well-defined morphology. Furthermore, the EOs have a plasticising effect on PLA, leading to a reduction of the glass transition temperature of the polymer and an increase in elongation-at-break of the fibres. The mechanical properties and bioactivity of the composite PLA-EOs mats make them promising as infection-resistant scaffolding materials for biomedical applications. Some of the results discussed in this Chapter have been published [40].

2.2. Literature review

2.2.1. Bioactive wound dressings

Electrospun scaffolds possess several advantages over traditional dressings for the treatment of chronic and acute wounds [169], [170]: high absorption of exudates from the wound site, efficient exchange of gases and nutrients to promote cells proliferation, physical protection of the injured tissue and possibility to release functional molecules. The combination of electrospinning with naturally-derived bioactive agents allows the development of advanced dressings with antibacterial, anti-inflammatory and anti-oxidant properties, for achieving efficient and rapid wound healing [163], [166], [178]–[187], [167], [188], [189], [171]–[177]. One of the objectives of this PhD project was to develop fibrous wound dressings with controlled mechanical and antibacterial properties by electrospinning essential oils. This section will discuss the

recent achievements in the field of nanofibrous dressings loaded with crude plant extracts, essential oils and plant-derived chemical components.

2.2.1.1. Crude plant extracts

Crude extracts are easily obtained by organic solvent extraction from fresh plants [171] or from milled dried plants [183]. Several crude plant extracts have been successfully encapsulated into electrospun fibres, such as *Centella asiatica* [171], baicalein [173], green tea [174], *Garcinia mangostana* [180], [183], *Tecomella undulata* [177], aloe vera [181], [190], *Grewia mollis* [191], chamomile [176], *Tridax procumbens* [192], *Gymnema sylvestre* [192], *Coptis chinensis* [192], *Coptidis rhizoma* [192], and grape seed [178]. Suwantong et al. produced cellulose acetate nanofibres loaded with asiaticoside (AC) from *Centella asiatica*, a herb that has shown healing activity on wounds, burns, ulcers and other skin problems [184]. An efficient release of the herb compounds from the electrospun mats was shown, if compared with as-cast cellulose acetate films, using total immersion method and transdermal diffusion through a pigskin method. The release behaviour was due to the high porosity of the electrospun meshes and consequently to the enhanced media absorption. Cytotoxicity tests on human dermal fibroblasts (HDFs) pointed out that no harmful substances were release from the scaffolds, which find potential application as topical/transdermal or wound dressing patches. In another study, grape seed extracts (GSEs) have been encapsulated into nanofibres of silk fibroin from *Bombyx mori* and polyethylene oxide (PEO) [178]. Release tests *in vitro* revealed a burst release of GSE in the first 50 hours from the surface of the fibres, followed by a continuous release phase from 50 to 100 hours. The antioxidant properties of GSE significantly enhanced the proliferation of fibroblasts when the elecrospun fibres were used as scaffolds, preventing oxidative stress. Silk fibroin fibres have been used also for the delivery of baicalein, a Chinese herbal extract with anti-inflammatory and antioxidant properties [173]. In this case fibroin was combined with polyvinylpyrrolidone (PVP), whose water solubility promoted the burst release of baicalein within 24 hours in an aqueous environment. The composite scaffolds were able to inhibit the proliferation of *Staphylococcus aureus* (*S. aureus*) and to reduce lipopolysaccharide-induced inflammation on macrophages model. Furthermore, *in vivo* tests on an infected wound

model showed enhanced wound closure, increased production of collagen fibres, angiogenesis and no bacteria colonisation.

The extracts of *Garcinia mangostana* (GM), a tropical fruit found in Southeast Asia, have been loaded into electrospun mats of chitosan-ethylenediaminetetraacetic acid/polyvinyl alcohol (CS-EDTA/PVA) [183]. Burst release of GM was obtained within 24 hours due to the swelling of chitosan in water. The antibacterial and antioxidant activity of GM was exploited for the treatment of wounds in an animal model. CS-EDTA/PVA fibres containing the fruit extracts had an inhibitor effect against *S. aureus* and *Escherichia coli* (*E. coli*), and accelerated skin re-epithelialisation and collagen synthesis. Suganya *et al*. have proposed the use of nanofibres of polycaprolactone (PCL) and PVP with crude bark extracts of *Tecomella undulata*, a medicinal plant from Thar Desert regions of northwest and western India, for the treatment of skin infections [177]. The extract was rapidly released *in vitro* from the composite mats in the first few hours due to the extract remained on fibres' surface, followed by a slow release causing by the diffusion over a prolonged period of time. Moreover, the fibres were characterised by a bactericidal activity against *Pseudomonas aeruginosa* (*P. aeruginosa*), *S. aureus* and *E. coli*, with zones of inhibition having diameters between 28 and 30 mm. Motealleh and co-workers reported instead on PCL/polystyrene (PS) nanofibrous mats containing chamomile, a medicinal plant of the *Asteraceae* family (Figure 14a) [176]. The PCL/PS/chamomile fibres exhibited an inhibition effect against bacteria (*S. aureus*) and fungi (*Candida albicans*), as shown in Fig1(b) and (c), and they were able to heal wounds in an animal model leading to fibroblast proliferation, re-epithelization and increased formation of granulation tissue. Other plant extracts have been encapsulated into PCL electrospun fibres, such as *Indigofera aspalathoides*, *Azadirachta indica*, *Memecylon edule* (ME) and *Myristica andamanica*, which are traditional Indian medical plants [172]. Biocompatibility studies revealed that HDFs proliferated on the scaffolds, and particularly PCL/ME fibres were metabolically active with increased cell-to-cell communication and high secretion of collagen. Furthermore, the therapeutic use of the PCL/ME scaffolds was demonstrated by the capability of inducing differentiation of adipose derived stem cells (ADSCs) in keratinized epithelial cells.

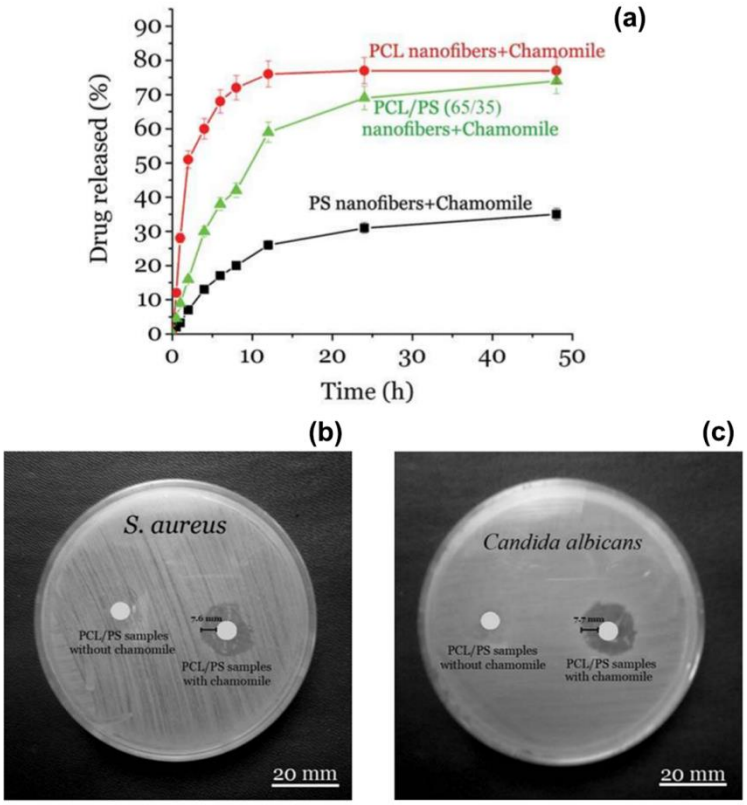

Figure 14 (a) Release profile of chamomile, during 48 hours, from PCL (red circles), PCL/PS (green triangles) and PS (black squares) electrospun nanofibres. PS samples showed a lower release if compared to PCL and PCL/PS samples. An-tibacterial and antifungal properties of the composite PCL/PS fibre loaded with chamomile agonist (b) S. aureus and (c) C. albicans. This figure has been published [160].

Torres Vargas *et al*. selected the medicinal plant *Calendula officinalis* (*C. officinalis*) as anti-inflammatory agent for wound healing applications [193]. They prepared hyperbranced polyglycerol (HPGL) electrospun membranes in order to control the delivery of *C. officinalis* in physiological conditions, by exploiting the high swelling ability and surface area of HPGL nanofibers. *In vivo* tests showed the anti-inflammatory properties of the fibres produced, together with regeneration of connective tissue and initiation of re-epithelialization.

2.2.1.2. Essential oils

Essential oils (EOs) are typically extracted from aromatic plants and, similar to crude plant extracts, are mixtures of different chemical compounds, such as linalool, pinene, eugenol, cymene [194]. When EOs are incorporated into electrospun fibres, they provide bioactivity to the final scaffolds and, in some cases, have an effect also on the mechanical properties. EOs that have been electrospun include orange [192], candeia [175], cinnamon [189], [195], eugenol [196], lemongrass and peppermint [189], peppermint and chamomile [196] tea tree [187], thyme [166] [196], sage and black pepper oil [38], ginger [197], plai [197], oregano [197], and lavender [167] [198]. PLA nanofibres containing Candeia (*Eremanthus erythropappus*) essential oil have been produced by electrospinning [175]. Thermal analysis showed that the addition of the EO decreased the glass transition and melting temperatures of the composite fibres, indicating the plasticiser effect of the oil on PLA. The study suggested that small molecules in essential oils increased the flexibility of polymer chain. Cinnamon EO has been combined with a blend of chitosan and PEO in order to produce scaffolds for the treatment of infections caused by *E. coli* and *P. aeruginosa* [163]. In another study, cellulose acetate nanofibres loaded with cinnamon, peppermint and lemon grass EOs have been proposed as antimicrobial scaffolds for preventing wound infections [189]. The scaffolds effectively stopped the proliferation of *E. coli*, without losing in biocompatibility. In fact, non-cytotoxicity effects were reported on two different cell lines: fibroblasts and human keratinocytes. Balasubramanian *et al*. produced electrospun mats of polyacrylonitrile (PAN) and *Syzygium aromaticum* (clove) oil with a superior antibacterial performance against Gram positive bacteria (*S. aureus* and *Bacillus subtilis*) and good fibroblasts viability [165].

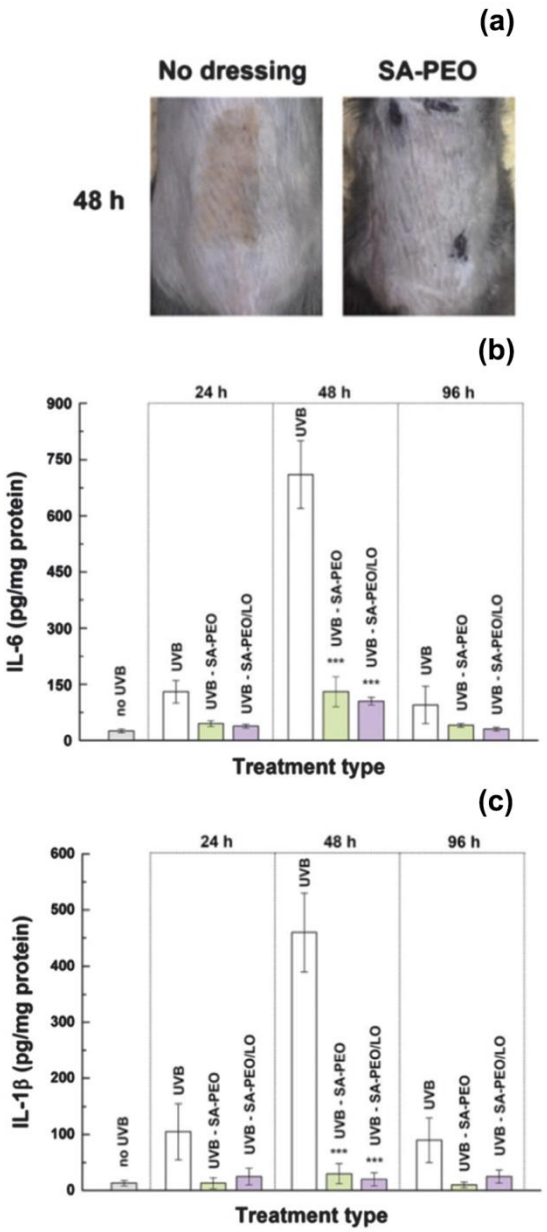

Figure 15 . (a) Photographs of the skin of mice after 48 hours from irradiation with ultraviolet light: untreated (no dressing) and treated with alginate-PEO fibres (SA-PEO). An evident burn mark (red area) was visible for animals without treatment, differently for mice treated with the electrospun dressings (no trace of erythema). Time course of the expression of (b) Interleukin-6 (IL-6) and (c) Interleukin-1β (IL-1β) for animals without treatment (UVB), and for animals treated with SA-PEO fibres (UVB-SA-PEO) and with SA-PEO fibre containing lavender essential oil (UVB-SA-PEO/LO). This figure has been published [160].

In another work, the authors showed that nanofibers of PAN containing lavender essential oil were able to stop the growth of *S. aureus* and *Klebsiella pneumoniae* (*K. pneumoniae*) [198]. Lavender essential oil has been also used in combination with sodium alginate for dressings suitable to treat skin burns [167]. The dressings were

effective to inhibit both the formation of biofilms of *S. aureus* and the production of pro-inflammatory cytokines *in vitro* (fibroblast cells) and *in vivo* (mice). The animals treated with the alginate-lavender EO mats rapidly recovered, without traces of skin inflammation (Figure 15(a)). In fact, after 24 hours from the treatment, the levels of pro-inflammatory cytokines (Interleukin-6 and Interleukin-1β) for treated animals were up to 10 times lower than for untreated ones, (Figure 15(b) and (c)). Recently, Wang and Mele incorporated black pepper EO and sage EO in electrospun PLA fibres [38]. The fibres possessed bacteria inactivation efficiency of 76 and 100% against *E. coli* and *S. epidermidis*. Incorporation of EOs also affected the fibre morphology. With sage EO, wrinkled surface was shown on fibres, and with black pepper EO, nano-textured surface was shown. Since the EOs were composed of chemicals with different evaporation rate and PLA was insoluble in them, phase separation was likely to take place in the system, resulting in non-smooth surface.

2.2.1.3. Single chemical components

A considerable number of studies are based on the use of pure bioactive chemical compounds obtained from plants, such as curcumin [186], [199], asiaticoside [184], emodin [182], shikonin [179], cinnamaldehyde [163], [200], lawsone [201], rosmarinic acid [201], α-Mangostin [201]. Comparing to crude extracts and essential oils, the incorporation of pure chemical components into electrospun scaffolds allows better study of chemical interactions, analysing the release behaviour and investigating biological processes.

Emodin, an extract of the medicinal plant *Polygonum cuspidate*, has been blended with PVP and electrospun in order to produce membranes for wound healing [182]. Animals treated with the composite fibrous dressings did not show adverse reactions, such as skin irritation and erythema, thanks to the high biocompatibility of the fibres. Most importantly, emodin promoted healing and accelerated wound closure in a 15 day test, with formation of new connective tissue and blood vessels. Another extract of interest in wound care is shikonin, which is the major component of the dried root of *Lithospermum erythrorhizon*, a Chinese herbal medicine [202]. Han and co-workers reported on the encapsulation of shikonin into electrospun PCL/poly(tri-

methylene carbonate) (PTMC) fibres. They observed that, initially, the drug was rapidly released from the electrospun mats and then at a constant rate for 50 hours. The shikonin-loaded PCL/PTMC fibres were characterised by anti-oxidant and antibacterial activity against *S. aureus* and *E. coli*, which was due to the formation of semiquinone radicals. The healing properties of shikonin have been also investigated in combination with alkannin, which is another naturally occurring hydroxynaphthoquinones, for the development of topical/transdermal dressings [203]. In this case, cellulose acetate, PLA and two different blends of poly(lactic-co-glycolic) were used as polymer matrices.

Curcumin, which is extracted from the root of *Curcuma longa L*., is well-known for its medicinal properties including strong anti-inflammatory, anti-oxidant and anti-cancer activity [199], [204]. Several works have been published on the electrospinning of curcuma-based fibres for wound healing applications. For instance, it has been demonstrated that PLA nanofibres with 0.125 wt% of curcumin induced fibroblast proliferation *in vitro*, and significantly increased the rate of wound closure in an animal model [199]. Composite scaffolds with anti-oxidant efficacy and low cytotoxicity have been produced by electrospinning curcumin and PCL-poly(ethylene glycol)-PCL copolymer (PCL-PEG-PCL) [188]. Furthermore, when the samples were tested on a full-thickness wound *in vivo*, the recovery of the animals was observed after 21 days post-operation, with 93% of wound closure. The curcumin-based scaffolds accelerated the re-epithelialization of tissue and collagen deposition. Another work demonstrated that nanofibres of PCL, PEG and curcumin facilitated wound healing [205]. In fact, they supported cell attachment and proliferation, and possessed anti-inflamatory and anti-bacterial activity against RAW264.7 mouse macrophages and *S. aureus*, respectively. Almost complete wound closure (99%) was achieved *in vivo* after 10 days of treatment. Curcumin-PCL fibres were also investigated as dressings for diabetic wounds [185]. A sustained release of curcumin was obtained for 72 hours, and anti-oxidant and anti-inflammatory activity was proved by oxygen radical absorbance capacity assay. The fibres preserved the viability of foreskin fibroblasts that were exposed to oxidative stress. Moreover, they down-regulated the production of Interlukin-6 in monocyte-macrophages, reducing inflammation. Finally, a rapid wound closure was detected in a streptozotocin-induced diabetic mice model.

Curcumin and its β-cyclodextrin (CD) inclusion complex were encapsulated into polyvinyl alcohol (PVA) electrospun nanofibres [206]. CDs are cyclic oligosaccharides with a cavity-shaped structure, composed of six to eight glucopyranose units that control the size of the cavity in the final structure [207]. CDs form complexes with hydrophobic compounds and are typically used as drug carrier. X-ray diffraction, differential scanning calorimetry (DSC) and scanning electron microscope (SEM) investigations of PVA/curcumin and PVA/CD-curcumin fibres showed that curcumin formed crystalline aggregates in the fibres, whereas CD-curcumin is homogeneously distributed. Curcumin was faster released from the fibres when the CD complex was used, and in both cases the stability of the natural drug was enhanced. Cyclodextrin inclusion complexes (CD-ICs) of plant extracts reduces the volatility of natural compounds, limiting loss of chemicals during the electrospinning process, enhancing thermal stability and also prolonging the storage period [208]. For these reasons, CD-ICs of natural compounds have been synthesised for both biomedical applications and food industry, as it will be discussed in the following paragraphs.

2.2.2. Tissue engineering

As it emerges from the above discussion, plant extracts have been extensively used in wound management for their biocompatibility, as well as antimicrobial, anti-inflammatory and anti-oxidant activity. Yet those characteristics are relevant also to other biomedical areas, including tissue engineering [209]–[211] [212] [212].
Medicinal plants with osteogenic properties, such as *Cissus quadrangularis* [209] and Asian Panax Ginseng root [210], have been proposed for bone regeneration. The combined effect of *Cissus quadrangularis* (CQ) and hydroxyapatite (HA) have been investigated by producing PCL-CQ-HA electrospun scaffolds [209]. Enhanced adhesion and proliferation of human foetal osteoblasts (hFOBs) on the composite scaffolds was observed, if compared with pristine PCL fibres. Moreover, increased levels of mineralisation and osteocalcin expression were detected, which are fundamental in bone formation. PCL scaffolds with osteo-inductive potential were produced also using Asian Panax Ginseng root extract [210]. The ginseng extract had a positive effect on the hydrophylicity and mechanical properties of the nanofibres. Moreover, it induced the osteogenic differentiation of rabbit mesenchymal stem cells

(MSCs), resulting in a significant expression of osteogenic genes. Selvakumar *et al.* produced anti-infective scaffolds for bone regeneration by electrospinning segmented polyurethane and Aloe vera wrapped mesoporous hydroxyapatite (Al-mHA) nanorods [211]. The incorporation of Al-mHA nanorods resulted in constructs with significantly improved mechanical properties and effectiveness against various human pathogenic bacteria. When implanted in rabbits, biomineralisation, cartilage formation and bone healing after 4 weeks was achieved, without toxicological effects. Recent studies have found that curcumin inhibits the growth of cancer cells by suppressing specific signalling pathways [213]. Therefore, curcumin-loaded electrospun nanofibres have been developed for the treatment of cancer. For instance, implantable PCL-PEG-PCL (PCEC) electrospun scaffolds incorporating curcumin have been prepared [214]. Curcumin-PCEC fibres were tested on rat Glioma 9L cells: whereas PCEC fibres were not cytotoxic and the effect of pure curcumin disappeared within 48 hours, the composite scaffolds had a prolonged antitumor activity. Moreover, the viability of cancer cells decreased with increasing curcumin content. This suggested that the curcumin-based scaffolds can find application for postoperative brain chemotherapy. In another study, the synergic effect of curcumin and aloe vera was exploited for the treatment of lung and breast cancers [215]. PCL fibres with 1% of aloe vera and 5% of curcumin were tested against human breast cancer and lung cancer cell lines *in vitro*, leading to an enhanced cytotoxicity if compared to PCL fibres laded with standard drugs [215].

2.2.3. Food industry

In food processing and packaging, the encapsulation of plant extracts in a polymer matrix is typically used to improve the stability and control the release profile of natural compounds, facilitating their storage and handling [216]. Main advantages of electrospinning for the encapsulation of naturally-derived materials for food industry are its cost-effectiveness and the possibility to preserve the integrity of the active ingredients because high processing temperatures are not required [207], [216]. Furthermore a wide range of polymers that are edible or approved for food contact can be successfully electrospun [217].

This section will discuss how electrospun nanofibres encapsulating plant extracts have been engineered in order to be used as food carriers and as systems for smart food packaging.

2.2.3.1. Nanofibres as carriers of plant extracts

For food-based applications, natural polymers which can be dissolved in water or ethanol were preferred. Zein, a protein of corn, is a good candidate for that purpose. A considerable number of studies have used electrospun fibres of zein as carrier. Electrospun nanofibres of zein have been proposed for the encapsulation of β-carotene, a natural antioxidant used as dietary supplement and food colorant [218]. The role of the fibres was to preserve the antioxidant activity of this light sensitive compound. The study compared the stability of β-carotene contained into nanofibres with pure β-carotene and fine powder β-carotene produced by solution cast. The results demonstrated that the photo-oxidation of the natural ingredient was remarkably delayed using the nanofibres, which blocked light and β-carotene interaction. Zein fibres have been also used as carriers for gallic acid, which is a phenolic acid with anti-inflammatory, anti-oxidant and antibacterial properties [219]. The interaction between zein and gallic acid at molecular level induced structural changes on both components, with changes in the degradation temperature of gallic acid but without affecting its antioxidant ability. In fact, gallic acid maintained 1,10-diphenyl-2-picrylhydrazyl (DPPH) radical scavenging effect. In another study, electrospun nanofibres of zein have been proposed as carriers and stabilisers of Epigallocatechin gallate (EGCG), a green tea polyphenol [108] with antioxidant and antimicrobial activity and health benefits [108]. EGCG and zein powder were dissolved in aqueous ethanol solutions and then electrospun. It was observed that freshly-prepared fibres were less effective in stabilizing EGCG than fibres aged at 21 ^{o}C and 0% humidity for 1 day. In fact, the results showed that, when in contact with water, mats without ageing resulted in 18% EGCG loss, while the aged mats exhibited no EGCG loss, which was desirable. However, mats aged at high relative humidity (75%) were characterised by even a higher loss (27-34%) than not aged ones, which was explained by the progressively degradation of the matrix during aging. Physical encapsulation and chemical interactions between zein and EGCG

(hydrogen bonds and hydrophobic interactions) are mainly responsible for the mechanism of stabilisation of zein nanofibres. Mats with increased bactericidal activity against *E.coli* and *Saccharomyce cerevisiae* (*S. cerevisiae*) have been produced by loading EGCG-Cu^{II} complex into PVA fibres [220]. The study believed that when contacting with bacteria, Cu^{II} reduced into Cu^{I}, which was responsible for the damage of bacteria surface.

As discussed in 2.2.1.3., cyclodextrin inclusion complexes of plant extracts have been synthesised in order to improve the stability of volatile chemicals encapsulated into electrospun nanofibres. In food industry, CD-ICs are of particular interest because they allow prolonging the shelf-life and thermal stability of additives [221], [222]. Kayaci *et al*. demonstrated the encapsulation of vanillin/CD-IC into PVA mats [223]. The antioxidant properties and the fragrance of vanillin make it a preservative largely used in food industry, even though the high volatility limits its functionality. The work showed that when PVA fibres are used as encapsulating matrix, the thermal stability of vanillin/CD-IC increased with vanillin release shifting at high temperature. Moreover, only 40% of vanillin was lost after 50 days of storage at room temperature, indicating that the shelf-life of the product was increased. PVA electrospun meshes encapsulating eugenol (EG) CD-IC were also produced (Figure 16) [224]. EG is a fragrance and a germicide extracted from plants, with limited stability when exposed to oxygen, light and temperature. High thermal stability of EG was instead achieved when EG/CD-ICs were electrospun in PVA, highlighted by the shift of EG degradation temperature at high values and a slow release at elevated temperatures. Similar behaviour was observed also for geraniol CD-ICs loaded into PVA electrospun membranes [225]. Geraniol is a component of plant essential oils and characterised by insect repellence, antimicrobial and antioxidant activity. Minimal loss of geraniol (10%) from the nanofibres was detected after two years of storage at room temperature and 25% relative humidity, confirming the improved stability and durability of chemical compound. A recent study on geraniol/CD-IC fibres has proved that the electrospun mats possessed DPPH radical scavenging activity and ability to inhibit the growth of *E. coli* and *S. aureus* [226].

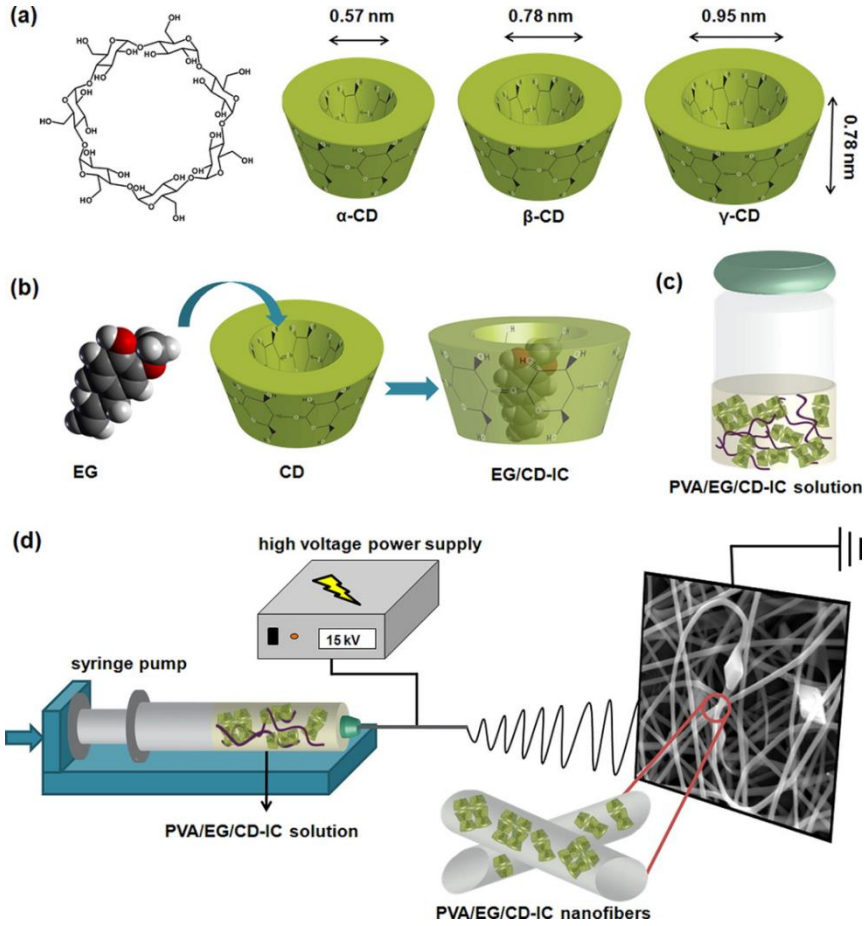

Figure 16 (a) Chemical structure of β-CD and dimensions of α-CD, β-CD, γ-CD. (b) Schematic representations of (b) the formation of EG/CD-IC, (c) the PVA/EG/CD-IC solution and (d) the electrospinning process leading to the production of PVA/EG/CD-IC fibres. This figure has been published [160].

Pullulan, an edible polysaccharide, and β-cyclodextrin have been used to encapsulate perillaldehyde that is an aroma compound extracted from the plant *Perilla frutescens* [227]. The fibres were stable for months in normal conditions without losses of the volatile chemicals, whose release can be controlled by modifying the ambient humidity. For instance, increasing the relative humidity at 92%, the release of almost 90% of perillaldehyde was achieved in one day. Hybrid fibres of pullulan and amaranth protein isolate (API) have been used for the production of food with potential health benefits, by encapsulating quercitin (a flavonoid present in vegetables, fruits and medicinal plants) and ferulic acid (a phenolic compound obtained from plant cell walls) [228]. *In vitro* digestion analysis demonstrated that quercitin and ferulic acid were quickly released at the beginning of the gastric process (19 and 21% for quercitin and ferulic acid, respectively), with an almost complete delivery at the end of the intestinal digestion. Importantly, the API:pullulan matrix was able to prevent the loss

of the antioxidant capacity of quercitin and ferulic acid if compared with not encapsulated compounds.

2.2.3.2. Active food packaging

For food packaging applications, functional molecules extracted from plants have been exploited for prolonging food shelf-life and avoiding bacteria colonisation[229]. In a recent study, electrospun mats of PVA, cinnamon essential oil (CEO) and β-cyclodextrin (PVA/CEO/β-CD) have been produced for their antimicrobial activity against *S. aureus* and *E. coli* [195]. CEO was chosen because it was more effective than clove, Artemisia and eucalyptus EOs, and the combination with β-CD further enhanced CEO antibacterial action. The study compared the electrospun nanofibrous mats with casting films, demonstrating that the fibrous PVA/CEO/β-CD substrates produced a larger bacteria inhibition zone than casting films. This was associated with the porosity of the electrospun mat, which facilitated the faster release of CEO. The electrospun package was evaluated in strawberry preservation tests, compared to commercial fresh-keeping films. Unpacked strawberries were easily perishable with a maximum storage life of four days, which was extended to six days when packed with fresh-keeping films. On the contrary, the fruit packed with PVA/CEO/β-CD fibres were stable for up to 6 days without losing their flavour. Cinnamaldehyde (CNMA), the bioactive chemical component of CEO with virucidal properties, has been encapsulated in zein electrospun nanofibres [230]. Biodegradable multilayer systems based on compression moulded polyhydroxybutyrate (PHB) films as outer layer and CNMA-zein fibres as inner layer have been developed. Virucidal activity of the system was tested by a modification of ISO 22196:2011 method. The produced systems were active against norovirus surrogates that are responsible for foodborne illness; therefore, they are promising in food safety for preventing contaminations of food contact surfaces.

Combinations of natural ingredients and nanomaterials have been proposed for preventing microbial contaminations of meat foodstuffs. In a recent work, electrospun polyurethane nanofibres containing zinc nanoparticles and virgin olive oil have been developed as hybrid packaging material [231]. Whilst pristine polyurethane fibres were not active against *S. aureus* and *Salmonella typhimurium* (*S. typhimurium*), the

addition of olive oil showed a greater inhibition effect, which was further strengthened by the use of ZnO nanoparticles. This nanofibrous hybrid packaging system is attractive for protecting fresh and processed meat against pathogen contaminations. Lin et al. encapsulated chrysanthemum EO in chitosan electrospun fibres for beef packaging application [201]. The study found that chrysanthemum EO showed strong antibacterial properties against *Listeria monocytogenes* by increasing its cell membrane permeability and restraining its respiratory metabolism. The cumulative release rate of chrysanthemum EO was 43.98%, 55.43%, 62.45% under 4 ºC, 12 ºC, 25 ºC, respectively, detected by gas chromatograph mass spectrometer, and inhibition rate of *L. monocytogenes* on beef was found up to 99.95%.
Tang et al. developed edible packaging composed of electrospun gelatin nanofibres encapsulating peppermint and chamomile EOs [212]. The incorporation of EOs increased the hydrophobicity of material. Water contact angle of fibres increased from 45º to (101.3 ± 4.3)º with 9 v/v % EO encapsulated. Peppermint EO and chamomile EO in fibres showed antibacterial properties against *E. coli* and *S. aureus*, either separately or combined. Fibres containing 9% peppermint EO showed higher inhibition value of 1 log unit (*E. coli*) and 1 log unit (*S. aureus*) than fibres containing 9% chamomile EO. Cell survival rates of all mats were similar, and all are above 95%, indicating the fibres were not cytotoxic.

2.2.4. Summary of Literature Review

This literature review focused on diverse studies that has demonstrated that naturally-derived bioactive agents are valid alternatives to synthetic counterparts for applications that include wound management and food industry. In particular, the possibility to encapsulate them in polymeric nanofibres using the electrospinning technique has promoted the creation of scaffolds with improved bioactivity for tissue regeneration. In fact, *in vitro* and *in vivo* tests have highlighted the efficacy of electrospun dressings based on plant extracts in stimulating cells proliferation, controlling inflammation response and preventing bacteria colonisation. Furthermore, the electrospinning of natural ingredients has been proposed for preserving the stability and integrity of food and for developing active packaging systems that prolong food shelf-

life and avoid biofilms formation. Future research in the field aims to create multi-functional electrospun architectures that combine the biological properties of diverse plant extracts.
In this chapter, Tea Tree essential oil (*Melaleuca alternifolia*) or manuka essential oil (*Leptospermum scoparium*) were combined with PLA to produce electrospun fibres with antibacterial properties for wound dressing application.

2.3. Experimental methods

2.3.1. Electrospinning process

Solutions for electrospinning were prepared by dissolving PLA (Ingeo™ 4060D supplied by Natureworks LLC) in acetone at 15% w/v concentration. PLA 4060D is an amorphous polymer with an l-lactide content of around 88 wt% and a weight average molecular weight (M_w) as determined by gel permeation chromatography (GPC) of 1.15×10^5 g/mol. The optimum concentration for defect-free nanofibre production is between 2 and 2.5 times the critical chain entanglement concentration (C_e) and the value of C_e for PLA/acetone was found to be 6% w/v [11]. Hence the concentration of 15% w/v was chosen.
Tea Tree essential oil (*Melaleuca alternifolia*) or manuka essential oil (*Leptospermum scoparium*) were added to the PLA/acetone solution at different concentrations: 2.5, 5.0, 7.5, 10.0 and 15.0% v/v. Tea Tree oil is mainly constituted by terpinen-4-ol, γ-terpinene, α-terpinene and 1,8-cineole; Manuka oil contains triketones, sesquiterpenes and *p*-cymene [232]–[234]. PLA, PLA/Tea Tree EO (PLA/TT EO) and PLA/Manuka EO (PLA/M EO) solutions were loaded into a 3 ml plastic syringe capped with one 18-gauge needle. The solutions were injected at a constant flow rate of 2 ml/h that was generated by a pump system (PHD ULTRA, Harvard Apparatus). A voltage of 18.5 kV was applied between the needle and an aluminium planar collector, placed at a relative distance of 15 cm. The electrospinning process was conducted at 20 °C, using the Spraybase® Electrospinning equipment.

2.3.2. Characterisation of the fibrous mats

The morphology of the electrospun fibres was observed using a scanning electron microscope (SEM), with a field emission gun system LEO1530VP. A gold/palladium coating was deposited onto the fibrous mats before imaging using an Emitech SC7640 sputter coater (90 s sputter time).
The chemical analysis of the fibres with and without the essential oils, and of the pristine essential oils was carried using Raman spectroscopy. Raman measurements were performed in a confocal back-scattering configuration with a HORIBA LabRAM HR spectrometer equipped with an Olympus microscope, a liquid-nitrogen cooled Charge-Coupled Detector and a He-Ne laser (excitation wavelength of 633 nm). The laser power on the sample surface was 3.75 mW.
Thermal characterisation of the mats was conducted using differential scanning calorimetry (DSC Q200, TA Instruments Calorimetric Analyser, USA) in a nitrogen atmosphere with a flow rate of 50 ml/min. Approximately 8 mg of each type of mat was sealed in an aluminium pan and heated from − 20 to 100 °C at 10 °C/min. Empty aluminium pans were used as reference. Data were analysed using the TA universal analysis software. All the reported values are the average of 3 samples.
For analysis of mechanical properties, the fibrous mats were detached from the aluminium foil and cut using an ISO527-2/5A die. Tensile tests were carried out using a single column table top Instron system at room temperature. The rate of extension was set at 2 mm/min for the preload stage and at 3 mm/min for the test. Side action grip clamps with flat jaw faces were used.

2.3.3. Antibacterial tests

The antibacterial activity of the nanofibrous mats containing Tea Tree oil or Manuka oil was tested against *Staphylococcus epidermidis*. PLA nanofibers without essential oils were used as control. Bacterial cultures were prepared in 2.5 mg/100 ml water LB broth, according to the manufacturer's instructions, and incubated at 37 °C overnight. 11.1 mg LB Agar was dissolved in 300 ml of water and then heated at 120 °C for 15 min. Agar plates were then prepared and inoculated with 1 ml of bacteria cul-

ture. The electrospun mats (weight 45 mg) were placed on top of the plates and incubated at 37 °C for two days. Photos of the plates were taken, and the zone of inhibition was measured.

2.4. Results and discussion

2.4.1. Morphology of fibres encapsulating different concentrations of essential oils

The solubility of PLA, Tea Tree oil and Manuka oil in acetone allowed homogeneous solutions to be obtained, as observed by the naked eye, which gave good dispersion of the essential oils in the polymer matrix. This had a positive effect on the morphology of the electrospun fibres.

As shown in Figure 17, SEM analysis of the fibrous mats revealed the absence of defects and beads. Fibres produced from PLA solution without EOs (Figure 17a), showed a cylindrical and well-defined shape, with overlapping but not merged fibres. The addition of 5% v/v of Tea Tree EO to PLA/acetone solution gave rise to the formation of junctions where fibres merged together, as shown in Figure 17b and highlighted by the blue circle in the inset of Fig. 4b. The extent of this inter-fibre bonding further increased with the increase of Tea Tree EO concentration, as seen in the inset of Figure 17c for PLA fibres electrospun from solutions containing 10% v/v of Tea Tree EO. This is explained in 2.4.3. Two or more fibres have fused together and formed bundles. When the concentration of EO reached 15% v/v, mats with highly interconnected fibres were produced. The fibrous structure is still visible, but fibres have merged together and lost their cylindrical shape (Figure 17d and inset).

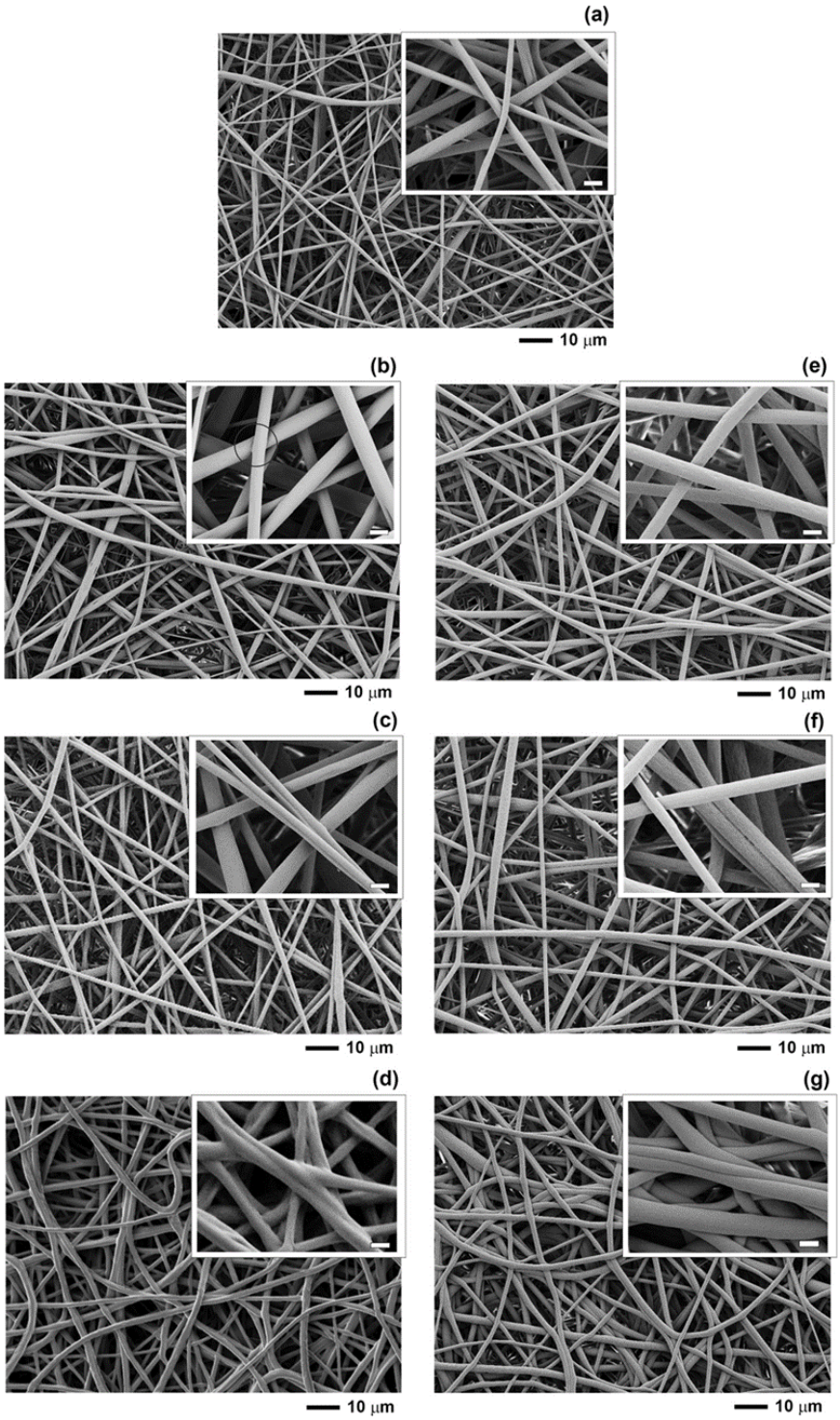

Figure 17 SEM images of electrospun fibres of (a) PLA, (b) PLA/TT EO (5% v/v), (c) PLA/TT EO (10% v/v), (d) PLA/TT EO (15% v/v), (e) PLA/M EO (5% v/v), (f) PLA/M EO (10% v/v) and (g) PLA/M EO (15% v/v). Insets: SEM images at higher magnification. Scale bar = 2 μm. This figure has been published on [40]**.**

The effect of oil concentration was less evident for fibres produced from PLA/Manuka EO solutions (Figure 17e–g). Only at EO concentration of 15% v/v, the morphology of the fibrous mat changed, with extended regions of contact between fibres but without fusion (Figure 17g and relative inset). The phenomenon of fibre coalescence has been already reported in the literature. For example, interconnected networks of Fe-N/C Polyvinylpyrrolidone can be formed as a consequence of water absorption [26]; Electrospun fibres of nitrile butadiene rubber tend to fuse together if the crosslinking degree is insufficient [27]. In the case of PLA and EOs, the changes observed in fibre morphology can be attributed to the thermal properties of the composite fibres, as discussed below.

2.4.2. Chemical characterisation

The Raman spectrum of Tea Tree oil (Melaleuca alternifolia) in Figure 18a is characterised by bands assigned to terpinen-4-ol, which is one of the main components of this essential oil [232]. Particularly, the peaks at 1678 cm^{-1}, 1376 cm^{-1}, 1307 cm^{-1} and 730 cm^{-1} correspond to C=C stretching modes of terpinen-4-ol. The presence of γ-terpinene and α-terpinene, which are two other components of Tea Tree EO, is confirmed by the peaks at 1702 cm− 1 (C=C stretching of γ-terpinene), 1612 cm^{-1} (C=C stretching of α-terpinene), 1425 cm^{-1} (C-H bending of γ-terpinene), 756 cm^{-1} (ring deformation of γ-terpinene). The bands at 1445 cm− 1 and 652 cm^{-1} are assigned to CH3/CH2 bending mode and to 1,8-cineole, respectively. The analysis of the PLA/TT EO fibres reveals the presence of the characteristic peaks of PLA and a reduction of the intensity of some of the bands of Tea Tree oil, particularly those associated with γ-terpinene and α-terpinene. This can be due to the evaporation of the oil during the electrospinning procedure. The bands of terpinen-4-ol are visible.

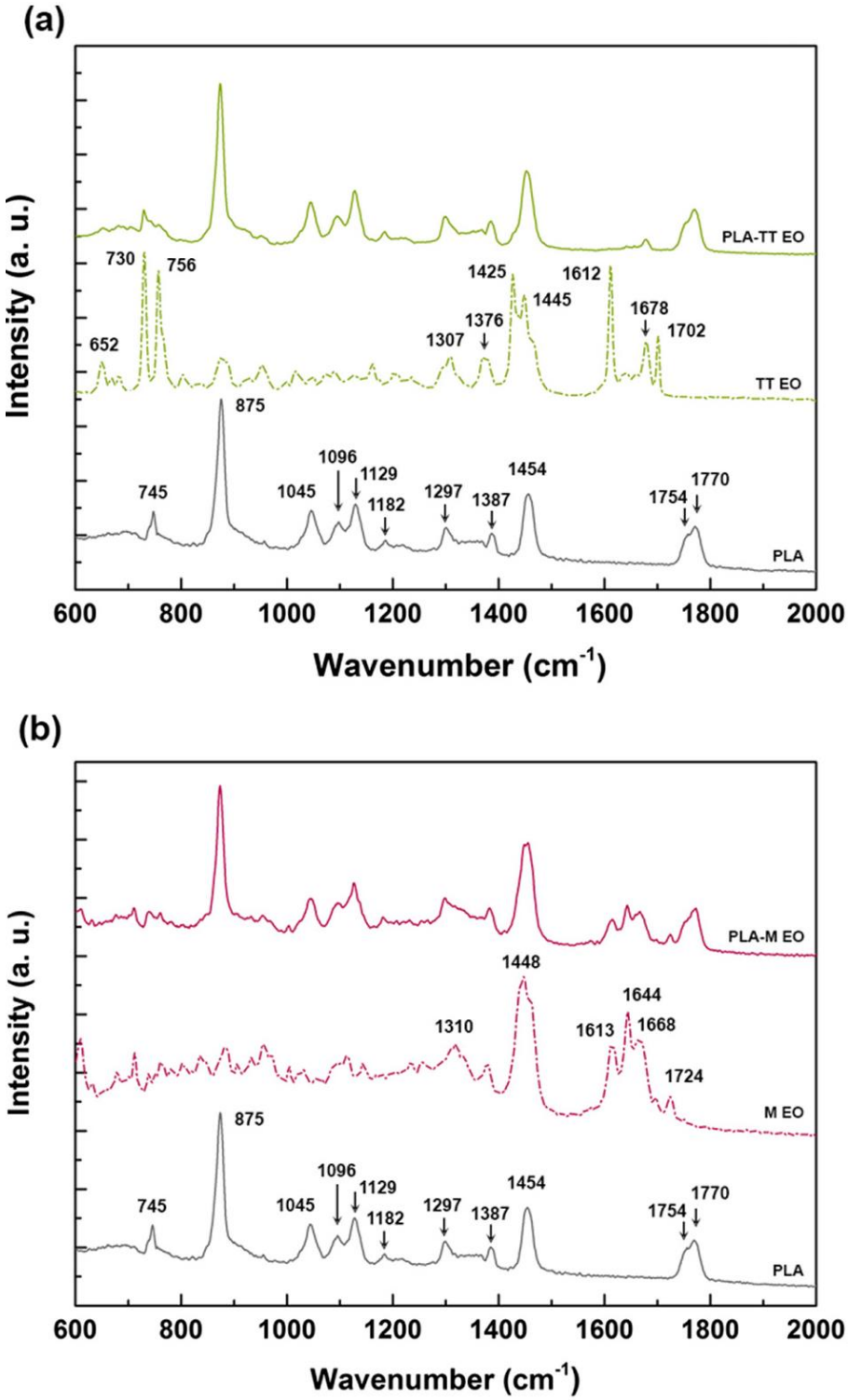

Figure 18 Comparison of the Raman spectra of PLA electrospun fibres (continuous grey line), essential oils and composite PLA/EOs fibres: (a) pristine Tea Tree oil (dashed green line) and PLA/TT EO (10% v/v) fibres (continuous green line); (b) pristine Manuka essential oil (dashed magenta line) and PLA/M EO (10% v/v) fibres (continuous magenta line). This figure has been published on [40]**.**

The main constituents of *M. alternifolia* oil are not present in Manuka essential oil (Leptospermum scoparium), for which the relevant compounds are flavonoids,

triketones (such as leptospermone and flavesone), sesquiterpenes (α-copaene and calamenene) and monoterpenes (α-pinene, myrcene, and p-cymene) [233], [234]. In Figure 18b, the Raman spectrum of the Manuka EO exhibits bands of triketones at 1724 cm^{-1}, 1668 cm^{-1}, 1448 cm^{-1}, and 1310 cm^{-1} [235], [236]. The peaks at 1644 cm^{-1} and 1613 cm^{-1} can be ascribed to C=C stretching mode and ring stretching mode of p-cymene, respectively [237].Those bands are still visible in the spectrum of PLA/M EO electrospun mats together with the peaks of PLA. Therefore, Manuka oil and particularly triketones, which are responsible for the antibacterial activity of this EO [235], are contained inside the fibres.

2.4.3. Thermal characterisation

DSC analysis was performed in order to evaluate the glass transition temperature (T_g) of PLA, PLA/TT EO and PLA/M EO fibres. As shown in Figure 19, the T_g of PLA fibres (grey bar) was (53 ± 1)°C, in agreement with previous reports [238]. However, PLA/TT EO (light green bars) and PLA/M EO (light magenta bars) electrospun mats exhibited a lower T_g, which decreased with increasing EO concentration. Fibres produced from PLA solutions with 2.5 and 5.0% v/v of Tea Tree and Manuka EO were characterised by similar values of T_g: around 35 °C and around 30 °C for 2.5 and 5.0% v/v, respectively. For concentrations ranging from 7.5 to 15.0% v/v, the difference in T_g between PLA/TT EO and PLA/M EO fibres became statistically significant, with Tea Tree EO having a greater effect on T_g than Manuka EO. When fibres were electrospun from PLA solutions with 7.5, 10.0 and 15.0% v/v of Tea Tree EO, T_g values of (23 ± 1)°C, (15 ± 1)°C and (12 ± 1)°C were recorded, respectively. On the other hand, for Manuka EO, T_g dropped to (19 ± 1)°C when 15% v/v of oil was used. Values of T_g in the range of 17–35 °C have been reported for PLA plasticised with low molecular weight molecules (less than 2000 g/mol), such as citrates or terpenes [239], [240]. Tea Tree and Manuka oil are compounds with low molecular weight (lower than 500 g/mol) and rich in terpenes [241]. Like plasticisers, they are able to drastically lower the T_g of PLA by enhancing polymer chain mobility and increasing polymer free volume [240], [242], [243]. The difference in thermal properties between PLA/TT EO and PLA/M EO fibres can be ascribed to the different

chemical composition of the two essential oils, as previously demonstrated by Raman spectroscopy.

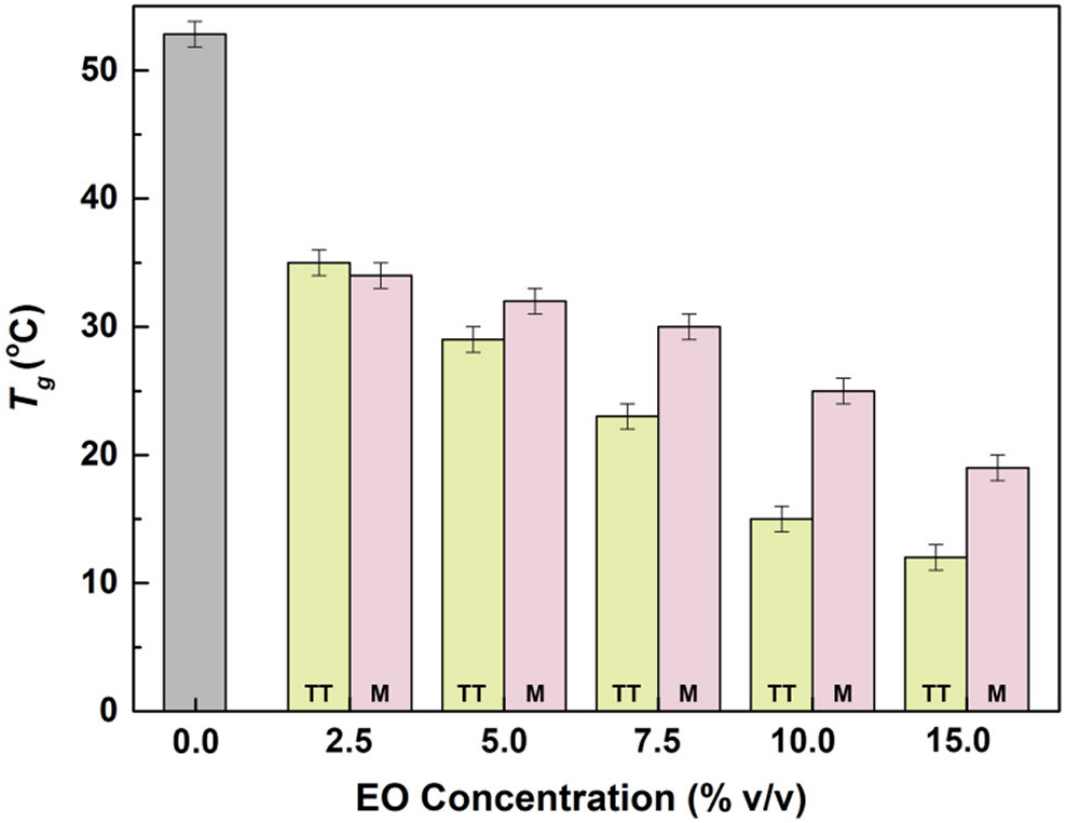

Figure 19 Glass transition temperature of PLA (grey bar), PLA/TT EO (light green bars) and PLA/M EO (light pink bars) fibres as a function of the EO concentration. This figure has been published on [40]**.**

The thermal properties of the PLA/EOs mats had an impact on their morphology. As previously discussed (Figure 17c, d and g), inter-fibre bonding was observed for high concentrations of Tea Tree and Manuka EO (10 and 15% v/v). At those concentrations, the samples produced had T_g in the range of 12–25 °C, which was comparable or slightly lower than room temperature (the electrospinning process was conducted at room temperature). As demonstrated in the literature, when electrospun fibres are annealed at a temperature close to their T_g, motions of the polymer chains at the fibre surface or in the bulk of the fibre, depending on the annealing temperature and polymer, give rise to fusion at the fibre-fibre junctions and eventually formation of collapsed structures [244]–[247]. Therefore, it can be assumed that PLA/TT EO mats exhibited more evident inter-fibre bonding than

PLA/M EO fibres because their T_g was much lower than the temperature at which the electrospinning process was carried out.

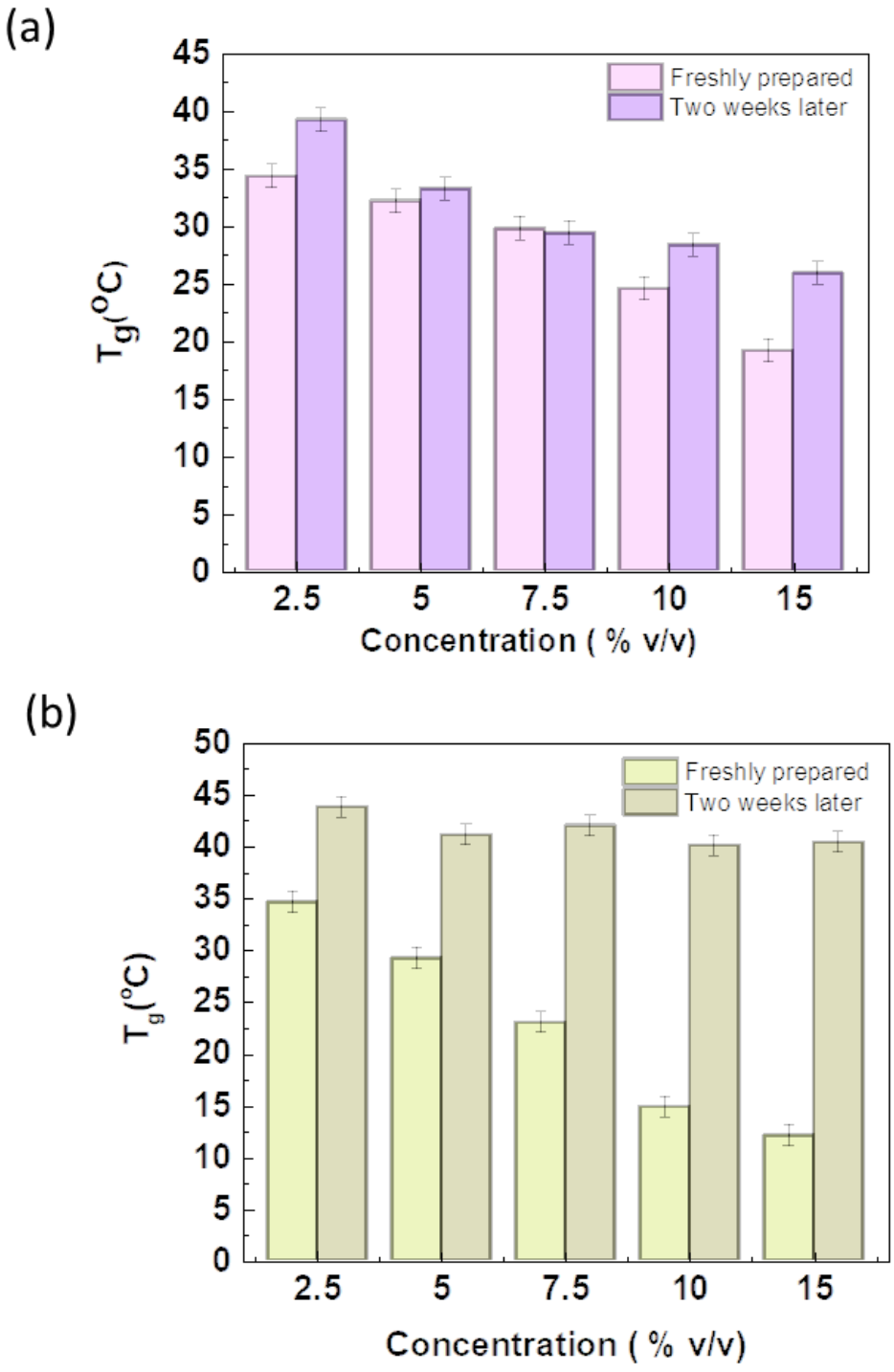

Figure 20 Glass transition temperature (Tg) of freshly prepared and exposed after two weeks PLA/EO with different EO concentrations: (a) Manuka EO and (b) tea tree EO

After two weeks of storage at room temperature, T_g increased for both PLA/M EO and PLA/TT EO for all concentrations, as shown in Figure 20a and b. This is likely caused by the evaporation of volatile molecules in two weeks. A more obvious increase was observed for PLA/TT EO samples, with the biggest increase (7.5 ^oC) for a concentration of 7.5% v/v. Additionally, for all PLA/TT EO stored for two weeks, T_g values were similar of (41.62±2.19) ^oC, indicating that most of the volatile molecules had evaporated in this period. For PLA/M EO samples, a less obvious increase in T_g was observed in samples stored for two weeks. These results confirmed that low molecular weight molecules, for example terpenes, with high volatility caused the plasticising effect for PLA nanofibres [248]. To maintain the volatile molecules, samples should be stored in sealed bags.

2.4.4. Mechanical characterisation

The plasticising effect of Tea Tree and Manuka oil on PLA also affected the mechanical properties of the composite fibres. PLA fibres exhibited tensile elongation at break (ε_b) and strength at break (σ_b) of (0.3 ± 0.1) and (2.4 ± 0.5) MPa, respectively, in agreement with previous studies, Figure 21 [247], [249]. The incorporation of Tea Tree and Manuka EOs resulted in a significant increase in both ε_b and σ_b. For PLA/TT EO fibres, Figure 21, ε_b reached values of (2.6 ± 0.2) when the lowest oil concentration was used (2.5% v/v), namely 8.7 times higher than the ε_b of PLA fibres. Then, with increasing TT EO concentration (up to 10.0% v/v), ε_b remained almost constant with values between 2.1 and 3.1. However, a drop in ε_b was recorded for fibrous mats produced from PLA solutions with 15.0% v/v of TT EO. While the high values of elongation at break (particularly for EO concentrations from 2.5 to 10.0% v/v) are mainly due to the plasticising effect of TT EO, the decrease of ε_b observed for 15.0% v/v concentration can be attributed to the morphology of the fibrous mat.

Previous studies have found that EOs worked as plasticisers for polymer films. For instance, Ahmed et al. incorporated cinnamon EO in PLA using solvent casting method [250]. Tensile strength of film decreased from (45.94 ± 2.99) MPa to (31.59 ± 1.95) MPa when 25% EO (w/w, PLA) was incorporated, and further decreased to (24.61 ± 0.65) MPa with 50% (w/w, PLA) EO incorporated. Thermal analysis of this

study found that glass transition temperature of the film decreased from (39.30 ± 0.27) ^{o}C, to 16.42 ^{o}C and 6.81 ^{o}C with increasing EO concentration (25% and 50%, w/w, PLA), which furthermore confirmed the plasticising effect of cinnamon EO on PLA. Researchers believed that low molecular weight EO could induced phase slipping and increased polymer chain flexibility, resulting in plasticising effect. Notably, in the study, the melting temperature of films also decreased from (146.94 ± 1.21) ^{o}C to 133.21 ^{o}C and 127.42 ^{o}C with increasing EO concentration (25% and 50%, w/w, PLA), which was explained by the localisation of the low molecular weight molecules at the interface between the crystalline and amorphous parts. Similar results were shown by incorporating: oregano EO into alginate films [251], PLA films [252], and starch-chitosan films [253]; Zataria multiflora EO into gelatin films [254]; cinnamon, clove, and oregano EOs into starch-gelatin films [255].

Plasticising effect of EOs usually cause increase in strain but decrease in strength for polymer films [250], [252], [256]. However, the breaking mechanism of films and electrospun fibres could be different, which could lead to different mechanical properties for the same material. Croisier et al. compared the mechanical properties of electrospun PCL fibres and extruded PCL films[257]. PCL nanofibrous mats were cut into 3×0.5 cm^2 rectangular shape and then tested by an electromechanical tensile tester. The study found that nanofibrous mats had higher strain at break (170 ± 10%) but lower Young's modulus (3.8 ± 0.8 MPa), which might be due to the porosity of fibre scaffolds, interactions between fibres and fibre orientation. Similar results were also shown in electrospun PLA and cellulose nanocrystals nanocomposite mats [249]. The study explained the breaking mechanism in detail. For the cast films, grazes or defects, which caused the rupture, occurred after polymer chains could not revert back to their original positions. However, for the nanofibrous mats, the SEM result showed that nanofibres started to align during the stretching, resulting in larger elongation at break.

As shown in Figure 22 and Figure 23, PLA/TT EO nanofibres showed a higher degree of alignment after stretching, which not only increased the elongation but also strengthened whole material at the stretching direction. Thus, strength and strain both increased. The alignment of nanofibres after stretching is different for all three materials (Figure 23), which is likely to be caused by the difference in flexibility of polymer chains. Monnier et al. detected the change in mesophase in electrospun PLA with or without plasticisation. The change of mesophase reflected the inter-

chain interactions between PLA and plasticisation which caused the loosening of PLA macromolecules [258]. In both PLA/M EO and PLA/TT EO fibres, inter-fibre adhesion, shown in the morphological analysis in Figure 17d, limits the sliding of fibres on top of each other during tensile deformation, resulting in a lower elongation. Similar behaviour has been observed, for example, for polyethersulfone electrospun membranes after thermal treatment and for composite
Polycaprolactone, collagen and elastin fibres [259], [260]. Once tight cohesion between the fibres has been established, the elongation at break of the electrospun mat decreases, contrary to the tensile strength, which increases.

As shown in Figure 21b, the addition of Tea Tree EO resulted in an increase of σ_b: values of (4.9 ± 1.1) MPa and (4.2 ± 1.2) MPa were measured for fibres electrospun from PLA solutions with 2.5 and 5.0% v/v oil, respectively. The effect of Tea Tree EO on the σ_b was much more evident for EO concentrations higher than 7.5% v/v, (10.5 ± 1.8) MPa, with the highest value reported for concentration of 15.0% v/v, (17.0 ± 1.0) MPa, as expected, due to the morphology of these mats. A previous study on thermally treated PLA electrospun membranes has demonstrated that, as a consequence of the temperature increase, the fibres undergo changes in morphology and fibre-fibre junctions become bonded [261]. Fibre coalescence increases as a function of the temperature together with the tensile strength of the membranes.

Tensile tests conducted on PLA/M EO electrospun samples also showed an increase of ε_b and σ_b with oil concentration (Figure 21). Differently from PLA/TT EO fibres, ε_b gradually increased from (1.2 ± 0.1) at 2.5% v/v EO concentration to (3.4 ± 0.2) at 5.0% v/v. Then, ε_b remained almost constant, with the highest value of (3.7 ± 0.2) at 15.0% v/v EO concentration. The trend observed for σ_b also differed from that of PLA/TT EO samples, with values in the range of 4.7–6.5 MPa, which were significantly lower than those of the PLA/TT EO samples, and without a large incremental change between the different EO concentrations. The lack of fibre coalescence in PLA/M EO mats, explained in 2.4.3, can be the reason for the difference in mechanical properties observed for the two types of composite fibres, particularly at higher EO concentrations.

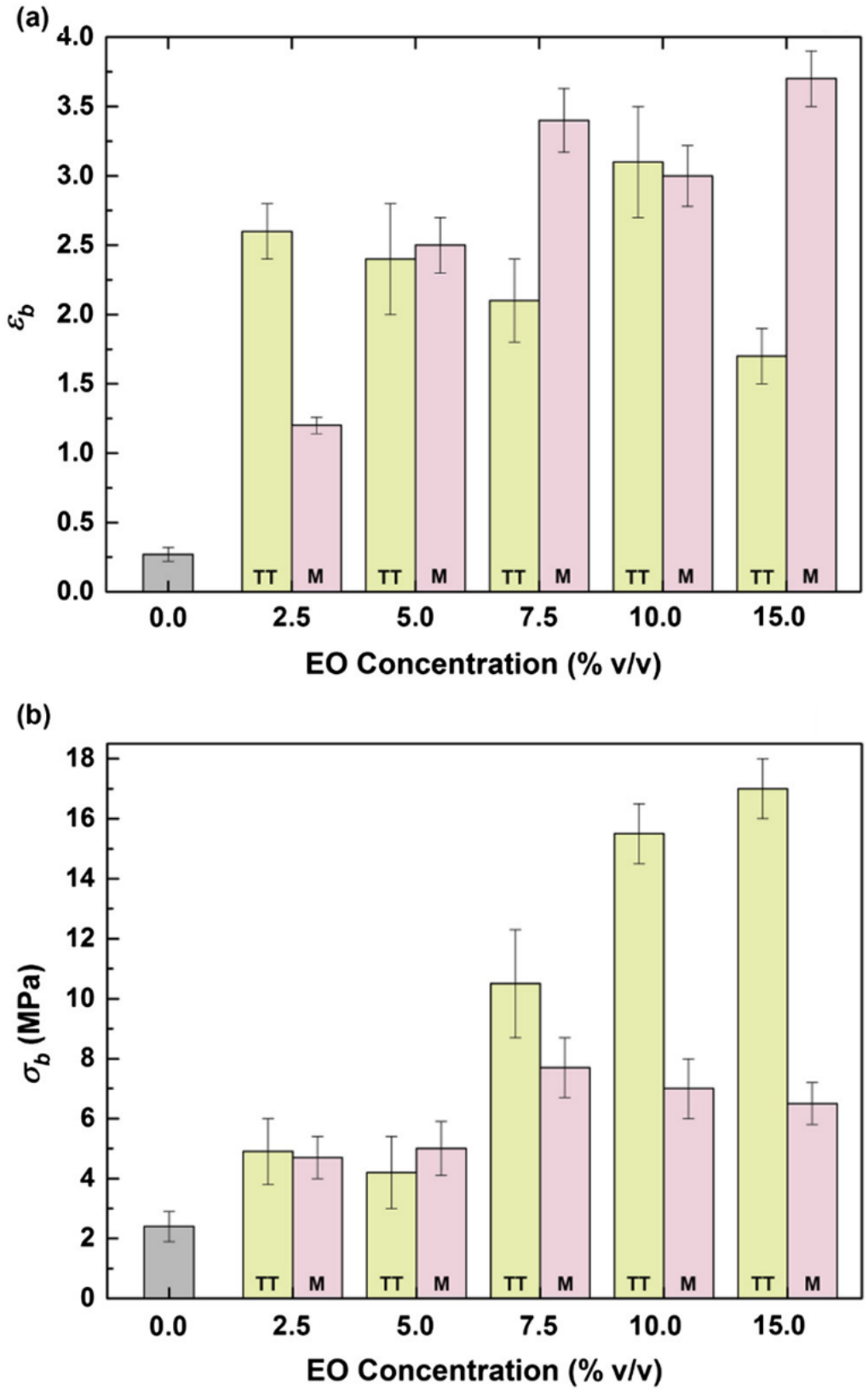

Figure 21. (a) Elongation-at-break and (b) tensile strength of PLA (grey bar), PLA/TT EO (light green bars) and PLA/M EO (light pink bars) fibres as a function of the EO concentration. This figure has been published on [40].

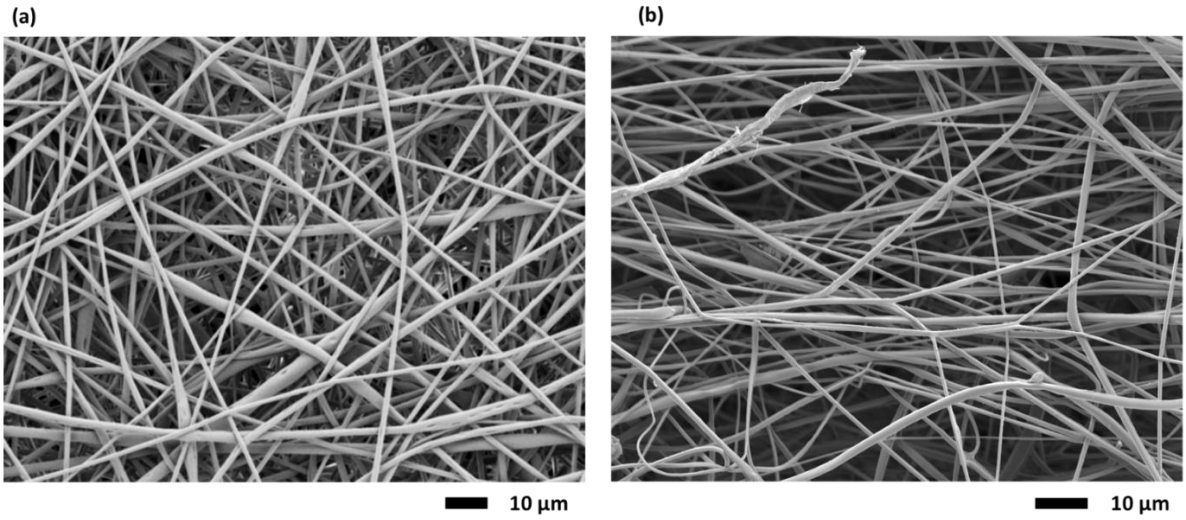

Figure 22 . FEG-SEM images of 15% w/v PLA(a) before stretch and (b)after stretch

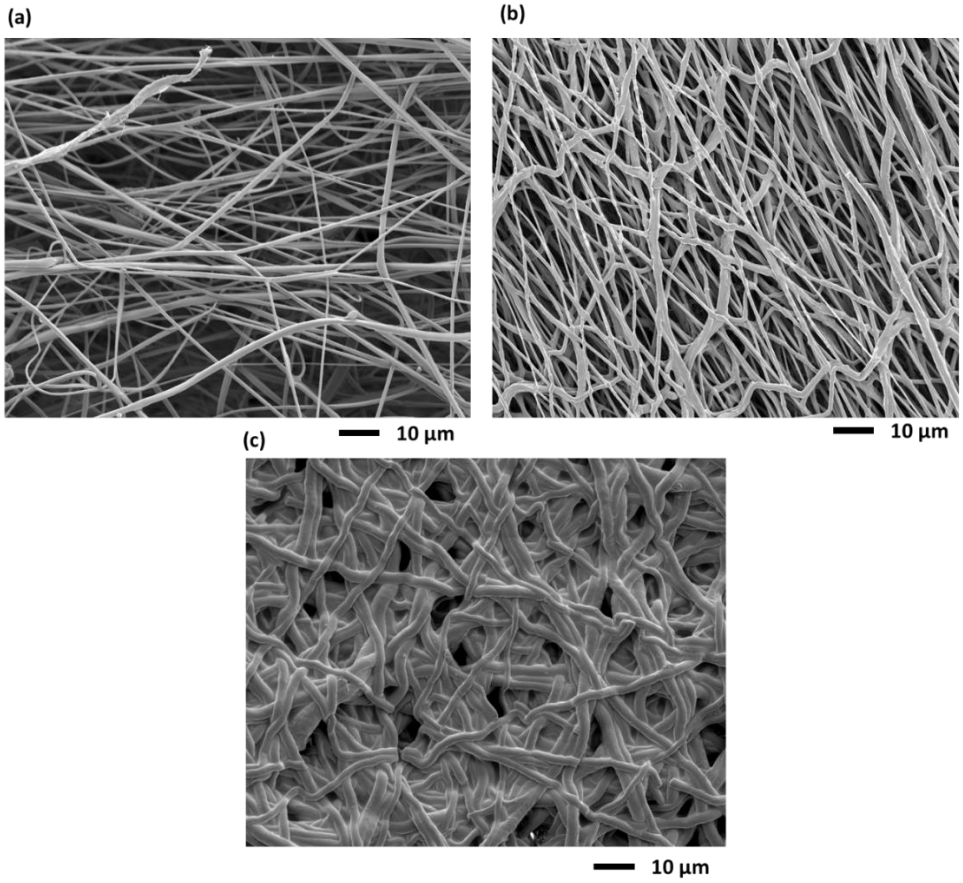

Figure 23 FEG-SEM images of electrospun fibres after stretching (a)PLA, (b)PLA/TT EO (15% v/v) and (c)PLA/M EO (15% v/v).

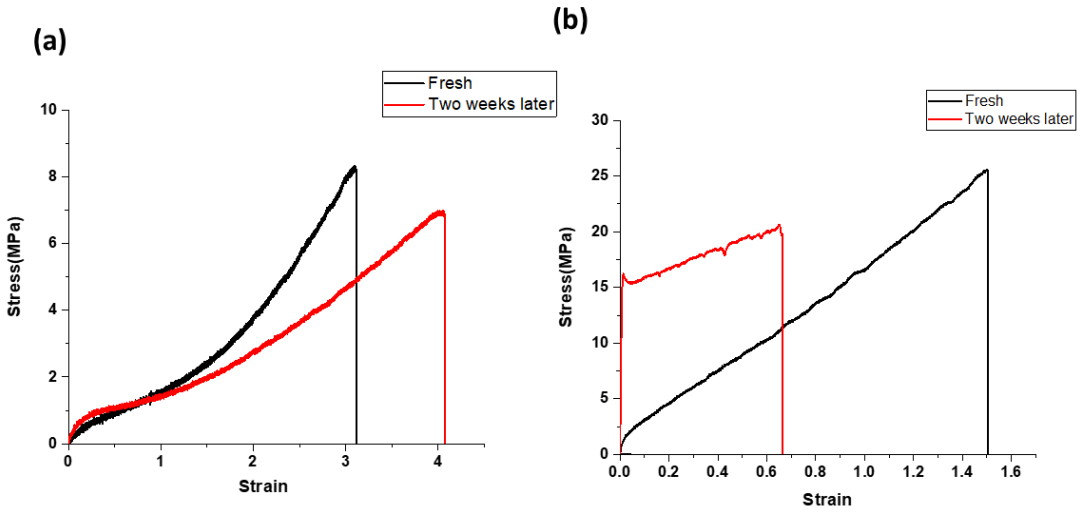

Figure 24 Typical stress-strain curves of electrospun fibres with 15% v/v Manuka EO concentration: freshly prepared (black line), after two weeks (red line) (a) PLA/TT EO, and (b) PLA/M EO

Mechanical tests were conducted after two weeks after electrospinning for PLA/M EO and PLA/TT nanofibres with 15% v/v EO. Typical stress-strain curves are shown in Figure 24. No big difference was shown for PLA/M EO nanofibres. However, for PLA/TT EO, modulus increased while strain decreased after two weeks, which indicated the nanofibres were less plasticised than the freshly prepared ones. Notably, the strength of nanofibres after two weeks was still close to freshly prepared one. This may be due to the fusion of fibres caused by the evaporation of EO on fibres' surface.

2.4.5. Antimicrobial

The antimicrobial properties of Tea Tree and Manuka EOs are attractive for preventing microorganism colonisation and biofilm formation [166] [262]. As reported in literature, the mechanism of action of essential oils against bacteria is mainly due to the hydrocarbons partition into the bacteria membrane [166]. The accumulation of hydrocarbons, such as terpene, in the bacteria membrane, causes a loss of integrity. This induces damages to the cytoplasmic membranes, with disruption of its functions and eventually cell lysis. The effectiveness of the composite fibres produced was tested against *S. epidermidis*. This bacterium is abundant on human skin and often

responsible for infections and formation of biofilms on indwelling medical devices [263]. PLA mats without EO (Figure 25a) and with Tea Tree oil (Figure 25b) were not able to inhibit the proliferation of *S. epidermidis*, and the presence of the biofilm was visible in the agar medium. On the other hand, an inhibition zone of 2 cm in diameter was detected for PLA fibres containing Manuka oil (Figure 25c), indicating the antibacterial activity of those mats. Although Tea Tree oil is used for the treatment of skin infections induced by *S. epidermidis* [263], in this case its efficacy was limited. This was probably due to the low amount of terpinen-4-ol, and α-terpinene available after the electrospinning process, as demonstrated by Raman spectroscopy. Conversely, Manuka oil was more stable during electrospinning, and the electrospun fibres still contained the compounds that confer antimicrobial properties on this essential oil (triketones) [235]. The glass transition temperature of the fibrous mats had also an effect on the release and diffusion of the active compounds inside the agar gel, leading to the inhibition zone observed.

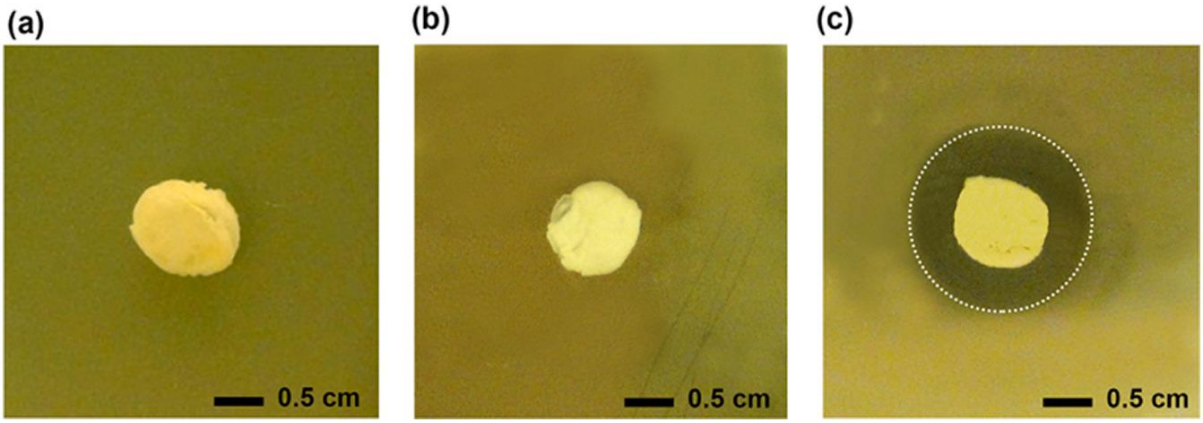

Figure 25 Photographs of the *in-vitro* test for analysing the activity of (a) PLA, (b) PLA-TT EO (10% v/v) and (c) PLA-M EO (10% v/v) electrospun mats against *S. epidermidis*. This figure has been published on [40].

2.5. Conclusion

In conclusion, it is demonstrated that essential oils of Tea Tree and Manuka can be used for enhancing the properties of PLA electrospun fibres, in terms of both mechanical and antibacterial characteristics. Chemical analysis of the fibres through Raman spectroscopy showed that the main components of Manuka oil were stable

after the electrospinning process. This was different from Tea Tree oil in which a strong reduction in the intensity of the characteristic peaks was detected. Consequently, the antibacterial activity of the composite PLA mats against S. epidermidis was affected. PLA/M EO fibres exhibited an inhibition effect against this pathogen, whereas PLA/TT EO mats were ineffective in preventing biofilm formation. Nevertheless, both EOs worked as plasticisers for PLA. In fact, the glass transition temperatures of PLA/TT EO and PLA/M EO fibres were reduced compared with the control PLA fibres. An increase in elongation-at-break as well as in tensile strength was observed for the composite fibres, and it was dependent on the EO concentration used. These results demonstrate that the PLA/EOs combinations studied have the potential to be exploited for the development of biomedical devices of which the mechanical behaviour and bioactivity can be controlled by using natural plant extracts.

Chapter 3 Phase separation in electrospun fibres of poly(ethyl cyanoacrylate) and polycaprolactone

3.1. Introduction

Hierarchical porous structures over different length scales, from nano- to macro-level, are widely available in nature [264], [265], [266]. They are fundamental for adaptation and provide unique properties to biological systems. Examples are: the outstanding mechanical properties of bone [267], which is composed of a dense cortical shell and a porous, cancellous interior of mineralised collagen fibres [268] [269]; the efficient light harvesting and nutrient transport capabilities of the green leaves of most photosynthesising plants, which possess a porous network of veins and irregular-shaped, loosely-packed spongy mesophyll cells [270].

The development of multi-scale hierarchical porous materials that mimic natural structures has drawn increasing research interest over the last decade, for application in catalysis, energy conversion and storage, tissue engineering and drug delivery [271], [272], [273], [274]. Among the diverse fabrication methods proposed, electrospinning [160] [275] has demonstrated the possibility of creating a variety of hierarchical primary and secondary structures with easy control over morphology, porosity and chemical composition [276], [277], [278], [279]. Porous electrospun fibres have been obtained by several methods, such as co-axial electrospinning [277], [280], [281], [282], selective removal [283], [284], [285], [286], [287], self-assembly [288], [289], breath figure [290], [291], [292], and phase separation [57], [290], [293], [294], [295], [296], [297], [298], [299], [300], [301]. Formation mechanisms of electrospun hierarchical porous fibres are explained in detail in literature review part.

So far, it has been demonstrated that phase separation is a useful approach to create porous electrospun fibres [302], [303]. However, phase separation events have not been used yet to promote the coexistence of micro- and nano-features with distinct morphology on the same fibre. Here we show that each single electrospun fibre of poly ethyl cyanoacrylate (PECA) and PCL can be partitioned in one region with aligned micro-grooved and one with circular nanopores by blending the polymers in a selected mixture of solvents. In order to elucidate the formation of those structures, we investigated the role played by diverse solvents (acetone, chloroform and acetonitrile) and their mixtures. We described the results obtained using a mechanism

based on the simultaneous happening of diverse types of phase separation events. The surface micro- and nanostructures and the internal porosity generated are of interest for biomedical applications as physical cues to locally influence cellular behaviour [47], [48] and to control the release of bioactive compounds [46].

3.2. Literature review

3.2.1. Hierarchical porous fibres

By manipulating the composition of polymer solutions and adjusting electrospinning parameters (applied voltage, flow rate, tip-to-collector distance, temperature, environmental humidity), researchers have achieved fibres with different morphologies. Most of them show smooth surface and thus possess only primary structures [11], [81]: cylinder or ribbon-like shape, with or without beads. Only a few of them possess hierarchical structures [57], [283], [309]–[311], [285], [290], [292], [304]–[308], such as wrinkled surface, porous surface, hollow or porous cores, etc.
Hierarchical structures for electrospun fibres have been achieved by different methods, which can be divided into two classes: selective removal and direct method. The selective removal method involves adding another material into the solution and creates porosity by removing this material after electrospinning [283], [285], [309]–[311]. For instance, Han et al. removed most of poly(3-hydroxybutyrate-co-3-hydroxyvalerate) from electrospun polyetherimide/poly(3-hydroxybutyrate-co-3-hydroxyvalerate) (PEI/PHBV) fibres via thermal degradation [285]. PEI/PHBV fibres with different ratios (75/25, 50/50, 25/75, w/w) were first prepared by electrospinning PEI/PHBV in chloroform. The miscibility of the two polymers was characterised by DSC. With the increase of PHBV content from 0% to 75%, glass transition temperature of PEI decreased from 220 °C to 194 °C, and glass transition temperature of PHBV increased form below 0.7 °C to 2.3°C, indicating that the two polymers were partially miscible. Fibres with average pore size of 80 nm were produced after thermal treatment at 210 °C for 90 min for PEI/PHBV (75/25) due to the degradation of PHBV. Zhang et al. created porous PCL fibres by leaching out gelatine from electrospun PCL/gelatine fibres [301]. Though PCL and gelatine were immiscible, continuous fibres were formed, indicating that the two polymers could interpenetrate each

other during electrospinning. Since this method is time-consuming and likely to deform fibres during the removal of the second material, direct methods are commonly used. These methods can produce hierarchical porous fibres directly during electrospinning, as used in this PhD project. The literature review discussed in the next section focuses on the two mechanisms of the direct method: breath figure [290], [292], [307] and phase separation [57], [290], [292], [304]–[308], [312].

3.2.1.1. Breath figure

Environmental humidity and choice of solvent play important roles in the breath figure mechanism. During electrospinning, the evaporation of volatile solvents causes significant temperature drop in the jet, which results in water from atmosphere condensing on the fibre surface and leaving pores after water evaporation [290], [292], [307]. The pores usually have a circular shape and are present only on the surface of the fibres [79]**,** [292] (Figure *26*). Volatile solvents with poor water miscibility are usually preferred, such as chloroform [79], [313], dichloromethane (DCM) [79], [314] [315], and tetrahydrofuran (THF) [290] [297], [316], [317]. For instance, Huang et al. reported that, though chloroform and acetone are both volatile solvents, porous PLA could only be obtained by using chloroform as solvent due to its immiscibility with water [79]. Magelski et al. found that polymer hydrophobicity was also required for breath figure to take place [290]. When using chloroform as solvent, porosity could be formed on PMMA, a hydrophobic polymer, but could not on PEO, a hydrophilic polymer. Similarly, Homarbakhsh et al. discovered that when using DCM as solvent, porosity on the surface of PLA/PEO blend fibre decreased with increasing content of hydrophilic PEO [315]. Casper et al found that when electrospinning PS in THF, porosity only appeared on fibres when environmental humidity was above 30% [291]. Increasing environmental humidity from 31% to 72% increased diameter of pores from 60-190 nm to 50-280 nm.

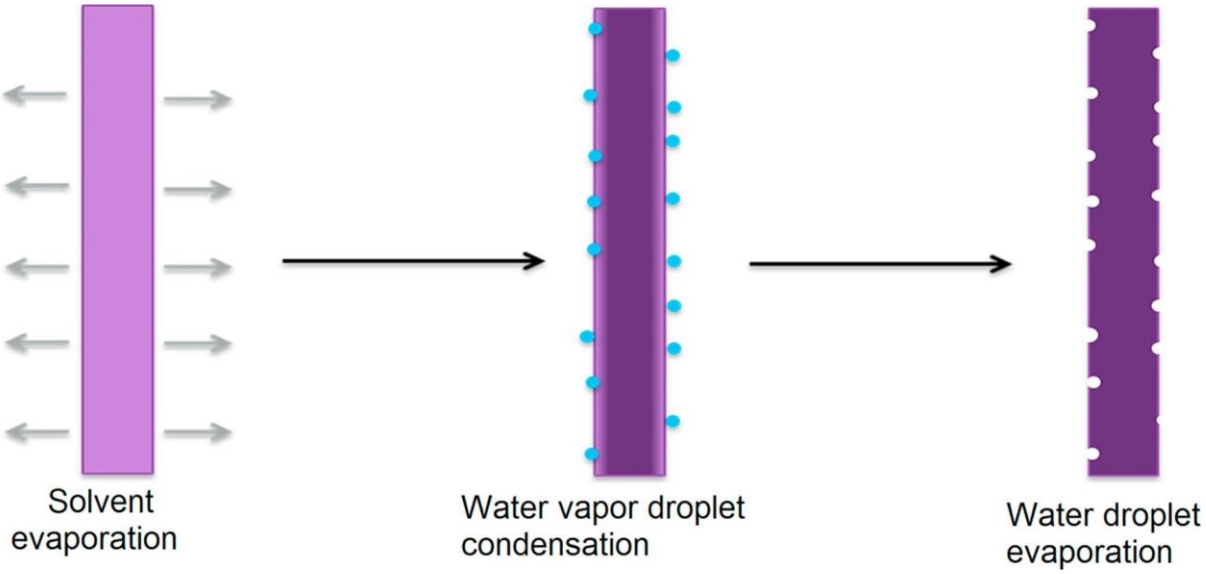

Figure 26. Schematic diagram of surface pore formation induced by breath figures mechanism [79].

3.2.1.2. Phase separation

Generally, there are two ways to induce phase separation in electrospun fibres: thermally-induced phase separation (TIPS) [290], [292], [307], [308], [312] and non-solvent induced separation (NIPS) [57], [304], [305], [307].

Figure 27 represents a typical phase diagram of TIPS in a binary system [318]. The solid line represents the binodal curve, above which the solution is homogeneous, and the dashed line represent the spinodal curve, below which is the unstable region. The region between binodal curve and spinodal curve is the metastable region, where polymer-rich phase and polymer-lean phase can co-exist [319]. Nucleation and growth take place in the metastable region, which leads to isolated circular pores. Spinodal decomposition takes place in the unstable region, which leads to interconnected pores [318].

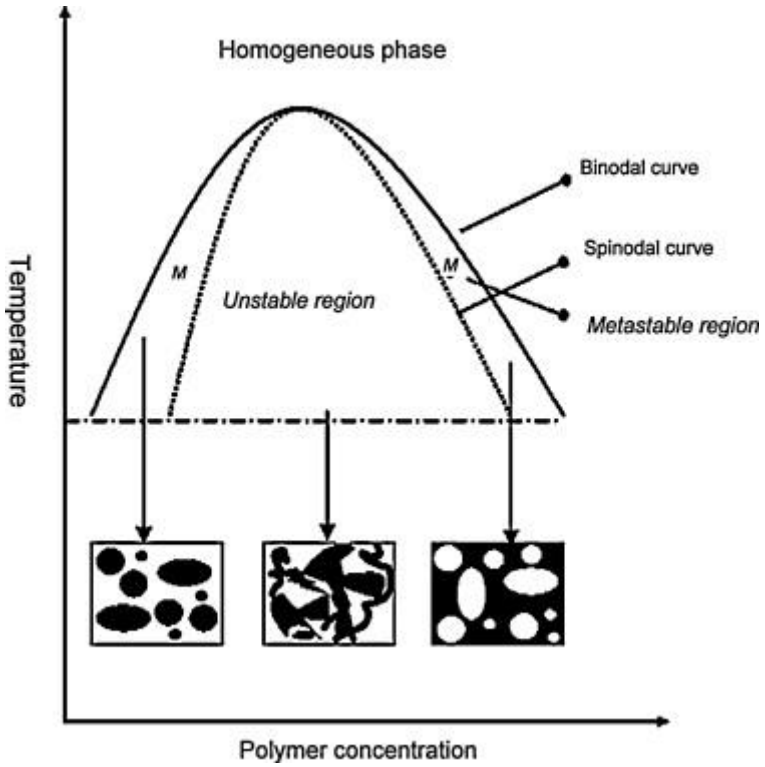

Figure 27. Schematic temperature–composition phase diagram of a binary polymer solution [318]**.**

TIPS in electrospinning usually involves solvents with high evaporation rate[290], [292], [307], [308], [312]. During electrospinning, rapid evaporation of solvent leads to the temperature drop of the jet, which causes the system to be thermodynamically unstable and thus phase separation can take place. Bognitzki et al. reported that [298] ellipse-shaped pores on electrospun PLA fibre surface were caused by a rapid thermal induced phase separation followed by a rapid solidification. The study found that when changing the solvent, DCM, with a less volatile solvent, chloroform, pores formation was reduced. Dayal et al. developed an electrospinning dynamic model to explain the formation of porous fibres [312]. Porous fibres would form when the polymer and solvent were partially miscible and electrospinning temperature was lower than the upper critical solution temperature (UCST) of the system. UCST is the maximum point of the spinodal and binodal curves in phase diagrams [318]. A simulation was carried out based on the theoretical model to test effect of different temperatures on porosity formation, see Figure 28. With the increase of temperature, the size of the phase-separation region got smaller, see Figure 28 (a). Higher temperature led to faster solvent evaporation, which caused rapid rise of polymer concentration

and faster crossing in phase diagram, resulting in single phase texture-less fibres to be produced, see Figure 28 (b).

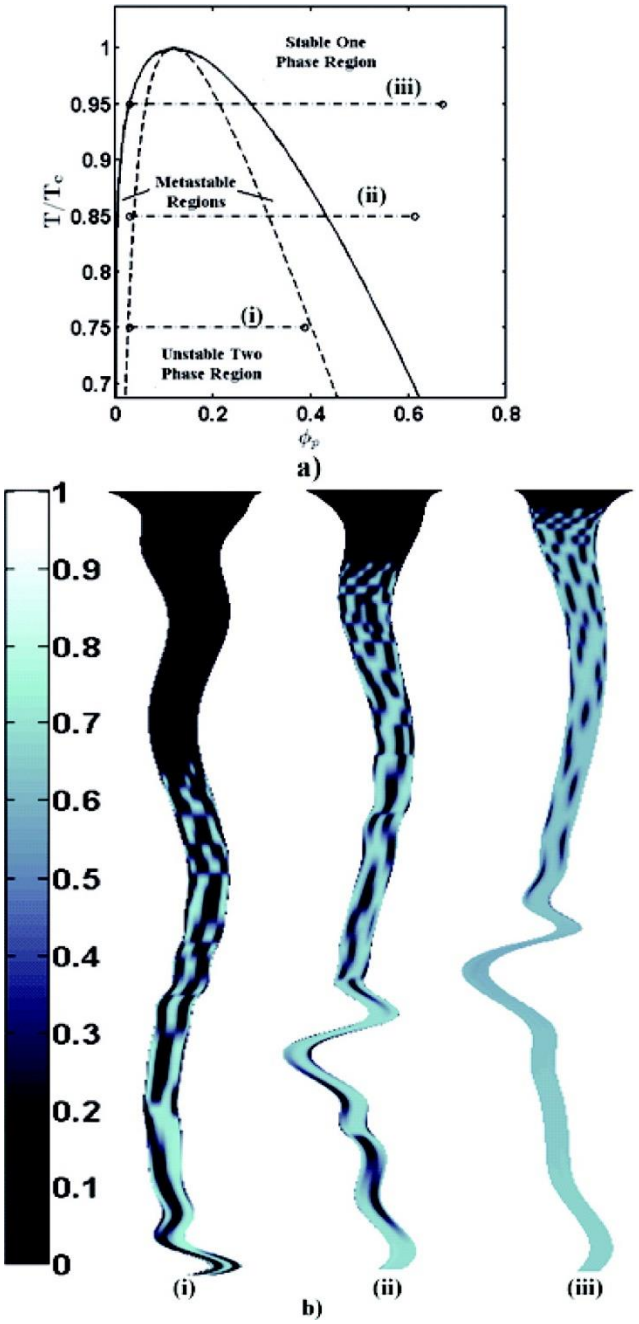

Figure 28 Simulated electrospun fiber from the spinneret (top) to the collector plate (bottom) with reference to the phase diagram (a) where (i), (ii) and (iii) represent the concentration sweeps at different temperatures. (b) Electrospun fibre in which dark regions represent solvent-rich regions and bright regions represent polymer rich regions. The pores are smaller in diameter as the temperature increases [312]**.**

Alternatively, Thermal induced phase separation can also take place when environmental temperature rapidly changes. McCann et al. demonstrated it using a bath of liquid nitrogen as collector and they produced electrospun PS fibres with smooth surface but porous internal structure [308]. Internal porosity was explained by TIPS and smooth surface was explained by sufficient tip-to-collector distance, which allowed solvent to evaporate from the surface. Notably, when PCL was used, porosity could also be found on the surface, which indicated porosity could be affected by crystallinity of polymer. Ye et al. induced TIPS to create isotactic polypropylene (iPP) and poly(vinylidene fluoride) (PVDF) porous fibres by high temperature electrospinning [320]. The syringe/needle system was heated by electric heating wires and maintained at 200 ^{o}C. High boiling point solvents were used in the study and an ionic liquid was added to improve conductivity. Porosity of fibres could be controlled by varying ionic liquid content, which affected polymer crystallisation, and co-diluent content, which determined the phase separation mechanism either solid-liquid or liquid-liquid. NIPS usually takes place in a multi-solvent system where a non-solvent is added. During electrospinning, the non-solvent causes phase separation and becomes part of polymer-lean phase, which later becomes pores, see Figure 29 [79]**.** Rezabeigi et al. demonstrated electrospun porous PLA fibres using PLA/DCM/hexane system [321]. Liquid-liquid phase separation was induced by the non-solvent hexane. Interestingly, the study also found that phase separation could increase crystallinity of PLA in polymer-rich phase, which resulted in difficulty in electrospinning. Qi et al. used butanol as non-solvent and DCM as solvent to successfully produced PLA porous fibres [322]. The study stated that a faster vaporising rate of solvent than non-solvent favoured phase separation to take place. Moreover, change of solvent/non-solvent ratio and applied voltage resulted in different pore morphology. Water could also be used as non-solvent. Ye et al. produced porous polyacrylonitrile (PAN) fibres using PAN/DMF/water system [323]. Ye et al. agreed with other studies that during the electrospinning, the system travelled from single phase region to unstable region in a phase diagram, resulting in spinodal decomposition and produced interconnected pores.

Notably, several studies have reported that when water-miscible solvents have been used, the system absorbed water from the atmosphere during solvent evaporation. Water played the role of non-solvent, which also caused phase separation. This is also called vapour-induced phase separation (VIPS) [305], [307], [79], [324] (Figure 30). Demir electrospun PS/DMF solution under 35% relative humidity and produced fibres with smooth surface and high internal porosity [324]. A “glass skin model” together with VIPS were used to explain this morphology. The study stated that polymer molecules were concentrated at the edge of jet which led to a fast solidification of the fibre surface forming a “glass skin”. Atmospheric moisture and DMF formed solvent-rich phase in the core which later became internal porosity. Similar results were obtained by Zheng et al. for PS/DMF electrospun under different humidity [297]. When the polymer concentration was lower than 20% w/v, polymer beads were formed. By increasing the humidity (from 20% to 40%), the roughness and porosity of the beads increased. When polymer concentration was fixed at 25% w/v, beadless fibres with smooth skin and internal porosity were formed at high humidity (60%). The study agreed that VIPS was the mechanism for porosity formation. Diffusing of water vapour into the jet caused the system to separate into a continuous polymer rich phase and dispersed polymer-lean droplets. The reason why porosity was observed on beads surface and only observed inside the fibres was explained by the difference of surface tension of solution and stretching process during electrospinning.

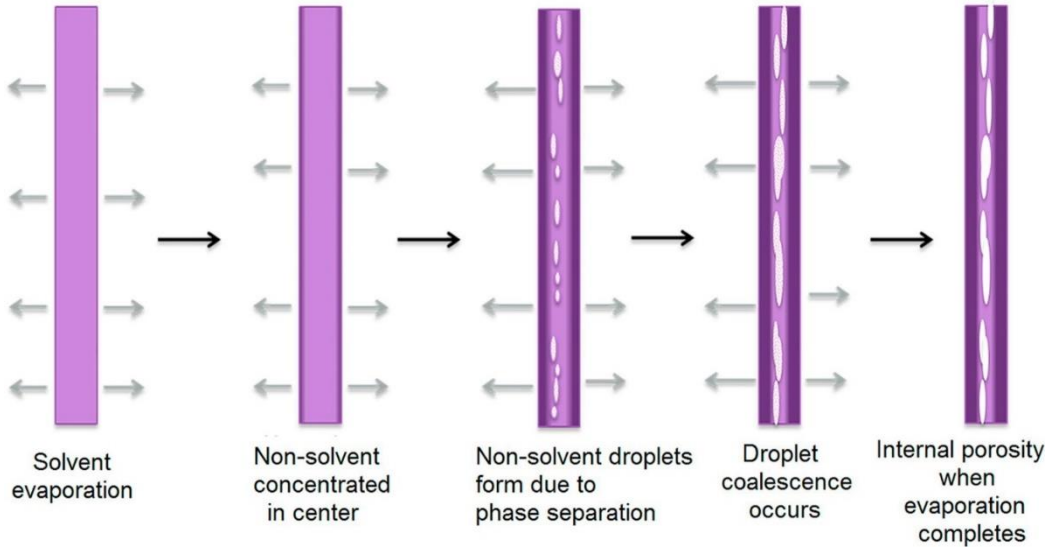

Figure 29. Schematic diagram of internal porosity induced by non-solvent induced phase separation (NIPS) [79]**.**

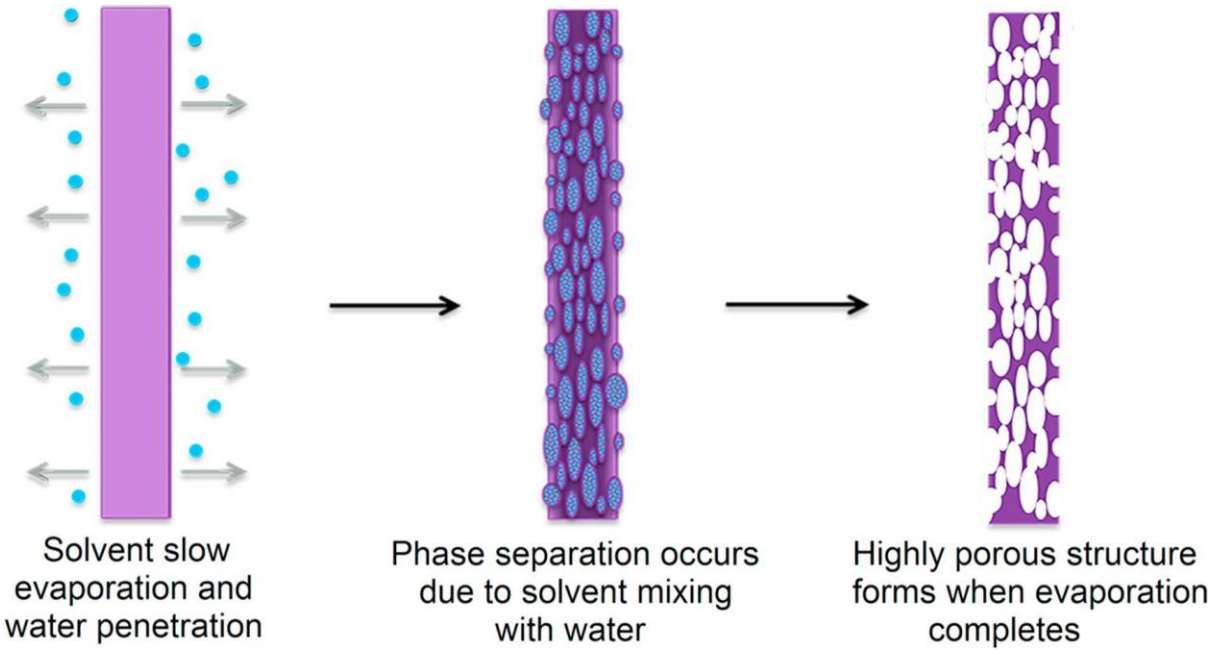

Figure 30. Schematic diagram of porosity induced by a vapour induced phase separation (VIPS) mechanism [79]**.**

Spinodal decomposition (SD) and/or nucleation and growth (NG) are also involved in non-solvent induced phase separation [296], [312], [321], [325], [326]. In a phase diagram of a ternary system, there are three regions: one phase region, metastable region, and unstable region, divided by the binodal and spinodal curves [296], [325], [326] (Figure 31). During the electrospinning, due to the solvent evaporation, water vapour and temperature change, the system could change from one region to another. Li et al. demonstrated the electrospinning of PMMA fibres with hierarchical structures from different solvent systems. They found that when the system passed the binodal curve and entered the metastable region, nucleation and growth took place, resulting in isolated circular pores. When the system passed the spinodal curve and entered the unstable region, spinodal decomposition took place, resulting in wrinkled surface and porous core [49]. The study showed that when acetone, THF and DMF were used as solvents, the features of PMMA fibres indicated a SD mechanism. When chloroform and DMF/DCM were used as solvents they showed features of the NG mechanism. In Qi et al.'s study, for a PLA/DCM/1-butanol system, with a low applied voltage, spinodal decomposition took place, while with a high ap-

plied voltage, nucleation and growth took place [322]. The study suggested that difference in applied voltage could cause difference in evaporation rate of both solvent and non-solvent, which led to the change in composition of system.

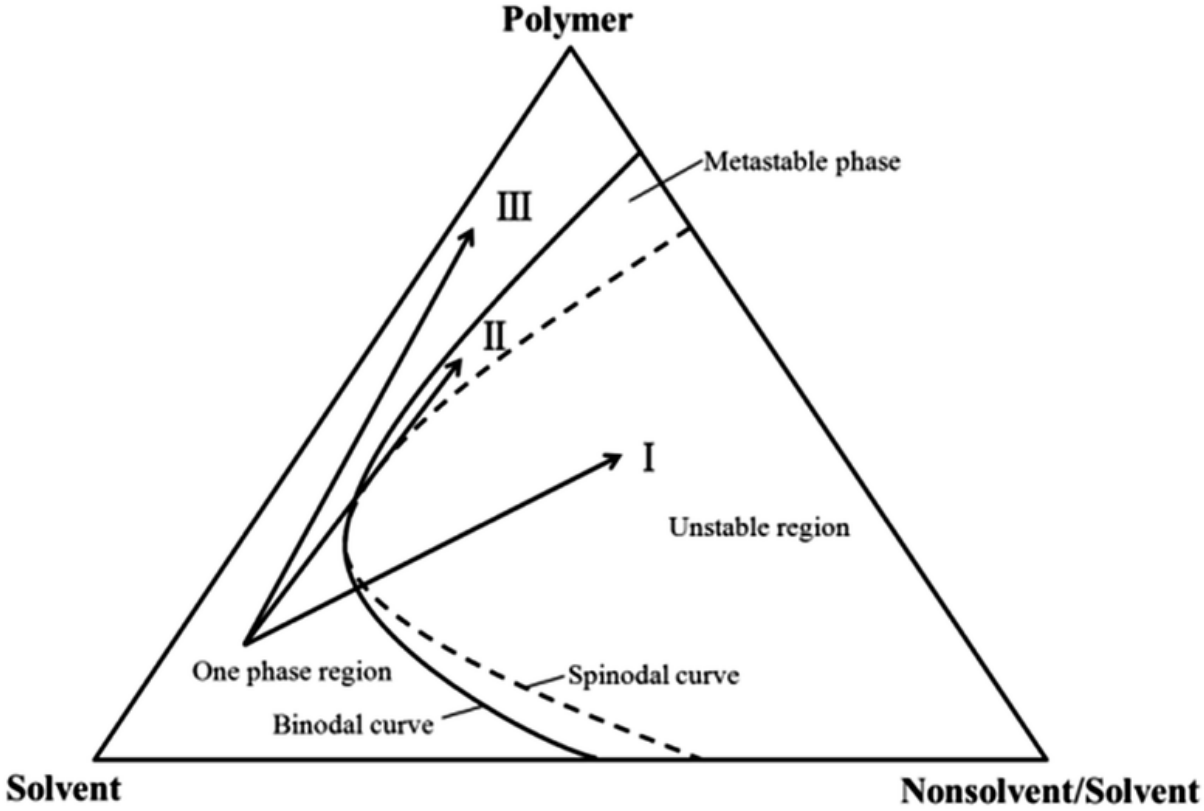

Figure 31. Ternary phase diagram for polymer solution system [296]**.**

Porous fibres can be formed by a combination of several mechanisms. For instance, Li et al used water bath as collector to induce thermal-nonsolvent phase separation, resulting in highly porous PLA fibres [327]. Zheng et al. suggested that when the electrospinning of PS in THF/DMF was conducted under high humidity environment, breath figure and VIPS both took place [297]. Honarbakhsh et al. concluded that when using DMF as solvent, electrospun PLA fibres with both elliptical pores on surface and internal porosity resulted from both breath figure and TIPS [315]. Casper et al. carefully controlled humidity level when electrospun PS with THF solvent [307]. Smooth fibres were produced up to 25% humidity. Surface with circular shaped pores were formed with the raising of humidity. When humidity was higher than 50%,

large irregular shaped pores started to appear. Both breath figure and phase contributed to pores formation in this case. With solvent evaporation, temperature of the jet decreased dramatically, which caused water vapour condensed on the surface of the fibre, leaving imprints. Additionally, water vapour caused thermodynamic instability, which led to phase separation and resulted in interior fibre porosity.

3.2.2. Hierarchical electrospun PCL fibres

This chapter discussed the production of electrospun PECA/PCL fibres with hierarchical structure. Previously, hierarchical PCL fibres have been produced using phase separation [328] [329] [64], leaching treatment [301], water bath [330], and co-axial electrospinning [250]. Huang et al. used chloroform as solvent and different non-solvents for PCL and found that the surface morphology of electrospun microspheres and fibres could be controlled by polymer concentration as well as non-solvent properties [329]. When PCL was dissolved in chloroform, both microspheres and fibres possessed smooth surface, indicating no TIPS or breath figure taking place during electrospinning. With the adding of ethanol, methanol, hexanol or DMF as non-solvents, fibres with rough or porous surface were produced. The study suggested that porosity of fibres was affected by both weight ratio between non-solvent and polymer (W_R), and non-solvent properties. High W_R could cause coalescence of the non-solvent during NIPS, which led to lower porosity. Interestingly, when propanediol was used as non-solvent, contradictory results were observed. With increasing W_R, fibre surface went from smooth to rough and highly porous. In this case, VIPS took place instead of NIPS due to the high viscosity and slow evaporation rate of propanediol. Katsogiannis et al. defined three requirements to produce porous PCL fibres using NIPS: appropriate good solvent, suitable good/non solvent ratio, suitable polymer concentration [64]. While using DMSO as non-solvent, among chloroform, DCM, THF and formic acid (FA), only chloroform could produce porous fibres. The fast evaporation rate of DCM and THF led to glass skin effect, and for FA, due to its similar evaporation rate with DMSO, it could not induce instability for phase separation. The study also found that different chloroform/DMSO ratios induced the following morphology transition: Bead-on-string→Porous fibres→Ribbon fibres→Porous bead-on string (Figure 32).

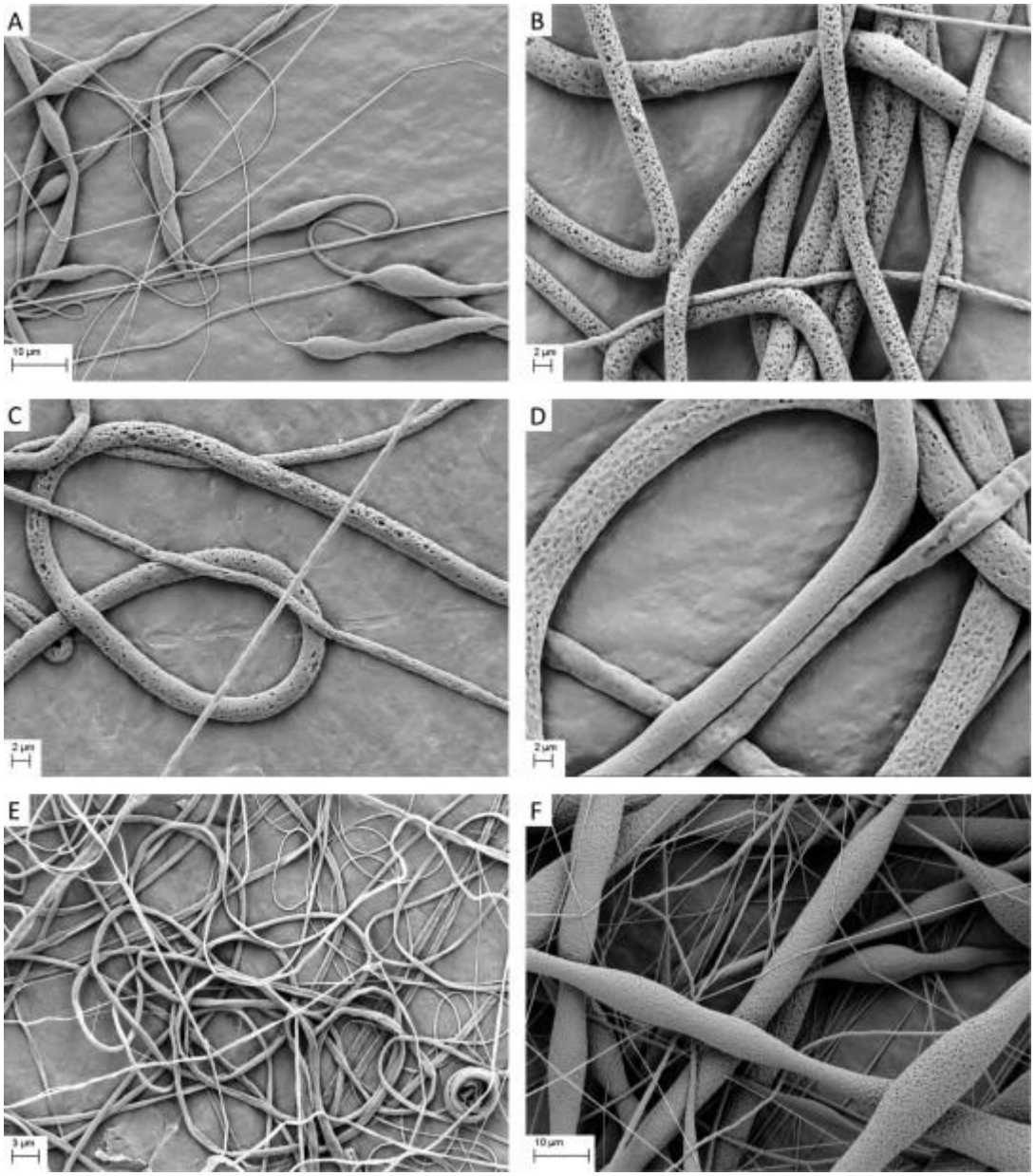

Figure 32.SEM pictures of the fibres produced by CF/DMSO solutions. The polymer concentration in the feed solution was 12.5% w/v in all cases and the concentration of good solvent in the good/poor solvent mixture was: (A) 100% v/v, (B) 90% v/v, (C) 80% v/v, (D) 70% v/v, (E) 60% v/v, and (F) 50% v/v [64]**.**

Pant et al. used a water bath as collector to induce porosity in PCL/methoxy poly(ethylene glycol) (MPEG) electrospun fibres [330]. While PCL/MPEG fibres collected without water bath showed smooth surface, fibres collected in the water bath showed a mixture of nano-sized and micro-sized irregular pores. In 25g of 10% w/v PCL solution, increasing MPEG content from 0.5 to 2.0 g increased pore size

and density due to the dissolution of MPEG in water. However, with a 4.0 g of MPEG, “rice-like” nanoparticles were formed on the fibre surface instead of pores. The study also found that blending MPEG with PCL decreased crystallinity and increased hydrophilicity of PCL, resulting in a better biocompatibility. Wu et al. produced magnetic nanoparticles and ketoconazole (KCZ) loaded hollow PCL by co-axial electrospinning using a solvent bath [250]. PCL and KCZ were dissolved in DCM first and Fe_3O_4 magnetic nanoparticles was dispersed in the solution. The resulting suspension was used as sheath liquid and dimethyl silicone oil was used as core liquid. The collected fibres were then immersed into secondary downstream selected solvent environment. The study found that using different downstream solvents and temperature could control the phase separation and produce different surface morphologies.

Due to the increased surface-to-volume ratio and biomimetic structure, hierarchical PCL fibres have showed potential for biomedical applications [331]. Buschle-Diller et al. reported using chloroform as solvent could produce PCL fibres with oval-shaped pores and PLA fibres with small circular shaped pores [332]. When blending PLA/PCL together, the bicomponent fibres shared similar morphology with PLA fibres. The release profile of antibiotics loaded in the three types of fibres (PLA, PCL, and PLA/PCL blend) was studied and PCL fibres was found to have a much faster release rate than PLA fibres. PLA/PCL fibres fell in between these two, indicating that the porosity of fibres played important role in the drug releasing profile. Jiang et al. believed porous fibres produced from PCL/chloroform/dimethyl sulfoxide (DMSO) was a result of both TIPS and NIPS [333]. After immersing these porous fibres in PCL/acetic acid/deionised water, “shish-kebab-structured” (SK) fibres could be formed by self-induced crystallisation (Figure 33). Both porous and SK structure showed better cell viability and proliferation compared with smooth PCL fibres, which could be applied for tissue regeneration.

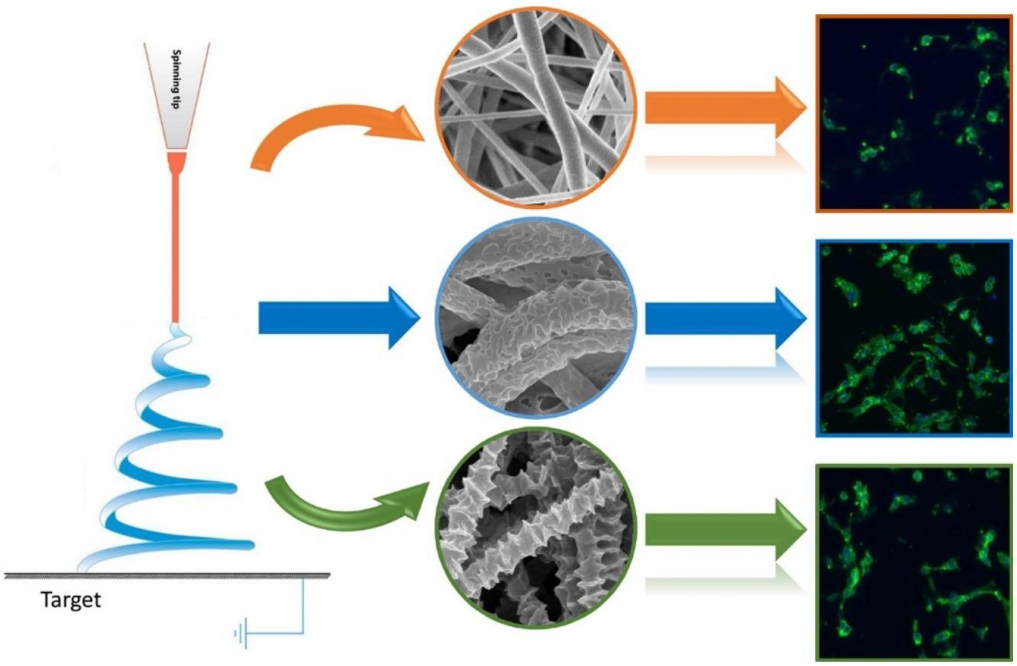

Figure 33 Smooth, porous, and "shish-kebab-structured" PCL fibres and their biocompatibility [333]**.**

3.2.3. Cyanoacrylate

Cyanoacrylates with their adhesion properties and biocompatibility have been used in wound closure and surgical applications [334]–[337]. However, traditional ways of depositing of cyanoacrylate, including injection, daub and spraying, are not able to produce continuous fibres and homogeneous mats, limiting their use for large-area complex wound [49], [338], [339]. Hence, there is a growing interest in the fabrication of cyanoacrylate-based fibres by electrospinning. Several studies have used different strategies for that purpose, such as *in-situ* electrospinning [338], [339], combination with another polymer [83], [340] and electrospinning after zwitterionic polymerisation [49].

Liu et al. demonstrated "solventless electrospinning" using only PMMA and ethyl-2-cyanoacrylate (ECA) monomers without solvents. ECA polymerised into poly-ethyl-2-cyanoacrylate (PECA) during electrospinning using water molecules (hydroxide ions) as initiator and terminator, mechanism showing in Figure 34. Increase in PMMA/ECA

ratio promoted the polymerisation of ECA and resulted in fibres with bigger diameter [340].

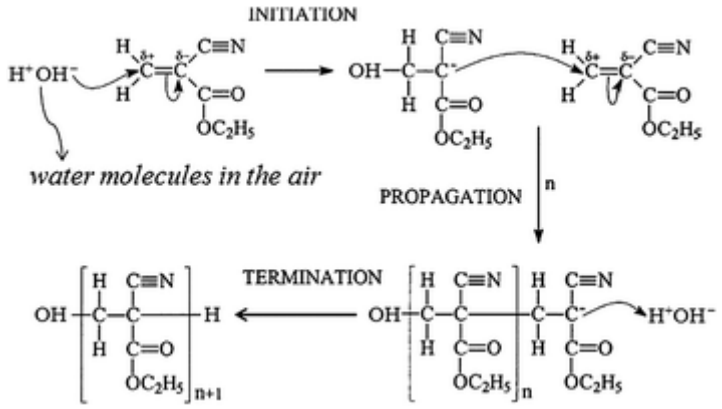

Figure 34.Curing mechanism of ethyl-2-cyanoacrylate(ECA) [340]**.**

Later, inspired by Liu's study, Jiang's group designed and demonstrated airflow-directed *in-situ* electrospinning device with an additional air pump to produce poly(N-octyl-2-cyanoacrylate) (POCA)/PMMA blend fibres (Figure 35) [338], [339]. Due to the good adhesion of OCA monomer, electrospun fibres could adhere on targeted tissues and soon polymerised into POCA and acted as a protective barrier. *In vivo* hemostasis of rat [338] and pig liver [339] proved that fibres possessed high strength and tissue bonding ability and could improve movement of cells to repair the injury sites. Romano et al. successfully electrospun POCA combined with polypropylene fumarate (PPF) using a more straightforward method [83]. PPF and POCA, which was firstly polymerised by mixing OCA and dimethylacetamide (DMAc), were dissolved in chloroform in ratio 3/7 (v/v) and then electrospun. Due to its anti-inflammatory properties, PPF worked not only as a structural component of the fibres but also as a bioactive agent. *In vivo* tests showed that POCA/PPF fibres promoted the healing of UVB-irradiated animal skin by reducing the cytokines production and neutrophils level.

Mele et al. first showed the successful electrospinning of PECA without adding other additives [49]. Different from Liu's method, ECA was polymerised in DMSO, initialised by the oxygen of the sulfoxide group and terminated by water molecule, mechanism showing in Figure 36. Macro-zwitterions of PECA was produced by this

polymerisation and could be easily electrospun. In the study, thermal treatment of the electrospun PECA fibres was used to form transparent and anti-staining films, which were able to promote the proliferation of myoblast cells.

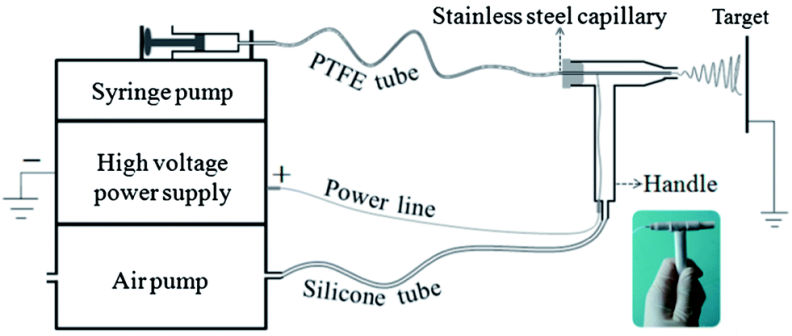

Figure 35.Schematic illustration of the airflow-directed in-situ electrospinning device. The inset is a camera picture showing the home-made handle and spinning head [339]**.**

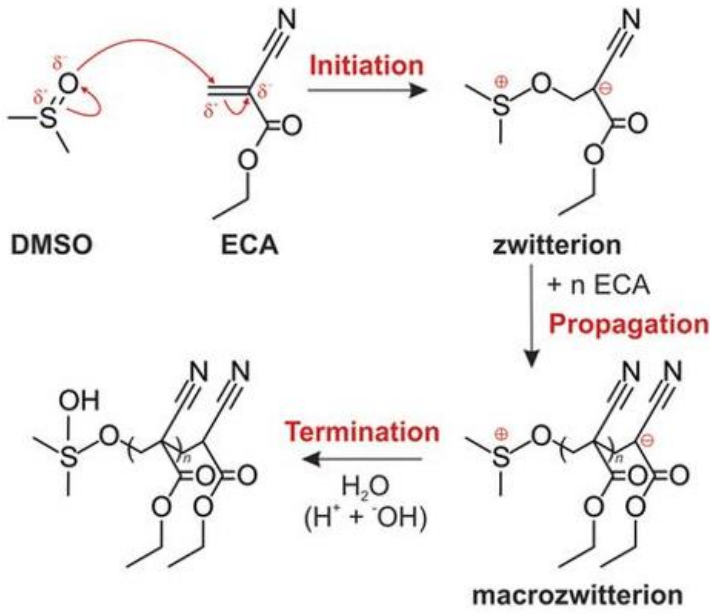

Figure 36 Proposed scheme of the reactions occurring for the zwitterionic polymerisation of ECA in DMSO (initiation, propagation and termination). For the termination reaction, the proton and hydroxide transfer from water molecules is shown [49]**.**

However, none of previous papers has developed cyanoacrylate-based hierarchical structures. In this PhD project, novel structured microfibres were produced by electrospinning PCL and PECA blends. PECA was previously polymerised using the same method developed in 2015 [49]. Two kinds of pores were found on a single fibre: near-circular shaped pores and elongated shaped pores. A dual phase separation mechanism was proposed for the pore formation. This structure further increased fibres' surface to volume ratio, which gives them a potential application in drug delivery and tissue engineering. The experimental procedures and the results are discussed in the next sections and they have been published in paper [53].

3.3. Experimental methods

3.3.1. Electrospinning process

All materials were purchased from Sigma Aldrich and used as received without further purification. Electrospinning solution was prepared by dissolving PECA (medium viscosity) in acetone (10% v/v) and PCL (80,000 g/mol) in chloroform (10% w/v). PECA was first prepared by mixing ethyl cyanoacrylate and DMSO at 1:1 ratio [49]. PECA/acetone and PCL/chloroform solutions were then mixed together at 1:1, 2:1, and 4:1 vol ratio and diluted in acetonitrile to achieve a 7% w/v mixture. The composition of polymers and solvents in each system is summarised in Table 2. All solutions/mixtures were then electrospun by keeping the tip-to-collector distance fixed at 15 cm, solution injection rate between 2 and 3 mL/hour (pump system PHD ULTRA, Harvard Apparatus), needle gauge of 21, and applied voltage between 10 and 12 kV, summarised in Table 3. The electrospinning process was conducted at room temperature, using a Linari srl. electrospinning system.

Table 2 Volume ratio of chloroform, acetone and acetonitrile in different systems.

PECA/PCL ratio (w/w)	Polymer concentration(w/v)	Chloroform concentration (v/v)	Acetone concentration (v/v)	Acetonitrile concentration (v/v)
4/1	5%	10.0%	40.0%	50.0%
	7%	14.0%	56.0%	30.0%
2/1	5%	16.7%	33.3%	50.0%
	7%	23.3%	46.7%	30.0%
1/1	5%	25.0%	25.0%	50.0%
	7%	35.0%	35.0%	30.0%

Table 3 Flow rate and applied voltage for three types of fibres.

Materials	Flow rate (ml/h)	Applied Voltage (kV)
PECA-PCL	3	12
PECA in all solvent systems	2	10
PCL in all solvents systems	2	12

3.3.2. Characterisations

The morphology of the electrospun fibres (surface and cross section) was observed using a scanning electron microscope (SEM), with a field emission gun system LEO1530VP. A gold/palladium coating was deposited onto the fibrous mats before imaging, using an Emitech SC7640 sputter coater (90 s sputter time). The fibres size, the distribution and alignment of the micro- and nanostructures presented onto the fibres surface were measured using ImageJ software (US National Institutes of Health). For each sample, ten SEM micrographs with different magnification were analysed and 50 measurements were used to perform statistical analysis. Attenuated total reflection-fourier transform infrared (ATR-FTIR, IRTracer-100, Shimadzu) was conducted to detect the chemical composition of PECA/PCL fibres. All spectra with 4000-600 cm^{-1} were recorded.

Differential scanning calorimetry (DSC Q200, TA Instruments Calorimetric Analyser) in a nitrogen atmos-phere with a flow rate of 50 ml/min was used to test the thermal properties of PCL, PECA and PECA/PCL fibres. Approximately 9 mg of each type of mat was sealed in an aluminium pan and heated from 0 to 200 °C at 10 °C/min. At least three samples were tested to obtain average.

3.4. Results and discussions

3.4.1. Morphology of fibres from different PCL/PECA ratios

Figure 37 to Figure 39 show the SEM images of the fibres produced from different PECA/PCL ratios and polymer concentrations. At 4/1 ratio, bead-on-string morphology was observed at low polymer concentration (5% w/v) [341]. When the concentration was increased to 7 w/v%, the beads disappeared, and uniform fibres were formed with wrinkled surface. At 2/1 ratio, the increased polymer concentration resulted in improved uniformity. Notably, dual porosity fibres were produced from both concentrations, with both near circular shaped pores and elongated grooves (this morphology will be discussed in further detail in Section 3.4.2). At 1/1 ratio, fibres produced from 5 w/v% concentration showed a morphology similar to that of fibres produced at 2/1 ratio. By increasing the polymer concentration to 7 w/v%, beads and fibres were both produced.

It has been widely agreed that beaded fibres are formed when the solution viscosity, which is related to polymer chain entanglement, is lower than a critical value [127], [342]. With the increasing of viscosity, the primary structure goes through: spherical beads→spindle shaped beads on string→fibres [343]. This was true for samples with PECA/PCL ratio at 4/1 and 2/1. Curiously, with ratio at 1/1, increasing polymer concentration from 5 w/v % to 7 w/v % led to beads formation. Fibres produced from 7 w/v% still possessed near circular shaped pores but elongated grooves could not be observed. Since the two types of porosity was associated with either PECA-rich or PCL-rich domain, as explained in section 3.4.3, a possible explanation could be that severe phase separation causing PCL and PECA to be formed independently.

As reviewed in literature review, secondary structures of electrospun fibres are results from breath figure, phase separation or a combination of both. In this case, breath figure was excluded since the porosity was neither shallow nor regular shaped. Though hierarchical porous electrospun fibres formed by phase separation have been demonstrated by many studies, none of them have produced nor discussed the formation of dual porosity on a single fibre. Hence, the 2/1 ratio was chosen for further study.

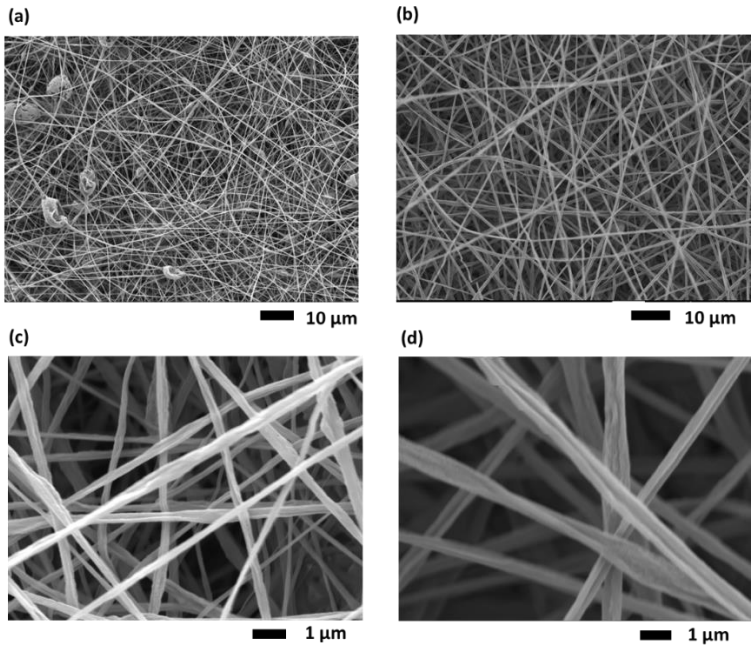

Figure 37.SEM images of fibres electrospun from PECA/PCL with ratio 4/1. Different polymer concentrations were selected: (a) and (c): 5% w/v; (b) and (d) 7% w/v.

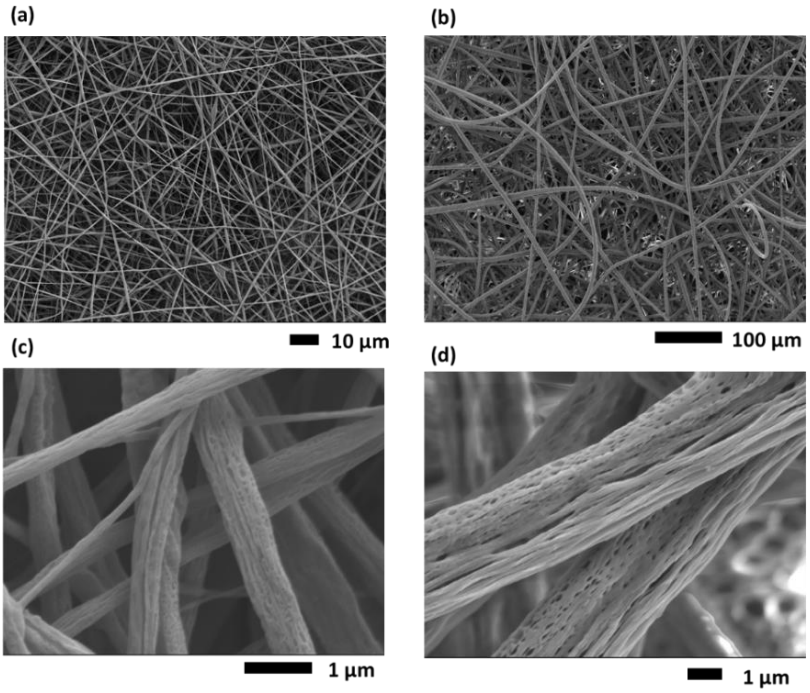

Figure 38.SEM images of fibres electrospun from PECA/PCL with ratio 2/1. Different polymer concentrations were selected: (a) and (c): 5% w/v; (b) and (d) 7% w/v.

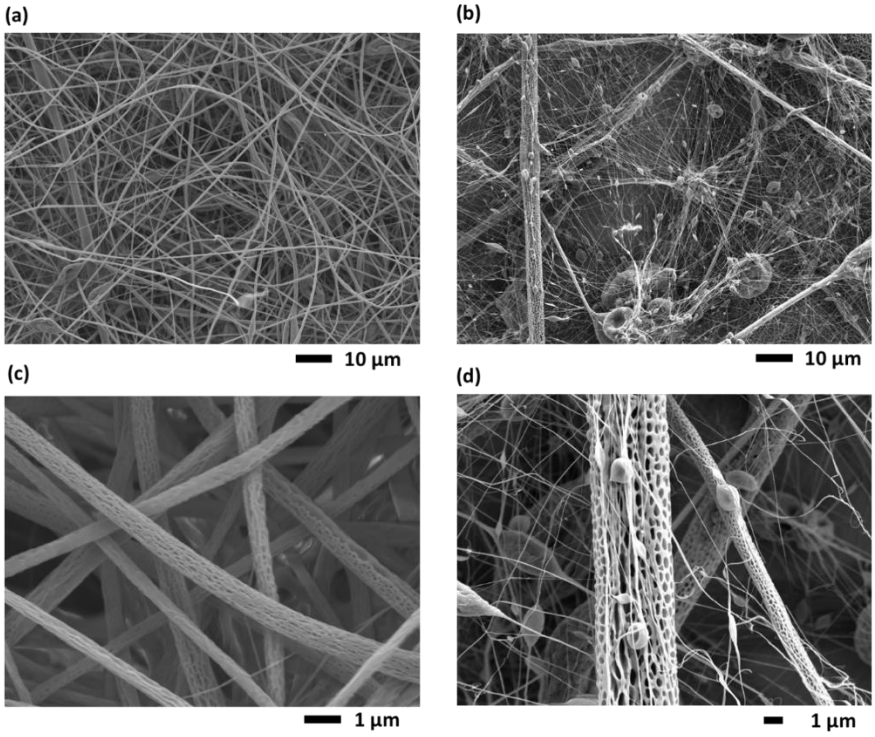

Figure 39 SEM images of fibres electrospun from PECA/PCL with ratio 1/1. Different polymer concentrations were selected: (a) and (c): 5 w/v%; (b) and (d) 7 w/v%.

3.4.2. Morphology analysis on 2/1 PECA/PCL hierarchical dual porosity fibres

The SEM images of Figure 40 a–c show that the resulting 2/1 PECA/PCL fibres were characterised by an average diameter of (4.5 ± 1.2) μm and, more interestingly, by two different types of porosity. Each single PECA/PCL fibre had one region with elongated and parallel grooves and one region with near-circular shaped **pores (**Figure 40 b and c**)**. Although several researchers have worked on the electrospinning of polymer blends [57], [283], [284], [285], [290], [292], [304], [307], [306], [308], [309], [312] no accounts have been reported so far on electrospun fibres with dual morphology. SEM investigations revealed a net separation between the two regions along the whole length of the PECA/PCL fibres. The fibre portion with circular-shaped pores (green area in the schematics of Figure 40d) had an average width (*a*) of (2.23 ± 0.30) μm, whereas the portion with elongated structures (orange area in Figure 40d) had an average width (*a'*) of (2.26 ± 0.30) μm. Therefore, the *a/a'* ratio was of (1.01 ± 0.30), indicating that half of each fibre was formed by pores and the other half by parallel micro-features. In particular, as shown in Figure 40e, the majority of the fibres population (60.5%) had *a/a'* values between 0.8 and 1.1; whereas *a/a'* was in the range of 0.5–0.8 and 1.1–1.6 for 15.8% and 23.7% of the fibres produced, respectively. Furthermore, both pores and grooves exhibited a degree of alignment to the main axis of the fibre. The polar diagram in Figure 40f (green symbols) shows that the angle (θ) formed by the main axis of the fibre and the main axis of the near-circular shape pore was in the range of 0–34°: 48% of the values were between 1° and 7° (included), and 24% between 7° (excluded) and 14°. The statistical analysis of θ values can be described by a broad bell curve centred at 3.9° with a variance of 8.4°. On the contrary, the angle (θ') formed by the main axis of the fibre and the main axis of the elongated structures (orange symbols in Figure 40f) ranged between 0 and 14°, with most of the values (90%) between 0° and 7°. The statistical distribution of the values had a mean of 3.0° and a variance of 2.1°. This denotes that the grooves were more aligned to the fibre direction than the pores. Alignment of both grooves and pores can be associated to the stretching of the polymer filaments during electrospinning, as previously reported in other studies, [57], [304], [312].

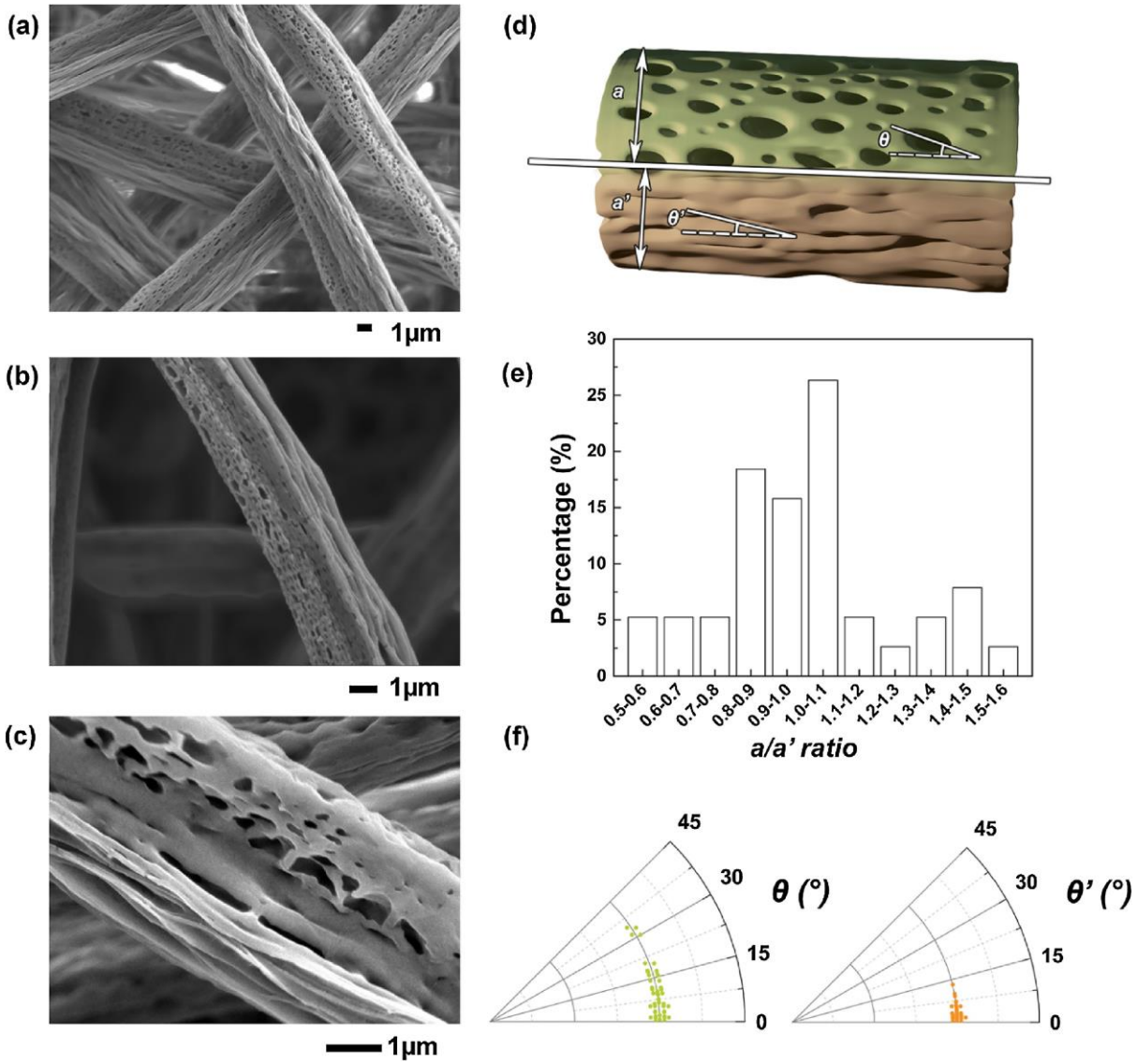

Figure 40. (a), (b) and (c) SEM images of electrospun PECA/PCL fibres at different magnifications. (d) Schematic diagram of one single fibre with dual porosity, where *a* is the size of the region with circular pores, *a'* is the size of the region with elongated structures, *θ* is the angle formed by the main axis of the fibres and the direction of the main diameter of the pores, and *θ'* is the angle formed by the main axis of the fibres and the main direction of the structures. (e) Statistical distribution of *a/a'* ratio. (f) Polar diagrams of *θ* (green symbols) and *θ '*(orange symbols). Data were obtained by analysing 50 structures for each shape (circular pores and grooves). Figure has been published [53]**.**

The formation of PECA/PCL fibres with dual morphology was likely to be determined by phase separation before and during the electrospinning process. In order to investigate this further, we firstly analysed the role played by solvent properties (boiling point and surface tension). PECA and PCL were separately electrospun using different solvents and solvent combinations: acetone, chloroform, acetonitrile,

acetone/chloroform (2/1 vol ratio), acetone/acetonitrile (14/9 vol ratio), chloroform/acetonitrile (7/9 vol ratio), and acetone/chloroform/ acetonitrile (14/7/9 vol ratio). The polymer concentration was fixed at 7% w/v for all solutions to have a direct comparison with the PECA/PCL system. Solvent ratios of binary and ternary solvent systems were calculated based on the solvent ratio of the PECA/PCL blend: 10% w/v PCL in chloroform and 10% w/v PECA in acetone were mixed at 1:2 vol ratio, and then acetonitrile was added to achieve a 14/7/9 solvent volume ratio. Since PCL had a poor solubility in acetone and insolubility in acetonitrile, the following solvent systems were studied for PCL: chloroform, chloroform/acetone, chloroform/acetonitrile, and acetone/chloroform/acetonitrile. The SEM images of the PCL fibres produced revealed a beads-on-string morphology for all solvent combinations used (Figure 42). The low polymer concentration was responsible for the formation of electrospun mats with beads, being widely accepted that a minimal concentration is required for producing uniform and defect-free fibres [[304], [344], [345], [346]]. For chloroform solutions, we observed spindle-like shape beads with micro-features (Figure 42a), similarly to golf-ball shaped particles discussed for the electrospray of PCL-chloroform at 1–4% w/v concentrations [347]. At these low polymer concentrations, a small amount of solvent was still present on the beads surface when they hit the collector. The successive evaporation of the solvent caused the formation of particles with a rough surface [348]. The effect of different solvents on the morphology of PCL electrospun mats is well documented in the literature [13][349]. Katsogiannis et al. have reported on the electrospinning of PCL (molecular weight of 80,000 g/mol) from chloroform solutions with a polymer concentration of 12.5% w/v [64]. When chloroform was used as a single solvent, they observed the presence of elongated beads, possibly due to the low dielectric constant of chloroform. The addition of dimethyl sulfoxide resulted in well-defined fibres but also in an increased fibre diameter. As shown in Figure 42b and d, for the binary (acetone/chloroform) and the ternary system (acetone/acetonitrile/chloroform), the beads presented a spindle-like shape along with a more rounded shape. They were also characterised by surface roughness, which could be caused by non-solvent induced phase separation (being PCL poorly soluble in acetone and not soluble in acetonitrile) and high vapour pressure of acetone and chloroform [297][347][350]. Bosworth and Downes have investigated the use of acetone in PCL solutions with polymer concentration of 5.0, 7.5 and

10.0%w/v [351]. They observed that beads were formed for 7.5%w/v solutions, irrespective of the electrospinning parameters used (increase in applied voltage and needle-collector distance). The beading effect has been reported also by Nottelet et al. for PCL solutions of acetone/chloroform (3:7 vol ratio, 5–15% w/v polymer concentration) [344]. For acetonitrile/chloroform mixtures (Figure 42c), the beads appeared more rounded in shape and with a smooth surface, which could be due to the relatively high boiling point (81.6 °C) and high surface tension (29.2 mN/m at 20 °C) of acetonitrile.

We investigated the effect of different solvent combinations on the electrospinning of PECA. As shown in Figure 41. In the single solvent systems, only acetone was suitable as single solvent for PECA, thanks to its high conductivity, which caused stretching of polymer solution with the electric field [11]. The fibres produced were well-defined and defect-free with a ribbon-like shape and a wrinkled surface (Figure 41a), in agreement with a previous study [49]. The wrinkled surface is expected to be due to the high volatility of acetone, which causes buckling instability during electrospinning [296][297][57]. Interestingly, although PECA could not be electrospun from acetonitrile and chloroform as single solvents, fibres were formed from the binary acetonitrile/chloroform system (Figure 41f), even if spindle-like beads were present along the fibre length. The combination of the two solvents could assist the formation of fibres by changing the conductivity, viscosity and evaporation rate of the system [81]. A similar phenomenon was found in electrospun PCL fibres from formic acid/acetic acid system even though only beads were produced from single formic acid and acetic acid solvent [81]. Beads along fibres were also observed for acetone/acetonitrile solutions of PECA (Figure 41e). The electrospinning of PECA from acetone/chloroform led to the formation of only beads. The ternary system (Figure 41g), instead, allowed us to obtain well-defined flat fibres decorated with near-circular nanopores.

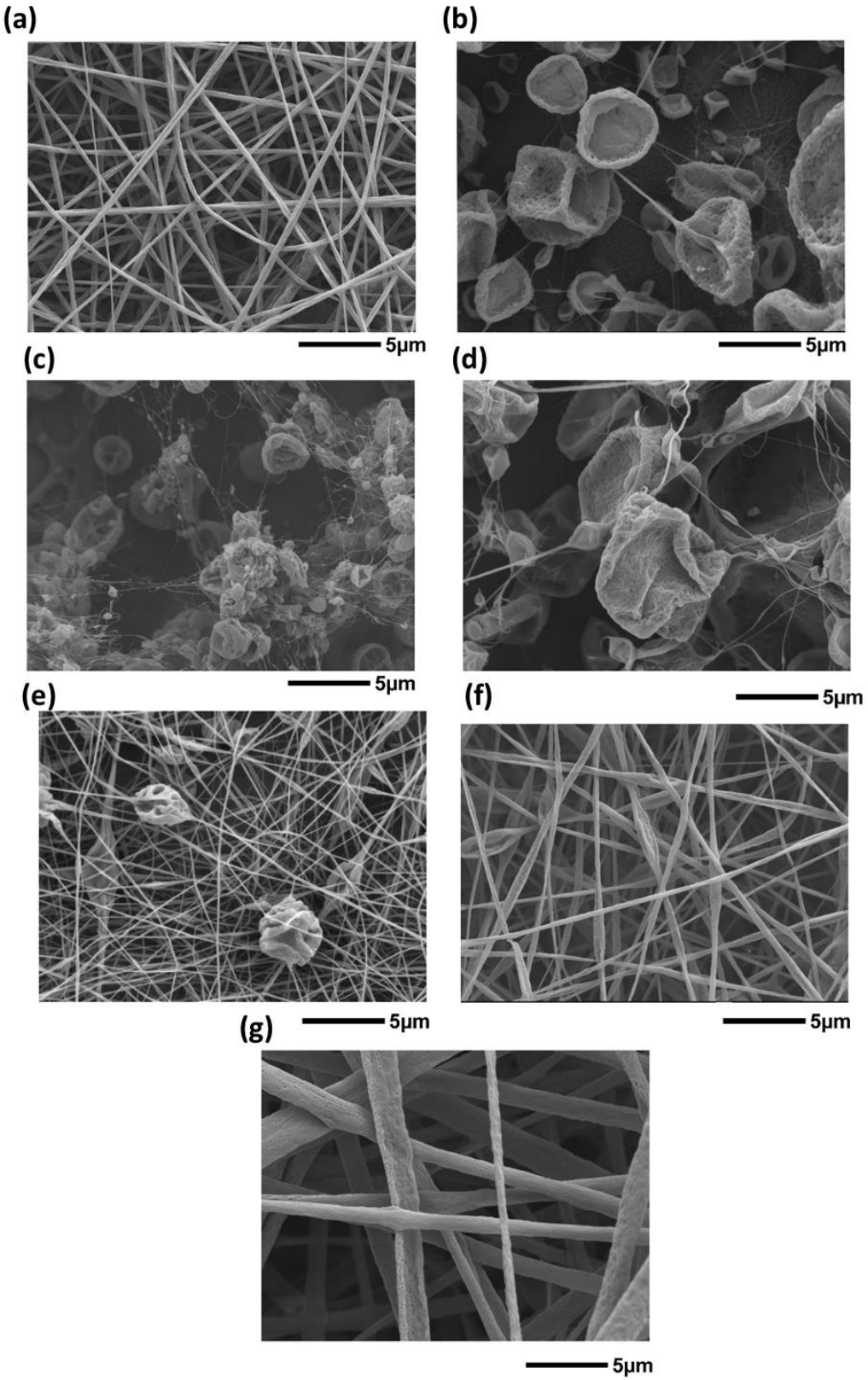

Figure 41.SEM images of PECA fibres electrospun from different solvent systems: (a) acetone, (b) chloroform, (c) acetonitrile, (d) acetonitrile/chloroform, (e) acetone/acetonitrile, (f) acetonitrile/chloroform, and (g) acetone/acetonitrile/chloroform. (a), (e), (f) and (g) have been published [53]**.**

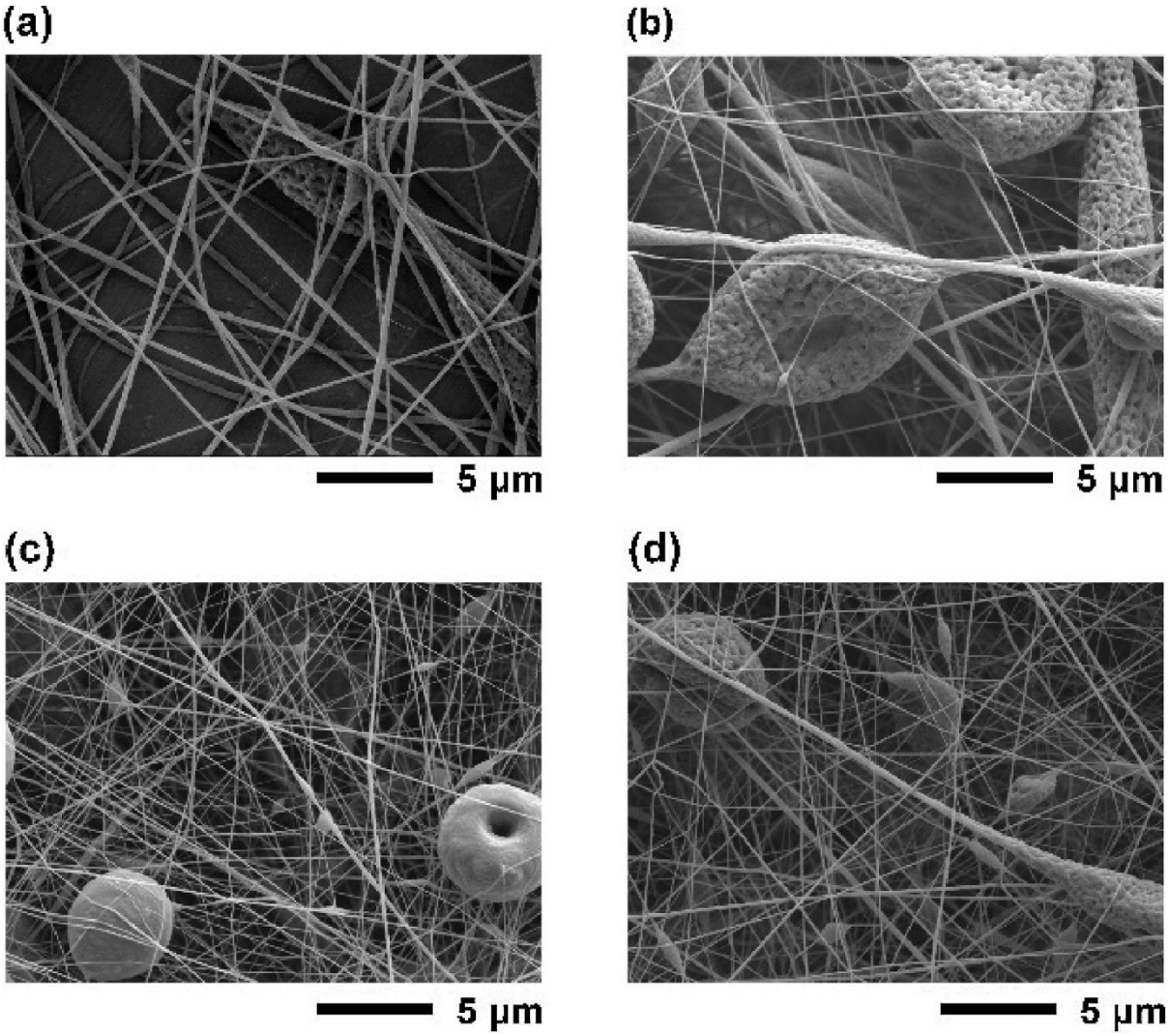

Figure 42. SEM images of PCL electrospun fibres formed using different solvent systems: (a) chloroform, (b) acetone/chloroform, (c) acetonitrile/chloroform, and (d) acetone/acetonitrile/chloroform. Figure has been published [53]**.**

The investigations conducted on the diverse solvent combinations revealed that chloroform and acetone were necessary to produce electrospun fibres with increased surface roughness, both for PCL and PECA. A direct comparison between PCL and PECA mats, separately electrospun from the ternary system, showed that PCL fibres were characterised by a rough surface (Figure 43a), whereas PECA fibres exhibited a wrinkled surface with circular nanopores (Figure 43b). The composite PECA/PCL fibres were much bigger in size than PCL and PECA fibres, and they consisted of elongated grooves and near-circular pores (Figure 43c). Investigations of the fibres cross section revealed that some PECA/PCL fibres possessed a cylindrical shape whereas others had a collapsed ribbon-like structure

(Figure 44a). In both cases, the porosity was not limited to the surface of the fibres, but cavities were visible throughout the fibre cross section. The fibres with a cylindrical shape were more likely to be hollow in some regions, as shown in Figure 44b. Li et al. have demonstrated the possibility to produce hollow electrospun fibres using a single nozzle instead of a coaxial needle (conventionally used to create core-shell and hollow fibres) [352]. The process was based on the electrospinning of phase-separated solutions of poly(vinyl pyrrolidone) (PVP), ethanol and tetraethyl orthosilicate (TEOS) in ethanol. During the fast ethanol evaporation, a concentration gradient was created along the fibre diameter: high concentration of TEOS, highly soluble in ethanol, in the core of the fibres; high concentration of PVP, immiscible with TEOS, at the edges of the fibres. After the complete evaporation of ethanol and TEOS, PVP nanotubes were formed. A similar approach has been reported also by Bazilevsky et al. for the fabrication of poly(methyl methacrylate) (PMMA)/polyacrylonitrile (PAN) core-shell fibres [353]. They electrospun emulsions of 100–200 μm-diameter drops of PMMA/DMF in a continuous phase of PAN/DMF. During electrospinning of the polymer blend, occasionally one PMMA/DMF drop (embedded in the PAN/DMF solution) reached the Taylor cone and a jet was formed at the drop edge. This resulted in core-shell fibres (PMMA core and PAN shell), whose structure was maintained until the drop was completely consumed.

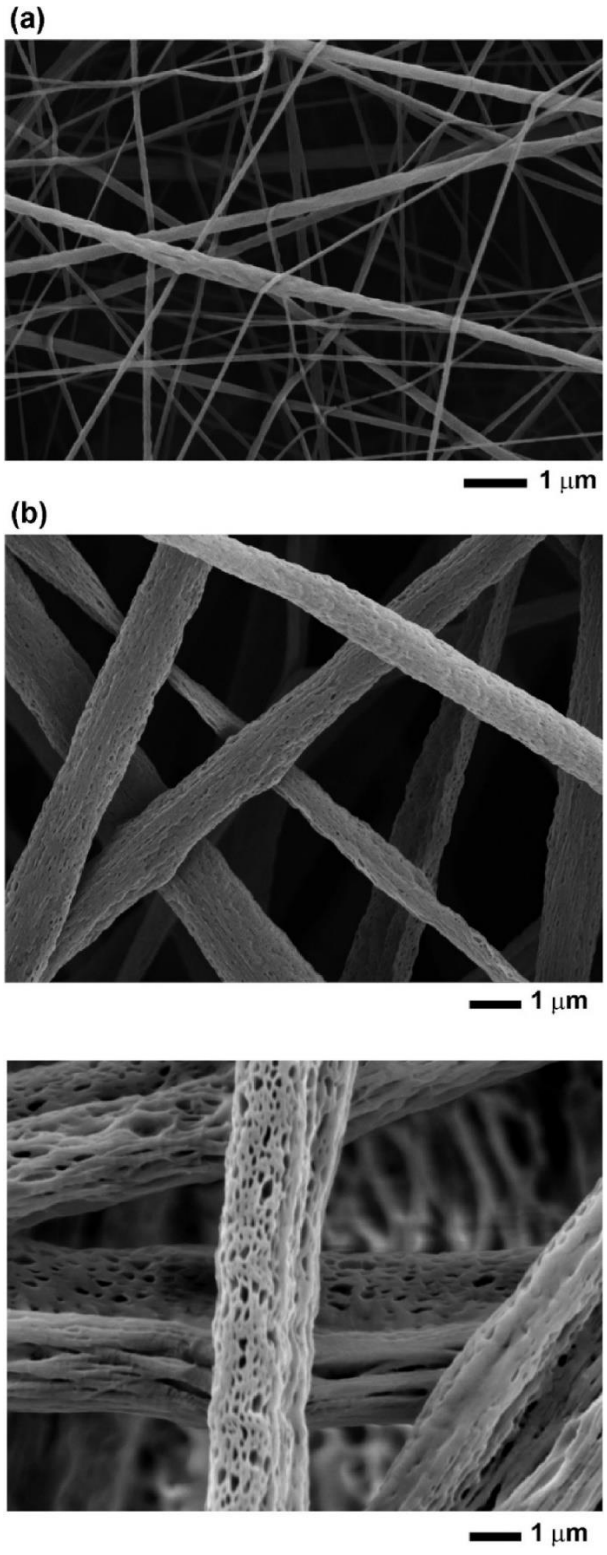

Figure 43.SEM images of (a) PCL (region of the mat without beads) and (b) PECA and (c) PECA-PCL fibres electrospun from the ternary system (acetone/acetonitrile/chloroform). Figure has been published [53]**.**

In our case, phase separation occurred in the PECA/PCL solution (ternary system) mainly between PECA-acetone and PCL-chloroform, due to the immiscibility of PECA and PCL (hydrophilic and hydrophobic polymer, respectively) [354], the limited solubility of PECA in chloroform and acetonitrile, the poor solubility of PCL in acetone and its insolubility in acetonitrile [349][355]. During fibre formation, solvents evaporation, mainly acetone and chloroform, determined a gradient in PECA and PCL concentration from the outer fibre surface (high concentration) to the inner core (low concentration) [352], [356], [357]. The acetonitrile concentration (being this a solvent with low evaporation rate) instead increased in the core of the fibres. Eventually, acetonitrile evaporated leading to fibres with a skin-core morphology.

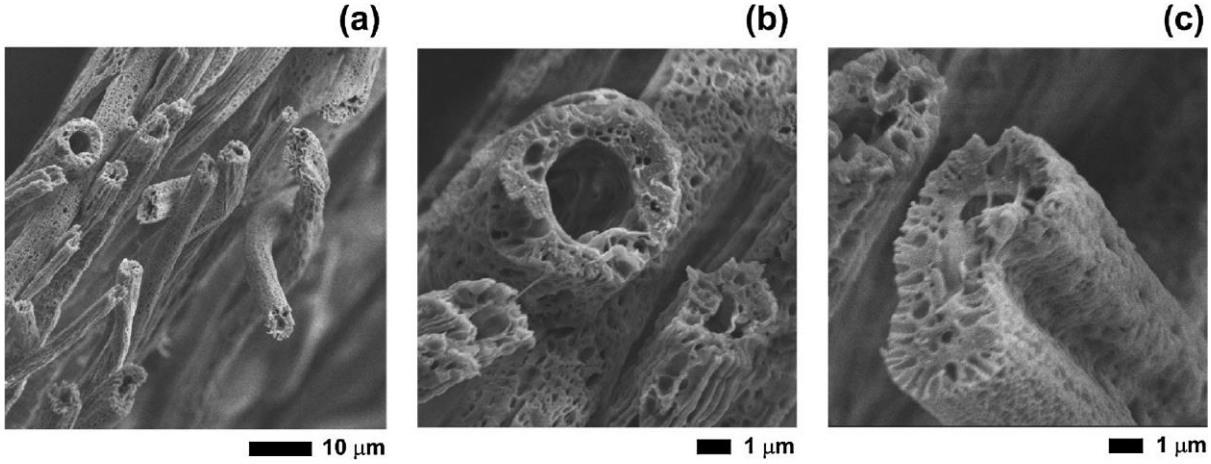

Figure 44.SEM images of the cross section of (a) PECA-PCL mats, (b) hollow PECA-PCL fibre with cylindrical shape, (c) PECA-PCL fibre with ribbon-like shape. Figure has been published [53]**.**

Some PECA/PCL fibres exhibited a ribbon-like structure with a peanut-shaped cross-section Figure 44c), due to the collapse of the outer porous shell. This morphology has been previously reported in the literature and it has been related to buckling instability: a thin skin layer is formed around the fibres due to solvent evaporation; when the solvent continues to evaporate from the core of the fibres, the skin collapses under atmospheric pressure and cohesive forces stick together the skin from the opposite sides of the fibre [296][358][359]. This phenomenon tends to be observed for fibres with large diameter (microfibres) due to the long drying time. The unique morphology of the skin layer of the PECA/PCL fibres (grooves and pores) can be described by considering phase separation events occurring during the electrospinning process, namely a complex interplay between nucleation and

growth and/or spinodal decomposition [321][296][312][325][326]. If a ternary system is considered, its phase diagram consists of three regions: one region where only one phase exists (good miscibility), one metastable region where phase separation proceeds via nucleation and growth, and one unstable region where phase separation proceeds via spinodal decomposition. The three regions are divided by the binodal and spinodal curves. When the system passes the binodal curve and enters the metastable region, nucleation and growth take place and the formation of isolated circular pores has been observed during electrospinning [321][322][325][326][360]. In case of spinodal decomposition (transition through the spinodal curve into the unstable region), instead, fibres with bi-continuous morphology and wrinkled/grooved surface have been produced [57][296][322][360] [361].

3.4.3. Dual-phase separation mechanism

We propose a dual phase separation mechanism for describing the hierarchical morphology and internal porosity of the PECA/PCL fibres, as schematically illustrated in Figure 45. When the two solutions, PCL in chloroform and PECA in acetone, were mixed together and then solubilised in acetonitrile, phase separation happened and caused the mixture to become partially cloudy. During electrospinning, polymer-lean nuclei appeared on one portion of the ejected filament and they were embedded into a polymer-rich matrix (left-hand side path of Figure 45). Due to the rapid solvent evaporation, the polymer-rich matrix solidified, and limited time was given to the nuclei to grow. Therefore, isolated pores emerged onto the fibre surface. They represent one of the morphologies (near circular pores) observed for the PECA/PCL fibres (coloured in green in the SEM image of the inset of Figure 45) and often associated with the nucleation and growth mechanism [322][360].

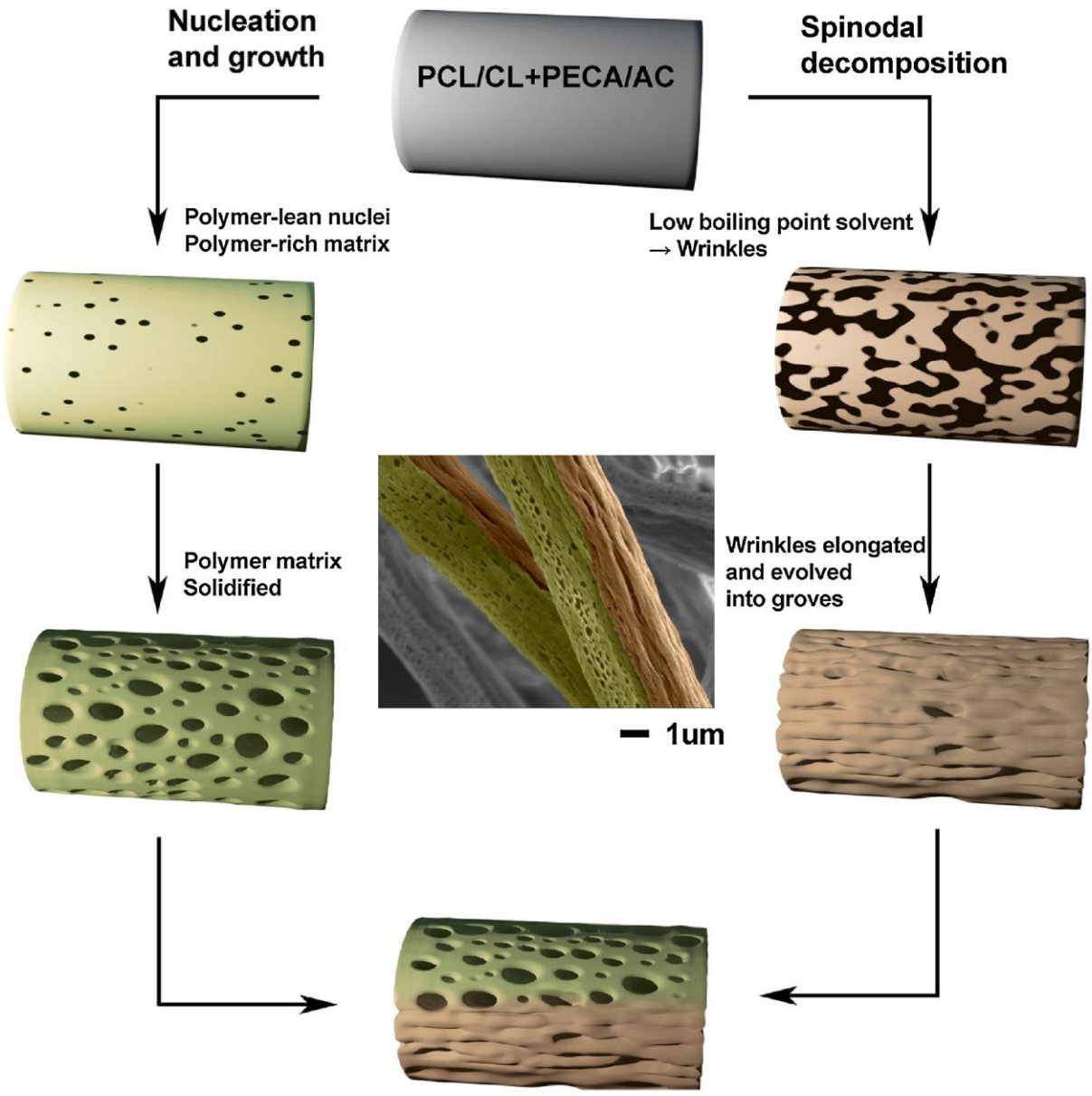

Figure 45.Schematic diagram (not in scale) of the dual phase separation process: green path shows nucleation and growth mechanism, while the orange path shows the spinodal decomposition mechanism. Central inset: Coloured SEM image of PECA-PCL fibres. Figure has been published [53]**.**

Simultaneously, polymer-rich phase and polymer-lean domains appeared also onto the other portion of the electrospun filament due to solvent evaporation and changes in polymer concentration (right-hand side path in Figure 45). After complete solvent evaporation, grooves aligned along the fibre direction were formed. Those microstructures are attributed to spinodal decomposition [296][360][343] combined with stretching of the polymer filament by electric force [361]. Electrospun fibres with a

grooved texture have been observed for polystyrene (PS) solutions of binary solvent systems with enough difference in evaporation rate between the two solvents [361]. Three different mechanisms of grooves formations have been proposed: void-based elongation, wrinkle-based elongation, and collapsed jet-based elongation. In the case of the PECA/PCL fibres, the characteristic elongated and aligned structures (coloured in orange in the SEM image of the inset of Fig. 19) were the result of the second mechanism. According to this mechanism (for a binary solvent system), a solvent with a low boiling point induces the formation of wrinkles at the fibre surface, while a solvent with high boiling point maintains the extruded filament wet and able to stretch because of the electric force [361]. The wrinkles then elongate and evolve into grooves upon fibre solidification. During the electrospinning of PECA/PCL fibres, we expect that the high evaporation rate of acetone (boiling point of 56 °C) and the slow one of acetonitrile (boiling point of 82 °C) influenced grooves formation. Since acetone and acetonitrile are a poor solvent and a non-solvent for PCL, respectively, while they solubilise PECA, we assume that the elongated microstructures consisted mainly of PECA.

In order to verify this, we treated the PECA/PCL mats with acetonitrile: a 5 µL drop of acetonitrile was deposited onto the mat and let it dry at room temperature. SEM investigations (Figure 46) of the treated mats show that the regions with near-circular pores survived the acetonitrile treatment, while the other regions were solubilised. This indicates that it is most likely that the grooved surface and the porous one contained a high amount of PECA and PCL, respectively. The spatial separation of the two polymers within the electrospun fibres can be associated to the presence of PECA-rich and PCL-rich domains (emulsion) in the starting solution before electrospinning. Those domains further segregated during fibre formation due to changes in solvent concentration.

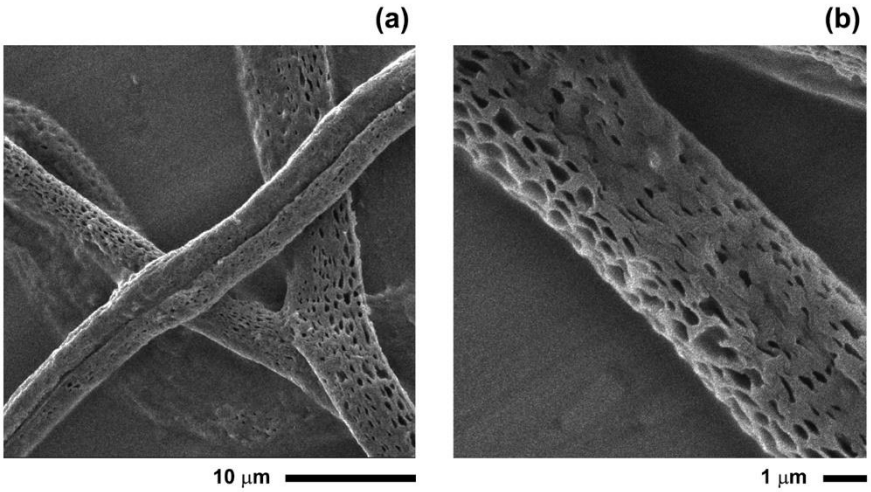

Figure 46 SEM images of PECA-PCL electrospun mats after treatment with acetonitrile. Figure has been published [53]**.**

3.4.4. Chemical characterisation

Fourier transform infrared spectroscopy (FTIR) was used to characterise the chemical composition of three materials PCL, PECA, and 2/1 PECA/PCL blend.

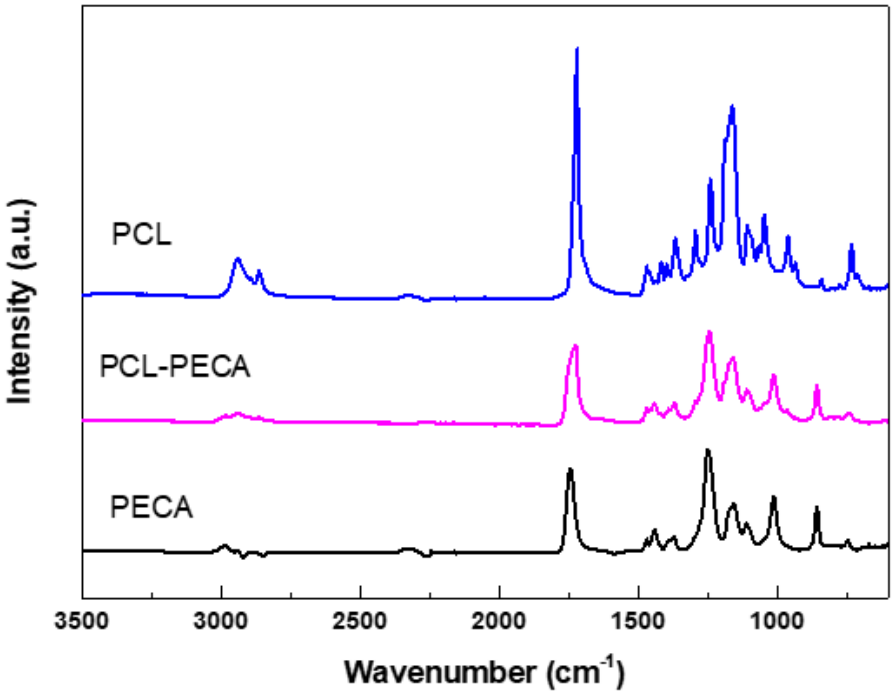

Figure 47.FTIR spectra of PCL, PECA, and PECA/PCL fibres

As shown in Table 4, the C≡N stretching of PECA was found at 2247 cm^{-1} in PECA spectra and at 2264 cm^{-1} in PECA/PCL spectra [49] [362]. The symmetric CH_2 stretching of PCL was found at 2866 cm^{-1} in PCL spectra and at 2864 cm^{-1} in PECA/PCL spectra. C-O and C-C stretching in the crystalline phase were found at 1294 cm^{-1} in both spectra [363]. Notably, CN stretching band in PECA/PCL spectra shifted to a higher frequency comparing to PECA spectra. This is likely due to the substitution of electronegative groups on the beta-carbon with the adding of PCL [364]. No chemical reaction took place in solution blending PCL and PECA.

Table 4 Functional groups and their peaks on FTIR spectroscopy

	PECA	PECA/PCL	PCL
CN stretching	2247	2261	/
C=O stretching	1743	1724	1720
single saturated C-O-C stretching	1248	1244	1240
asymmetric CH2 stretching	2945	2943	2943
symmetric CH2 stretching	/	2864	2866
C-O, and C-C stretching in the crystalline phase	/	1294	1294

3.4.5. Thermal characterisation

Similar melting temperatures were detected for all samples with PCL: (59.4±0.3) °C for 1/1 blend, (59.6±0.4) °C for 2/1 blend, (59.0±0.3) °C for 4/1 blend, and (61.0±0.3) °C for PCL (Figure 48). Since PCL was the only crystallised polymer in the blend and amount of PCL decrease with increasing PECA ratio, the crystallinity of blend decreases as well. Glass transition temperature (T_g) of PECA here was found at (134.0±0.5) °C, similar to a previous study [365]. Endothermal flow was shown above 150 °C, likely to be caused by degradation, see insert of Figure 48. Previous studies have found that PECA possessed poor thermal stability [293], [365], [366]. Initial degradation temperature of PECA was detected at 150-160 °C by TGA [293], [366] , and T_g was 140 °C by TMA [365].

Kim et al. mixed ethyl cyanoacrylate and starch and successfully produced PECA/starch blend. Glass transition of blend decreased from 113 °C to 106 °C with increasing starch content from 48 w/w % to 65 w/w% [367]. In theory, if two polymers were miscible, Flory-Fox equation could be applied to estimate the T_g of the blend [368]. If T_g of PECA was assumed to be 140 °C and PCL was -60 °C, T_g of 1/1, 2/1, and 4/1 PECA/PCL blend should be found at 8, 40, and 75 °C. However, no transition was found between (0-100) °C in DSC test, indicating the miscibility of two polymers was poor.

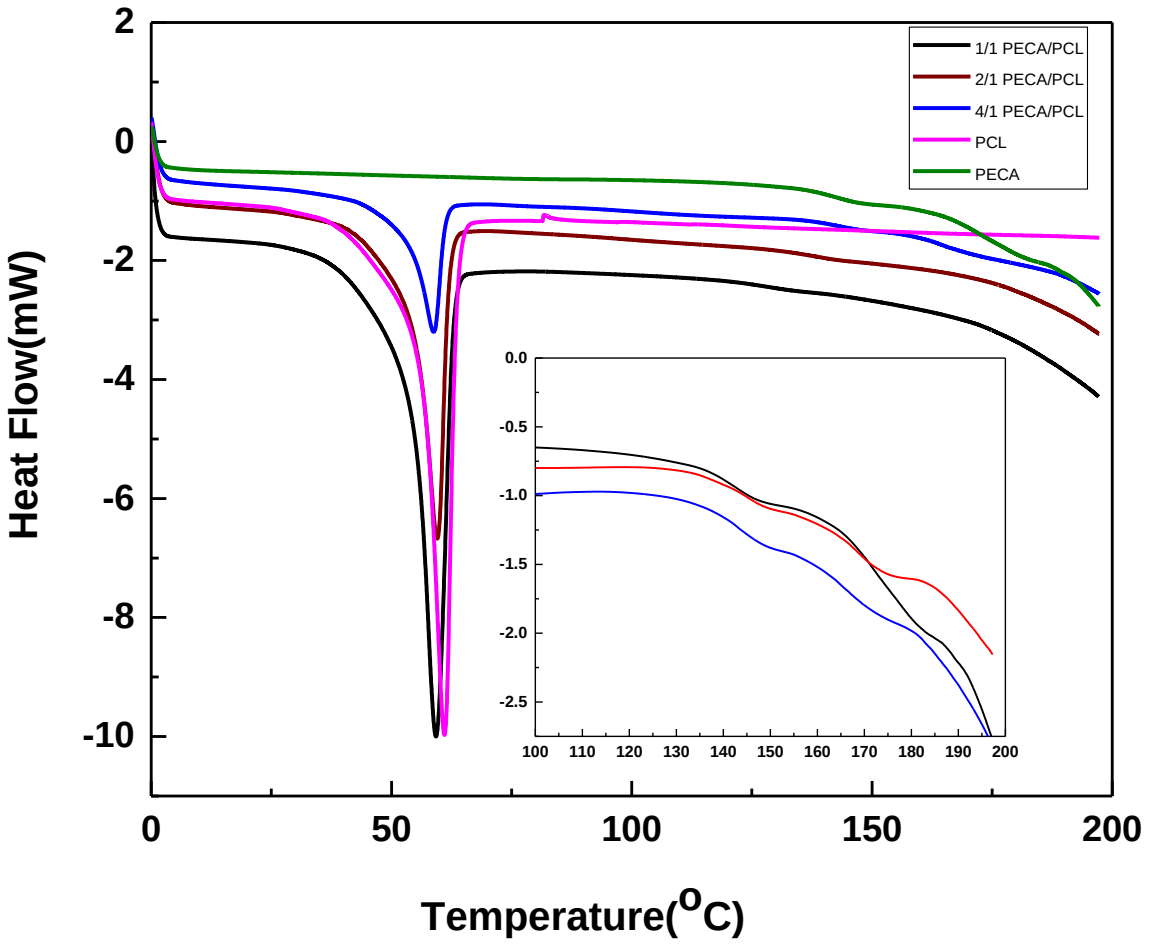

Figure 48 DSC curves of PCL, PECA, and blend samples with insert focus on the glass transition and degradation of PECA.

3.5. Conclusion

In conclusion, we demonstrated the formation of structured PECA/PCL fibres with dual-porosity by inducing phase separation during the electrospinning process. The fibres were constituted by two distinct regions: one with elongated and parallel grooves, possibly caused by spinodal decomposition; the other one with near-circular nanopores as result of nucleation and growth phenomena. Compared with previous studies on hierarchical micro- and nano-structures, the method here discussed allows the easy and cost-effective production of fibres with a unique morphology. Those hierarchical, multi-scale electrospun mats have potential applications as scaffolds for tissue engineering and devices for drug delivery.

Chapter 4 Electrospinning of zein fibres containing *in-situ* generated ZnO nanoparticles within a polyethyleneimine (PEI) matrix

4.1. Introduction

Zein is found in the endosperm of corn and belongs to the group of storage protein known as prolamins, which are the main repository for nitrogen in cereal seeds [369]. Zein mainly contains nonpolar amino acids, such as leucine, proline and alanine. The lack of polarity arises from the dipole cancellation effect of the constituent amine and acid groups through internal associations, which determine the hydrophobic character and poor water solubility of this protein [370]. For this reason, ethanol or alkaline solutions are used to process zein from “stocks” of solutions or dopes. Biocompatibility, biodegradability and processing versatility for a wide range of products, such as films, nanoparticles and nanofibres, make zein a material of interest for biomedical applications, particularly for tissue engineering and drug delivery [371]. Zein-based nanofibres have been produced by electrospinning from alcoholic solutions [372], [373] and have also been proposed for the release of antibacterial compounds and drugs, such as eucalyptus essential oil [374], gallic acid [375], curcumin [376], indomethacin [377], aceclofenac [378] and silver [379], and for promoting skin regeneration [380], [381], [382], [383]. The addition of biofunctional metal oxides to zein in the production of nanofibres by electrospinning has been reported by several authors. Babitha and Korrapati have evaluated zein and polydopamine (PDA) nanofibrous scaffolds incorporating TiO_2 nanoparticles for the treatment of skin wounds [380].

The sol-gel method is widely used to produce nanoparticles of metal oxides within a polymer matrix starting with a metal alkoxide or a metal carboxylate, through controlled successive steps of hydrolysis and condensation reactions [384]. Zhang et al. have used a solution mixture at 1:1:1 molar ratio of zinc acetate ($ZnAc_2$), 2- methoxyethanol as solvent and monoethyl amine as micro-suspension “stabiliser” and catalyst for the sol-gel reactions to produce piezoelectric coatings [385]. Rui Zang et al, on the other hand, have produced discrete ZnO nanorods in an alcoholic sodium hydroxide solution [386]. Other researchers have used procedures where the ZnO particles were used as suspensions, omitting a final thermal treatment at high tempera-

tures. For instance, Sun et al. have used a one-step hydrothermal method to produce ZnO nanoparticles, using hexamethylenetetramine to create the required basic conditions. The micro suspension was stabilised with the addition of a cationic surfactant [387]. Hong et al., on the other hand, have produced ZnO nanoparticles in a basic aqueous solution containing polyethylene glycol as a suspension stabiliser [388].

More recently Zinc acetylacetonate dihydrate (ZnAc-Ac.$2H_2O$) has attracted attention as a precursor for producing ZnO nanoparticles. However, as discussed in this chapter's literature review, there has been no report on the *in-situ* generation the ZnO nanoparticles within a PEI matrix. One previous work has been identified on the use of small amounts (1-2 %) polyethyleneimine as a suspension stabiliser for ex-situ produced ZnO nanoparticles in an aqueous medium containing measured quantities of NH_4OH [389]. In this work the ZnO nanoparticles are produced in-situ with much larger quantities of PEI to bring about the required basic condition within the reaction medium, and then incorporated within zein fibre.

This work investigates the effect of branched polyethyleneimine as a co-polymer for blends with zein for electrospinning of fibres. The use of PEI for the plasticisation and/or toughening of zein for films or fibres has not yet been reported in the literature. The feasibility of producing stable suspensions of ZnO nanoparticles within the PEI matrix by the sol-gel method, prior to the incorporation into the zein electrospinning solution, is also a novel idea that is explored in the present work, which is enhanced by the low toxicity rating of the reactants and solvents. Some of the result discussed in this Chapter has been accepted to be published on ACS Applied Polymer Materials [390].

4.2. Literature review

4.2.1. Synthesis of zinc oxide nanoparticles

There are three ways to synthesis ZnO nanoparticles from zinc acetylacetonate ($Zn(AcAc)_2$): thermal decomposition [391], [392], [393], [394], chemical vapour deposition [395], [396], [397], [398], and precipitation method [399],**[400]** [400], [401], [403].

Thermal decomposition is a straightforward process, involving direct heating of zinc acetylacetonate. Due to the high temperature, there is usually no organic residues left in the final nanoparticles. In ambient environment, ZnO formation starts at 195 ^{o}C, followed by crystallisation at 260 ^{o}C [391]. Music et al. studied the effect of temperature on ZnO nanoparticles formation from 200 to 600 ^{o}C in 2010 and found that, with increasing decomposition temperature, ZnO particle size increased due to aggregation/sintering processes [391]. Finest ZnO particles were produced at 200 ^{o}C, with size range of 20 to 40 nm. Later, in 2012, Schwartz et al. synthesised ZnO nanoparticles with average size of 23±6 nm in argon environment at 240 ^{o}C [392]. These particles were then mixed with poly (N-isopropylacrylamide) using solvent casting method to form a hydrogel mix. For a good dispersibility, two surfactants, oleylamine and oleic acid, were added together with zinc acetylacetonate during thermal decomposition, acting as hydrophobic coating. The hydrogel showed good antibacterial property against *E. coli*, as well as good biocompatibility. Ultraviolet light could be used to assist the formation of ZnO nanowires, as demonstrated by Wu et al. [393]. Zinc acetylacetonate was firstly spin-coated on glass substrates and exposed to UV light with a power intensity of 76 mWcm^{-2} while being heated at 200 ^{o}C, ambient environment. Comparing with the ZnO nanowires formed without UV light, ZnO nanowires formed with UV light assistance showed smoother, less mesoporous structure and relatively low intensity of visible emission. The study suggested that UV light promoted electronic transitions in $Zn(OH)_2$, which led to faster dissociation, resulting in the aggregation of ZnO nuclei and further, the formation of larger ZnO nanoparticles. However, from application perspective, ZnO nanowires formed without UV light showed better photocatalytical properties because of more defects and smaller particle size. Fauteux et al. used a laser as heat source to induce decomposition of zinc acetylacetonate [394]. Zinc acetylacetonate/water/ethanol suspension was irradiated by an unfocused CO_2 laser with wavelength 10.6 μm. ZnO nanowires/nanorods morphology was controlled by different laser powers and irradiation time.

The mechanism of chemical vapour/spray deposition (CVD) is similar to thermal decomposition. However, in CVD, metal precursors and dopants were vaporised first and introduced into high temperature reactor for decomposition to take place and later collected on a substrate (usually glass) surface. Back in 1994, Minami et al demonstrated polycrystallined ZnO synthesised from zinc acetylacetonate via CVD

method [395]. Since the gas glow was N_2, deionised water was necessary as an oxygen source. Lowest resistivity undoped ZnO film was obtained at 550 ^oC. By adding aluminium acetylacetonate as dopant, the reaction temperature can be reduced to 350 ^oC. Similar experiment was conducted by Maldonado et al. [396]. Instead of vaporising, zinc acetylacetonate was dissolved in acetic acid/alcohol (ethanol, methanol, isopropyl)/water and indium nitrate, the dopant was dissolved in water, then both were sprayed onto heated substrates. Lower resistivity was reached by using ethanol due to the good uniformity of grains.

Precipitation method involves reduction of zinc acetylacetonate solution using alkali solution as reducing agent via hydrothermal synthesis, followed by precipitation of ZnO nanoparticles from solution. The method was firstly used in 1997, Iwasaki et al. successfully produced ZnO nanoparticles with diameter 8.9 nm by adding zinc acetylacetonate/alcohol solution dropwise into sodium hydroxide/ethanol solution and refluxing for 1 hour [399]. The study suggested that the reaction processed via an attack of anions on the zinc cation in zinc acetylacetonate forming the ZnO particles. In 1998, the same group proposed a more detailed mechanism for the same process (Figure 49 and Figure 50) [400]. Gas-liquid chromatography (GLC) and high-performance liquid chromatograph (HPLC) detected the presence of $CH_3COCH_2COCH_3$, CH_3CO_2H, and CH_3COCH_3, which indicated that part of $acac^-$ ligands was attacked by EtO- , followed by hydrolysis forming $Zn(OH)_2$/Zn(acac)OH. The growth of ZnO was through a dehydration-condensation of $Zn(OH)_2$/ Zn(acac)OH. Similar procedure was used by two studies of Music et al. [401], [402] with heating post-treatment. The study in 2011 obtained squire plate-like ZnO/$Zn(OH)_2$-citrate complex particles by hydrolysis of zinc acetylacetonate in sodium hydroxide and trisodium citrate ethanol solution [402]. Pure uniform ZnO nanoparticles were formed after 300 ^oC heating post-treatment. With continue heating at 600 ^oC, crystal growth continued and larger size of hexagonal ZnO particles were obtained. The other study added zinc acetylacetonate powder into sodium hydroxide water solution to synthesis hollow ZnO nanoparticles [401]. The study found that the concentration of zinc acetylacetonate affected the morphology of ZnO. At lower concentration, narrow ZnO nanoneedles were formed. With the increasing of concentration, ZnO formed larger and more hexagon shaped nanorods. Morphology of these samples remained the same after 300 ^oC heating post-treatment. In 2014, Music et al. demonstrated hydrolysis of zinc acetylacetonate ethanol/water solution using aqueous NH_3 solution at 160 ^oC [403].

With increasing reaction time, ZnO particles changed from hexagonal hollow shells to hexagonal pencil-type rods caused by dissolution/recrystallisation of ZnO. Comparing with hydrolysis without aqueous NH_3 solution, the process of ZnO dissolution was accelerated by forming $[Zn(NH_3)_4]^{2}$+ and $[Zn\ (OH)_4]^{2}$- complex.

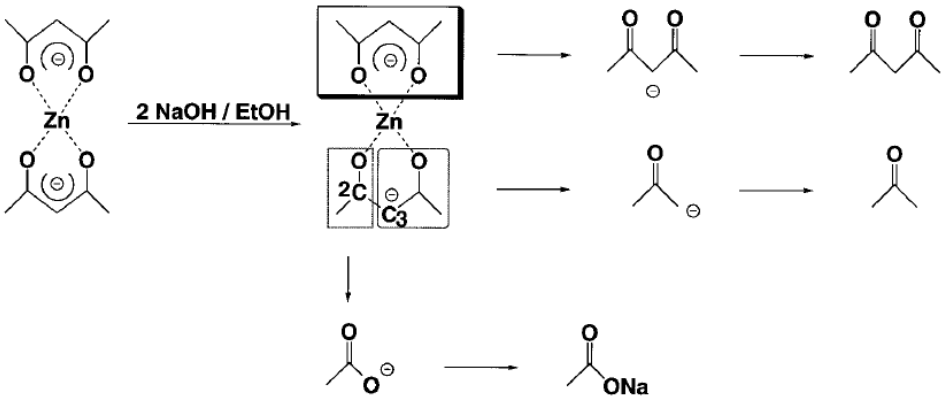

SCHEME 1

Figure 49 The reaction proceeds with decomposition of acac$^-$ ligand. The reaction seems to involve the cleavage of C2-C3 bonds of acac$^-$ ligand $H_3C(1)CO(2)CH(3)CO(4)CH_3$(5) [400]**.**

In this PhD project, *in-situ* hydrothermal process was used to generate ZnO/polyethyleneimine (PEI) nanocomposite. PEI served as a polymer matrix as well as a reduction agent, since -NH_2 groups could promote hydrolysis of zinc acetylacetonate. Previously, there has been no study used zinc acetylacetonate as precursor for *in-situ* composite generation. Abdullah et al. developed ZnO/poly(ethylene glycol) (PEG) nanocomposite using zinc acetate as precursor via *in-situ* method [404]. Zinc acetate ethanol solution was mixed with lithium hydroxide/PEG ethanol solution and reacted at 40 ^oC. Blue to yellow luminescence was detected from produced nanocomposite. The study suggested that the spectral shift was caused by the change in particle size, which is consistent with a later study by Wu et al. [393]. Furthermore, with the adding of europium acetate as dopant, the Eu-doped ZnO/PEG composite provided red luminescence.

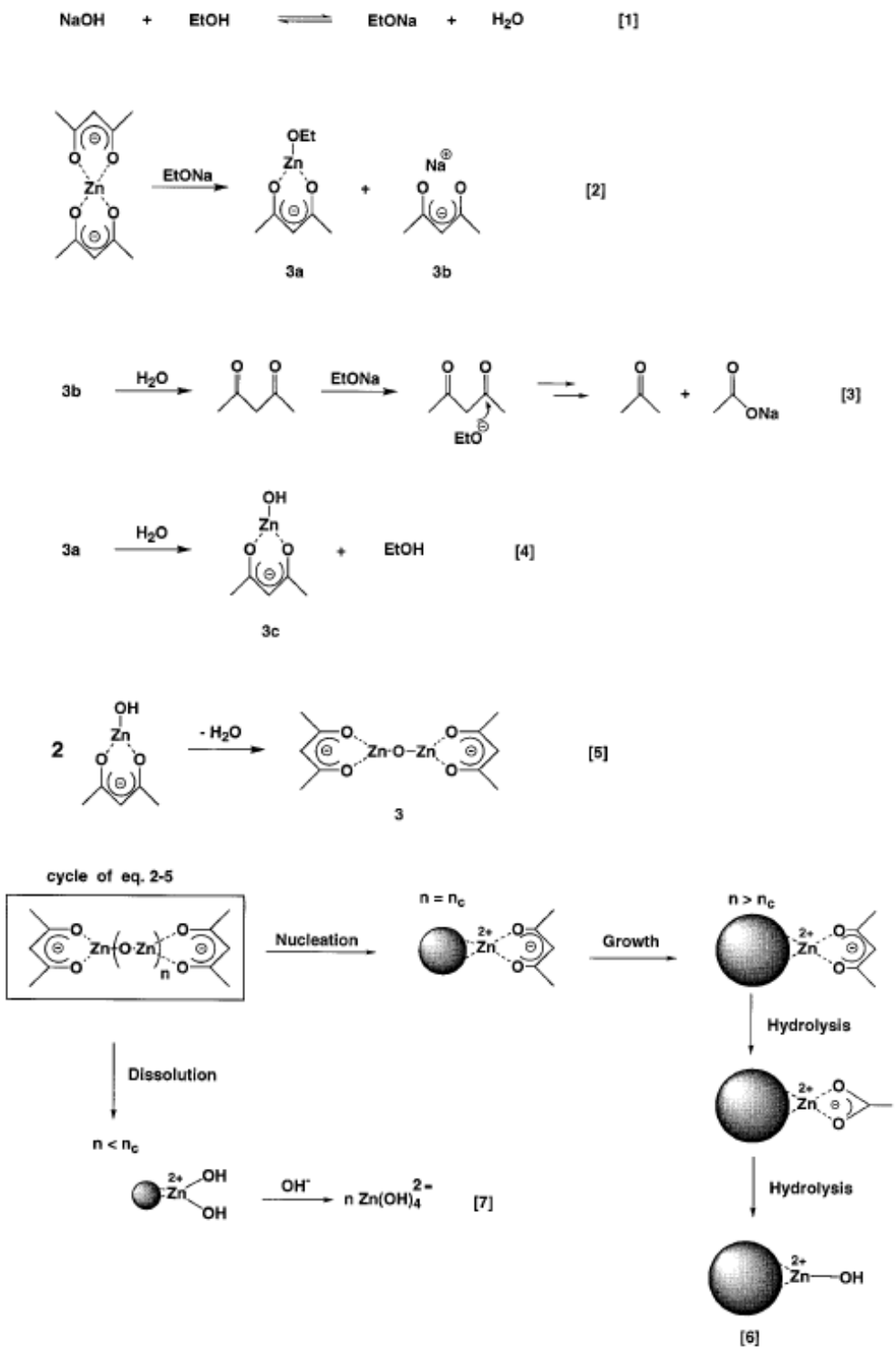

SCHEME 2

Figure 50 There are two remarkable features in this reaction system; the first is that a stable chelate complex ([Zn(acac)$_2$]) can be used as a starting compound, and the second is that H_2O is only furnished by the equilibrium reaction of NaOH and EtOH. [400]**.**

4.2.2. Zinc oxide (ZnO) nanoparticles in electrospinning

Passive loading is the most commonly used method to combine ZnO nanoparticles in electrospinning. In this method, as-received ZnO nanoparticles are dispersed into a polymer solution, using ultrasonic bath [405], [406], [407], [408], [238], [239] or magnetic stirring [409] and then electrospun into fibres. ZnO nanoparticles are usually embedded inside the polymer fibres by this method, while some studies showed that some of the ZnO nanoparticles can also be detected on the surface or semi-exposed [409][410].

Augustine's group have been working on electrospinning fibres of polycaprolactone (PCL) and ZnO nanoparticles using passive loading method with different ZnO loading content (0.1-1 wt% and 1-6 wt%) [405], [407], [411], [412]. PCL is a widely studied for biomedical applications due to its biocompatibility and biodegradability, as reviewed in Chapter 2. The group discovered that, 1 wt% was the critical value for ZnO nanoparticles, where the fibres with smallest average diameter occurred. Below it, ZnO nanoparticles themselves could accumulate charge density on the surface of the electrospinning jet and change viscosity of electrospinning solution [411], causing the fibre diameter decreased with increased ZnO nanoparticles content. With higher ZnO nanoparticles content, agglomeration of ZnO nanoparticles happened, which caused rougher surface and larger diameter of the fibres [407] [411]. The dispersion of ZnO nanoparticles also affected thermal properties. The group found that adding ZnO nanoparticles caused less crystallinity of PCL, which was possibly caused by the restriction of polymer chain mobility [411]. With below 1 wt% of ZnO nanoparticles, thicker lamellar crystals of PCL were more likely to form which caused a higher melting temperature; above 1 wt%, lower melting temperature was observed due to nucleation and thinner lamellar crystal [405]. The difference in crystallinity together with interaction between ZnO nanoparticles and carbonyl groups of PCL [411] affected fibres mechanical properties [405], [411]. Below 1 wt% of ZnO nanoparticles, ZnO nanoparticles worked as reinforcement of fibres, boosting their strength from (1.40±0.21) to (1.60±0.23) MPa, and modulus from (3.70±0.23) to (5.52±0.21) MPa. However, above 1 wt%, agglomeration of ZnO nanoparticles acted as stress concentration, which decreased the strength of fibres. With 2, 4, 6 wt% of ZnO added, the strength of fibres were (1.17±0.12), (0.93±0.04), and (0.98±0.11)

MPa. The group thoroughly studied biological performance of PCL/ZnO nanoparticles fibres and found that ZnO nanoparticles helped to improve the antibacterial property against *E. coli* and *S. aureus* and cell proliferation (up to 120% of cell viability comparing to control) [411], which enhanced wound healing process [407]. Furthermore, fibroblast proliferation was also improved since ZnO nanoparticles could generate reactive oxygen species which helped the expression of growth factors and receptors[407]. Additionally, another study showed that the adding of ZnO nanoparticles accelerated degradation of fibres in simulated body fluid [405]. Weight loss test observed up to 42% weight loss of ZnO loaded PCL fibres, while weight loss of neat PCL fibres was only 20%.

Since in the passive loading method ZnO nanoparticles are mostly embedded inside the polymer fibres, other studies focused on how to make ZnO nanoparticles attached to the fibre surface to further improve their performance. Electrospinning/electrospraying and surface coating have been used for this purpose. Electrospinning/electrospraying involves simultaneously electrospinning polymer solution and electrospraying ZnO nanoparticles. A study on the production of polyacrylonitrile (PAN)/ZnO nanoparticles electrospun fibres compared electrospinning ultrasonicated ZnO nanoparticles loaded PAN solution, as the “in” method, and electrospinning/electrospraying, as the “on” method [413]. The study showed that ZnO nanoparticles were more evenly dispersed inside and on the surface of the PAN fibres with “in” method; while spherical aggregates of ZnO nanoparticles were found on the surface of fibres with “on” method. Different morphologies of the two types of fibres contributed to the different properties. Fibres produced with the “in” method exhibited better mechanical properties, while fibres produced with the “on” method exhibited faster photocatalytic properties on degradation of methylene blue dye and better antibacterial property against *S. aureus*. A similar study was also done on PLA/ZnO nanoparticles electrospun fibres [414]. Passive loading and electrospinning/electrospraying methods were both used for comparison. Dispersions and agglomerates of ZnO nanoparticles were both found inside and semi-exposed onto the fibres for passive loading methods, while well dispersed ZnO nanoparticles with few agglomerates were found on the surface of fibres for electrospinning/electrospraying method. In agreement with the PAN/ZnO nanoparticles study, fibres produced from electrospinning/electrospraying exhibited better antibacterial properties against *E. coli* and *S. aureus* due to the direct exposure of ZnO nanoparticles. However, in this study,

fibres produced from the passive loading showed better mechanical properties due to the H- bonding formed between PLA and ZnO nanoparticles. The different results obtained in these two studies show that the effect of the mechanical properties of ZnO nanoparticles could be influenced by concentration and dispersion of nanoparticles, and the chemical groups of the polymers used.

Surface coating is another method to produce electrospun fibres with ZnO nanoparticles on the surface. A study produced polyamide 6 (PA6)/polyaniline (PANI)/ZnO nanoparticles fibrous composites by immersing electrospun PA6/PANI into a liquid dispersion of ZnO nanoparticles [406]. Near spherical ZnO nanoparticles were produced by hydrothermal synthesis using zinc nitrate as precursor, potassium hydroxide to adjust pH and polyethylene glycol (PEG) as surfactant. Researchers observed that the ZnO nanoparticles were connected to the fibre's surface via H-bonding and the nanoparticles remained after a washing process. After the ZnO treatment, the electron transfer kinetic of the fibres was improved, which makes the resulting mats suitable for electrochemical applications. Surface coating can also be used to grow ZnO nanorods on the surface of electrospun fibres. In a recent study by Kim et al. [415], electrospun polyurethane (PU) fibres were firstly immersed in dopamine hydrochloride solution to have a polydopamine (Pdopa) coating and then soaked in a solution containing ZnO nanoparticles. Hydrothermal treatment using zinc nitrate hexahydrate as precursor was then used to grow ZnO nanorods. Pdopa was used as "adhesive" in this study, since some of its catechol groups forms hydrogen bonding with PU and the others with ZnO nanoparticles. As a result, the dispersion of ZnO nanoparticles was much better. After hydrothermal treatment, ZnO nanorods with 10-30 nm diameter fully covered the fibres surface. The resulting mats showed good photocatalytic and antibacterial properties. Notably, hydrothermal method has been used to produce ZnO fibres with structure similar to Kim's study [416]. Electrospun Zinc acetate/polyvinylpyrrolidone (PVP) fibres were firstly calcinated into ZnO fibres and then hydrothermally treated to grow ZnO nanorods on the fibres surface.

4.2.3. Structure of zein

Many studies have been conducted to detect the structure of zein [417], [418], [419], [420], [421]. There are four types of zein: α, β, γ, δ, classified based on their solubility. Among them, α-zein is the one that is highly hydrophobic and widely used and studied [417], [418]. It mainly contains nonpolar amino acids, such as leucine, proline and alanine. Lack of polarity arises from the dipole cancellation effect of the constituent amine and acid groups through internal associations, determining hydrophobicity and poor water solubility. The secondary and ternary structures of zein still remain unclear.

The first structural model of zein was proposed by Argos et al. in 1982 [417]. 50-60% α-helical content with turn or random coil configuration was detected by circular dichroic method. They suggested a “turn-helix-turn” model, which was an oval cross-sectioned cylinder formed by “9 topologically antiparallel and adjacent helices”. However, the model was questioned in 1993 by Tatham et al. with the discovery of elongated asymmetric structures for zein in solution using small angle X-ray scattering and viscometry [418]. This was consistent with the study of Matsushima et al. in 1997 [419]. Matsushima suggested linear stacks of antiparallel α-helical joined by glutamine-rich “‘turns’ or loops” (Figure 51). This model had been widely accepted. Until then, all studies stated that there was no β-sheet content in zein. However, later in 2004, two studies confirmed the existence of β-sheets by two different methods [420], [421].

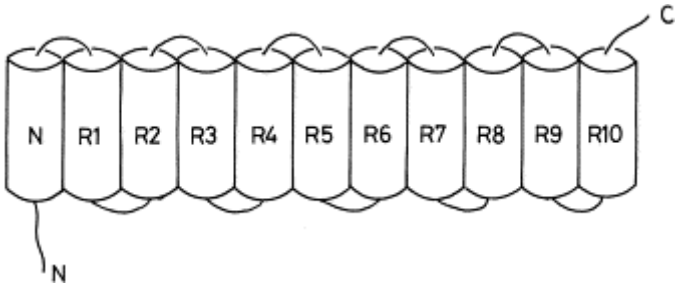

Figure 51 Zein structural model suggested by Matsushima. Each of the tandem repeat units formed by a single α-helix is presented by the cylinder and glutamine-rich “turns” or loops joining them by the curve. The antiparallel helices of tandem repeats stack linearly in the direction perpendicular to the helical axis (the c-axis) [419]**.**

4.2.4. Plasticising of zein fibres

Although zein has several desired properties as stated previously, it is brittle and difficult to process. Several studies have successfully modified the mechanical properties of zein using glycerol [422], [423], water [423], oleic acid [424], 2-mercaptoethanol [423], amphiphilic plasticisers [422], co-protein [425], and biodegradable polyethers [425], as plasticisers. An early study by Gioia et al. compared plasticising effect of polar (water and glycerol) and amphiphilic (palmitic acid, octanoic acid, dibutyl tartrate, dibutyl phthalate, and diacetyl tartaric acid ester of mono-diglycerides) plasticisers on zein, and discovered that amphiphilic plasticisers had higher plasticising efficiency than polar plasticisers when the molar content was the same [422]. It was also found that higher molecular weight and lower hydrophilicity helped to increase efficiency. The study developed a plasticising mechanism involving breaking physical bonds in zein and forming new plasticiser-zein bonds. Plasticisers firstly “wet” and solvate zein surface. This is followed by the diffusion and dissolution of plasticisers in amorphous regions of zein, resulting in reformation of the structure. Since H-bond and nonpolar interactions were responsible for the stabilisation of zein, interactions of non-polar groups of zein and amphiphilic plasticisers led to better efficiency comparing with polar plasticisers, which were more likely to interacted with polar groups. However, later studies are more likely to choose polar plasticisers [423] [424] [425]. This is probably due to higher plasticising efficiency of polar plasticisers with the same volume fraction [422]. Notably, the preparation method used in the study of Gioia et al. was thermal mixing using a Brabender counter coating batch mixer, while later studies usually use solution casting [423], [424], [425]. Polymer chain relaxation during mixing could be different in the two methods, which might change plasticising efficiency. A study in 2012 further investigated plasticising mechanism of water and glycerol using FTIR and found a reduction of amide II band, which suggested a breaking of amide-amide H-bonding and an increase of amide-plasticiser interaction [423], which is consistence with the early study [422]. Similar result was also found in another study by comparing the plasticiser effect of oleic acid and glycerol on zein [424]. The study suggested that the mechanism for glycerol was structural plasticisation since change of H-bonding could be seen in FTIR, while mechanism for oleic acid was molecular plasticisation because of the increase of mobility of zein chains

caused by the hydrophobicity of oleic acid. The study observed no obvious change in amide I band, which related to secondary structure of zein, in the FTIR of oleic acid. However, later in 2014, another study observed a change in low frequency β-sheet secondary structure in zein plasticised by oleic acid using FTIR [425]. A recent study discovered that combining poly (ethylene glycol) (PEG) with glycerol could enhance zein plasticisation, though PEG on its own did not have any plasticising effect [426]. XRD analysis showed that the inter-α-helix packing of zein was disrupted by an insertion of plasticisers. In ATR-FTIR analysis, researchers used the area ratio of α-helix/β-sheets to indicate the change in secondary structures. The result showed that combination of glycerol and PEG had the lowest ratio, followed by glycerol, indicating that the plasticising effect was caused by change in secondary structure [426], agreed with the study in 2014 [425]. It is noteworthy that, though glycerol is the most studied plasticiser for zein, it could also act as anti-plasticiser, suggested by a study in 2015 [427]. At high content (>20%), glycerol increased local dipolar relaxation of amorphous zein matrix suggested by phosphorescence measurement, and bound zein into aggregation state as suggested by AFM. Thus, it worked as plasticisers. However, at low content (<10%), glycerol decreased local dipolar relaxation, and the surface seemed smooth under AFM. At molecular level, it worked as anti-plasticiser.

4.2.5. Zein structures for biomedical applications

4.2.5.1. Micro/nano particles

Zein has been proposed for the production of micro/nanoparticles because its hydrophobicity facilitates particle generation in a self-assembly manner with limited energy consumption [428]. Furthermore, zein particles have been further processed to manufacture tablets for instance [429] and to encapsulate actives compounds [428].
The method widely used to produce zein micro/nano particles is phase separation [430] [431] [432]. Zein solution, of which the solvent is usually ethanol/water, is poured or added drop-by-drop into an antisolvent, which is usually water. For instance, zein and ivermectin, a poorly water soluble parasiticide, were firstly dissolved

in ethanol/water, and ultrapure water was then added into the solution to create microparticles encapsulating ivermectin with size between 0.3-1.2 μm (Figure 52) [429]. The microparticles were then directly compressed into tablets. *In vitro* release tests showed a biphasic releasing curve for microparticles with an initial burst release. In the tablet form, the release became much slower since the release rate was depending on drug diffusion. *In vitro* release rate result was obtained by using pepsin, an enzyme, to degrade zein matrix. After the treatment with pepsin, release rate was controlled mainly by the matrix degradation. In another study reported on encapsulating peppermint oil in zein nanoparticles, zein was dissolved with and without peppermint oil in propylene glycol (PG)/water [432]. Gum Arabic solution was added as a stabiliser, which helped zein nanoparticles stabilised at wider pH range. Without peppermint oil, using gum Arabic decreased mean diameter of zein nanoparticle from 250 nm to 143 nm. The adding of peppermint oil, mean diameter further decreased to 129 nm. *In vitro* release test showed a pH-controlled release of peppermint oil with a faster release at lower pH.

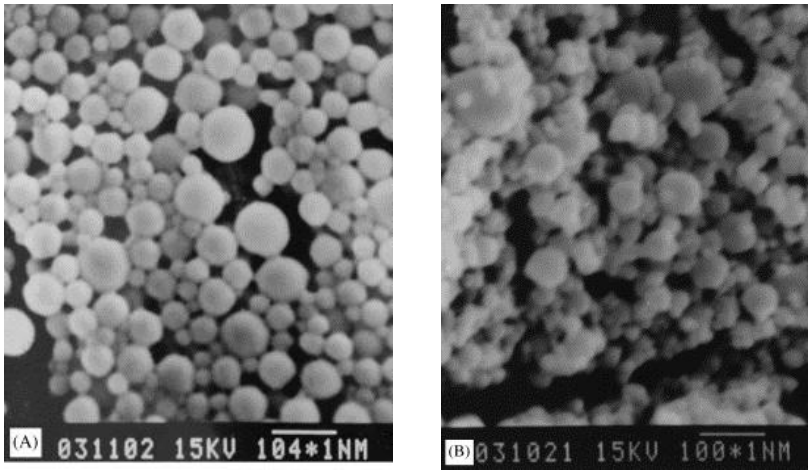

Figure 52 SEM images of ivermectin loaded zein microparticles: (A) freshly prepared, scale bar is 1.04 μm. (B) after compressing and shaping in wet box at 37 °C for 3 days, scale bar is 1 μm [429]**.**

Surface coated zein micro/nano particles have also been developed [433]. Based on the encapsulating peppermint study, a recent study developed soluble soybean polysaccharide (SSPS) surface coated zein nanoparticles for encapsulation of quercetin, a beneficial natural flavonol [433]. Zein, together with quercetin, was dissolved in

ethanol/water, and the solution was then added drop-by-drop directly in SSPS solution. XRD revealed the formation of the amorphous complex between zein and SSPS and, in FTIR, a chemical shift was identified in OH stretching bands. Together, they indicated noncovalent interaction existed between zein and SSPS. The study compared the antioxidation activity of quercetin before and after encapsulation using 2,2'-azino-bis(3-ethylbenzothiazoline-6-sulphonic acid) (ABTS) radical solution and observed no obvious change. Barkoula et al. demonstrated hydroxyapatite crystals growing on crosslinked zein microparticles to achieve ceramic coatings via mineralisation [434]. The study found that particle size played an important role in deposition of minerals. No mineral layer could be observed until the diameter of particles was larger than 1.13 μm, due to the number of active sites on particle surface. Since the hydroxyapatite crystals were characterised by thin and plate-like structure, which was similar to bone apatite, and no cytotoxicity was shown, the material showed potential to be used in bone tissue engineering.

More interestingly, supercritical CO_2 has been used as an antisolvent to produce zein micro/nano particles. For instance, in 2008, an aerosol solvent extraction system was assembled for this purpose (Figure 53) [435]. The study tested different factors that could change morphology of zein particles, and found that larger zein concentration, increasing the CO_2 flow rate and use less polarity alcohol, helped to produce larger and more uniform particles. Later, in 2009, researchers loaded lysozyme, an antimicrobial, in zein particles using a similar process [436]. Lysozyme was firstly dissolved with zein in ethanol/water and then went through phase separation using supercritical CO_2 as antisolvent. Red-blood-cell shaped particles were formed with smooth surface but interconnected, porous internal structure. *In vitro* release test observed a long-time sustained release of lysozyme in potassium phosphate buffer in near-neutral pH (7 and 8) condition. The release was faster at low pH (2-5), in agreement with a previous study [432]. Smaller and more regular shaped zein particles as drug carrier were achieved in 2012 [437]. In this study, lutein, a natural pigment, replaced lysozyme, as drug, and acetone/DMSO replaced ethanol/water, as solvent. The study found that changing the combination of temperature, solvent flow rate and pressure, zein particle size varied from (198±16) to (355±40) nm. A much slower release with no initial burst release were observed from zein nanoparticle system comparing with lutein and lutein/zein physical mixer in *in vitro* release test.

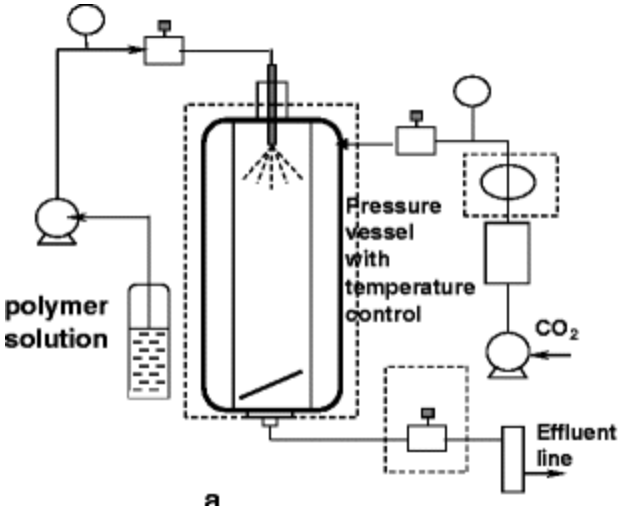

Figure 53 The supercritical antisolvent process [435]**.**

Electrospraying is another method to produce zein micro/nano particles [438] [439]. Comparing with phase separation, electrospraying does not require removing particles from a liquid environment and can achieve high encapsulation efficiency for active materials [438]. Gomez-Estaca et al. produced zein nanoparticles with sizes between 175 to 900 nm, from 2.5% to 15% (w/w) zein/aqueous ethanol solution using electrospraying (Figure 54) [438]. Researchers successfully encapsulated curcumin, an antioxidant plant extract, in those nanoparticles with 85-90% efficiency. Curcumin encapsulated particles could stay stable for three months in a dark ambient environment. Liu et al. recently proposed a co-axial electrospraying system using solvent as sheath liquid to prevent clogging, which usually happens when natural polymers are used [439]. Comparing with single-fluid electrosprayed tamoxifen citrate encapsulated zein microparticles (P1 sample), co-axial electrosprayed ones (P4 sample) possessed smaller diameter (0.68±0.07 μm) and more regular shape. A more gradual release was observed with co-axial electrosprayed particles. Releasing time for 50% of encapsulated tamoxifen citrate was 1.14 h for P1 and 4.22 h for P4.

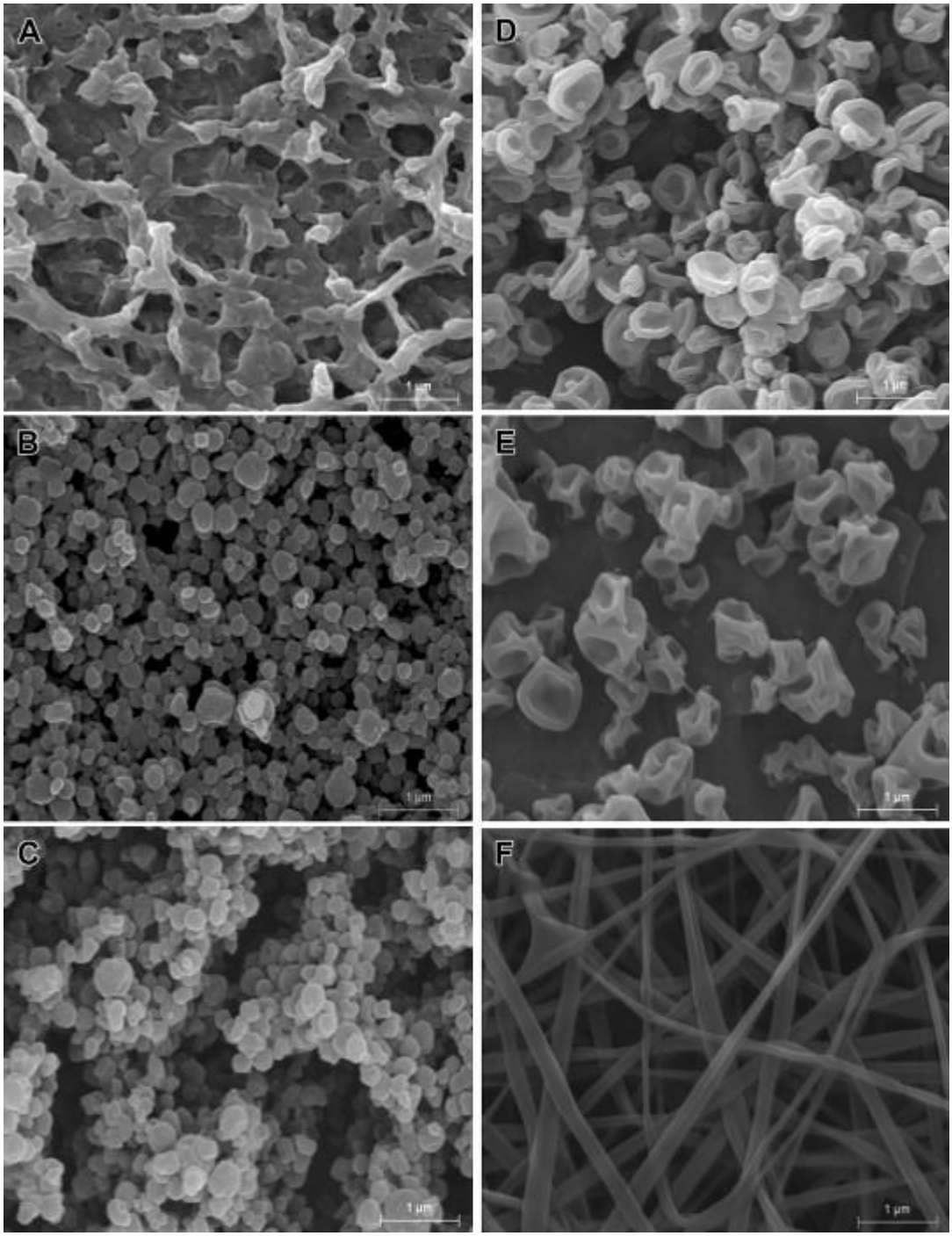

Figure 54 SEM of electrospraying samples of different zein concentrations: A. 1%; B. 2.5%; C. 5%; D. 10%, E. 15%; F. 20% [438]**.**

4.2.5.2. Electrospun fibres

Zein-based nanofibres have also been proposed for the release of antibacterial compounds and drugs, such as eucalyptus essential oil [374], fish oil [111], curcumin

[376], and nanoparticles [440] [441] [383] [442]. Babitha and Korrapati have evaluated zein and polydopamine (PDA) nanofibrous scaffolds incorporating TiO_2 nanoparticles for the treatment of skin wounds [440]. The fibres produced from ethanol solutions (90%) displayed a ribbon-like structure with an average diameter of 150 nm. Cell viability studies on keratinocytes showed an enhanced cell adhesion and proliferation on zein-PDA-TiO_2 nanofibres, possibly due to the increased surface roughness. Animal studies (rats) on full-thickness excisional wound model have revealed a complete reepithelialisation of the injured skin after 15 days for the group treated with zein-PDA-TiO_2 fibres, whereas the group treated with the zein-PDA required 17 days to heal. Hydroxyapatite (HA) nanoparticles can also been incorporated in the similar way. Zhang et al. compared effectiveness of magnetic stirring and ultrasonic mixing in preparing a zein/HA solution for electrospinning [441]. With the adding of HA, fibre diameter increased in both methods, magnetic stirred samples showed bigger increase than ultrasonic mixed samples due to the more agglomerates. Interestingly, though magnetic stirred samples showed worse mechanical properties, the hydrophilicity was improved, which favoured cell proliferation. On the other hand, ultrasonic mixing made the material stronger, but did not improved bioactivity. Electrospun zein fibres with *in-situ* generated metal nanoparticles have also been developed. For instance, Dashdorj et al. have prepared zein/Ag composite nanofibres by dissolving zein in citric acid, ethanol and sodium hydroxide, and then adding $AgNO_3$ [383]. Citric acid was used for its dual function, as cross-linking agent for zein and reducing component for the *in-situ* production of silver. Electrospinning of the fibres was followed by thermal curing of the collected mats at 150 °C for 150 minutes. No information was provided, however, about possible thermal degradation effects on properties. The silver nanoparticles had an average diameter of 20 nm and were homogenously dispersed within the zein electrospun fibres. *In vitro* tests on fibroblasts showed that the composite fibres were non-cytotoxic and were able to promote cell proliferation. The presence of silver nanoparticles rendered the nanofibres effective in stopping the growth of *E. coli* and *S. aureus*. Chen et al. developed crosslinked electrospun zein fibres coated with gold nanoparticles for the biosensor application [442]. Zein was firstly dissolved in glacial acetic acid and then crosslinker, glyoxal, was added before electrospinning. After electrospinning and crosslinking in ambient temperature, Au nanoparticles were *in-situ* generated on the surface of the fibres with $HAuCl_4$ as precursor in PEI solution at 60°C. FTIR suggested H-bonds

formed between zein and PEI and a vigorous reaction took place between amino groups of PEI and aldehyde groups of glyoxal. The study showed that the crosslinking improved water resistance and thermal stability of fibres, which maintained the morphology of fibres during *in-situ* generation. Au nanoparticles were successfully deposited on the surface of fibres with good dispersion (Figure 55).

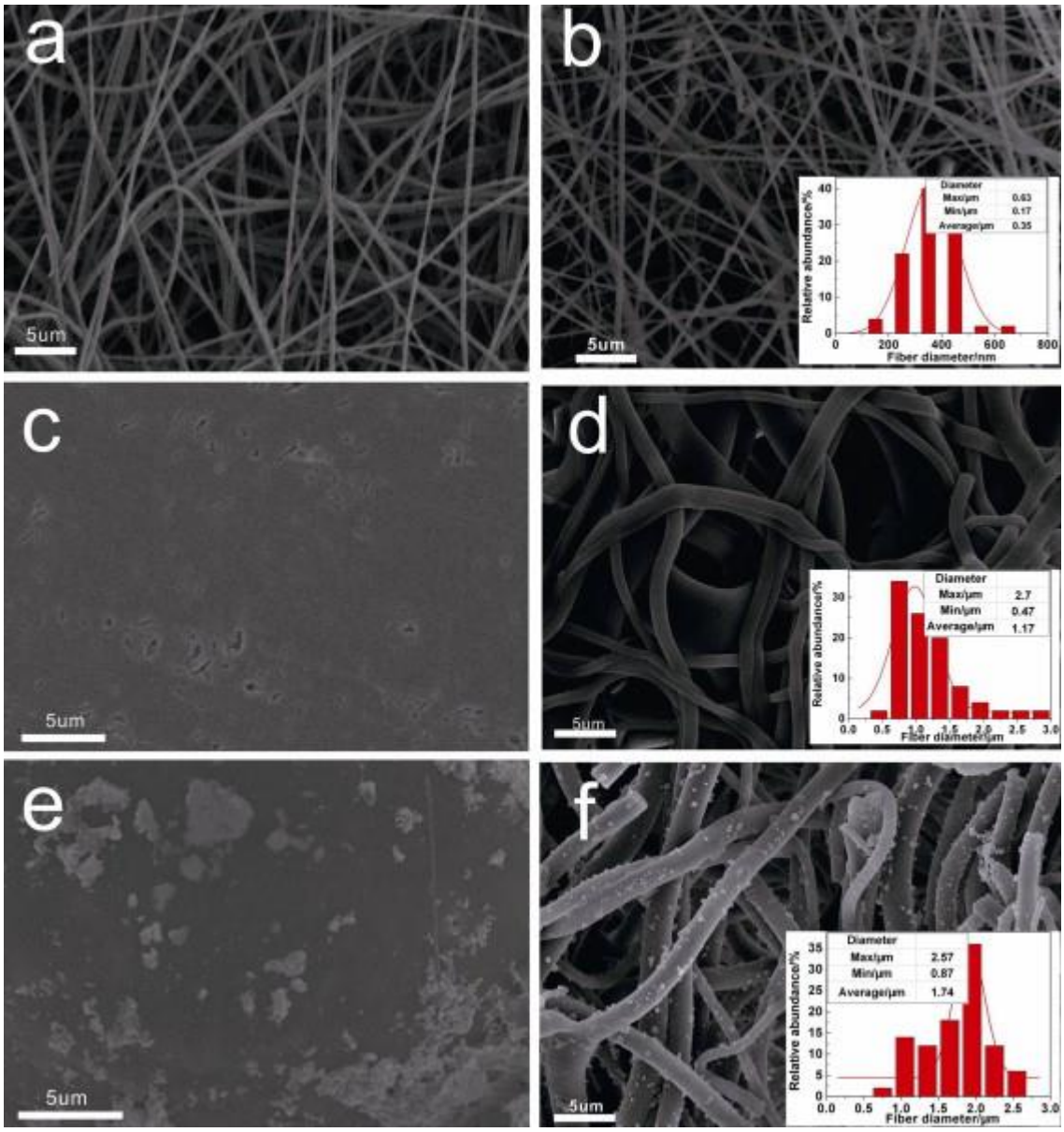

Figure 55 SEM images of (a) Non-crosslinked zein nanofibres, (b) Crosslinked zein nanofibres, (c) Non-crosslinked and (d) crosslinked zein nanofibres in water environment, (e) Au coated zein film developed from (c), and (f) Au coated crosslinked zein nanofibres. Inset: diameter distribution of fibres [442]**.**

Due to its poor mechanical properties, researches have blended other polymers with zein to achieve electrospun mats that are easier to handle. For instance, Dippold et al. have demonstrated electrospinning of blends of poly(glycerol sebacate) (PGS) and zein in acetic acid solutions [443]. The PGS-zein fibres were flat with diameters in the 300-350 nm range. The composite scaffolds were proposed for the development of tissue engineered cardiac patches. Hu et al. produced oriented zein/PCL blend fibres by dissolving zein and PCL together in DMF, acetic acid and DCM, and using a rotating drum as the collector [444]. With the increasing content of PCL, diameter of fibres decreased, but tensile strength increased from 1.54 MPa to 5.18 MPa, and elongation at break increased from 1.65% to 27.5%. The improvement of the mechanical properties was explained by partially miscibility of zein and PCL, as confirmed by change in shift of glass transition temperature. Researchers used this system to load poly (ε-lysine) and found that, with the loading of poly (ε-lysine), hydrophilicity of fibres was increased, and fibres showed successful antibacterial properties against L. monocytogenes, which made them potential candidates for tissue engineering and drug delivery applications.

Apart from synthetic polymers, several studies have been done on combining natural polymers with zein. For instance, Yang et al. produced zein/gelatin fibres by dissolving them in 1,1,1,3,3,3-hexafluoro-2-propanol (HFIP) and then electrospinning [445]. After blending with gelatin, fibre diameter increased remarkably from 69±22 nm (pure zein) to 950±356 nm (zein/gelatin ratio: 2/1). Mechanical properties were greatly improved with 138% raise in tensile strength and 278% raise of elastic modulus. Biocompatibility was also improved due to the binding and hydrophilicity of gelatin. A recent study on using zein/gelatin blend compared two film fabrication methods, electrospinning and solvent casting [446]. In the study 1:1 w/w zein and gelatin were dissolved in acetic aqueous solution, and then either electrospun or air-dried into films. The study showed that phase separation took place in solvent casting method while solution remained homogeneous during electrospinning. To further improve the mechanical property, crosslinking could be used, as demonstrated by Deng et al. [447]. Zein, gelatin, and 5% glucose (crosslinker) were dissolved in acetic aqueous solution. Crosslinking took place in the oven after electrospinning. No obvious change in fibre morphology was observed after crosslinking. FTIR results confirmed the bonds forming between carbonyl groups of glucose and amino groups of proteins, which helped to improve thermal stability and mechanical properties. Antimicrobial ultrathin

zein-based nanofibres have also been produced from blends of zein with chitosan [448]. The study found that the compatibility of zein and chitosan can be increased by the addition of polyvinyl pyrrolidone.

In the past five years, studies have produced bi-layered or tri-layered electrospun fibrous membrane to enhance drug release and mechanical properties by alternating different solutions during electrospinning to obtain different layers[449][450][451]. For instance, a salicylic acid loaded bi-layered membrane was designed for tissue engineering purpose [449]. The first layer was composed of chitosan, zein, and salicylic acid, to obtain anti-inflammatory and antimicrobial properties. The second layer was composed of PCL and hyaluronic acid to provide mechanical support and physical barrier. The membrane showed good biocompatibility and active antibacterial action for 5 days. Salicylic acid showed a burst release from the membranes, followed by slow release which could favour elimination of bacteria when first applied and inhibits bacterial growth later. A more recent study produced tri-layered zein/PCL for the controlled release of tetracycline [451]. Tetracycline was loaded by dissolving tetracycline, PCL, and zein together in 2,2,2-trifluoroethanol (TFE)/DCM for electrospinning and it was only loaded in the middle layer. The tri-layered membrane showed slow release of tetracycline, and good antibacterial property against S. aureus *in-vitro* and *ex vivo* on pig skin, as well as good biocompatibility. The study found that adding PCL increased the diameter of fibres because of the increase of viscosity. Interestingly, this was inconsistent with a PCL/zein blend study mentioned earlier in this section [444]. The variation in fibre size could be caused by different collectors used in the two studies.

4.2.6. Polyethyleneimine (PEI) and its use in electrospinning

PEI, with its high density of primary, secondary and tertiary amine groups, has been used in the synthesis and surface modification of electrospun fibres for different applications, for instance, ion sensor[452] [453] [454], tissue engineering [455] [456], cancer cell capture [457] [458], CO_2 capture [459], catalysts [460], biological imaging [461], gene delivery[462] [463] [464].

Uzel et al. used PEI and Al_2O_3 nanoparticles to modify polysulfone (PSF) nanofibres [465]. The adding of PEI and Al_2O_3 decreased diameter of fibres by decreasing solution viscosity and increasing conductivity. Though FTIR showed no reaction and interaction between PSF and PEI, a new C=O bond was introduced by Al_2O_3 nanoparticles. The new bond partially explained the improvement of mechanical properties. Other explanations for the improvement include the coupling effect of PEI with nanoparticles and PSF, and the reinforcement due to the nanoparticles.

PEI has been combined with PVA to immobilise active agents via a facile approach in several studies [456] [459] [465]. In this approach, electrospun PVA/PEI was crosslinked with glutaraldehyde (GA) vapour first to increase water stability, as demonstrated by Fang et al. [466]. Heated fibres were immersed in GA solution and also exposed to GA vapour in a desiccator. FTIR results showed that crosslinking happened through interaction between GA aldehyde groups and hydroxyl/amino groups of PVA/PEI. It also showed that primary amines of PEI remained after crosslinking, which were responsible for a fast methyl blue dye absorption in the study. Due to the availability of PEI's primary amines, PEI here not only provided active sites for crosslinking, but was also used to bind active agents. Zhao et al. immobilized lactobionic acid (LA), a targeting agent for hepatocellular carcinoma (HCC) cells, onto crosslinked PVA/PEI electrospun fibres via PEG spacer [458]. LA was modified with NH_2-PEG-COOH to form LA-PEG-COOH conjugate, and then reacted with amines through an N-(3-dimethylaminopropyl)-N'-ethylcarbodiimide hydrochloride (EDC)/N-hydroxysuccinimide (NHS) coupling reaction. Similar study was also done by Fan et al. immobilizing folic acid for cancer cell detection [457]. In both studies, smooth and uniformed fibres were produced with active agents successfully attached on fibres surface, as proven by FTIR.

Recently, Hu et al. *in-situ* generated Au/Ag nanoparticles inside PVA/PEI nanofibres for catalytic applications [460] with a process similar to Chen et al. [442], as described in the last section. Crosslinked electrospun PVA/PEI fibres acted as nanoreactors to generate Au/Ag particles using $HAuCl_4$ and $AgNO_3$ as precursors (Figure 56). Bimetallic nanoparticles with average diameter of 4.9±1.8 nm were observed both on the surface and inside the fibres using TEM, indicating the diffusion of $AuCl_4^-$ and Ag^+.

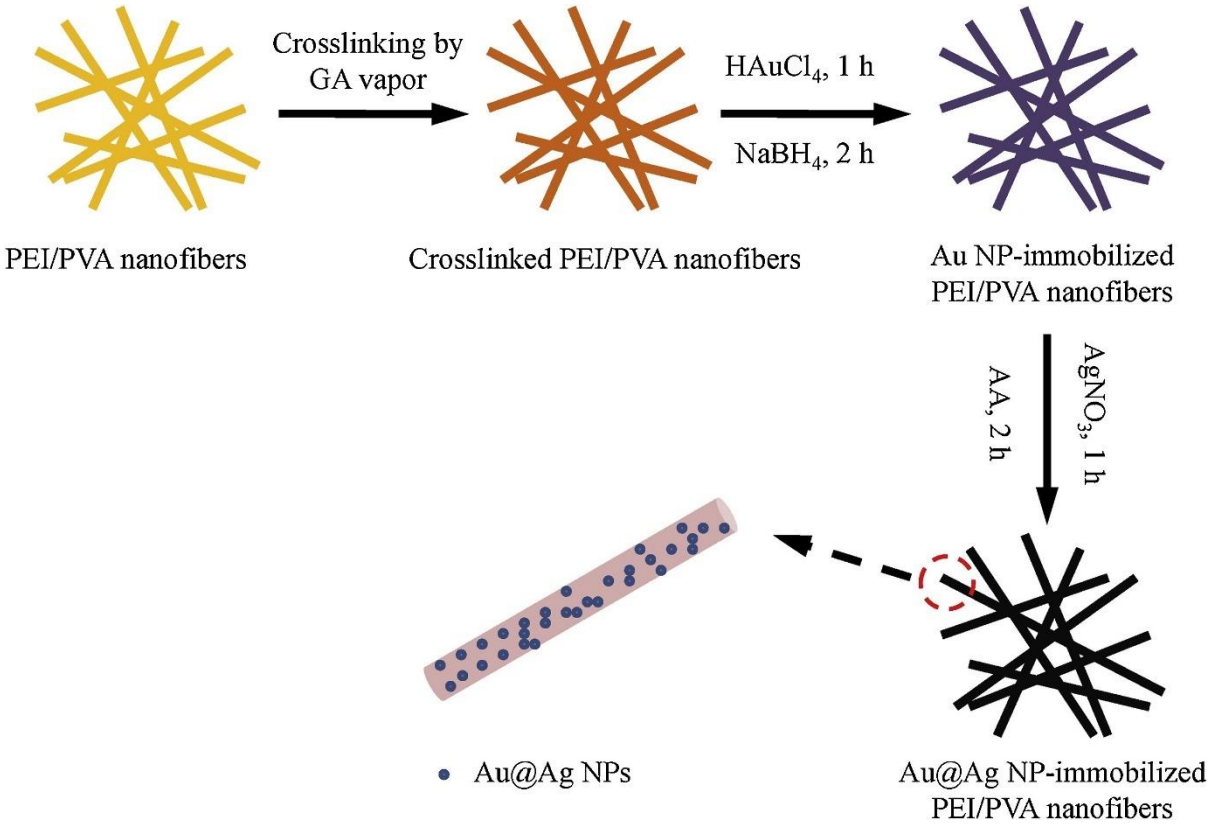

Figure 56 Schematic of the formation of Au/Ag nanoparticles immobilized onto electrospun PVA/PEI nanofibres [460]**.**

4.2.7. Summary

Loading Zinc oxide nanoparticles in electrospun fibres has recently seen widespread studies for a variety of biomedical and electrical applications due to its antibacterial properties and conductivity. In general, thermal decomposition, chemical vapour deposition, and precipitation method can be used to synthesise zinc oxide nanoparticles from zinc acetylacetonate and passive loading is the most common method to combine them into electrospun fibres. Here, zinc oxide was synthesised via *in-situ* hydrolysis and PEI was chosen as polymer matrix. A natural protein, zein, was chosen to be the electrospun material. Properties and applications of zein and PEI were also reviewed here.

4.3. Experimental methods

4.3.1. *In-situ* production of micro-suspensions of ZnO nanoparticles

The PEI used in this study is grade b-25 kDa, Mn = 10,000 Da; Mw = 25, 000 Da, obtained from Sigma Aldrich. This is represented with a raw formula $[CH_2-CH_2)_{11}(NH_2)4(NH)_3N_4]_n$ where n ~ 20. This can be schematically represented with a graphical structure where each repeating unit contains short branches, both linear and bifurcated, with terminal NH_2 groups.

The details for the *in-situ* production of ZnO nanoparticles within the PEI matrix at NH_2:Zn ratio equal to 2:1 (low ZnO content) and NH_2:Zn = 1:1 (high ZnO content) are as follows:

2.5 mmol amount of zinc acetylacetonate hydrate were dispersed in 30 ml ethanol at room temperature and mechanical stirred to form a milky suspension. A 2.5 w/v% PEI/ethanol solution was mixed with the suspension of ZnAcAc at the two NH_2:Zn ratios indicated above and then heated up to 80 ºC under gentle steering conditions and reacted for 16 hrs. The reaction product was poured into a shallow PTFE evaporation dish and allowed to dry for 48 hrs in a fume cupboard to collect the solvent free micro-suspension of ZnO nanoparticles in PEI.

4.3.2. Electrospinning zein/PEI/ZnO fibres

Both PEI/ZnO micro-suspensions and pure PEI were mixed with zein at weight ratio 3:1 and dispersed in ethanol/water mixtures (7/3 v/v) at room temperature to form 30 w/v% micro-suspensions. A 30 w/v% solution of zein in ethanol/water was also prepared and used as the main control sample.

Electrospinning of the fibres was then carried out at room temperature with an apparatus manufactured by Linari Engineering, which was run under an applied voltage of 18 kV and a flow rate of 1 ml/h and setting the tip-to-collector distance from the end of the needle at 15 cm. The syringes used have a 1 mL capacity with a 21G needle with a length of 80 mm and a bore diameter of 0.6 mm. At the stated flow rate the exit velocity of the jet is around 0.4 mm/s.

4.3.3. Characterisation methods

4.3.3.1. Morphology studies

Field emission scanning electron microscopy (FE-SEM, Joel 7800) was used to study the morphology of ZnO nanoparticles /PEI micro-suspensions and electrospun fibres. Samples were coated with Au/Pb for 60 s. Energy dispersive X-ray spectroscopy (EDS) was used to determine the present of zinc. For observation, the applied voltage was set at 5 kV and for EDS was set at 15-20 kV. Inlens SEM (Zeiss) was used to have clearer images of ZnO nanoparticles on the surface at 10 kV.

4.3.3.2. X-ray diffraction (XRD)

X-ray diffraction (XRD) was used to determine the presence of ZnO in micro-suspensions in the 2θ range of 20° to 70°. Applied voltage was set at 20 kV and CuKα radiation of 8.04 keV and wavelength of 0.154 nm was used.

4.3.3.3. Differential scanning calorimetry (DSC)

Thermal characterisation of the mats was conducted using differential scanning calorimetry (DSC Q200, TA Instruments Calorimetric Analyser) in a nitrogen atmosphere with a flow rate of 50 ml/min. Approximately 9 mg of each type of mat was sealed in an aluminium pan and experienced a heating-cooling-heating cycle from 0 to 200 °C at 10 °C/min. Empty aluminium pans were used as reference. Data were analysed using the TA universal analysis software. All the reported values are the average of 3 samples.

4.3.3.4. Thermogravimetric analysis (TGA)

Thermogravimetric analysis (TGA) was conducted in a nitrogen atmosphere, from room temperature (25ºC) to 800 ºC with a heating rate at 10 °C/min. Approximately 10 mg of each type of mat were used.

4.3.3.5. Fourier transform infrared (FTIR)

Attenuated total reflection-fourier transform infrared (ATR-FTIR, IRTracer-100, Shimadzu) and FTIR was conducted to detect the chemical change of PEI. All spectra with 4000-1000 cm^{-1} were recorded

4.3.3.6. Mechanical test

For analysis of mechanical properties, the fibrous mats were detached from the aluminium foil and cut into 20mm×4mm size. Tensile tests were carried out using a single column table top Instron system at room temperature. The rate of extension was set at 1 mm/min for easy observation of fragile materials. Side action grip clamps with flat jaw faces were used.

4.4. Results and discussion

4.4.1. Characterisation of ZnO/PEI micro-suspensions

4.4.1.1. SEM characterisation of *in-situ* generated ZnO

Figure 57 and Figure 58 show SEM images of as prepared ZnO/PEI micro-dispersions with different ZnO concentrations. Low concentration sample showed much less density and better dispersion of ZnO NPs comparing with high concentration samples. As proven by EDS mapping and spectrum, bright spots in the SEM images

(Figure 57(a) and Figure 58(a)) are believed to be agglomerates of ZnO nanoparticles. To obtain a closer look and better estimation of particle sizes, PEI matrix was washed once with ethanol, and In-lens SEM was used, shown in Figure 58.

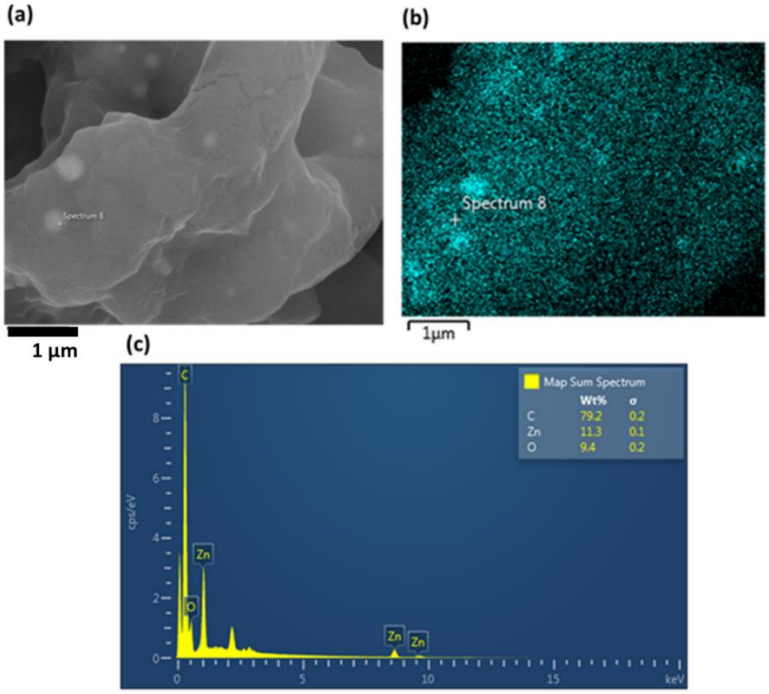

Figure 57 SEM (a) and EDS mapping (b) and (c) of as prepared in-situ generated low concentration ZnO/PEI micro-dispersion.

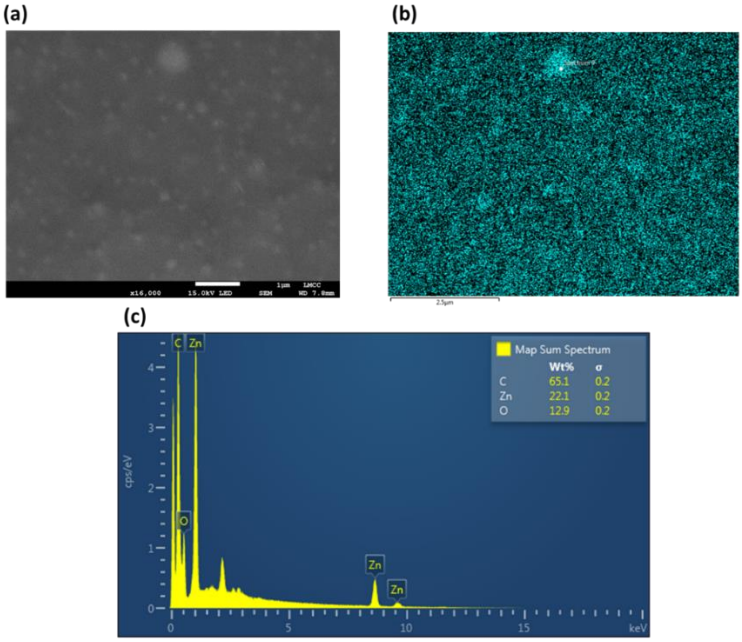

Figure 58 SEM (a) and EDS mapping (b) and (c) of as prepared in-situ generated high concentration ZnO/PEI micro-dispersion.

The In-lens SEM micrographs show that the ZnO nanoparticles, for the low concentration samples, have a spherical shape, while those of the high concentration samples are irregular with a higher incidence of larger agglomerates. The analysis has also revealed a discrepancy for the size and the size distribution of the ZnO nanoparticles in the two samples. The average diameter of the nanoparticles formed in the samples at low ZnO concentration is (121±44) nm, while for the sample at high ZnO concentration the recorded value is (163±51) nm.

The presence of more PEI in the low concentration sample seemed to slow down the ZnO NPs formation. This could be caused by steric effect of PEI. Previous studies [401], [403], [467] have found that ZnO crystals formed by hydrolysis of zinc acetylacetonate show nanowire/nanotube shape. The further growth of these nanowire/nanotube ZnO could explain the irregular shape of ZnO NPs in high concentration sample.

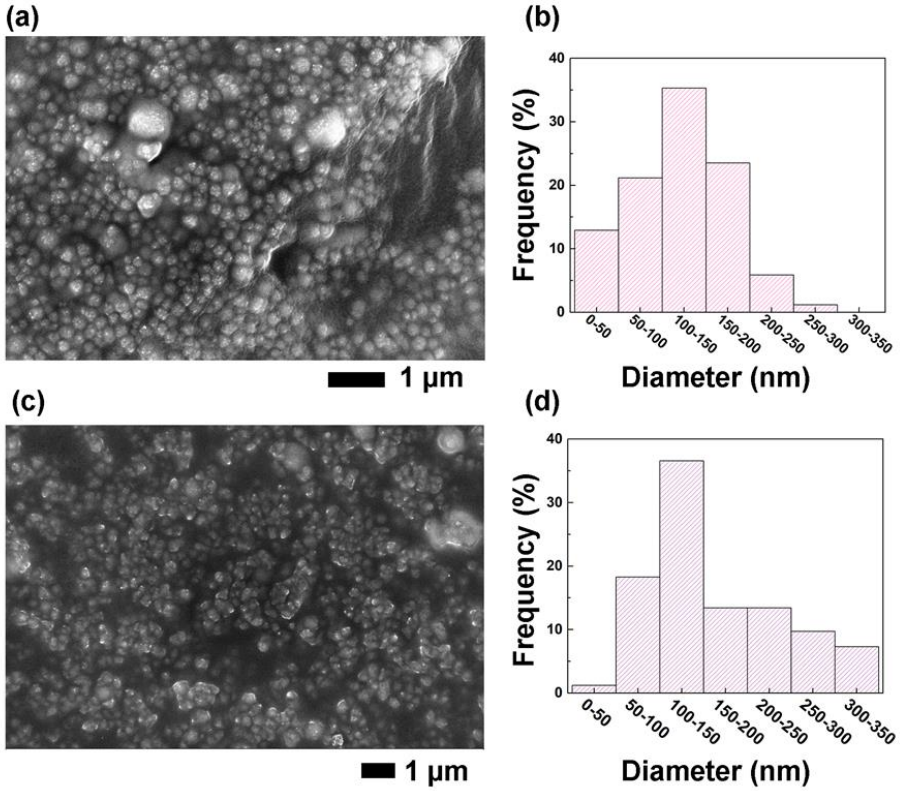

Figure 59 SEM images of in-situ generated ZnO/PEI micro-dispersion and size distribution of nanoparticle agglomerates: (a) and (b) are images for samples at high ZnO concentration. (c) and (d) are corresponding images at low ZnO concentration.

In Figure 60, SEM images at different magnifications are shown for the dried residue obtained in the “control synthesis” experiments conducted in ethanol solution of ZnAcAc.2H_2O without PEI, reacted under the same conditions (i.e. heating for 16 hours at 80 ^oC) and at concentration equivalent to that used to obtain the higher ZnO content for the synthesis in a PEI matrix. Only few ZnO particles are formed from the original ZnAcAc.2H_2O, which are clearly seen as large crystals in the background formed by recrystallisation while drying the reaction products at room temperature.

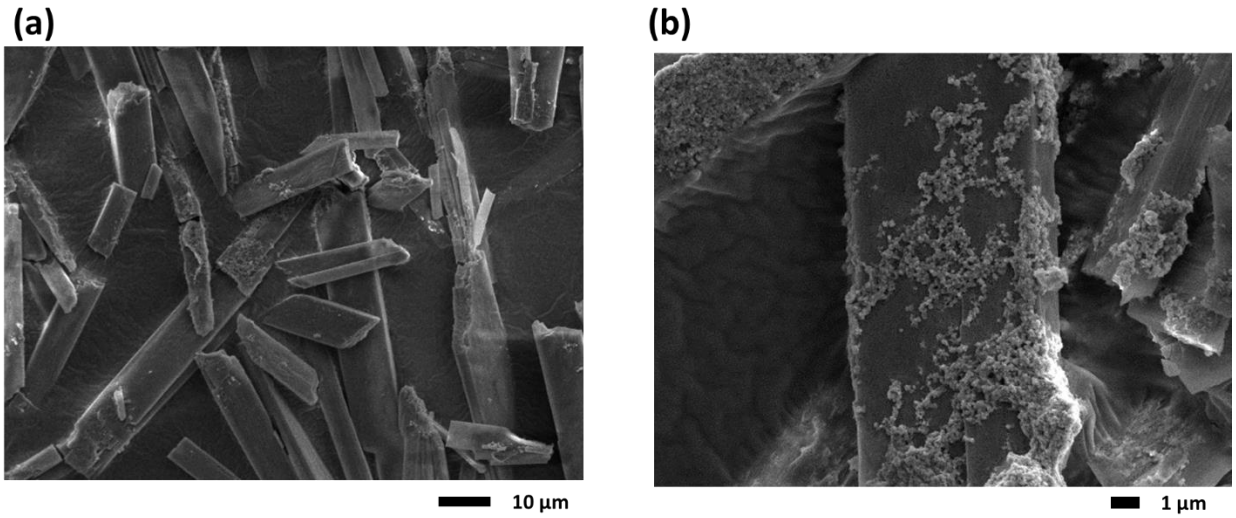

Figure 60 SEM micrographs of ex-situ ZnO particles produced without PEI at high ZnAcAc.2H_2O content. This figure has been accepted to be published on ACS Applied Polymer Materials [390].

4.4.1.2. XRD characterisation of *in-situ* generated ZnO

Since the ZnO is embedded inside the amorphous PEI matrix, the obtained XRD patterns are slightly noisy, especially for the low concentration sample (Figure 61). However, peaks can still be identified at 31.4°, 34.0°, 35.8°, 47.1°, 56.2°, 62.3°, and 67.6° for high concentration sample and 32.0°, 34.6°, 36.5°, 56.7°, 63.0°, and 67.6° for low concentration sample. These peaks correspond to (100), (002), (101), (102) (missing in low concentration sample), (110), (103), (112) planes, which are assigned to the wurtzite-type hexagonal ZnO crystal structure. The missing of (102) peak for low concentration sample could be caused by the submergence of the peak and the

noise. Notably, there is a peak at 27.7° for the low concentration sample, this may be assigned to ZnAcAc, as seen in a previous study [468]. XRD results confirmed successful conversion of ZnAcAc to ZnO.

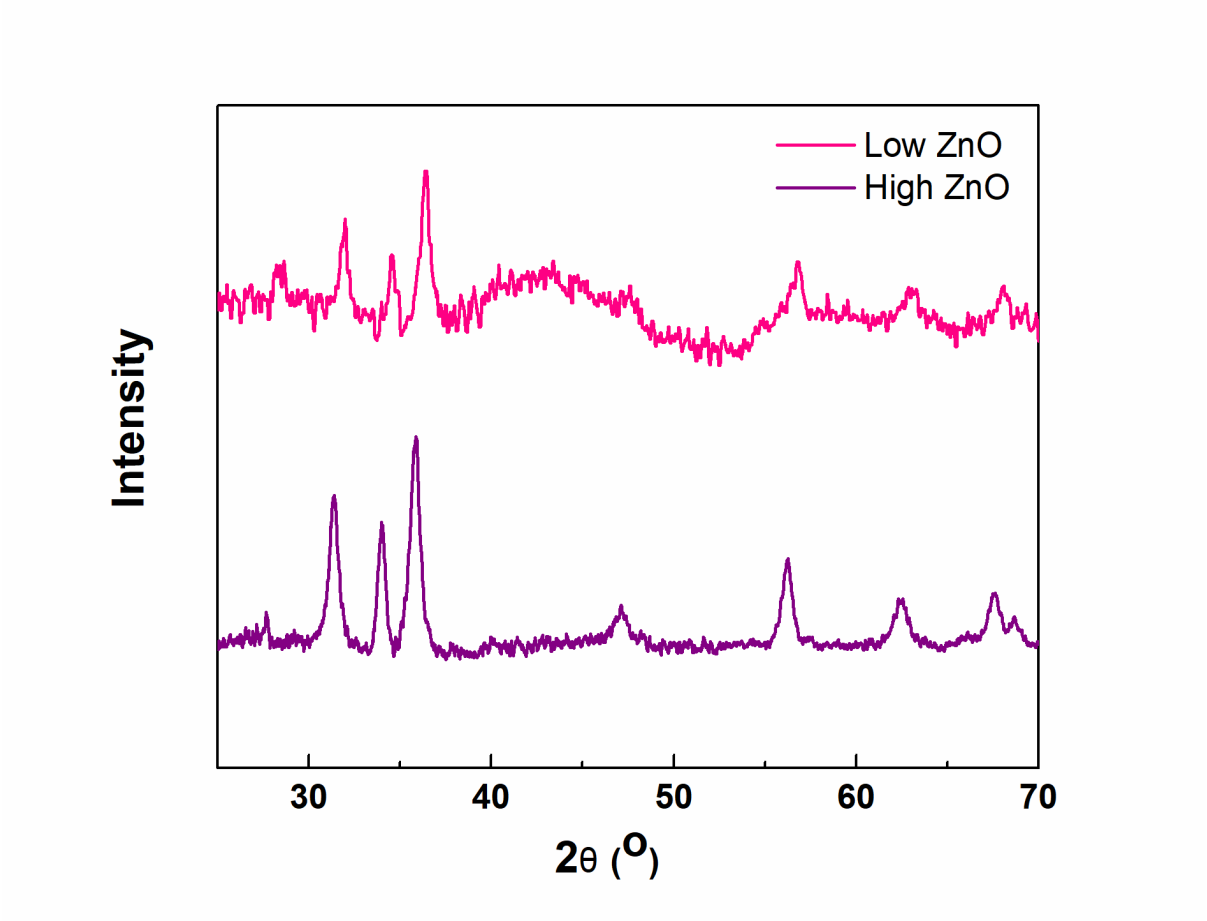

Figure 61 XRD spectra of high and low concentration ZnO nanoparticle micro-suspensions. This figure has been accepted to be published on ACS Applied Polymer Materials [390].

4.4.1.3. Chemical characterisation of ZnO/PEI micro-suspensions

The FTIR spectra obtained on the micro-suspensions of ZnO in PEI are shown in Figure 62 and the relevant absorption peaks are summarised in Table 5. The FTIR spectra show that the characteristic peaks of PEI within the absorption band in the range 1700 - 1500 cm^{-1} shift to lower wave numbers takes place for the samples containing ZnO particles.

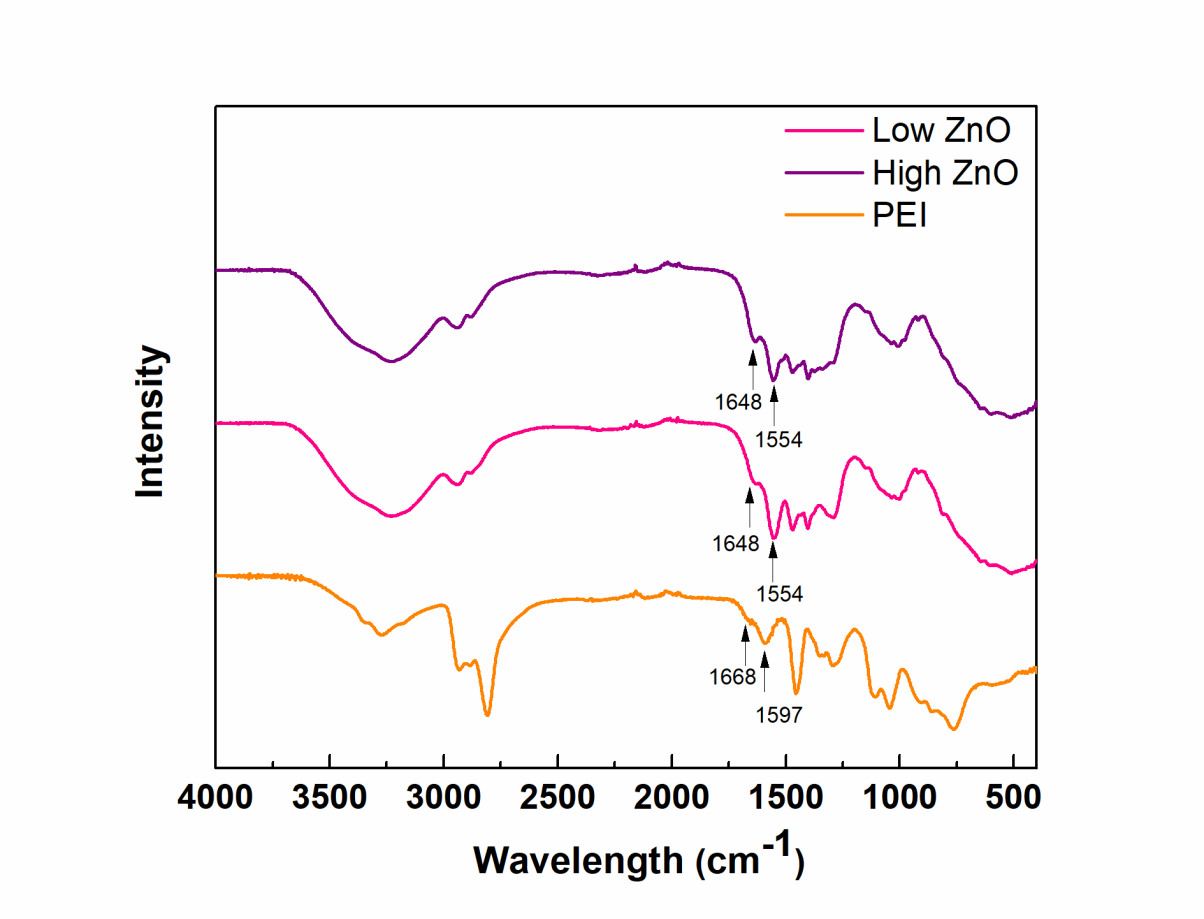

Figure 62 FTIR spectra for micro-suspensions of ZnO in PEI. This figure has been accepted to be published on ACS Applied Polymer Materials [390].

These data can be taken as evidence for the presumed interfacial interactions in accordance with the mechanism outlined in Figure 63, supported from data reported by other authors on comparable systems. Similar interactions of NH_2 groups have been identified for polyacrylamide with $Zn(OH)_2$, where a corresponding shift was observed in the absorption peak from 1610 cm $^{-1}$ to 1600 cm $^{-1}$ [31]. For a composite containing ZnO nanoparticles dispersed in a matrix consisting of a mixture of polypyrrole and chitosan, a downward shift has been noted from 1708 cm $^{-1}$ to 1654 cm $^{-1}$, which was also attributed to interfacial interactions [32].

Table 5 Summary of relevant absorption peaks (cm^{-1}) for micro-suspensions of ZnO nanoparticles in PEI.

PEI	PEI/high ZnO content	PEI/low ZnO content
1668	1648	1648
1595	1556	1556

The systems of the present study can be considered to be closer to the first example insofar as it can be argued that under the basic conditions imposed by the presence of PEI, pH around 10 -12, the surface layers of ZnO contain large proportions of hydrated negatively charged zinc hydroxide moieties, such as $Zn(OH)_3^-$ [33], which are capable of producing ionic interactions with the slightly positively charged -NH_2 groups within the short branches along the backbone chains of PEI. It should also be noted that the expected peak at 1716 cm^{-1} for the C=O band in ZnAcAc has not been identified in the spectra of either micro-suspensions.

Zinc acetyl acetonate dihydrate (ZnAcAc) was used as the precursor material for producing Zinc oxide according to the reaction

$$(CH_3CO{=}CHCOCH_3)_2Zn{\cdot}2H_2O = 2\ CH_3COCH_2COCH_3 + ZnO + H_2O \quad (1)$$

The formation of ZnO particles within the PEI matrix is expected to take place through successive steps, namely (a) the decomplexation of $ZnAcAc \cdot 2H_2O$ comprising the formation of soluble intermediates and (b) the nucleation and growth of ZnO nanoparticles, according to the scheme presented in Figure 63.

The diagram in Figure 63 indicates that decomplexation of $ZnAcAc.2H_2O$ takes place owing to its intrinsic instability and that the conversion to ZnO occurs at faster rate due to the basic environment conditions provided by the multitude of accessible NH_2 groups in the PEI. The formation of unstable soluble intermediate products provides the required conditions for a self-assembling of hydrated ZnO nuclei into a spatial configuration favourable for the formation of stable Wurtzite crystals, through stacking sequences into a tetrahedral geometry for the growth into structurally stable hexagonal faced platelets. It should be noted, however, that the high density of ZnO crystals (d = 5.6 g/cm^3) makes it very difficult to obtain stable suspensions in a liquid medium of much lower density unless they are strong interfacial interactions, which

is the reason for choosing a multifunctional polyamine as the matrix medium for the resulting micro-suspension.

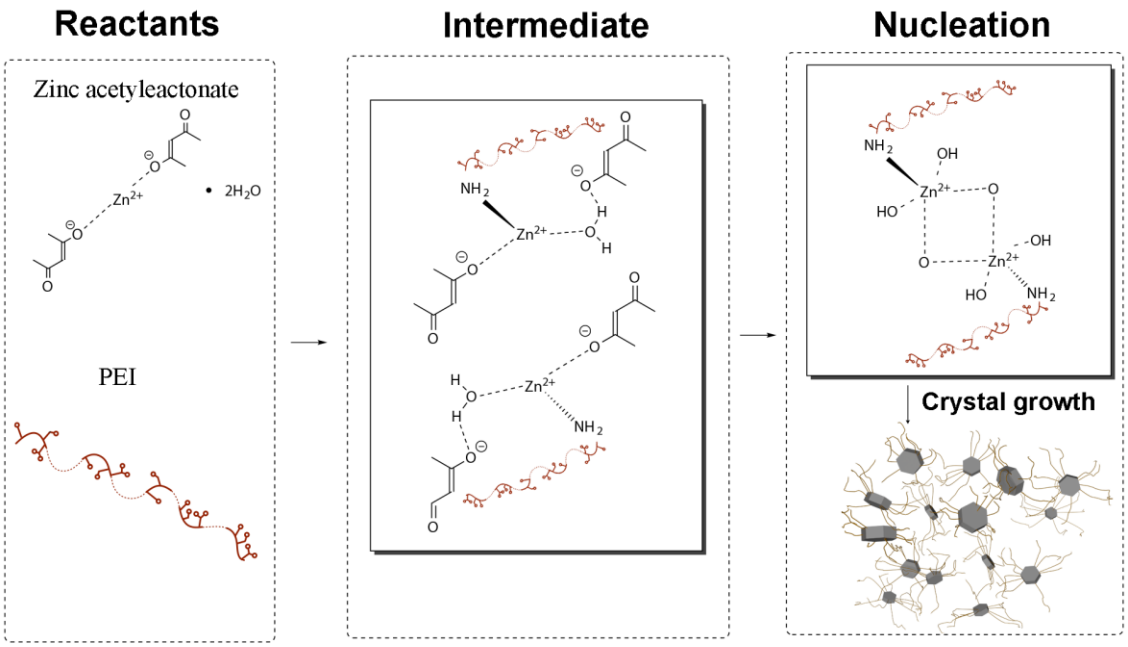

Figure 63 Schematic illustration of the production of ZnO nanoparticles within the PEI matrix. This figure has been accepted to be published on ACS Applied Polymer Materials [390].

4.4.2. Characterisation of electrospun zein/PEI/ZnO fibres

4.4.2.1. Morphology study

SEM images taken for the fibres produced from mixtures of PEI and ZnO/PEI micro-spensions with zein are shown in Figure 64, and a graphical presentation of the corresponding analysis of the fibre diameter is Figure *65*. All fibres were free of beads and displayed an average diameter in the region of 1.62 μm for zein, 0.66 μm for zein/PEI, 1.25 μm for zein/PEI/high ZnO and 1.06 μm for zein/PEI/low ZnO. Notably, the lowest fibre diameter is exhibited by the mixture zein/PEI followed by the system with the lowest ZnO content. These could be affected by the expected lower viscosity of the spinning solution. [245].

From an examination of the data in Figure 64 and Figure *65* it is noted that not only the diameter is different but also the shape of the cross-sectional area varied considerably for the four types of fibres produced. The fibres obtained from the “neat” zein system were ribbon-shaped. This is caused by the formation of a rigid skin as the result of the rapid evaporation of the solvent in the outer layers of the jet, which prevents the occurrence of a homogeneous shrinkage with further solvent evaporation from the inner sections. The rigid skin effect causes the original circular cross section to become first elliptical and then flat as a way of accommodating the reduction in cross-section area without further reduction in the perimeter [358], [380], [469]. It is interesting to note that the incorporation of PEI in zein gave rise to the formation of fibres more cylindrical in shape, while the presence of ZnO nanoparticle as PEI micro-suspensions in the fibres tended to reverse this feature to a ribbon-shaped cross-section. The SEM images for the zein/PEI fibres reveals also the high incidence of splays connecting adjacent fibres.

Previous studies on the electrospinning of PCL fibres containing ZnO nanoparticles have suggested that, at low concentration, ZnO nanoparticles could assist the accumulation of charges on the surface of the jet, thereby decreasing the fibre diameter and narrowing the size distribution. Higher ZnO concentrations (over 1% wt) gave rise to the formation of fibres with larger diameter, which was attributed to the agglomeration of nanoparticles [411]. However, the agglomeration of particles can also be expected to have the opposite effect through a concomitant reduction in the viscosity of the fluid, which can in turn reduce the incidence of splays within in the formation of the fibres [245], [358].

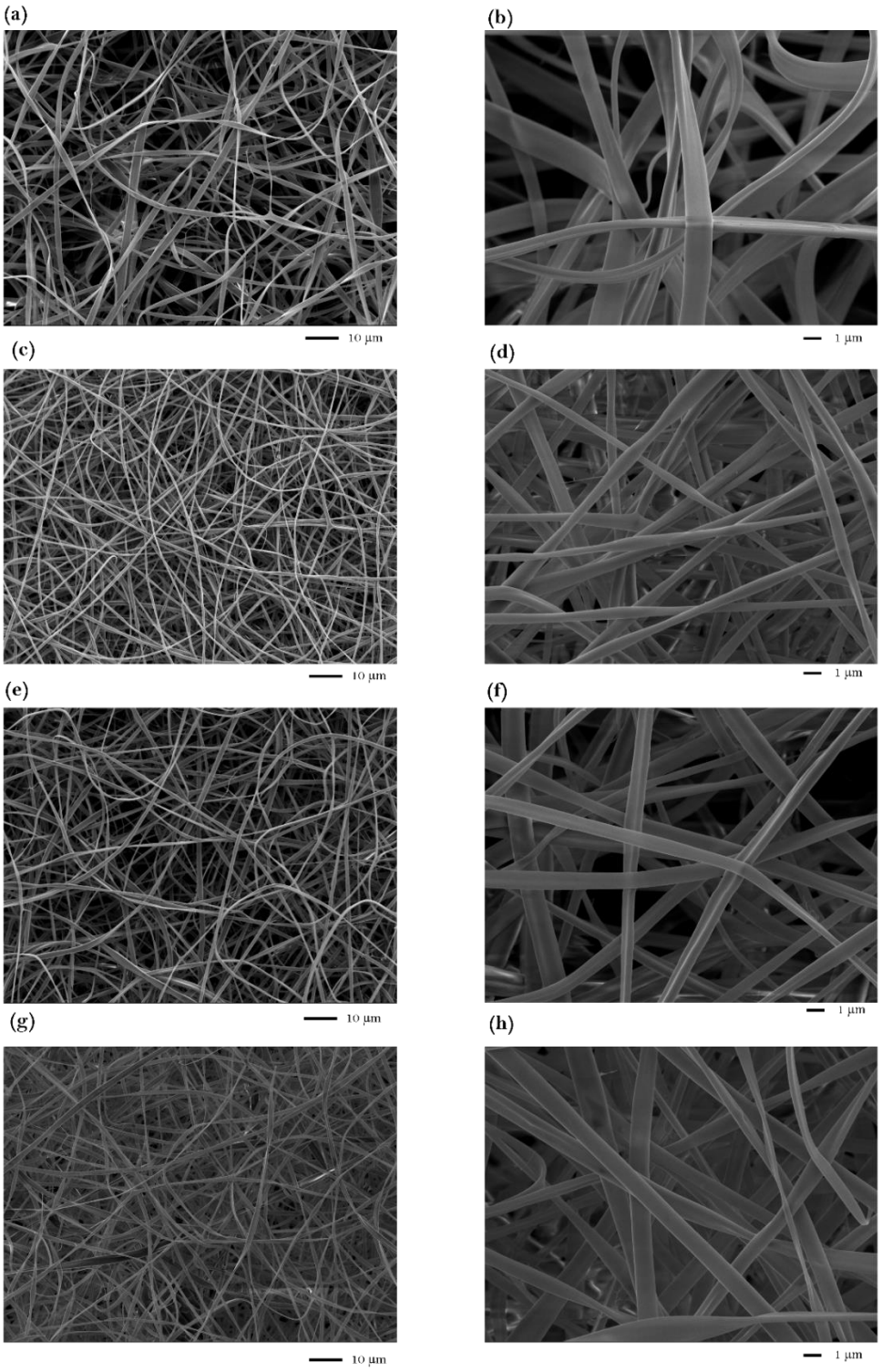

Figure 64 SEM figures of electrospun zein fibres (a) and (b), zein/PEI fibres (c) and (d), zein/PEI/Low ZnO fibres (e) and (f), zein/PEI/High ZnO fibres (g) and (h). (b), (d), (f) and (h) have been accepted to be published on ACS Applied Polymer Materials [390].

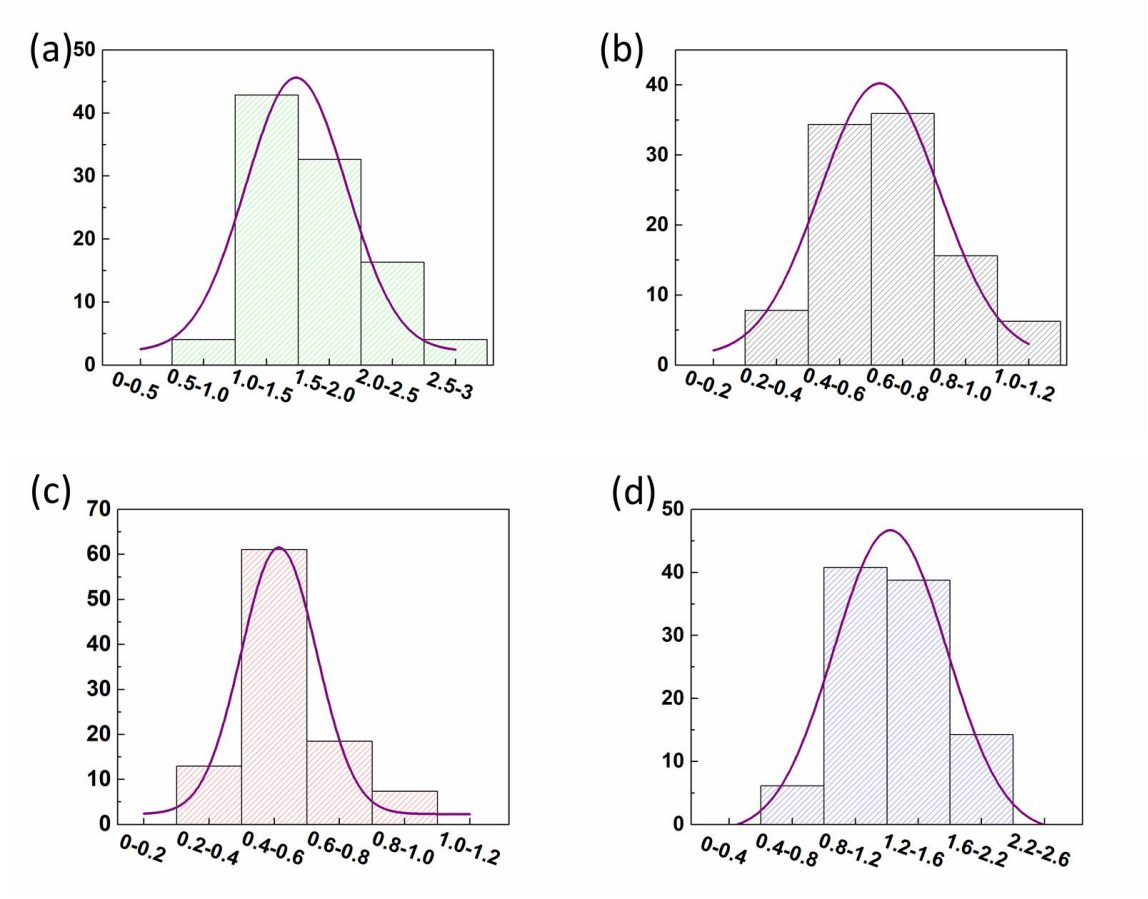

Figure 65 Analysis of fibre diameter distribution: zein fibres (a), zein/PEI fibres (b), zein/PEI/Low ZnO fibres (c), zein/PEI/High ZnO fibres (d).

4.4.2.2. Thermal study

The DSC thermograms in Figure 66 show the plasticisation effect of PEI on zein, which can be attributed to the strong interactions of NH_2 groups of PEI with the COOH groups of the constituent amino acids. It is noted that the presence of ZnO in the two PEI plasticised systems not only exhibit higher glass transition temperatures due to the lower PEI content but display also a narrower transition range, which is analogous to the behaviour exhibited by the fibres produced from unmodified zein. Furthermore, the presence of ZnO restores part of the small endotherm at the upper end of the glass transition exhibited by the unmodified zein fibre, which is associated with the erasing of physical ageing, which is a behaviour often found in DSC scans of glassy polymers [470]. At the same time, one notes an increase in the gradient of the DSC trace before the onset of the glass transition for the samples containing only

PEI and the total disappearance of the physical ageing feature. Insert in Figure 66 shows comparison of zein/PEI samples dried at ambient and dried at 80 °C in oven for 1 hour. Gioia et al. previous showed that water had plasticising effect on zein [422]. The drying test is to show that the solvents in electrospun samples were totally evaporated before DSC test. Since there was no obvious difference between two samples, it could be proven that plasticising effect was only caused by PEI.

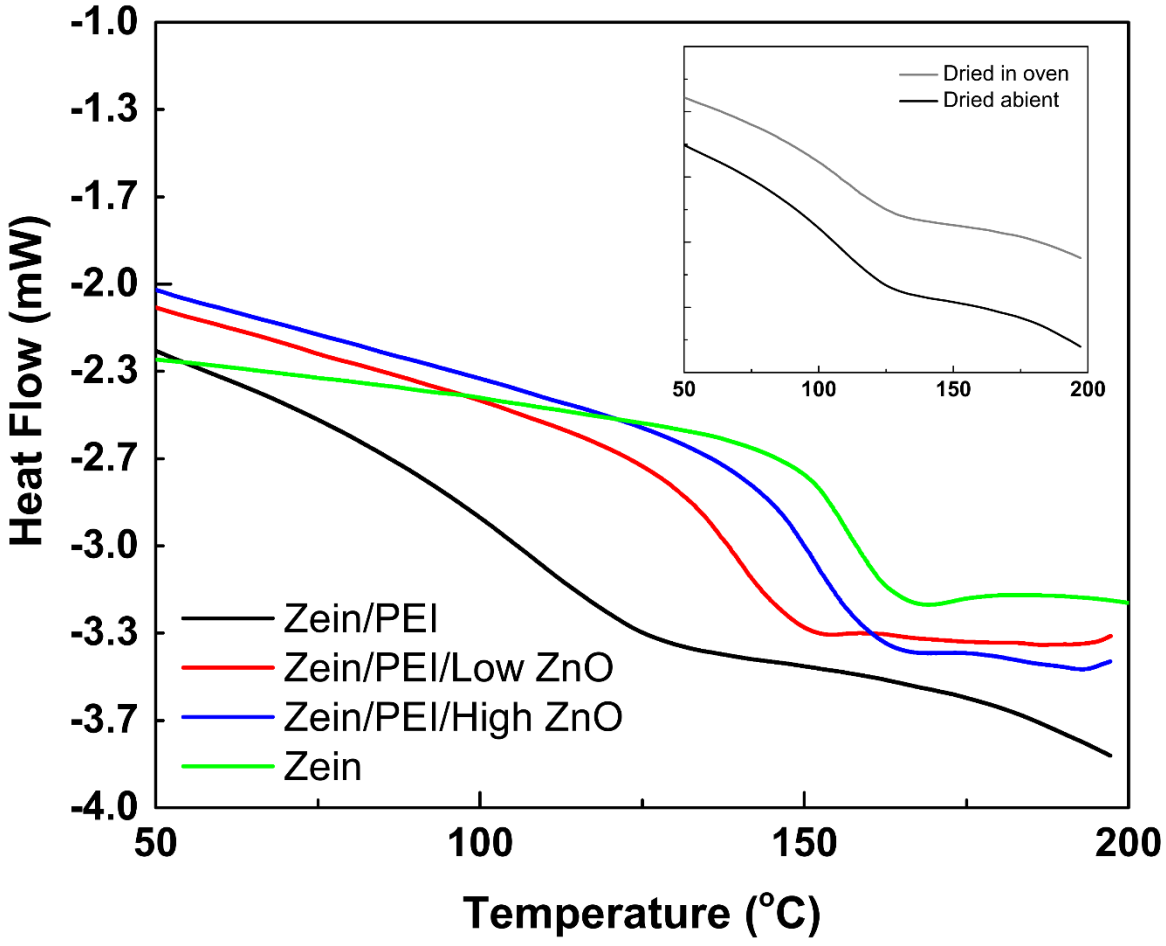

Figure 66 DSC curves of electrospun fires of zein, zein/PEI, zein/PEI/low ZnO, and zein/PEI/high ZnO. This figure has been accepted to be published on ACS Applied Polymer Materials [390].

The corresponding glass transition temperature (T_g) values, taken at the transition "mid-point" of the DSC traces, are respectively (165.1±1.8) °C for zein, (125.6±0.8) °C for zein/PEI, (147.8±1.9) °C zein/PEI/low ZnO and (160.6±1.0) °C zein/PEI/high ZnO.

The TGA data are presented in Figure 67. These show that the initial weight loss at temperatures up to about 100 °C, due to the evaporation of residual solvent, and the subsequent plateau at temperatures in the region of 200 – 250 °C both increased with the amount of PEI present in the fibres. The peak temperature for the derivative weight/time are shown in the corresponding thermograms.

The derivative TGA curves show that the starting point of first decomposition step for all electrospun fibres occurs at around 250 °C. For the electrospun zein fibres the first rate of decomposition peak was found at 321 °C, which is consistent with the results from previous studies [471]. The addition of PEI to zein causes this peak to become broader and to shift towards lower temperatures. Since the incorporation of ZnO nanoparticles does not change the position of these two peaks, it is deduced that the presence of ZnO encapsulated in a PEI-rich matrix does not affected the thermal decomposition kinetics of the fibres under anaerobic conditions. Accordingly, the reduction in loss of volatiles at temperatures above 350 °C displayed by the sample with high ZnO can be attributed the obstacles imposed to the diffusion of volatiles in the presence of such particles, which is a typical behaviour displayed by nanocomposites [384]. This explanation is supported by the observation that the residue at 800 °C (not shown) for the sample with the higher ZnO content was ~ 9 w%, whereas the lower ZnO content was undistinguishable from the other samples within the range 3-5 w%.

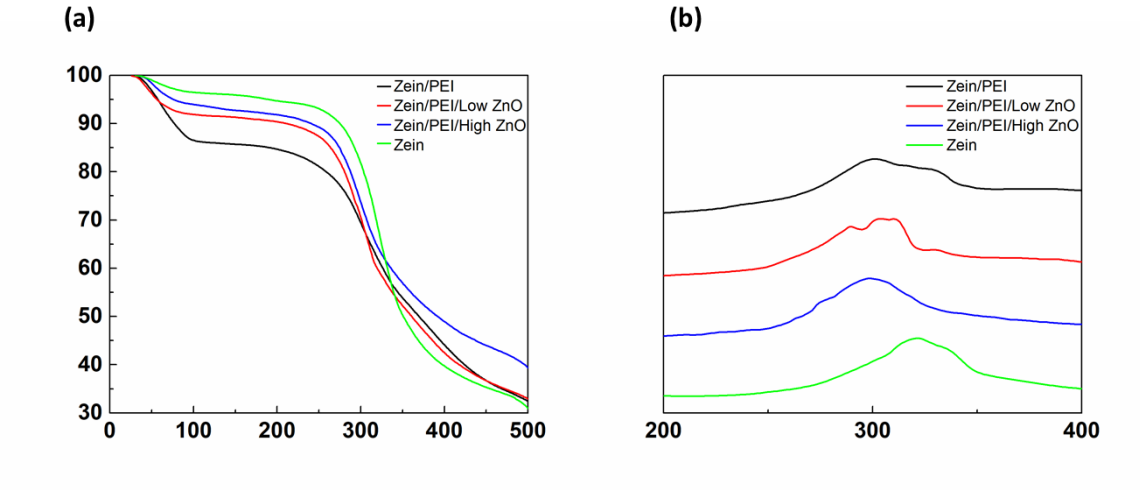

Figure 67 TGA thermograms for weight (left) and derivative weight/time (right) of electrospun fibres: zein (green), zein/PEI (black), zein/PEI/low ZnO (red) and zein/PEI/high ZnO (blue). This figure has been accepted to be published on ACS Applied Polymer Materials [390].

4.4.2.3. Mechanical study

Tests on fibres produced from pure zein solutions were not carried out as the mats were too fragile to handle. Average yield stress of Zein/PEI, Zein/PEI/low ZnO, and Zein/PEI/high ZnO were found to be 1.0, 0.8, and 0.2 MPa. Average elongation at break of three samples were found to be 6%, 7%, 14%, respectively.
Zein/PEI/low ZnO samples exhibit the lowest scatter in the stress -extension curves, while the high ZnO system exhibits a much higher ductility, associated with the higher compliance of the fibres mats. The implications are that, although the onset of fracture occurs at lower tensile loads in the presence of agglomerated ZnO nanoparticles, the onset of fibre breakage takes place at higher extensions, which would allow the mats to bend over larger angles without fracture. The behaviour displayed by this system would be beneficial for applications requiring easily tearing mats, which would be supported by eternal fastening such as microporous tapes. The higher consistency of data for fibres containing ZnO can also be related to the residual acetylacetone that could have a “stabilizing role” on the fibre consolidation stage through an attenuation of the solvent evaporation rate.

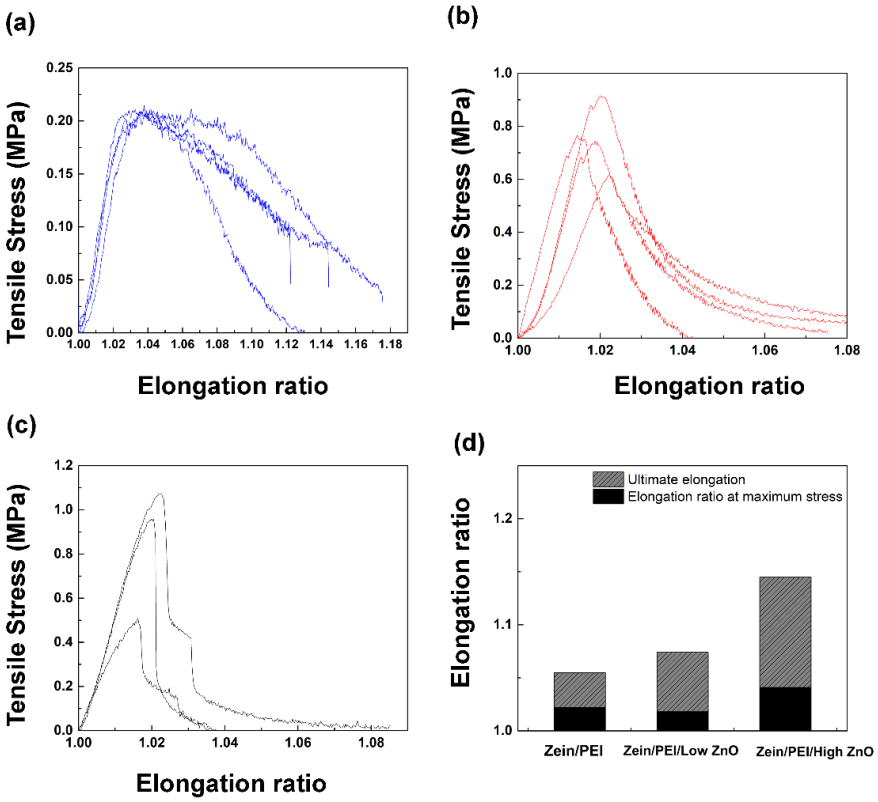

Figure 68 Tensile test data on fibre mats and ductility comparison: a) Zein/PEI/low ZnO; b) Zein/PEI/low ZnO; c) Zein/PEI; d) Elongation at strength and end.

4.5. Conclusion

Experiments were carried out with the view of producing novel zein based fibres by electrospinning. Polyethylene imine (PEI) was used for its dual function, namely as a potential plasticiser for zein and as favourable medium for the *in-situ* generation of ZnO nanoparticles. Zinc acetylacetonate dihydrate was chosen as the owing to its low stability, which facilitates the formation of ZnO through successive sol-gel reaction steps, consisting of decomplexation of Zinc acetylacetonate, formation of solid nuclei and growth into stable Wurtzite crystals. The obtained ZnO/PEI micro-suspension in ethanol was mixed in an ethanol/water solution of zein at two concentration levels and used for electrospinning of different types of zein-modified fibres. DSC

analysis has revealed that PEI acts as an “effective” plasticiser for zein, causing also a broadening of the glass transition. TGA data have shown that the presence of PEI increases as the solvent retention of the fibres produced, which is reduced considerably when ZnO nanoparticles are present as a micro-suspension in PEI. This study has provided useful new insights for formulating fibres, films and coatings exhibiting antibacterial characteristics, as well as higher mechanical flexibility and toughness relative to plain zein.

Chapter 6. Conclusions and future outlook

In this thesis, three types of electrospun fibres with potential for biomedical applications were demonstrated: PLA fibres containing tea tree/manuka essential oils (Chapter 2), hierarchical porous PECA/PCL fibres (Chapter 3), and zein fibres encapsulating in-situ generated ZnO nanoparticles (Chapter 4).

Setup of electrospinning and its controlling parameters were discussed in Background (Chapter 1). The electrospinning system generally composes of a high voltage generator, a supply system with syringe pump and metal needle, and a collector. The choice of polymer concentration and solvent, as well as applied voltage flow rate, and tip-to-collector distance, have direct influence on the fibre morphology and diameters. Different collecting systems could alter alignment and porosity of produced fibres. To produce desired beadless fibres, through this PhD, various combinations of polymer concentration, applied voltage, and tip-to-collector distance were tested in preliminary studies.

Tea tree and Manuka essential oils and ZnO nanoparticles were encapsulated in fibres with aim to give antibacterial properties. In Chapter 2, electrospun PLA-Manuka oil fibres were found successfully against *S. epidermidis*. The adding of both essential oils also reduced glass transition temperature, showing plasticising effect on PLA. In Chapter 4, ZnO nanoparticles, the antibacterial agent, was firstly *in-situ* generated in PEI. The obtained composite was then mixed with zein in solution and produced electrospun fibres. Plasticising effect of PEI on zein improved mechanical properties of fibres and made them easier for handle. The antibacterial activity of the fibres has been tested in collaboration with the Italian Institute of Technology (Genoa, Italy).

Hierarchical structured PECA/PCL fibres were produced with aim to improve surface roughness and surface-to-volume ratio, therefore, to improve cell attachment and proliferation. Two distinct types of porosity were observed on fibres: one with elongated and parallel grooves, possibly caused by spinodal decomposition; the other one with near-circular nanopores as result of nucleation and growth phenomena.

Though the electrospun mats developed during the PhD project show promising properties for biomedical applications, some improvements and further studies are required:

- Fast evaporation of essential oils can have an impact on antibacterial properties. Tests on evaporation rate of essential oils encapsulating in fibres in different environment (humidity, temperature, packages) should be carried out.
- Further investigation of hierarchical structured PECA/PCL to indicate the composition of each region. Simulation may be applied to verify the dual-phase separation mechanism.
- Various concentrations of ZnO could be generated to obtain the optimum concentration for antibacterial application.
- TEM could be carried out to detect the average size of single ZnO nanoparticles.
- Further investigation on aggregation of ZnO nanoparticles in PEI using different drying temperature and time.

Reference:

[1] N. Bhardwaj and S. C. Kundu, “Electrospinning: A fascinating fiber fabrication technique,” *Biotechnology Advances*, vol. 28, no. 3. pp. 325–347, 2010.

[2] L. A. Smith and P. X. Ma, “Nano-fibrous scaffolds for tissue engineering,” *Colloids Surfaces B Biointerfaces*, vol. 39, no. 3, pp. 125–131, 2004.

[3] W. E. Teo and S. Ramakrishna, “A review on electrospinning design and nanofibre assemblies,” *Nanotechnology*, vol. 17, no. 14, 2006.

[4] D. Liang, B. S. Hsiao, and B. Chu, “Functional electrospun nanofibrous scaffolds for biomedical applications,” *Advanced Drug Delivery Reviews*, vol. 59, no. 14. pp. 1392–1412, 2007.

[5] J. Wu, N. Wang, Y. Zhao, and L. Jiang, “Electrospinning of multilevel structured functional micro-/nanofibers and their applications,” *J. Mater. Chem. A*, vol. 1, no. 25, pp. 7290–7305, 2013.

[6] S. Agarwal, J. H. Wendorff, and A. Greiner, “Use of electrospinning technique for biomedical applications,” *Polymer (Guildf).*, vol. 49, no. 26, pp. 5603–5621, 2008.

[7] T. D. Brown, P. D. Dalton, and D. W. Hutmacher, “Melt electrospinning today: An opportune time for an emerging polymer process,” *Prog. Polym. Sci.*, vol. 56, pp. 116–166, 2016.

[8] E. Mele *et al.*, “Biomimetic approach for liquid encapsulation with nanofibrillar cloaks,” *Langmuir*, vol. 30, no. 10, pp. 2896–2902, 2014.

[9] R. Sridhar, R. Lakshminarayanan, K. Madhaiyan, V. A. Barathi, K. H. C. Limh, and S. Ramakrishna, “Electrosprayed nanoparticles and electrospun nanofibers based on natural materials: Applications in tissue regeneration, drug delivery and pharmaceuticals,” *Chem. Soc. Rev.*, vol. 44, no. 3, pp. 790–814, 2015.

[10] A. K. Haghi and M. Akbari, “Trends in electrospinning of natural nanofibers,” *Phys. Status Solidi Appl. Mater. Sci.*, vol. 204, no. 6, pp. 1830–1834, 2007.

[11] R. Casasola, N. L. Thomas, A. Trybala, and S. Georgiadou, “Electrospun poly

lactic acid (PLA) fibres: Effect of different solvent systems on fibre morphology and diameter," *Polymer (Guildf).*, vol. 55, no. 18, pp. 4728–4737, 2014.

[12] Q. P. Pham, U. Sharma, and A. G. Mikos, "Electrospun poly (ε-caprolactone) microfiber and multilayer nanofiber/microfiber scaffolds: Characterization of scaffolds and measurement of cellular infiltration," *Biomacromolecules*, vol. 7, no. 10, pp. 2796–2805, 2006.

[13] A. Cipitria, A. Skelton, T. R. Dargaville, P. D. Dalton, and D. W. Hutmacher, "Design, fabrication and characterization of PCL electrospun scaffolds - A review," *J. Mater. Chem.*, vol. 21, no. 26, pp. 9419–9453, 2011.

[14] S. Sukigara, M. Gandhi, J. Ayutsede, M. Micklus, and F. Ko, "Regeneration of Bombyx mori silk by electrospinning - Part 1: Processing parameters and geometric properties," *Polymer (Guildf).*, vol. 44, no. 19, pp. 5721–5727, 2003.

[15] S. L. Shenoy, W. D. Bates, H. L. Frisch, and G. E. Wnek, "Role of chain entanglements on fiber formation during electrospinning of polymer solutions: good solvent, non-specific polymer–polymer interaction limit," *Polymer (Guildf).*, vol. 46, no. 10, pp. 3372–3384, 2005.

[16] J. Tao and S. Shivkumar, "Molecular weight dependent structural regimes during the electrospinning of PVA," *Mater. Lett.*, vol. 61, no. 11–12, pp. 2325–2328, 2007.

[17] S. S. Goki Eda, James Liu, "Flight path of electrospun polystyrene solutions: Effects of molecular weight and concentration," *Mater. Lett.*, vol. 61, pp. 1451–1455, 2007.

[18] G. Eda, J. Liu, and S. Shivkumar, "Solvent effects on jet evolution during electrospinning of semi-dilute polystyrene solutions," *Eur. Polym. J.*, vol. 43, no. 4, pp. 1154–1167, 2007.

[19] I. Greenfeld and E. Zussman, "Polymer entanglement loss in extensional flow: Evidence from electrospun short nanofibers," *J. Polym. Sci. Part B Polym. Phys.*, vol. 51, no. 18, pp. 1377–1391, 2013.

[20] C. Wang, Y. Wang, and T. Hashimoto, "Impact of Entanglement Density on Solution Electrospinning: A Phenomenological Model for Fiber Diameter,"

Macromolecules, vol. 49, no. 20, pp. 7985–7996, 2016.

[21] N. Bhattarai, Z. Li, D. Edmondson, and M. Zhang, “Alginate-based nanofibrous scaffolds: Structural, mechanical, and biological properties,” *Adv. Mater.*, vol. 18, no. 11, pp. 1463–1467, 2006.

[22] H. Nie *et al.*, “Effect of poly(ethylene oxide) with different molecular weights on the electrospinnability of sodium alginate,” *Polymer (Guildf).*, vol. 50, no. 20, pp. 4926–4934, 2009.

[23] P. Songchotikunpan, J. Tattiyakul, and P. Supaphol, “Extraction and electrospinning of gelatin from fish skin,” *Int. J. Biol. Macromol.*, vol. 42, no. 3, pp. 247–255, 2008.

[24] T. Tzanov *et al.*, “Electrospinning of gelatin fibers using solutions with low acetic acid concentration: Effect of solvent composition on both diameter of electrospun fibers and cytotoxicity,” *J. Appl. Polym. Sci.*, vol. 132, no. 25, p. n/a-n/a, 2015.

[25] J. H. Song, H. E. Kim, and H. W. Kim, “Production of electrospun gelatin nanofiber by water-based co-solvent approach,” *J. Mater. Sci. Mater. Med.*, vol. 19, no. 1, pp. 95–102, 2008.

[26] A. K. Moghe, R. Hufenus, S. M. Hudson, and B. S. Gupta, “Effect of the addition of a fugitive salt on electrospinnability of poly(ε-caprolactone),” *Polymer (Guildf).*, vol. 50, no. 14, pp. 3311–3318, 2009.

[27] L. Van Der Schueren, I. Steyaert, B. De Schoenmaker, and K. De Clerck, “Polycaprolactone/chitosan blend nanofibres electrospun from an acetic acid/formic acid solvent system,” *Carbohydr. Polym.*, vol. 88, no. 4, pp. 1221–1226, 2012.

[28] S. V. Nair, V. K. Bhaskaran, A. Natarajan, D. Menon, U. Mony, and N. S. Binulal, “PCL–gelatin composite nanofibers electrospun using diluted acetic acid–ethyl acetate solvent system for stem cell-based bone tissue engineering,” *J. Biomater. Sci. Polym. Ed.*, vol. 25, no. 4, pp. 325–340, 2013.

[29] X. Geng, O. H. Kwon, and J. Jang, “Electrospinning of chitosan dissolved in concentrated acetic acid solution,” *Biomaterials*, vol. 26, no. 27, pp. 5427–

5432, 2005.

[30] H. Liu and Y. Lo Hsieh, “Ultrafine fibrous cellulose membranes from electrospinning of cellulose acetate,” *J. Polym. Sci. Part B Polym. Phys.*, vol. 40, no. 18, pp. 2119–2129, 2002.

[31] H. Homayoni, S. A. H. Ravandi, and M. Valizadeh, “Electrospinning of chitosan nanofibers: Processing optimization,” *Carbohydr. Polym.*, vol. 77, no. 3, pp. 656–661, 2009.

[32] L. Wu, X. Yuan, and J. Sheng, “Immobilization of cellulase in nanofibrous PVA membranes by electrospinning,” *J. Memb. Sci.*, vol. 250, no. 1–2, pp. 167–173, 2005.

[33] L. Wannatong, A. Sirivat, and P. Supaphol, “Effects of solvents on electrospun polymeric fibers: Preliminary study on polystyrene,” *Polym. Int.*, vol. 53, no. 11, pp. 1851–1859, 2004.

[34] H. Liu and C. Tang, “Electrospinning of Cellulose Acetate in Solvent Mixture N,N-Dimethylacetamide (DMAc)/Acetone,” *Polym. J.*, vol. 39, no. 1, pp. 65–72, 2007.

[35] A. Celebioglu and T. Uyar, “Electrospun porous cellulose acetate fibers from volatile solvent mixture,” *Mater. Lett.*, vol. 65, no. 14, pp. 2291–2294, 2011.

[36] B. Tarus, N. Fadel, A. Al-Oufy, and M. El-Messiry, “Effect of polymer concentration on the morphology and mechanical characteristics of electrospun cellulose acetate and poly (vinyl chloride) nanofiber mats,” *Alexandria Eng. J.*, vol. 55, no. 3, pp. 2975–2984, 2016.

[37] K. T. Shalumon, K. H. Anulekha, C. M. Girish, R. Prasanth, S. V. Nair, and R. Jayakumar, “Single step electrospinning of chitosan/poly(caprolactone) nanofibers using formic acid/acetone solvent mixture,” *Carbohydr. Polym.*, vol. 80, no. 2, pp. 413–419, 2010.

[38] P. Wang and E. Mele, “Effect of antibacterial plant extracts on the morphology of electrospun poly(lactic acid) fibres,” *Materials (Basel).*, vol. 11, no. 6, p. 923, 2018.

[39] M. A. Jahangir, T. M. Rumi, A. Wahab, M. A. Rahman, and Z. Bin Sayed, “Poly

Lactic Acid (PLA) Fibres: Different Solvent Systems and Their Effect on Fibre Morphology and Diameter," *Am. J. Chem.*, vol. 2017, no. 6, pp. 177–186, 2017.

[40] W. Zhang, C. Huang, O. Kusmartseva, N. L. Thomas, and E. Mele, "Electrospinning of polylactic acid fibres containing tea tree and manuka oil," *React. Funct. Polym.*, vol. 117, no. May, pp. 106–111, 2017.

[41] J. Zeng *et al.*, "Biodegradable electrospun fibers for drug delivery," *J. Control. Release*, vol. 92, no. 3, pp. 227–231, 2003.

[42] H. Yang, L. Wang, C. Xiang, and L. Li, "Electrospun porous PLLA and poly(LLA-co-CL) fibers by phase separation," *New J. Chem.*, vol. 42, no. 7, pp. 5102–5108, 2018.

[43] X. Y. Yuan, Y. Y. Zhang, C. Dong, and J. Sheng, "Morphology of ultrafine polysulfone fibers prepared by electrospinning," *Polym. Int.*, vol. 53, no. 11, pp. 1704–1710, 2004.

[44] S. Piperno, L. Lozzi, R. Rastelli, M. Passacantando, and S. Santucci, "PMMA nanofibers production by electrospinning," *Appl. Surf. Sci.*, vol. 252, no. 15, pp. 5583–5586, 2006.

[45] S. S. Murthe, M. S. Mohamed Saheed, V. Perumal, N. M. Mohamed, and M. S. Mohamed Saheed, "Effects of solvent ratio on the encapsulation of carbon nanotubes/Arthrospira platensis composite within electrospun poly(methyl methacrylate) nanofiber," *J. Phys. Conf. Ser.*, vol. 1123, no. 1, 2018.

[46] Z. Liu, J. H. Zhao, P. Liu, and J. H. He, "Tunable surface morphology of electrospun PMMA fiber using binary solvent," *Appl. Surf. Sci.*, vol. 364, pp. 516–521, 2016.

[47] J. Zeng *et al.*, "Ultrafine fibers electrospun from biodegradable polymers," *J. Appl. Polym. Sci.*, vol. 89, no. 4, pp. 1085–1092, 2003.

[48] H. Hazim, C. Deeptangshu, and D. Yu, "Electrospun PLA/PCL Fibers with Tubular Nanoclay: Morphological and Structural Analysis," *J. Appl. Polym. Sci.*, vol. 124, pp. 3930–3939, 2012.

[49] E. Mele *et al.*, "Zwitterionic Nanofibers of Super-Glue for Transparent and

Biocompatible Multi-Purpose Coatings," *Sci. Rep.*, vol. 5, p. 14019, 2015.

[50] M. Wang *et al.*, "Electrospun Nylon6 Nanofibrous Membrane as SPE Adsorbent for the Enrichment and Determination of Three Estrogens in Environmental Water Samples," *Chromatographia*, vol. 71, no. 5–6, pp. 487–492, 2009.

[51] F. Ignatious, L. Sun, C. P. Lee, and J. Baldoni, "Electrospun nanofibers in oral drug delivery," *Pharm. Res.*, vol. 27, no. 4, pp. 576–588, 2010.

[52] H. S. Bang, D. Kim, S. S. Hwang, and J. Won, "Surface-modified porous membranes with electrospun Nafion/PVA fibres for non-aqueous redox flow battery," *J. Memb. Sci.*, vol. 514, pp. 186–194, 2016.

[53] W. Zhang and E. Mele, "Phase separation events induce the coexistence of distinct nanofeatures in electrospun fibres of poly(ethyl cyanoacrylate) and polycaprolactone," *Mater. Today Commun.*, vol. 16, no. May, pp. 135–141, 2018.

[54] C. Zhijiang, Z. Ruihan, and S. Xingjuan, "Preparation and characterization of polyindole nanofibers by electrospinning method," *Synth. Met.*, vol. 162, no. 23, pp. 2069–2074, 2012.

[55] M. Kang, R. Jung, H. S. Kim, and H. J. Jin, "Preparation of superhydrophobic polystyrene membranes by electrospinning," *Colloids Surfaces A Physicochem. Eng. Asp.*, vol. 313–314, pp. 411–414, 2008.

[56] K. H. Lee, H. Y. Kim, H. J. Bang, Y. H. Jung, and S. G. Lee, "The change of bead morphology formed on electrospun polystyrene fibers," *Polymer (Guildf).*, vol. 44, no. 14, pp. 4029–4034, 2003.

[57] J. Lin, B. Ding, J. Yu, and Y. Hsieh, "Direct Fabrication of Highly Nanoporous Polystyrene Fibers via Electrospinning," *Appl. Mater. Interfaces*, vol. 2, no. 2, p. 521, 2010.

[58] S. Huan *et al.*, "Effect of experimental parameters on morphological, mechanical and hydrophobic properties of electrospun polystyrene fibers," *Materials (Basel).*, vol. 8, no. 5, pp. 2718–2734, 2015.

[59] T. Isık and M. M. Demir, "Tailored electrospun fibers from waste polystyrene

for high oil adsorption," *Sustain. Mater. Technol.*, vol. 18, 2018.

[60] N. Kattamuri, J. Shawon, and C. M. Sung, "Electrospinning of polycarbonate nanofibers with THF and DMF.," *Abstr. Pap. Am. Chem. Soc.*, vol. 225, pp. U652–U653, 2003.

[61] K. H. Lee, H. Y. Kim, Y. M. La, D. R. Lee, and N. H. Sung, "Influence of a mixing solvent with tetrahydrofuran and N,N-dimethylformamide on electrospun poly(vinyl chloride) nonwoven mats," *J. Polym. Sci. Part B Polym. Phys.*, vol. 40, no. 19, pp. 2259–2268, 2002.

[62] K. H. Lee, H. Y. Kim, Y. J. Ryu, K. W. Kim, and S. W. Choi, "Mechanical behavior of electrospun fiber mats of poly(vinyl chloride)/polyurethane polyblends," *J. Polym. Sci. Part B Polym. Phys.*, vol. 41, no. 11, pp. 1256–1262, 2003.

[63] M. S. Khil, D. Il Cha, H. Y. Kim, I. S. Kim, and N. Bhattarai, "Electrospun Nanofibrous Polyurethane Membrane as Wound Dressing," *J. Biomed. Mater. Res. - Part B Appl. Biomater.*, vol. 67, no. 2, pp. 675–679, 2003.

[64] K. A. G. Katsogiannis, G. T. Vladisavljević, and S. Georgiadou, "Porous electrospun polycaprolactone (PCL) fibres by phase separation," *Eur. Polym. J.*, vol. 69, pp. 284–295, 2015.

[65] M. Putti, M. Simonet, R. Solberg, and G. W. M. Peters, "Electrospinning poly(ε-caprolactone) under controlled environmental conditions: Influence on fiber morphology and orientation," *Polymer (Guildf).*, vol. 63, pp. 189–195, 2015.

[66] K. H. Lee, H. Y. Kim, M. S. Khil, Y. M. Ra, and D. R. Lee, "Characterization of nano-structured poly(ε-caprolactone) nonwoven mats via electrospinning," *Polymer (Guildf).*, vol. 44, no. 4, pp. 1287–1294, 2003.

[67] G. Bruni, S. Pisani, I. Genta, T. Modena, B. Conti, and R. Dorati, "Design of copolymer PLA-PCL electrospun matrix for biomedical applications," *React. Funct. Polym.*, vol. 124, no. July 2017, pp. 77–89, 2018.

[68] M. Herrero-Herrero, J. A. Gómez-Tejedor, and A. Vallés-Lluch, "PLA/PCL electrospun membranes of tailored fibres diameter as drug delivery systems," *Eur. Polym. J.*, vol. 99, no. November 2017, pp. 445–455, 2018.

[69] M. N. Akhtar, A. B. Sulong, S. A. Karim, C. H. Azhari, and M. R. Raza, “Evaluation of thermal, morphological and mechanical properties of PMMA/NaCl/DMF electrospun nanofibers: an investigation through surface methodology approach,” *Iran. Polym. J. (English Ed.*, vol. 24, no. 12, pp. 1025–1038, 2015.

[70] Z. Zhou and X. F. Wu, “Electrospinning superhydrophobic-superoleophilic fibrous PVDF membranes for high-efficiency water-oil separation,” *Mater. Lett.*, vol. 160, pp. 423–427, 2015.

[71] A. Sadighzadeh, M. Valinejad, A. Gazmeh, and B. Rezaiefard, “Synthesis of Polymeric Electrospun Nanofibers for Application in Waterproof-Breathable Fabric,” *Polym. eng. sci*, vol. 56, no. 2, pp. 143–149, 2015.

[72] H. Jiang, D. Fang, B. S. Hsiao, B. Chu, and W. Chen, “Optimization and characterization of dextran membranes prepared by electrospinning,” *Biomacromolecules*, vol. 5, no. 2, pp. 326–333, 2004.

[73] C. J. Luo, M. Nangrejo, and M. Edirisinghe, “A novel method of selecting solvents for polymer electrospinning,” *Polymer (Guildf).*, vol. 51, no. 7, pp. 1654–1662, 2010.

[74] Y. Liu, G. Ma, D. Fang, J. Xu, H. Zhang, and J. Nie, “Effects of solution properties and electric field on the electrospinning of hyaluronic acid,” *Carbohydr. Polym.*, vol. 83, no. 2, pp. 1011–1015, 2011.

[75] A. Celebioglu, F. Topuz, Z. I. Yildiz, and T. Uyar, “One-step green synthesis of antibacterial silver nanoparticles embedded in electrospun cyclodextrin nanofibers,” *Carbohydr. Polym.*, vol. 207, no. November 2018, pp. 471–479, 2019.

[76] J. Liu *et al.*, “Hydrophobic electrospun polyimide nanofibers for self-cleaning materials,” *Macromol. Mater. Eng.*, vol. 300, no. 3, pp. 358–368, 2015.

[77] X. Huang *et al.*, “Hierarchical electrospun nanofibers treated by solvent vapor annealing as air filtration mat for high-efficiency PM2.5 capture,” *Sci. China Mater.*, vol. 62, no. 3, pp. 423–436, 2019.

[78] S. Gautam, A. K. Dinda, and N. C. Mishra, “Fabrication and characterization of

PCL/gelatin composite nanofibrous scaffold for tissue engineering applications by electrospinning method," *Mater. Sci. Eng. C*, vol. 33, no. 3, pp. 1228–1235, 2013.

[79] C. Huang and N. L. Thomas, "Fabricating porous poly(lactic acid) fibres via electrospinning," *Eur. Polym. J.*, vol. 99, pp. 464–476, 2018.

[80] I. Bonadies, A. Longo, R. Androsch, and M. L. Di Lorenzo, "Biodegradable electrospun PLLA fibers containing the mosquito-repellent DEET," *Eur. Polym. J.*, vol. 113, pp. 377–384, 2019.

[81] L. Van Der Schueren, B. De Schoenmaker, Ö. I. Kalaoglu, and K. De Clerck, "An alternative solvent system for the steady state electrospinning of polycaprolactone," *Eur. Polym. J.*, vol. 47, no. 6, pp. 1256–1263, 2011.

[82] X. Liu, S. Zheng, W. Dan, and N. Dan, "Ultrasound-mediated preparation and evaluation of a collagen/PVP-PCL micro- and nanofiber scaffold electrospun from chloroform/ethanol mixture," *Fibers Polym.*, vol. 17, no. 8, pp. 1186–1197, 2016.

[83] I. Romano *et al.*, "Fumarate-loaded electrospun nanofibers with anti-inflammatory activity for fast recovery of mild skin burns," *Biomed. Mater.*, vol. 11, no. 4, p. 041001, 2016.

[84] J. Ahne, Q. Li, E. Croiset, and Z. Tan, "Electrospun cellulose acetate nanofibers for airborne nanoparticle filtration," *Text. Res. J.*, vol. 0, no. 00, pp. 1–13, 2018.

[85] Y. Xiao *et al.*, "Electrospun natural cellulose/polyacrylonitrile nanofiber: simulation and experimental study," *Text. Res. J.*, vol. 0, no. 00, pp. 1–11, 2018.

[86] Y. Liu *et al.*, "Fabrication and characterization of electrospun cellulose/polyacrylonitrile nanofibers with Cu(II) ions," *Cellulose*, vol. 25, no. 5, pp. 2955–2963, 2018.

[87] Y. K. Kang, C. H. Park, J. Kim, and T. J. Kang, "Application of electrospun polyurethane web to breathable water-proof fabrics," *Fibers Polym.*, vol. 8, no. 5, pp. 564–570, 2007.

[88] C. W. Kim, M. W. Frey, M. Marquez, and Y. L. Joo, “Preparation of submicron-scale, electrospun cellulose fibers via direct dissolution,” *J. Polym. Sci. Part B Polym. Phys.*, vol. 43, no. 13, pp. 1673–1683, 2005.

[89] X.-X. Shen *et al.*, “Electrospinning of Concentrated Polymer Solutions,” *Macromolecules*, vol. 43, no. 24, pp. 10743–10746, 2010.

[90] G. Z. Yang, H. P. Li, J. H. Yang, J. Wan, and D. G. Yu, “Influence of Working Temperature on The Formation of Electrospun Polymer Nanofibers,” *Nanoscale Res. Lett.*, vol. 12, no. 1, p. 55, 2017.

[91] C. Su, Y. Li, Y. Dai, F. Gao, K. Tang, and H. Cao, “Fabrication of three-dimensional superhydrophobic membranes with high porosity via simultaneous electrospraying and electrospinning,” *Mater. Lett.*, vol. 170, pp. 67–71, 2016.

[92] L. G. Liu and J. H. He, “Solvent evaporation in a binary solvent system for controllable fabrication of porous fibers by electrospinning,” *Therm. Sci.*, vol. 21, no. 4, pp. 1821–1825, 2017.

[93] J. Zhang, C. C. Han, A. He, S. Xu, J. Li, and H. Zhang, “Electrospinning of native cellulose from nonvolatile solvent system,” *Polymer (Guildf).*, vol. 49, no. 12, pp. 2911–2917, 2008.

[94] S. L. Quan, S. G. Kang, and I. J. Chin, “Characterization of cellulose fibers electrospun using ionic liquid,” *Cellulose*, vol. 17, no. 2, pp. 223–230, 2010.

[95] L. Hardelin, J. Thunberg, E. Perzon, G. Westman, P. Walkenstrom, and P. Gatenholm, “Electrospinning of Cellulose Nanofibers from Ionic Liquids: The Effect of Different Cosolvents,” *J. Appl. Polym. Sci.*, vol. 125, p. 1901, 2012.

[96] L. Kong and G. R. Ziegler, “Fabrication of pure starch fibers by electrospinning,” *Food Hydrocoll.*, vol. 36, pp. 20–25, 2014.

[97] J. Sunthornvarabhas, P. Chatakanonda, K. Piyachomkwan, and K. Sriroth, “Electrospun polylactic acid and cassava starch fiber by conjugated solvent technique,” *Mater. Lett.*, vol. 65, no. 6, pp. 985–987, 2011.

[98] L. Kong and G. R. Ziegler, “Role of molecular entanglements in starch fiber formation by electrospinning,” *Biomacromolecules*, vol. 13, no. 8, pp. 2247–2253, 2012.

[99] W. Wang, H. Wang, X. Jin, H. Wang, T. Lin, and Z. Zhu, “Effects of hydrogen bonding on starch granule dissolution, spinnability of starch solution, and properties of electrospun starch fibers,” *Polymer (Guildf).*, vol. 153, no. August, pp. 643–652, 2018.

[100] H. Wang, L. Kong, and G. R. Ziegler, “Fabrication of starch - Nanocellulose composite fibers by electrospinning,” *Food Hydrocoll.*, vol. 90, no. November 2018, pp. 90–98, 2019.

[101] K. Lin, K. N. Chua, G. T. Christopherson, S. Lim, and H. Q. Mao, “Reducing electrospun nanofiber diameter and variability using cationic amphiphiles,” *Polymer (Guildf).*, vol. 48, no. 21, pp. 6384–6394, 2007.

[102] S. Wang, H. Pan, Z. Xiong, W. Cai, J. Liu, and J. Yang, “Facile fabrication of porous carbon nanofibers by electrospun PAN/dimethyl sulfone for capacitive deionization,” *J. Mater. Chem. A*, vol. 3, no. 26, pp. 13827–13834, 2015.

[103] L. Sabantina *et al.*, “Stabilization of polyacrylonitrile nanofiber mats obtained by needleless electrospinning using dimethyl sulfoxide as solvent,” *J. Ind. Text.*, vol. 0, no. 0, 2019.

[104] L. Sebantina, J. R. Mirasol, T. Cordero, K. Finsterbusch, and A. Ehrmann, “Investigation of needleless electrospun PAN nanofiber mats,” *AIP Conf. Proc.*, vol. 1952, no. 1, 2018.

[105] Z. X. Meng, W. Zheng, L. Li, and Y. F. Zheng, “Fabrication and characterization of three-dimensional nanofiber membrance of PCL-MWCNTs by electrospinning,” *Mater. Sci. Eng. C*, vol. 30, no. 7, pp. 1014–1021, 2010.

[106] S. H. Kim, Y. S. Nam, T. S. Lee, and W. H. Park, “Silk Fibroin Nanofiber. Electrospinning, Properties, and Structure,” *Polym. J.*, vol. 35, no. 2, pp. 185–190, 2003.

[107] H. C. Chen, W. C. Jao, and M. C. Yang, “Characterization of gelatin nanofibers electrospun using ethanol/formic acid/water as a solvent,” *Polym. Adv. Technol.*, vol. 20, no. 2, pp. 98–103, 2009.

[108] Y. Li, L. T. Lim, and Y. Kakuda, “Electrospun zein fibers as carriers to stabilize (-)-epigallocatechin gallate,” *J. Food Sci.*, vol. 74, no. 3, pp. 233–240, 2009.

[109] Y. Zhang, Y. Yang, and K. Tang, “Physicochemical Characterization and Antioxidant Activity of Quercetin-Loaded Chitosan Nanoparticles Yuying,” *Polym. Polym. Compos.*, vol. 21, no. 7, pp. 449–456, 2007.

[110] T. Miyoshi, K. Toyohara, and H. Minematsu, “Preparation of ultrafine fibrous zein membranes via electrospinning,” *Polym. Int.*, vol. 54, no. 8, pp. 1187–1190, 2005.

[111] K. Moomand and L. T. Lim, “Effects of solvent and n-3 rich fish oil on physicochemical properties of electrospun zein fibres,” *Food Hydrocoll.*, vol. 46, pp. 191–200, 2015.

[112] S. Torres-Giner, M. J. Ocio, and J. M. Lagaron, “Novel antimicrobial ultrathin structures of zein/chitosan blends obtained by electrospinning,” *Carbohydr. Polym.*, vol. 77, no. 2, pp. 261–266, 2009.

[113] T. Y. Song, C. Yao, and X. S. Li, “Electrospinning of zein/chitosan composite fibrous membranes,” *Chinese J. Polym. Sci. (English Ed.*, vol. 28, no. 2, pp. 171–179, 2010.

[114] C. Yao, X. Li, and T. Song, “Fabrication of zein/hyaluronic acid fibrous membranes by electrospinning,” *J. Biomater. Sci. Polym. Ed.*, vol. 18, no. 6, pp. 731–742, 2007.

[115] C. Shi, S. Xi, Y. Han, H. Zhang, J. Liu, and Y. Li, “Structure, rheology and electrospinning of zein and poly(ethylene oxide) in aqueous ethanol solutions,” *Chinese Chem. Lett.*, vol. 30, no. 2, pp. 305–310, 2019.

[116] T. S. Lee, Y. S. Nam, S. H. Kim, B.-M. Min, W. H. Park, and G. Lee, “Electrospinning of silk fibroin nanofibers and its effect on the adhesion and spreading of normal human keratinocytes and fibroblasts in vitro,” *Biomaterials*, vol. 25, no. 7–8, pp. 1289–1297, 2003.

[117] J. Zhu, J. Luo, X. Zhao, J. Gao, and J. Xiong, “Electrospun homogeneous silk fibroin/poly (ϵ-caprolactone) nanofibrous scaffolds by addition of acetic acid for tissue engineering,” *J. Biomater. Appl.*, vol. 31, no. 3, pp. 421–437, 2016.

[118] W. H. Park, L. Jeong, D. Il Yoo, and S. Hudson, “Effect of chitosan on morphology and conformation of electrospun silk fibroin nanofibers,” *Polymer*

(Guildf)., vol. 45, no. 21, pp. 7151–7157, 2004.

[119] C. S. Ki, D. H. Baek, K. D. Gang, K. H. Lee, I. C. Um, and Y. H. Park, “Characterization of gelatin nanofiber prepared from gelatin-formic acid solution,” *Polymer (Guildf).*, vol. 46, no. 14, pp. 5094–5102, 2005.

[120] Y. J. Ryu, H. Y. Kim, K. H. Lee, H. C. Park, and D. R. Lee, “Transport properties of electrospun nylon 6 nonwoven mats,” *Eur. Polym. J.*, vol. 39, no. 9, pp. 1883–1889, 2003.

[121] P. Supaphol, C. Mit-Uppatham, and M. Nithitanakul, “Ultrafine electrospun polyamide-6 fibers: Effect of emitting electrode polarity on morphology and average fiber diameter,” *J. Polym. Sci. Part B Polym. Phys.*, vol. 43, no. 24, pp. 3699–3712, 2005.

[122] S. V. Fridrikh, J. H. Yu, M. P. Brenner, and G. C. Rutledge, “Controlling the Fiber Diameter during Electrospinning,” *Phys. Rev. Lett.*, vol. 90, no. 14, pp. 144502–1, 2003.

[123] J. M. Deitzel, J. Kleinmeyer, D. Harris, and N. C. Beck Tan, “The effect of processing variables on the morphology of electrospun,” *Polymer (Guildf).*, vol. 42, pp. 261–272, 2001.

[124] M. M. Hohman, M. Shin, G. Rutledge, and M. P. Brenner, “Electrospinning and electrically forced jets. I. Stability theory,” *Phys. Fluids*, vol. 13, no. 8, pp. 2201–2220, 2001.

[125] T. Uyar and F. Besenbacher, “Electrospinning of uniform polystyrene fibers: The effect of solvent conductivity,” *Polymer (Guildf).*, vol. 49, no. 24, pp. 5336–5343, 2008.

[126] T. Jarusuwannapoom *et al.*, “Effect of solvents on electro-spinnability of polystyrene solutions and morphological appearance of resulting electrospun polystyrene fibers,” *Eur. Polym. J.*, vol. 41, no. 3, pp. 409–421, 2005.

[127] H. Fong, I. Chun, and D. H. Reneker, “Beaded nanofibers formed during electrospinning,” *Polymer (Guildf).*, vol. 40, no. 16, pp. 4585–4592, 1999.

[128] K. Arayanarakul, N. Choktaweesap, D. Aht-ong, C. Meechaisue, and P. Supaphol, “Effects of poly(ethylene glycol), inorganic salt, sodium dodecyl

sulfate, and solvent system on electrospinning of poly(ethylene oxide),” *Macromol. Mater. Eng.*, vol. 291, no. 6, pp. 581–591, 2006.

[129] B. Kim, H. Park, S. H. Lee, and W. M. Sigmund, “Poly(acrylic acid) nanofibers by electrospinning,” *Mater. Lett.*, vol. 59, no. 7, pp. 829–832, 2005.

[130] L. R. Manea, R. Cramariuc, B. Cramariuc, I. G. Lupu, O. Cramariuc, and R. Scarlet, “Fiber diameter in electrospinning process,” *J. Electrostat.*, vol. 71, no. 3, pp. 189–198, 2013.

[131] C. Zhang, X. Yuan, L. Wu, Y. Han, and J. Sheng, “Study on morphology of electrospun poly(vinyl alcohol) mats,” *Eur. Polym. J.*, vol. 41, no. 3, pp. 423–432, 2005.

[132] M. Dhanalakshmi, A. K. Lele, and J. P. Jog, “Electrospinning of Nylon11: Effect of processing parameters on morphology and microstructure,” *Mater. Today Commun.*, vol. 3, pp. 141–148, 2015.

[133] K. H. K. Chan *et al.*, “Effect of Molecular Orientation on Mechanical Property of Single Electrospun Fiber of Poly[(*R*)-3-hydroxybutyrate- *co* -(*R*)-3-hydroxyvalerate],” *J. Phys. Chem. B*, vol. 113, no. 40, pp. 13179–13185, 2009.

[134] M. V. Kakade, S. Givens, K. Gardner, K. H. Lee, D. B. Chase, and J. F. Rabolt, “Electric field induced orientation of polymer chains in macroscopically aligned electrospun polymer nanofibers,” *J. Am. Chem. Soc.*, vol. 129, no. 10, pp. 2777–2782, 2007.

[135] J. Ma *et al.*, “Thermal conductivity of electrospun polyethylene nanofibers,” *Nanoscale*, vol. 7, no. 40, pp. 16899–16908, 2015.

[136] D. B. Chase, K. Gardner, J. F. Rabolt, S. Givens, K. H. Lee, and M. V. Kakade, “Electric Field Induced Orientation of Polymer Chains in Macroscopically Aligned Electrospun Polymer Nanofibers,” *J. Am. Chem. Soc.*, vol. 129, no. 10, pp. 2777–2782, 2007.

[137] T. Kongkhlang, K. Tashiro, M. Kotaki, and S. Chirachanchai, “Electrospinning as a new technique to control the crystal morphology and molecular orientation of polyoxymethylene nanofibers,” *J. Am. Chem. Soc.*, vol. 130, no. 46, pp. 15460–15466, 2008.

[138] S. Bazgir, R. Damerchely, S. Zargham, A. S. Rashidi, and A. Tavakoli, “The Effect of Flow Rate on Morphology and Deposition Area of Electrospun Nylon 6 Nanofiber,” *J. Eng. Fiber. Fabr.*, vol. 7, no. 4, p. 155892501200700, 2018.

[139] R. Ranjith, S. Balraj, J. Ganesh, and M. C. J. Milton, “Effect of Flow Rate on Fiber Morphology and Naringin Release of Electrospun Naringin Loaded Polycaprolactone Nanofibers,” *Int. J. Sci. Res. Sci. Technol.*, vol. 3, no. 7, pp. 05–08, 2017.

[140] X. P. Tang, N. Si, L. Xu, and H. Y. Liu, “Effect of flow rate on diameter of electrospun nanoporous fibers,” *Therm. Sci.*, vol. 18, no. 5, pp. 1447–1449, 2014.

[141] J. A. Matthews, G. E. Wnek, D. G. Simpson, and G. L. Bowlin, “Electrospinning of collagen nanofibers,” *Biomacromolecules*, vol. 3, no. 2, pp. 232–238, 2002.

[142] C. Y. Xu, R. Inai, M. Kotaki, and S. Ramakrishna, “Aligned biodegradable nanofibrous structure: A potential scaffold for blood vessel engineering,” *Biomaterials*, vol. 25, no. 5, pp. 877–886, 2004.

[143] P. Katta, M. Alessandro, R. D. Ramsier, and G. G. Chase, “Continuous electrospinning of aligned polymer nanofibers onto a wire drum collector,” *Nano Lett.*, vol. 4, no. 11, pp. 2215–2218, 2004.

[144] J. J. Ng and P. Supaphol, “Rotating-disk electrospinning: needleless electrospinning of poly(caprolactone), poly(lactic acid) and poly(vinyl alcohol) nanofiber mats with controlled morphology,” *J. Polym. Res.*, vol. 25, no. 7, 2018.

[145] N. A. Grigoryev and K. Levon, “Novel Method of Electrospinning; Rotating Dual Electrode Collector Design,” *J. Microelectromechanical Syst.*, vol. 27, no. 2, pp. 312–320, 2018.

[146] L. Wang, B. Wang, Z. Ahmad, J. S. Li, and M. W. Chang, “Dual rotation centrifugal electrospinning: a novel approach to engineer multi-directional and layered fiber composite matrices,” *Drug Deliv. Transl. Res.*, vol. 9, no. 1, pp. 204–214, 2019.

[147] D. Li, Y. Wang, and Y. Xia, “Electrospinning Nanofibers as Uniaxially Aligned

Arrays and Layer-by-Layer Stacked Films," *Adv. Mater.*, vol. 16, no. 4, pp. 361–366, 2004.

[148] P. D. Dalton, D. Klee, and M. Möller, "Electrospinning with dual collection rings," *Polymer (Guildf).*, vol. 46, no. 3, pp. 611–614, 2005.

[149] K. W. Kim, K. H. Lee, M. S. Khil, Y. S. Ho, and H. Y. Kim, "The effect of molecular weight and the linear velocity of drum surface on the properties of electrospun poly(ethylene terephthalate) nonwovens," *Fibers Polym.*, vol. 5, no. 2, pp. 122–127, 2004.

[150] M. D. Edwards, G. R. Mitchell, S. D. Mohan, and R. H. Olley, "Development of orientation during electrospinning of fibres of poly(e-caprolactone)," *Eur. Polym. J.*, vol. 46, no. 6, pp. 1175–1183, 2010.

[151] M. Oudega *et al.*, "Creation of highly aligned electrospun poly-L-lactic acid fibers for nerve regeneration applications," *J. Neural Eng.*, vol. 6, no. 1, p. 016001, 2008.

[152] E. Smit, U. Buttner, and R. D. Sanderson, "Continuous yarns from electrospun fibers," *Polymer (Guildf).*, vol. 46, no. 8, pp. 2419–2423, 2005.

[153] C. Nah, S. H. Han, M. H. Lee, J. S. Kim, and D. S. Lee, "Characteristics of polyimide ultrafine fibers prepared through electrospinning," *Polym. Int.*, vol. 52, no. 3, pp. 429–432, 2003.

[154] Q. Z. Yu, M. M. Shi, M. Deng, M. Wang, and H. Z. Chen, "Morphology and conductivity of polyaniline sub-micron fibers prepared by electrospinning," *Mater. Sci. Eng. B Solid-State Mater. Adv. Technol.*, vol. 150, no. 1, pp. 70–76, 2008.

[155] H. Wang, L. Kong, and G. R. Ziegler, "Aligned wet-electrospun starch fiber mats," *Food Hydrocoll.*, vol. 90, no. December 2018, pp. 113–117, 2019.

[156] X. Wang *et al.*, "Poly(ethyleneimine) nanofibrous affinity membrane fabricated via one step wet-electrospinning from poly(vinyl alcohol)-doped poly(ethyleneimine) solution system and its application," *J. Memb. Sci.*, vol. 379, no. 1–2, pp. 191–199, 2011.

[157] G. Sun, J. Yu, M. Sun, B. Ding, and X. Wang, "Nanofibrous polyethyleneimine

membranes as sensitive coatings for quartz crystal microbalance-based formaldehyde sensors," *Sensors Actuators B Chem.*, vol. 144, no. 1, pp. 11–17, 2009.

[158] A. H. Hekmati, A. Rashidi, R. Ghazisaeidi, and J. Y. Drean, "Effect of needle length, electrospinning distance, and solution concentration on morphological properties of polyamide-6 electrospun nanowebs," *Text. Res. J.*, vol. 83, no. 14, pp. 1452–1466, 2013.

[159] C. J. Uchko, L. C. Chen, Y. Shen, and D. C. Martina, "Processing and microstructural characterization of porous biocompatible\rprotein polymer thin films," *Polymer (Guildf).*, vol. 40, pp. 7397–7407, 1999.

[160] W. Zhang, S. Ronca, and E. Mele, "Electrospun Nanofibres Containing Antimicrobial Plant Extracts," *Nanomaterials*, vol. 7, no. 2, p. 42, Feb. 2017.

[161] K. A. Hammer, C. F. Carson, and T. V. Riley, "Antimicrobial activity of essential oils and other plant extracts," *J. Appl. Microbiol.*, vol. 86, no. 6, pp. 985–990, Jun. 1999.

[162] M. P. Kähkönen *et al.*, "Antioxidant activity of plant extracts containing phenolic compounds," *J. Agric. Food Chem.*, vol. 47, no. 10, pp. 3954–3962, 1999.

[163] K. A. Rieger and J. D. Schiffman, "Electrospinning an essential oil: Cinnamaldehyde enhances the antimicrobial efficacy of chitosan/poly(ethylene oxide) nanofibers," *Carbohydr. Polym.*, vol. 113, pp. 561–568, 2014.

[164] I. Liakos *et al.*, "Fibrous wound dressings encapsulating essential oils as natural antimicrobial agents," *J. Mater. Chem. B*, vol. 3, no. 8, pp. 1583–1589, 2015.

[165] R. Yadav and K. Balasubramanian, "Polyacrylonitrile/Syzygium aromaticum hierarchical hydrophilic nanocomposite as a carrier for antibacterial drug delivery systems," *RSC Adv.*, vol. 5, no. 5, pp. 3291–3298, 2015.

[166] Z. Karami, I. Rezaeian, P. Zahedi, and M. Abdollahi, "Preparation and performance evaluations of electrospun poly(ε- caprolactone), poly(lactic acid), and their hybrid (50/50) nanofibrous mats containing thymol as an herbal drug for effective wound healing," *J. Appl. Polym. Sci.*, vol. 129, no. 2, pp. 756–766,

2013.

[167] H. Hajiali *et al.*, “Alginate-lavender nanofibers with antibacterial and anti-inflammatory activity to effectively promote burn healing,” *J. Mater. Chem. B*, vol. 4, no. 9, pp. 1686–1695, 2016.

[168] P. Wen *et al.*, “Fabrication of electrospun polylactic acid nanofilm incorporating cinnamon essential oil/β-cyclodextrin inclusion complex for antimicrobial packaging,” *Food Chem.*, vol. 196, pp. 996–1004, 2016.

[169] P. Zahedi, I. Rezaeian, S. O. Ranaei-Siadat, S. H. Jafari, and P. Supaphol, “A review on wound dressings with an emphasis on electrospun nanofibrous polymeric bandages,” *Polym. Adv. Technol.*, vol. 21, no. 2, pp. 77–95, 2010.

[170] J. R. Hanna and J. A. Giacopelli, “A review of wound healing and wound dressing products,” *J. Foot Ankle Surg.*, vol. 36, no. 1, pp. 2–14, 1997.

[171] C. H. Yao, J. Y. Yeh, Y. S. Chen, M. H. Li, and C. H. Huang, “Wound-healing effect of electrospun gelatin nanofibres containing Centella asiatica extract in a rat model,” *J. Tissue Eng. Regen. Med.*, vol. 11, no. 3, pp. 905–915, 2017.

[172] G. Jin, M. P. Prabhakaran, D. Kai, S. K. Annamalai, K. D. Arunachalam, and S. Ramakrishna, “Tissue engineered plant extracts as nanofibrous wound dressing,” *Biomaterials*, vol. 34, no. 3, pp. 724–734, 2013.

[173] W. P. Chan, K. C. Huang, and M. Y. Bai, “Silk fibroin protein-based nonwoven mats incorporating baicalein Chinese herbal extract: preparation, characterizations, and in vivo evaluation,” *J. Biomed. Mater. Res. - Part B Appl. Biomater.*, vol. 105, no. 2, pp. 420–430, 2017.

[174] M. Sadri, S. Arab-Sorkhi, H. Vatani, and A. Bagheri-Pebdeni, “New wound dressing polymeric nanofiber containing green tea extract prepared by electrospinning method,” *Fibers Polym.*, vol. 16, no. 8, pp. 1742–1750, Aug. 2015.

[175] C. L. S. de O. Mori *et al.*, “Nanostructured Polylactic Acid/Candeia Essential Oil Mats Obtained by Electrospinning,” *J. Nanomater.*, vol. 2015, no. 4, pp. 1–9, 2015.

[176] B. Motealleh, P. Zahedi, I. Rezaeian, M. Moghimi, A. H. Abdolghaffari, and M.

A. Zarandi, “Morphology, drug release, antibacterial, cell proliferation, and histology studies of chamomile-loaded wound dressing mats based on electrospun nanofibrous poly(ε-caprolactone)/polystyrene blends,” *J. Biomed. Mater. Res. - Part B Appl. Biomater.*, vol. 102, no. 5, pp. 977–987, 2014.

[177] S. Suganya, T. Senthil Ram, B. S. Lakshmi, and V. R. Giridev, “Herbal drug incorporated antibacterial nanofibrous mat fabricated by electrospinning: An excellent matrix for wound dressings,” *J. Appl. Polym. Sci.*, vol. 121, no. 5, pp. 2893–2899, 2011.

[178] S. Lin *et al.*, “Green electrospun grape seed extract-loaded silk fibroin nanofibrous mats with excellent cytocompatibility and antioxidant effect,” *Colloids Surfaces B Biointerfaces*, vol. 139, pp. 156–163, 2016.

[179] J. Han, T.-X. Chen, C. J. Branford-White, and L.-M. Zhu, “Electrospun shikonin-loaded PCL/PTMC composite fiber mats with potential biomedical applications,” *Int. J. Pharm.*, vol. 382, no. 1, pp. 215–221, 2009.

[180] O. Suwantong, P. Pankongadisak, S. Deachathai, and P. Supaphol, “Electrospun poly(L-lactic acid) fiber mats containing a crude Garcinia cowa extract for wound dressing applications,” *J. Polym. Res.*, vol. 19, no. 6, pp. 9896–9906, 2012.

[181] S. Agnes Mary and V. R. Giri Dev, “Electrospun herbal nanofibrous wound dressings for skin tissue engineering,” *J. Text. Inst.*, vol. 106, no. 8, pp. 886–895, 2015.

[182] X. Y. Dai, W. Nie, Y. C. Wang, Y. Shen, Y. Li, and S. J. Gan, “Electrospun emodin polyvinylpyrrolidone blended nanofibrous membrane: A novel medicated biomaterial for drug delivery and accelerated wound healing,” *J. Mater. Sci. Mater. Med.*, vol. 23, no. 11, pp. 2709–2716, 2012.

[183] N. Charernsriwilaiwat, T. Rojanarata, T. Ngawhirunpat, M. Sukma, and P. Opanasopit, “Electrospun chitosan-based nanofiber mats loaded with Garcinia mangostana extracts,” *Int. J. Pharm.*, vol. 452, no. 1, pp. 333–343, 2013.

[184] O. Suwantong, U. Ruktanonchai, and P. Supaphol, “Electrospun cellulose acetate fiber mats containing asiaticoside or Centella asiatica crude extract

and the release characteristics of asiaticoside," *Polymer (Guildf).*, vol. 49, no. 19, pp. 4239–4247, 2008.

[185] J. G. Merrell, S. W. McLaughlin, L. Tie, C. T. Laurencin, A. F. Chen, and L. S. Nair, "Curcumin-loaded poly(ε-caprolactone) nanofibres: Diabetic wound dressing with anti-oxidant and anti-inflammatory properties," *Clin. Exp. Pharmacol. Physiol.*, vol. 36, no. 12, pp. 1149–1156, 2009.

[186] V. Kant, A. Gopal, N. N. Pathak, P. Kumar, S. K. Tandan, and D. Kumar, "Antioxidant and anti-inflammatory potential of curcumin accelerated the cutaneous wound healing in streptozotocin-induced diabetic rats," *Int. Immunopharmacol.*, vol. 20, no. 2, pp. 322–330, 2014.

[187] M.-Y. Bai, T.-C. Chou, J.-C. Tsai, and H.-C. Yang, "Active ingredient-containing chitosan/polycaprolactone nonwoven mats: Characterizations and their functional assays," *Mater. Sci. Eng. C*, vol. 33, no. 1, pp. 224–233, 2013.

[188] S.-Z. Fu *et al.*, "Acceleration of dermal wound healing by using electrospun curcumin-loaded poly(ε-caprolactone)-poly(ethylene glycol)-poly(ε-caprolactone) fibrous mats," *J. Biomed. Mater. Res. Part B Appl. Biomater.*, vol. 102, no. 3, pp. 533–542, Apr. 2014.

[189] I. Liakos *et al.*, "Fibrous wound dressings encapsulating essential oils as natural antimicrobial agents," *J. Mater. Chem. B*, vol. 3, no. 8, pp. 1583–1589, 2015.

[190] N. A. A. Shukry, K. A. Sekak, M. R. Ahmad, and T. J. B. Effendi, "Characteristics of Electrospun PVA-Aloe vera Nanofibres Produced via Electrospinning," in *Proceedings of the International Colloquium in Textile Engineering*, ICTEFAD 20., M. R. Ahmad and M. F. Yahya, Eds. Singapore: Springer Singapore, 2014, pp. 7–11.

[191] H. M. Al-Youssef *et al.*, "Herbal drug loaded poly(D,L-lactide-co-glycolide) ultrafine fibers: Interaction with pathogenic bacteria," *Macromol. Res.*, vol. 21, no. 6, pp. 589–598, Jun. 2013.

[192] M. Suryamathi, C. Ruba, P. Viswanathamurthi, V. Balasubramanian, and P. Perumal, "Tridax Procumbens Extract Loaded Electrospun PCL Nanofibers: A

Novel Wound Dressing Material," *Macromol. Res.*, vol. 27, no. 1, pp. 55–60, 2019.

[193] E. A. T. Vargas, N. C. do Vale Baracho, J. de Brito, and A. A. A. de Queiroz, "Hyperbranched polyglycerol electrospun nanofibers for wound dressing applications," *Acta Biomater.*, vol. 6, no. 3, pp. 1069–1078, Mar. 2010.

[194] M. H. Gracia-Valenzuela, C. Orozco-Medina, and C. Molina-Maldonado, "Essential oils: their antibacterial properties and potential applications in foods—a review," *Hidrobiologica*, vol. 22, no. 3, pp. 201–206, 2012.

[195] P. Wen, D. H. Zhu, H. Wu, M. H. Zong, Y. R. Jing, and S. Y. Han, "Encapsulation of cinnamon essential oil in electrospun nanofibrous film for active food packaging," *Food Control*, vol. 59, pp. 366–376, 2016.

[196] M. Dadras Chomachayi, A. Solouk, S. Akbari, D. Sadeghi, F. Mirahmadi, and H. Mirzadeh, "Electrospun nanofibers comprising of silk fibroin/gelatin for drug delivery applications: Thyme essential oil and doxycycline monohydrate release study," *J. Biomed. Mater. Res. - Part A*, vol. 106, no. 4, pp. 1092–1103, 2018.

[197] F. T. da Silva *et al.*, "Action of ginger essential oil (Zingiber officinale) encapsulated in proteins ultrafine fibers on the antimicrobial control in situ," *Int. J. Biol. Macromol.*, vol. 118, pp. 107–115, 2018.

[198] K. Balasubramanian and K. M. Kodam, "Encapsulation of therapeutic lavender oil in an electrolyte assisted polyacrylonitrile nanofibres for antibacterial applications," *RSC Adv.*, vol. 4, no. 97, pp. 54892–54901, 2014.

[199] T. T. T. Nguyen, C. Ghosh, S. G. Hwang, L. D. Tran, and J. S. Park, "Characteristics of curcumin-loaded poly (lactic acid) nanofibers for wound healing," *J. Mater. Sci.*, vol. 48, no. 20, pp. 7125–7133, 2013.

[200] K. A. Rieger, N. P. Birch, and J. D. Schiffman, "Electrospinning chitosan/poly(ethylene oxide) solutions with essential oils: Correlating solution rheology to nanofiber formation," *Carbohydr. Polym.*, vol. 139, pp. 131–138, 2016.

[201] M. Adeli-Sardou, M. M. Yaghoobi, M. Torkzadeh-Mahani, and M. Dodel,

“Controlled release of lawsone from polycaprolactone/gelatin electrospun nano fibers for skin tissue regeneration,” *Int. J. Biol. Macromol.*, vol. 124, pp. 478–491, 2019.

[202] X. Chen *et al.*, “Shikonin , a Component of Chinese Herbal Medicine , Inhibits Chemokine Receptor Function and Suppresses Human Immunodeficiency Virus Type 1,” *Antimicrob. Agents Chemother.*, vol. 47, no. 9, pp. 2810–2816, 2003.

[203] K. N. Kontogiannopoulos, A. N. Assimopoulou, I. Tsivintzelis, C. Panayiotou, and V. P. Papageorgiou, “Electrospun fiber mats containing shikonin and derivatives with potential biomedical applications,” *Int. J. Pharm.*, vol. 409, no. 1, pp. 216–228, 2011.

[204] O. Suwantong, P. Opanasopit, U. Ruktanonchai, and P. Supaphol, “Electrospun cellulose acetate fiber mats containing curcumin and release characteristic of the herbal substance,” *Polymer (Guildf).*, vol. 48, no. 26, pp. 7546–7557, 2007.

[205] H. T. Bui, O. H. Chung, J. Dela Cruz, and J. S. Park, “Fabrication and characterization of electrospun curcumin-loaded polycaprolactone-polyethylene glycol nanofibers for enhanced wound healing,” *Macromol. Res.*, vol. 22, no. 12, pp. 1288–1296, Dec. 2014.

[206] X. Z. Sun, G. R. Williams, X. X. Hou, and L. M. Zhu, “Electrospun curcumin-loaded fibers with potential biomedical applications,” *Carbohydr. Polym.*, vol. 94, no. 1, pp. 147–153, 2013.

[207] M. Noruzi, “Electrospun nanofibres in agriculture and the food industry: a review,” *J. Sci. Food Agric.*, vol. 96, no. 14, pp. 4663–4678, 2016.

[208] A.-C. Vega-Lugo and L.-T. Lim, “Controlled release of allyl isothiocyanate using soy protein and poly(lactic acid) electrospun fibers,” *Food Res. Int.*, vol. 42, no. 8, pp. 933–940, 2009.

[209] S. Suganya, J. Venugopal, S. Ramakrishna, B. S. Lakshmi, and V. R. Giri Dev, “Herbally derived polymeric nanofibrous scaffolds for bone tissue regeneration,” *J. Appl. Polym. Sci.*, vol. 131, no. 3, 2014.

[210] S. Pajoumshariati, S. K. Yavari, and M. A. Shokrgozar, “Physical and Biological Modification of Polycaprolactone Electrospun Nanofiber by Panax Ginseng Extract for Bone Tissue Engineering Application,” *Ann. Biomed. Eng.*, vol. 44, no. 5, pp. 1808–1820, 2016.

[211] M. Selvakumar, H. S. Pawar, N. K. Francis, B. Das, S. Dhara, and S. Chattopadhyay, “Excavating the Role of Aloe Vera Wrapped Mesoporous Hydroxyapatite Frame Ornamentation in Newly Architectured Polyurethane Scaffolds for Osteogenesis and Guided Bone Regeneration with Microbial Protection,” *ACS Appl. Mater. Interfaces*, vol. 8, no. 9, pp. 5941–5960, 2016.

[212] D. Huang *et al.*, “Electrospun gelatin nanofibers encapsulated with peppermint and chamomile essential oils as potential edible packaging,” *J. Agric. Food Chem.*, vol. 67, pp. 2227–2234, 2019.

[213] G. P. Nagaraju, S. Aliya, S. F. Zafar, R. Basha, R. Diaz, and B. F. El-Rayes, “The impact of curcumin on breast cancer,” *Integr. Biol. (United Kingdom)*, vol. 4, no. 9, pp. 996–1007, 2012.

[214] G. Guo *et al.*, “Preparation of curcumin loaded poly(ε-caprolactone)-poly(ethylene glycol)-poly(ε-caprolactone) nanofibers and their in vitro antitumor activity against Glioma 9L cells,” *Nanoscale*, vol. 3, no. 9, pp. 3825–3832, 2011.

[215] R. Sridhar *et al.*, “Curcumin- and natural extract-loaded nanofibres for potential treatment of lung and breast cancer: *in vitro* efficacy evaluation,” *J. Biomater. Sci. Polym. Ed.*, vol. 25, no. 10, pp. 985–998, 2014.

[216] J. Anu Bhushani and C. Anandharamakrishnan, “Electrospinning and electrospraying techniques: Potential food based applications,” *Trends Food Sci. Technol.*, vol. 38, no. 1, pp. 21–33, 2014.

[217] B. Ghorani and N. Tucker, “Fundamentals of electrospinning as a novel delivery vehicle for bioactive compounds in food nanotechnology,” *Food Hydrocoll.*, vol. 51, pp. 227–240, 2015.

[218] A. Fernandez, S. Torres-Giner, and J. M. Lagaron, “Novel route to stabilization of bioactive antioxidants by encapsulation in electrospun fibers of zein

prolamine," *Food Hydrocoll.*, vol. 23, no. 5, pp. 1427–1432, 2009.

[219] Y. P. Neo *et al.*, "Encapsulation of food grade antioxidant in natural biopolymer by electrospinning technique: A physicochemical study based on zein-gallic acid system," *Food Chem.*, vol. 136, no. 2, pp. 1013–1021, 2013.

[220] L. Sun, C. Zhang, and P. Li, "Characterization, Antimicrobial Activity, and Mechanism of a High-Performance (−)-Epigallocatechin-3-gallate (EGCG)−Cu ^{II} /Polyvinyl Alcohol (PVA) Nanofibrous Membrane," *J. Agric. Food Chem.*, vol. 59, no. 9, pp. 5087–5092, May 2011.

[221] H. M. C. Marques, "A review on cyclodextrin encapsulation of essential oils and volatiles," *Flavour Fragr. J.*, vol. 25, no. 5, pp. 313–326, 2010.

[222] Z. Aytac, S. I. Kusku, E. Durgun, and T. Uyar, "Quercetin/β-cyclodextrin inclusion complex embedded nanofibres: Slow release and high solubility," *Food Chem.*, vol. 197, pp. 864–871, Apr. 2016.

[223] F. Kayaci and T. Uyar, "Encapsulation of vanillin/cyclodextrin inclusion complex in electrospun polyvinyl alcohol (PVA) nanowebs: Prolonged shelf-life and high temperature stability of vanillin," *Food Chem.*, vol. 133, no. 3, pp. 641–649, 2012.

[224] F. Kayaci, Y. Ertas, and T. Uyar, "Enhanced thermal stability of eugenol by cyclodextrin inclusion complex encapsulated in electrospun polymeric nanofibers," *J. Agric. Food Chem.*, vol. 61, no. 34, pp. 8156–8165, 2013.

[225] F. Kayaci, H. S. Sen, E. Durgun, and T. Uyar, "Functional electrospun polymeric nanofibers incorporating geraniol-cyclodextrin inclusion complexes: High thermal stability and enhanced durability of geraniol," *Food Res. Int.*, vol. 62, pp. 424–431, 2014.

[226] Z. Aytac, Z. I. Yildiz, F. Kayaci-Senirmak, N. O. San Keskin, T. Tekinay, and T. Uyar, "Electrospinning of polymer-free cyclodextrin/geraniol-inclusion complex nanofibers: Enhanced shelf-life of geraniol with antibacterial and antioxidant properties," *RSC Adv.*, vol. 6, no. 52, pp. 46089–46099, 2016.

[227] E. Mascheroni *et al.*, "Encapsulation of volatiles in nanofibrous polysaccharide membranes for humidity-triggered release," *Carbohydr. Polym.*, vol. 98, no. 1,

pp. 17–25, 2013.

[228] M. Aceituno-Medina, S. Mendoza, B. A. Rodríguez, J. M. Lagaron, and A. López-Rubio, “Improved antioxidant capacity of quercetin and ferulic acid during in-vitro digestion through encapsulation within food-grade electrospun fibers,” *J. Funct. Foods*, vol. 12, pp. 332–341, 2015.

[229] P. Appendini and J. H. Hotchkiss, “Review of antimicrobial food packaging,” *Innov. Food Sci. Emerg. Technol.*, vol. 3, no. 2, pp. 113–126, 2002.

[230] M. J. Fabra *et al.*, “Efficacy of Cinnamaldehyde Against Enteric Viruses and Its Activity After Incorporation Into Biodegradable Multilayer Systems of Interest in Food Packaging,” *Food Environ. Virol.*, vol. 8, no. 2, pp. 125–132, Jun. 2016.

[231] T. Amna, J. Yang, K.-S. Ryu, and I. H. Hwang, “Electrospun antimicrobial hybrid mats: Innovative packaging material for meat and meat-products,” *J. Food Sci. Technol.*, vol. 52, no. 7, pp. 4600–4606, Jul. 2015.

[232] D.-W. Sun, *Modern Techniques for Food Authentication*. Academic Press, 2008.

[233] F. Christoph, K. H. KubecZka, and E. Stahl-Biskup, “The composition of commercial manuka oils from New Zealand,” *J. Essent. Oil Res.*, vol. 11, no. 6, pp. 705–710, 1999.

[234] N. G. Porter and A. L. Wilkins, “Chemical, physical and antimicrobial properties of essential oils of Leptospermum scoparium and Kunzea ericoides,” *Phytochemistry*, vol. 50, no. 3, pp. 407–415, 1998.

[235] D. P. Killeen, L. Larsen, F. E. Dayan, K. C. Gordon, N. B. Perry, and J. W. Van Klink, “Nortriketones: Antimicrobial Trimethylated Acylphloroglucinols from Mānuka (Leptospermum scoparium),” *J. Nat. Prod.*, vol. 79, no. 3, pp. 564–569, 2016.

[236] D. P. Killeen, J. W. van Klink, B. M. Smallfield, K. C. Gordon, and N. B. Perry, “Herbicidal β-triketones are compartmentalized in leaves of Leptospermum species: Localization by Raman microscopy and rapid screening,” *New Phytol.*, vol. 205, no. 1, pp. 339–349, 2015.

[237] P. Jentzsch, L. Ramos, and V. Ciobotă, “Handheld Raman Spectroscopy for

the Distinction of Essential Oils Used in the Cosmetics Industry," *Cosmetics*, vol. 2, no. 2, pp. 162–176, 2015.

[238] S. Pirani, H. M. N. Abushammala, and R. Hashaikeh, "Preparation and characterization of electrospun PLA/nanocrystalline cellulose-based composites," *J. Appl. Polym. Sci.*, vol. 130, no. 5, pp. 3345–3354, 2013.

[239] M. P. Arrieta, J. López, S. Ferrándiz, and M. A. Peltzer, "Characterization of PLA-limonene blends for food packaging applications," *Polym. Test.*, vol. 32, no. 4, pp. 760–768, 2013.

[240] T. Mekonnen, P. Mussone, H. Khalil, and D. Bressler, "Progress in bio-based plastics and plasticizing modifications," *J. Mater. Chem. A*, vol. 1, no. 43, pp. 13379–13398, 2013.

[241] J. S. Raut and S. M. Karuppayil, "A status review on the medicinal properties of essential oils," *Ind. Crops Prod.*, vol. 62, pp. 250–264, 2014.

[242] M. G. A. Vieira, M. A. Da Silva, L. O. Dos Santos, and M. M. Beppu, "Natural-based plasticizers and biopolymer films: A review," *Eur. Polym. J.*, vol. 47, no. 3, pp. 254–263, 2011.

[243] V. Nagarajan, A. K. Mohanty, and M. Misra, "Perspective on Polylactic Acid (PLA) based Sustainable Materials for Durable Applications: Focus on Toughness and Heat Resistance," *ACS Sustain. Chem. Eng.*, vol. 4, no. 6, pp. 2899–2916, 2016.

[244] S. J. Lee, S. H. Oh, J. Liu, S. Soker, A. Atala, and J. J. Yoo, "The use of thermal treatments to enhance the mechanical properties of electrospun poly(ε-caprolactone) scaffolds," *Biomaterials*, vol. 29, no. 10, pp. 1422–1430, 2008.

[245] L. Mascia, R. Su, J. Clarke, Y. Lou, and E. Mele, "Fibres from blends of epoxidized natural rubber and polylactic acid by the electrospinning process: Compatibilization and surface texture," *Eur. Polym. J.*, vol. 87, pp. 241–254, 2017.

[246] S.-S. Choi, S. G. Lee, C. W. Joo, S. S. Im, and S. H. Kim, "Formation of interfiber bonding in electrospun poly(etherimide) nanofiber web," *J. Mater.*

Sci., vol. 39, no. 4, pp. 1511–1513, Feb. 2004.

[247] Y. You, S. Won Lee, S. Jin Lee, and W. H. Park, “Thermal interfiber bonding of electrospun poly(l-lactic acid) nanofibers,” *Mater. Lett.*, vol. 60, no. 11, pp. 1331–1333, May 2006.

[248] C. F. Carson, K. a Hammer, T. V Riley, C. F. Carson, K. a Hammer, and T. V Riley, “Melaleuca alternifolia (Tea Tree) Oil : a Review of Antimicrobial and Other Medicinal Properties Melaleuca alternifolia (Tea Tree) Oil : a Review of Antimicrobial and Other Medicinal Properties,” *Clin. Microbiol. Rev.*, vol. 19, no. 1, pp. 50–62, 2006.

[249] Q. Shi, C. Zhou, Y. Yue, W. Guo, Y. Wu, and Q. Wu, “Mechanical properties and in vitro degradation of electrospun bio-nanocomposite mats from PLA and cellulose nanocrystals,” *Carbohydr. Polym.*, vol. 90, no. 1, pp. 301–308, 2012.

[250] J. Ahmed, M. Z. Mulla, and Y. A. Arfat, “Thermo-mechanical, structural characterization and antibacterial performance of solvent casted polylactide/cinnamon oil composite films,” *Food Control*, vol. 69, pp. 196–204, Nov. 2016.

[251] S. Benavides, R. Villalobos-Carvajal, and J. E. Reyes, “Physical, mechanical and antibacterial properties of alginate film: Effect of the crosslinking degree and oregano essential oil concentration,” *J. Food Eng.*, vol. 110, no. 2, pp. 232–239, 2012.

[252] M. Llana-Ruiz-Cabello *et al.*, “Development of PLA films containing oregano essential oil (Origanum vulgare L. virens) intended for use in food packaging,” *Food Addit. Contam. - Part A Chem. Anal. Control. Expo. Risk Assess.*, vol. 33, no. 8, pp. 1374–1386, 2016.

[253] D. Phebe and P. T. Ong, “Antimicrobial, Mechanical, and barrier properties of cassava starch-chitosan films incorporated with oregano essential oil,” *Int. Food Res. J.*, vol. 17, no. 1, pp. 63–69, 2010.

[254] G. Kavoosi, A. Rahmatollahi, S. M. M. Dadfar, and A. M. Purfard, “Effects of essential oil on the water binding capacity, physico-mechanical properties, antioxidant and antibacterial activity of gelatin films,” *Lwt-Food Sci. Technol.*,

vol. 57, no. 2, pp. 556–561, 2014.

[255] S. Acosta, A. Chiralt, P. Santamarina, J. Rosello, C. González-Martínez, and M. Cháfer, “Antifungal films based on starch-gelatin blend, containing essential oils,” *Food Hydrocoll.*, vol. 61, pp. 233–240, 2016.

[256] Y. Qin, W. Li, D. Liu, M. Yuan, and L. Li, “Development of active packaging film made from poly (lactic acid) incorporated essential oil,” *Prog. Org. Coatings*, vol. 103, pp. 76–82, 2017.

[257] F. Croisier *et al.*, “Mechanical testing of electrospun PCL fibers,” *Acta Biomater.*, vol. 8, no. 1, pp. 218–224, 2012.

[258] X. Monnier *et al.*, “Molecular dynamics in electrospun amorphous plasticized polylactide fibers,” *Polym. (United Kingdom)*, vol. 73, pp. 68–78, 2015.

[259] S. Homaeigohar, J. Koll, E. T. Lilleodden, and M. Elbahri, “The solvent induced interfiber adhesion and its influence on the mechanical and filtration properties of polyethersulfone electrospun nanofibrous microfiltration membranes,” *Sep. Purif. Technol.*, vol. 98, pp. 456–463, Sep. 2012.

[260] R. Erdem *et al.*, “Electrospinning of single and multilayered scaffolds for tissue engineering applications,” *J. Text. Inst.*, vol. 108, no. 6, pp. 935–946, 2017.

[261] S. Ramaswamy, L. I. Clarke, and R. E. Gorga, “Morphological, mechanical, and electrical properties as a function of thermal bonding in electrospun nanocomposites,” *Polymer (Guildf).*, vol. 52, pp. 3183–3189, 2011.

[262] F. Kayaci, O. C. O. Umu, T. Tekinay, and T. Uyar, “Antibacterial electrospun poly(lactic acid) (PLA) nanofibrous webs incorporating triclosan/cyclodextrin inclusion complexes,” *J. Agric. Food Chem.*, vol. 61, no. 16, pp. 3901–3908, 2013.

[263] M. Otto, “Staphylococcus epidermidis — the ‘accidental’ pathogen,” *Nat. Rev. Microbiol.*, vol. 7, pp. 555–567, 2009.

[264] P. Fratzl and R. Weinkamer, “Nature’s hierarchical materials,” *Prog. Mater. Sci.*, vol. 52, no. 8, p. 1263, Nov. 2007.

[265] R. Lakes, “Materials with structural hierarchy,” *Nature*, vol. 361, p. 511, Feb.

1993.

[266] F. Vollrath and D. P. Knight, “Liquid crystalline spinning of spider silk.,” *Nature*, vol. 410, no. 6828, p. 541, Mar. 2001.

[267] D.-G. Yu, X.-Y. Li, X. Wang, J.-H. Yang, S. W. A. Bligh, and G. R. Williams, “Nanofibers Fabricated Using Triaxial Electrospinning as Zero Order Drug Delivery Systems,” *ACS Appl. Mater. Interfaces*, vol. 7, no. 33, p. 18891, Aug. 2015.

[268] J.-Y. Rho, L. Kuhn-Spearing, and P. Zioupos, “Mechanical properties and the hierarchical structure of bone,” *Med. Eng. Phys.*, vol. 20, no. 2, pp. 92–102, Mar. 1998.

[269] N. Reznikov, R. Shahar, and S. Weiner, “Bone hierarchical structure in three dimensions,” in *Acta Biomaterialia*, 2014, vol. 10, no. 9, pp. 3815–3826.

[270] H. Zhou, J. Guo, P. Li, T. Fan, D. Zhang, and J. Ye, “Leaf-architectured 3D Hierarchical Artificial Photosynthetic System of Perovskite Titanates Towards CO2 Photoreduction Into Hydrocarbon Fuels,” *Sci. Rep.*, vol. 3, no. 1, p. 1667, Dec. 2013.

[271] J. Liu, S. Z. Qiao, S. B. Hartono, G. Qing, and M. Lu, “Monodisperse Yolk – Shell Nanoparticles with a Hierarchical Porous Structure for Delivery Vehicles and Nanoreactors **,” pp. 4981–4985, 2010.

[272] C. M. A. Parlett, K. Wilson, and A. F. Lee, “Hierarchical porous materials: Catalytic applications,” *Chemical Society Reviews*, vol. 42, no. 9. pp. 3876–3893, 2013.

[273] W. Huang, H. Zhang, W. Wang, and S. Wei, “Hierarchical porous carbon obtained from animal bone and evaluation in electric double-layer capacitors,” *Carbon N. Y.*, vol. 49, no. 3, pp. 838–843, 2010.

[274] Y. G. Ko, N. Kawazoe, T. Tateishi, and G. Chen, “Preparation of chitosan scaffolds with a hierarchical porous structure,” *J. Biomed. Mater. Res. - Part B Appl. Biomater.*, vol. 93, no. 2, pp. 341–350, 2010.

[275] C.-L. Zhang and S.-H. Yu, “Spraying functional fibres by electrospinning,” *Mater. Horizons*, vol. 3, no. 3, p. 266, 2016.

[276] E. Rezabeigi *et al.*, “Electrospinning of porous polylactic acid fibers during nonsolvent induced phase separation,” *J. Appl. Polym. Sci.*, vol. 134, no. 20, 2017.

[277] J. Wu, X. Qin, C. Miao, Y. He, and G. Liang, “A honeycomb-cobweb inspired hierarchical core e shell structure design for electrospun silicon / carbon fi bers as lithium-ion battery anodes,” *Carbon N. Y.*, vol. 98, pp. 582–591, 2016.

[278] S. Sankar, C. S. Sharma, S. N. Rath, and S. Ramakrishna, “Electrospun nanofibres to mimic natural hierarchical structure of tissues: application in musculoskeletal regeneration,” *Journal of Tissue Engineering and Regenerative Medicine*, vol. 12. pp. 604–619, 2018.

[279] S. M. Bhaway *et al.*, “Hierarchical Electrospun and Cooperatively Assembled Nanoporous Ni/NiO/MnO x /Carbon Nanofiber Composites for Lithium Ion Battery Anodes,” *ACS Appl. Mater. Interfaces*, vol. 8, no. 30, pp. 19484–19493, 2016.

[280] S. Zhan, D. Chen, X. Jiao, and S. Liu, “Facile fabrication of long α-Fe2O3, α-Fe and γ-Fe2O3 hollow fibers using sol-gel combined co-electrospinning technology,” *J. Colloid Interface Sci.*, vol. 308, no. 1, pp. 265–270, Apr. 2007.

[281] D. Li, J. T. McCann, and Y. Xia, “Use of electrospinning to directly fabricate hollow nanofibers with functionalized inner and outer surfaces,” *Small*, vol. 1, no. 1, pp. 83–86, 2005.

[282] Y. Z. Zhang, J. Venugopal, Z. M. Huang, C. T. Lim, and S. Ramakrishna, “Characterization of the surface biocompatibility of the electrospun PCL-Collagen nanofibers using fibroblasts,” *Biomacromolecules*, vol. 6, no. 5, pp. 2583–2589, 2005.

[283] A. Gupta, C. D. Saquing, M. Afshari, A. E. Tonelli, S. A. Khan, and R. Kotek, “Porous Nylon-6 Fibers via a Novel Salt-Induced Electrospinning Method,” *Macromolecules*, vol. 42, no. 3, p. 709, Feb. 2009.

[284] Z. Wei *et al.*, “Porous Electrospun PES/PEG Ultrafine Fibers for the Removal of Endocrine Disruptors,” *Sep. Sci. Technol.*, vol. 48, no. 15, pp. 2287–2292, 2013.

[285] S. O. Han, W. K. Son, D. Cho, J. H. Youk, and W. H. Park, “Preparation of porous ultra-fine fibres via selective thermal degradation of electrospun polyetherimide/poly(3-hydroxybutyrate-co-3-hydroxyvalerate) fibres,” *Polym. Degrad. Stab.*, vol. 86, no. 2, pp. 257–262, Nov. 2004.

[286] L. Jun, Y. Zhang, Y. Hao, L. Cheng, and J. J. Zhang, “Preparation of porous electro-spun UPM fibers via photocrosslinking,” *J. Appl. Polym. Sci.*, vol. 112, no. 4, pp. 2247–2254, 2009.

[287] W. S. Lyoo, J. H. Youk, S. W. Lee, and W. H. Park, “Preparation of porous ultra-fine poly(vinyl cinnamate) fibers,” *Mater. Lett.*, vol. 59, no. 28, pp. 3558–3562, 2005.

[288] T. Ruotsalainen *et al.*, “Towards Internal Structuring of Electrospun Fibers by Hierarchical Self-Assembly of Polymeric Comb-Shaped Supramolecules,” *Adv. Mater.*, vol. 17, no. 8, p. 1048, Apr. 2005.

[289] T. Ruotsalainen *et al.*, “Tailoring of the hierarchical structure within electrospun fibers due to supramolecular comb-coil block copolymers: Polystyrene-block-poly(4-vinyl pyridine) plasticized by hydrogen bonded pentadecylphenol,” *Soft Matter*, vol. 3, no. 8, pp. 978–985, 2007.

[290] S. Megelski, J. S. Stephens, D. B. Chase, and J. F. Rabolt, “Micro-and Nanostructured Surface Morphology on Electrospun Polymer Fibers,” *Macromolecules*, vol. 35, no. 22, p. 8456, 2002.

[291] C. L. Casper, J. S. Stephens, N. G. Tassi, D. B. Chase, and J. F. Rabolt, “Controlling surface morphology of electrospun polystyrene fibers: Effect of humidity and molecular weight in the electrospinning process,” *Macromolecules*, vol. 37, no. 2, pp. 573–578, 2004.

[292] Y. Li, C. T. Lim, and M. Kotaki, “Study on structural and mechanical properties of porous PLA nanofibers electrospun by channel-based electrospinning system,” *Polymer (Guildf).*, vol. 56, p. 572, Jan. 2015.

[293] B. Ding, J. Yang, J. Lin, G. Sun, and J. Yu, “Subtle regulation of the micro- and nanostructures of electrospun polystyrene fibers and their application in oil absorption,” *Nanoscale*, vol. 4, no. 1, pp. 176–182, 2011.

[294] Y. Wang *et al.*, “Electrospun TiO2-SiO2 fibres with hierarchical pores from phase separation,” *CrystEngComm*, vol. 19, no. 19, pp. 2673–2680, 2017.

[295] L. Natarajan, J. New, A. Dasari, S. Yu, and M. A. Manan, “Surface morphology of electrospun PLA fibers: mechanisms of pore formation,” *RSC Adv.*, vol. 4, no. 83, p. 44082, Sep. 2014.

[296] L. Li, Z. Jiang, M. Li, R. Li, and T. Fang, “Hierarchically structured PMMA fibers fabricated by electrospinning,” *RSC Adv.*, vol. 4, p. 52973, 2014.

[297] J. Zheng, H. Zhang, Z. Zhao, and C. C. Han, “Construction of hierarchical structures by electrospinning or electrospraying,” *Polymer (Guildf).*, vol. 53, no. 2, pp. 546–554, 2012.

[298] M. Bognitzki *et al.*, “Nanostructured fibers via electrospinning,” *Adv. Mater.*, vol. 13, no. 1, pp. 70–72, 2001.

[299] J. T. Mccann, M. Marquez, and Y. Xia, “Highly Porous Fibers by Electrospinning into a Cryogenic Liquid,” pp. 1436–1437, 2006.

[300] P. Dayal, J. Liu, S. Kumar, and T. Kyu, “Experimental and theoretical investigations of porous structure formation in electrospun fibers,” *Macromolecules*, vol. 40, no. 21, pp. 7689–7694, 2007.

[301] Y. Z. Zhang, Y. Feng, Z. M. Huang, S. Ramakrishna, and C. T. Lim, “Fabrication of porous electrospun nanofibres,” *Nanotechnology*, vol. 17, no. 3, pp. 901–908, 2006.

[302] H. Li, Y. Xu, H. Xu, and J. Chang, “Electrospun membranes: Control of the structure and structure related applications in tissue regeneration and drug delivery,” *Journal of Materials Chemistry B*, vol. 2, no. 34. pp. 5492–5510, 2014.

[303] R. J. Wade and J. A. Burdick, “Advances in nanofibrous scaffolds for biomedical applications : From electrospinning to self-assembly,” *Nano Today*, vol. 9, no. 6, pp. 722–742, 2014.

[304] C.-M. Hsu and S. Shivkumar, “Nano-sized beads and porous fiber constructs of Poly(ε-caprolactone) produced by electrospinning,” *J. Mater. Sci.*, vol. 39, no. 9, p. 3003, 2004.

[305] J. Lin, B. Ding, J. Yang, J. Yu, and G. Sun, “Subtle regulation of the micro- and nanostructures of electrospun polystyrene fibers and their application in oil absorption,” *Nanoscale*, vol. 4, no. 1, p. 176, Dec. 2012.

[306] M. Bognitzki *et al.*, “Nanostructured Fibers via Electrospinning,” *Adv. Mater.*, vol. 13, no. 1, p. 70, Jan. 2001.

[307] C. L. Casper, J. S. Stephens, N. G. Tassi, D. B. Chase, and J. F. Rabolt, “Controlling Surface Morphology of Electrospun Polystyrene Fibers: Effect of Humidity and Molecular Weight in the Electrospinning Process,” *Macromolecules*, vol. 37, no. 2, p. 573, 2004.

[308] J. T. Mccann, M. Marquez, and Y. Xia, “Highly Porous Fibers by Electrospinning into a Cryogenic Liquid,” *J. Am. Chem. Soc.*, vol. 128, no. 5, p. 1436, 2006.

[309] W. S. Lyoo, J. H. Youk, S. W. Lee, and W. H. Park, “Preparation of porous ultra-fine poly(vinyl cinnamate) fibers,” *Mater. Lett.*, vol. 59, no. 28, pp. 3558–3562, Dec. 2005.

[310] L. Jun, Y. Zhang, Y. Hao, L. Cheng, and J. J. Zhang, “Preparation of porous electro-spun UPM fibers via photocrosslinking,” *J. Appl. Polym. Sci.*, vol. 112, no. 4, pp. 2247–2254, May 2009.

[311] Z. Wei *et al.*, “Porous Electrospun PES/PEG Ultrafine Fibers for the Removal of Endocrine Disruptors,” *Sep. Sci. Technol.*, vol. 48, no. 15, p. 2287, Oct. 2013.

[312] P. Dayal, J. Liu, S. Kumar, and T. Kyu, “Experimental and Theoretical Investigations of Porous Structure Formation in Electrospun Fibers,” *Macromolecules*, vol. 40, no. 21, p. 7689, 2007.

[313] M. Ma *et al.*, “Decorated electrospun fibers exhibiting superhydrophobicity,” *Adv. Mater.*, vol. 19, no. 2, pp. 255–259, 2007.

[314] M. F. Leong, K. S. Chian, P. S. Mhaisalkar, W. F. Ong, and B. D. Ratner, “Effect of electrospun poly(D,L-lactide) fibrous scaffold with nanoporous surface on attachment of porcine esophageal epithelial cells and protein adsorption,” *J. Biomed. Mater. Res. - Part A*, vol. 89, no. 4, pp. 1040–1048,

2009.

[315] S. Honarbakhsh and B. Pourdeyhimi, “Scaffolds for drug delivery, part I: Electrospun porous poly(lactic acid) and poly(lactic acid)/poly(ethylene oxide) hybrid scaffolds,” *J. Mater. Sci.*, vol. 46, no. 9, pp. 2874–2881, 2011.

[316] P. Lu and Y. Xia, “Maneuvering the internal porosity and surface morphology of electrospun polystyrene yarns by controlling the solvent and relative humidity,” *Langmuir*, vol. 29, no. 23, pp. 7070–7078, 2013.

[317] M. M. Demir, N. Horzum, A. Taşdemirci, K. Turan, and M. Güden, “Mechanical interlocking between porous electrospun polystyrene fibers and an epoxy matrix,” *ACS Appl. Mater. Interfaces*, vol. 6, no. 24, pp. 21901–21905, 2014.

[318] J. S. Chen, S. L. Tu, and R. Y. Tsay, “A morphological study of porous polylactide scaffolds prepared by thermally induced phase separation,” *J. Taiwan Inst. Chem. Eng.*, vol. 41, no. 2, pp. 229–238, 2010.

[319] P. Vandeweerdt, H. Berghmans, and Y. Tervoort, “Temperature-Concentration Behavior of Solutions of Polydisperse, Atactic Poly(methyl methacrylate) and Its Influence on the Formation of Amorphous, Microporous Membranes,” *Macromolecules*, vol. 24, no. 12, pp. 3547–3552, 1991.

[320] X.-Y. Ye, F.-W. Lin, X.-J. Huang, H.-Q. Liang, and Z.-K. Xu, “Polymer fibers with hierarchically porous structure: combination of high temperature electrospinning and thermally induced phase separation,” *RSC Adv.*, vol. 3, no. 33, p. 13851, 2013.

[321] E. Rezabeigi *et al.*, “Electrospinning of porous polylactic acid fibers during nonsolvent induced phase separation,” *J. Appl. Polym. Sci.*, vol. 134, no. 20, p. 44862, May 2017.

[322] Z. Qi, H. Yu, Y. Chen, and M. Zhu, “Highly porous fibers prepared by electrospinning a ternary system of nonsolvent/solvent/poly(l-lactic acid),” *Mater. Lett.*, vol. 63, no. 3–4, pp. 415–418, 2009.

[323] X. Yu, H. Xiang, Y. Long, N. Zhao, X. Zhang, and J. Xu, “Preparation of porous polyacrylonitrile fibers by electrospinning a ternary system of PAN/DMF/H2O,” *Mater. Lett.*, vol. 64, no. 22, pp. 2407–2409, 2010.

[324] M. M. Demir, “Investigation on glassy skin formation of porous polystyrene fibers electrospun from DMF,” *Express Polym. Lett.*, vol. 4, no. 1, pp. 2–8, 2010.

[325] S. O. Han, W. K. Son, J. H. Youk, T. S. Lee, and W. H. Park, “Ultrafine porous fibers electrospun from cellulose triacetate,” *Mater. Lett.*, vol. 59, no. 24–25, p. 2998, Oct. 2005.

[326] H. Fashandi and M. Karimi, “Characterization of porosity of polystyrene fibers electrospun at humid atmosphere,” *Thermochim. Acta*, vol. 547, p. 38, Nov. 2012.

[327] X. Li *et al.*, “Electrospun preparation of polylactic acid nanoporous fiber membranes via thermal-nonsolvent induced phase separation,” *J. Taiwan Inst. Chem. Eng.*, vol. 60, pp. 636–642, 2016.

[328] K. A. G. Katsogiannis, G. T. Vladisavljević, and S. Georgiadou, “Porous electrospun polycaprolactone fibers: Effect of process parameters,” *J. Polym. Sci. Part B Polym. Phys.*, vol. 54, no. 18, pp. 1878–1888, Sep. 2016.

[329] X. Huang, J. Gao, W. Li, H. Xue, R. K. Y. Li, and Y. W. Mai, “Preparation of poly(ε-caprolactone) microspheres and fibers with controllable surface morphology,” *Mater. Des.*, vol. 117, no. 2017, pp. 298–304, 2017.

[330] H. R. Pant *et al.*, “Fabrication of highly porous poly (ε-caprolactone) fibers for novel tissue scaffold via water-bath electrospinning,” *Colloids Surfaces B Biointerfaces*, vol. 88, no. 2, pp. 587–592, 2011.

[331] Y. Z. Zhang, B. Su, J. Venugopal, S. Ramakrishna, and C. T. Lim, “Biomimetic and bioactive nanofibrous scaffolds from electrospun composite nanofibers,” *Int. J. Nanomedicine*, vol. 2, no. 4, pp. 623–638, 2007.

[332] G. Buschle-Diller, J. Cooper, Z. Xie, Y. Wu, J. Waldrup, and X. Ren, “Release of antibiotics from electrospun bicomponent fibers,” *Cellulose*, vol. 14, no. 6, pp. 553–562, 2007.

[333] L. Jiang *et al.*, “Fabrication of polycaprolactone electrospun fibers with different hierarchical structures mimicking collagen fibrils for tissue engineering scaffolds,” *Appl. Surf. Sci.*, vol. 427, pp. 311–325, 2018.

[334] L. Elemen, T. H. Seyidov, and M. Tugay, “The advantages of cyanoacrylate wound closure in circumcision,” *Pediatr. Surg. Int.*, vol. 27, no. 8, p. 879, Aug. 2011.

[335] A. T. Trott, “Cyanoacrylate Tissue Adhesives: An Advance in Wound Care,” *JAMA*, vol. 277, no. 19, p. 1559, May 1997.

[336] R. Kang *et al.*, “Cyanoacrylate medical glue application in intervertebral disc annulus defect repair: Mechanical and biocompatible evaluation,” *J. Biomed. Mater. Res. Part B Appl. Biomater.*, vol. 105, no. 1, p. 14, Jan. 2017.

[337] S. Wu, H. Yu, Y. Fan, J. Kong, and X. Yu, “Liver retraction using n -butyl-2-cyanoacrylate glue during single-incision laparoscopic upper abdominal surgery,” *Br. J. Surg.*, vol. 101, no. 5, p. 546, Apr. 2014.

[338] R. H. Dong *et al.*, “In situ precision electrospinning as an effective delivery technique for cyanoacrylate medical glue with high efficiency and low toxicity,” *Nanoscale*, vol. 7, no. 46, pp. 19468–19475, Nov. 2015.

[339] K. Jiang *et al.*, “Airflow-directed in situ electrospinning of a medical glue of cyanoacrylate for rapid hemostasis in liver resection,” *Nanoscale*, vol. 6, no. 14, p. 7792, Jun. 2014.

[340] S.-L. Liu *et al.*, “Solventless electrospinning of ultrathin polycyanoacrylate fibers,” *Polym. Chem.*, vol. 4, no. 23, p. 5696, Oct. 2013.

[341] N. E. Zander, “Hierarchically structured electrospun fibers,” *Polymers (Basel).*, vol. 5, no. 1, pp. 19–44, 2013.

[342] J. Liu, A. Rasheed, H. Dong, W. W. Carr, M. D. Dadmun, and S. Kumar, “Electrospun micro- and nanostructured polymer particles,” *Macromol. Chem. Phys.*, vol. 209, no. 23, pp. 2390–2398, 2008.

[343] L. Li, R. Li, M. Li, Z. Rong, and T. Fang, “Theoretical selection of solvent for production of electrospun PMMA fibers with wrinkled surfaces,” *RSC Adv.*, vol. 4, no. 53, pp. 27914–27921, 2014.

[344] B. Nottelet *et al.*, “Factorial design optimization and in vivo feasibility of poly(ε-caprolactone)-micro- and nanofiber-based small diameter vascular grafts,” *J. Biomed. Mater. Res. Part A*, vol. 89A, no. 4, p. 865, Jun. 2009.

[345] N. Bhardwaj and S. C. Kundu, “Electrospinning: A fascinating fiber fabrication technique,” *Biotechnology Advances*, vol. 28, no. 3. pp. 325–347, 2010.

[346] S.-H. Tan, R. Inai, M. Kotaki, and S. Ramakrishna, “Systematic parameter study for ultra-fine fiber fabrication via electrospinning process,” *Polymer (Guildf).*, vol. 46, no. 16, p. 6128, Jul. 2005.

[347] Y. Wu and R. L. Clark, “Controllable porous polymer particles generated by electrospraying,” *J. Colloid Interface Sci.*, vol. 310, no. 2, p. 529, Jun. 2007.

[348] R. V. N. Krishnappa, K. Desai, and C. Sung, “Morphological study of electrospun polycarbonates as a function of the solvent and processing voltage,” *J. Mater. Sci.*, vol. 38, no. 11, p. 2357, 2003.

[349] C. J. Luo, E. Stride, and M. Edirisinghe, “Mapping the influence of solubility and dielectric constant on electrospinning polycaprolactone solutions,” *Macromolecules*, vol. 45, no. 11, pp. 4669–4680, 2012.

[350] I. M. Smallwood, *Handbook of organic solvent properties*. Arnold, 1996.

[351] L. A. Bosworth and S. Downes, “Acetone, a Sustainable Solvent for Electrospinning Poly(ε-Caprolactone) Fibres: Effect of Varying Parameters and Solution Concentrations on Fibre Diameter,” *J. Polym. Environ.*, vol. 20, no. 3, pp. 879–886, 2012.

[352] X. H. Li, C. L. Shao, and Y. C. Liu, “A simple method for controllable preparation of polymer nanotubes via a single capillary electrospinning,” *Langmuir*, vol. 23, no. 22, pp. 10920–10923, 2007.

[353] A. V. Bazilevsky, A. L. Yarin, and C. M. Megaridis, “Co-electrospinning of core-shell fibers using a single-nozzle technique,” *Langmuir*, vol. 23, no. 5, pp. 2311–2314, 2007.

[354] S. W. Choi, I. W. Cheong, J. H. Kim, and Y. Xia, “Preparation of uniform microspheres using a simple fluidic device and their crystallization into close-packed lattices,” *Small*, vol. 5, no. 4, pp. 454–459, 2009.

[355] G. Yazgan *et al.*, “Steering surface topographies of electrospun fibers: Understanding the mechanisms,” *Sci. Rep.*, vol. 7, no. 1, pp. 1–13, 2017.

[356] Q. Zhang, Y. Li, Z. Ren, Z. Ahmad, X. Li, and G. Han, “Synthesis of porous CaTiO3nanotubes with tunable hollow structures via single-nozzle electrospinning,” *Mater. Lett.*, vol. 152, pp. 82–85, 2015.

[357] D. Durgalakshmi and S. Balakumar, “Phase separation induced shell thickness variations in electrospun hollow Bioglass 45S5 fiber mats for drug delivery applications,” *Phys. Chem. Chem. Phys.*, vol. 17, no. 23, pp. 15316–15323, 2015.

[358] S. Koombhongse, W. Liu, and D. H. Reneker, “Flat Polymer Ribbons and Other Shapes by Electrospinning,” *J. Polym. Sci. Part B Polym. Phys.*, vol. 39, no. 1, pp. 2363–2377, 2001.

[359] C. L. Pai, M. C. Boyce, and G. C. Rutledge, “Morphology of porous and wrinkled fibers of polystyrene electrospun from dimethylformamide,” *Macromolecules*, vol. 42, no. 6, pp. 2102–2114, 2009.

[360] H. Fashandi and M. Karimi, “Pore formation in polystyrene fiber by superimposing temperature and relative humidity of electrospinning atmosphere,” *Polymer (Guildf).*, vol. 53, no. 25, pp. 5832–5849, 2012.

[361] W. Liu, C. Huang, and X. Jin, “Electrospinning of Grooved Polystyrene Fibers: Effect of Solvent Systems,” *Nanoscale Res. Lett.*, vol. 10, no. 1, p. 237, 2015.

[362] O. R. Rodig, “Spectrometric Identification of Organic Compounds,” *J. Med. Chem.*, vol. 6, no. 6, pp. 826–827, 1963.

[363] X. Wang, H. Zhao, L. S. Turng, and Q. Li, “Crystalline morphology of electrospun poly(ε-caprolactone) (PCL) nanofibers,” *Ind. Eng. Chem. Res.*, vol. 52, no. 13, pp. 4939–4949, 2013.

[364] R. E. Kitson and N. E. Griffith, “Infrared Absorption Band Due to Nitrile Stretching Vibration,” *Anal. Chem.*, vol. 24, no. 2, pp. 334–337, 1952.

[365] T. YinChao, H. SuongHyu, and I. Yoshito, “Modification of synthesis and investigation of properties for 2-cyanoacrylate,” *Biomaterials*, vol. 11, no. 1, pp. 73–79, 1990.

[366] M. G. Han, S. Kim, and S. X. Liu, “Synthesis and degradation behavior of poly(ethyl cyanoacrylate),” *Polym. Degrad. Stab.*, vol. 93, no. 7, pp. 1243–

1251, 2008.

[367] K. Sanghoon and P. Steven C., “Development of Degradable Polymer Composites From Starch and Poly(ethyl cyanoacrylate),” *Polym. Compos.*, vol. 33, no. 6, pp. 904–911, 2012.

[368] Avraam I. Isayev, *Encyclopedia of Polymer Blends, Volume 3: Structure*. Wiley-VCH, 2016.

[369] R. Shukla and M. Cheryan, “Zein: The industrial protein from corn,” *Ind. Crops Prod.*, vol. 13, no. 3, pp. 171–192, 2001.

[370] S. Rishi and C. Munir, “Zein: industrial protein from corn,” *Ind. Crops Prod.*, vol. 13, pp. 171–192, 2001.

[371] M. Demir, L. Ramos-rivera, R. Silva, S. N. Nazhat, and A. R. Boccaccini, “Zein-based composites in biomedical applications,” pp. 1656–1665, 2017.

[372] S. Torres-Giner, E. Gimenez, and J. M. Lagaron, “Characterization of the morphology and thermal properties of Zein Prolamine nanostructures obtained by electrospinning,” *Food Hydrocoll.*, vol. 22, no. 4, pp. 601–614, 2008.

[373] E. Shoba *et al.*, “Electrospun protein nanofibers in healthcare: A review,” *Int. J. Pharm.*, vol. 523, no. 1, pp. 52–90, 2017.

[374] M. Dias Antunes *et al.*, “Antimicrobial electrospun ultrafine fibers from zein containing eucalyptus essential oil/cyclodextrin inclusion complex,” *Int. J. Biol. Macromol.*, vol. 104, pp. 874–882, 2017.

[375] F. Acevedo *et al.*, “Gallic acid loaded PEO-core/zein-shell nanofibers for chemopreventive action on gallbladder cancer cells,” *Eur. J. Pharm. Sci.*, vol. 119, no. February, pp. 49–61, 2018.

[376] H. Wang, L. Hao, P. Wang, M. Chen, and S. Jiang, “Release kinetics and antibacterial activity of curcumin loaded zein fi bers,” *Food Hydrocoll.*, vol. 63, pp. 437–446, 2017.

[377] H. Lu, Q. Wang, G. Li, Y. Qiu, and Q. Wei, “Electrospun water-stable zein / ethyl cellulose composite nano fi ber and its drug release properties,” vol. 74, pp. 86–93, 2017.

[378] K. Karthikeyan, S. Guhathakarta, R. Rajaram, and P. S. Korrapati, “Electrospun zein/eudragit nanofibers based dual drug delivery system for the simultaneous delivery of aceclofenac and pantoprazole,” *Int. J. Pharm.*, vol. 438, no. 1–2, pp. 117–122, 2012.

[379] S. Yang *et al.*, “Optimum Conditions for the Fabrication of Zein/Ag Composite Nanoparticles from Ethanol/H2O Co-Solvents Using Electrospinning,” *Nanomaterials*, vol. 6, no. 12, p. 230, 2016.

[380] S. Babitha and P. S. Korrapati, “Biodegradable zein-polydopamine polymeric scaffold impregnated with TiO2 nanoparticles for skin tissue engineering,” *Biomed. Mater.*, vol. 12, no. 5, 2017.

[381] C.-H. Chen, S.-H. Chen, K. T. Shalumon, and J.-P. Chen, “Dual functional core–sheath electrospun hyaluronic acid/polycaprolactone nanofibrous membranes embedded with silver nanoparticles for prevention of peritendinous adhesion,” *Acta Biomater.*, vol. 26, pp. 225–235, Oct. 2015.

[382] A. R. Unnithan, G. Gnanasekaran, Y. Sathishkumar, Y. S. Lee, and C. S. Kim, “Electrospun antibacterial polyurethane–cellulose acetate–zein composite mats for wound dressing,” *Carbohydr. Polym.*, vol. 102, pp. 884–892, Feb. 2014.

[383] U. Dashdorj *et al.*, “Fabrication and characterization of electrospun zein / Ag nanocomposite mats for wound dressing applications,” *Int. J. Biol. Macromol.*, vol. 80, pp. 1–7, 2015.

[384] L. Mascia, “Fillers Generated In-Situ: Organic-Inorganic Hybrids,” in *Functional Fillers for Plastics*, Wiley-VCH, 2010.

[385] Z. Keming, Z. Yapu, H. Faquan, and L. Dongqing, “Piezoelectricity of ZnO Films Prepared by Sol-Gel Method,” *Chinese J. Chem. Phys.*, vol. 20, p. 721, 2007.

[386] R. Zhang, P. G. Yin, N. Wang, and L. Guo, “Photoluminescence and Raman scattering of ZnO nanorods,” *Solid State Sci.*, vol. 11, no. 4, pp. 865–869, 2009.

[387] Y. Sun *et al.*, “Synthesis and characterization of twinned flower-like ZnO

structures grown by hydrothermal methods," *Ceram. Int.*, vol. 42, no. 8, pp. 9648–9652, 2016.

[388] R. Hong, T. Pan, J. Qian, and H. Li, "Synthesis and surface modification of ZnO nanoparticles," *Chem. Eng. J.*, vol. 119, no. 2–3, pp. 71–81, 2006.

[389] F. Tang, T. Uchikoshi, and Y. Sakka, "Electrophoretic deposition behavior of aqueous nanosized zinc oxide suspensions," *J. Am. Ceram. Soc.*, vol. 85, no. 9, pp. 2161–2165, 2002.

[390] L. Mascia, W. Zhang, F. Gatto, A. Scarpellini, P. P. Pompa, and E. Mele, "In situ generation of ZnO nanoparticles within a polyethyleneimine matrix for antibacterial zein fibres," *ACS Appl. Polym. Mater.*, vol. XXXX, no. XXX, pp. XXX–XXX, 2019.

[391] S. Musić, A. Šarić, and S. Popović, "Formation of nanosize ZnO particles by thermal decomposition of zinc acetylacetonate monohydrate," *Ceram. Int.*, vol. 36, no. 3, pp. 1117–1123, 2010.

[392] V. B. Schwartz *et al.*, "Antibacterial surface coatings from zinc oxide nanoparticles embedded in poly(N-isopropylacrylamide) hydrogel surface layers," *Adv. Funct. Mater.*, vol. 22, no. 11, pp. 2376–2386, 2012.

[393] J. M. Wu and Y. R. Chen, "Ultraviolet-light-assisted formation of ZnO nanowires in ambient air: Comparison of photoresponsive and photocatalytic activities in zinc hydroxide," *J. Phys. Chem. C*, vol. 115, no. 5, pp. 2235–2243, 2011.

[394] C. Fauteux, R. Longtin, J. Pegna, and D. Therriault, "Fast synthesis of ZnO nanostructures by laser-induced decomposition of zinc acetylacetonate," *Inorg. Chem.*, vol. 46, no. 26, pp. 11036–11047, 2007.

[395] H. Minami, T., Sonohara, H., Takata, S. and Sato, "Transparent and Conductive ZnO Thin Films Prepared by Atmospheric-Pressure Chemical Vapor Deposition Using Zinc Acetylacetonate," *Jpn. J. Appl. Phys.*, vol. 33, pp. L743–L746, 1994.

[396] A. Maldonado, M. D. L. L. Olvera, S. T. Guerra, and R. Asomoza, "Indium-doped zinc oxide thin films deposited by chemical spray starting from zinc

acetylacetonate: Effect of the alcohol and substrate temperature," *Sol. Energy Mater. Sol. Cells*, vol. 82, no. 1–2, pp. 75–84, 2004.

[397] J.-J. Wu and S.-C. Liu, "Catalyst-Free Growth and Characterization of ZnO Nanorods," *J. Phys. Chem. B*, vol. 106, no. 37, pp. 9546–9551, 2002.

[398] J. R. Jensen, T. Johannessen, S. Wedel, and H. Livbjerg, "Preparation of ZnO – Al 2 O 3 particles in a premixed flame," *J. Nanoparticle Res.*, pp. 363–373, 2000.

[399] M. Iwasaki, Y. Inubushi, and S. Ito, "New route to prepare ultrafine ZnO particles and its reaction mechanism," *J. Mater. Sci. Lett.*, vol. 16, no. 18, pp. 1503–1505, 1997.

[400] Y. Inubushi, R. Takami, M. Iwasaki, H. Tada, and S. Ito, "Mechanism of Formation of Nanocrystalline ZnO Particles through the Reaction of [Zn (acac)2] with NaOH in EtOH," *J. Colloid Interface Sci.*, vol. 200, no. 2, pp. 220–227, 1998.

[401] S. Musić and A. Šarić, "Formation of hollow ZnO particles by simple hydrolysis of zinc acetylacetonate," *Ceram. Int.*, vol. 38, no. 7, pp. 6047–6052, 2012.

[402] A. Šarić, S. Musić, and M. Ivanda, "Varying the microstructural properties of ZnO particles using different synthesis routes," *J. Mol. Struct.*, vol. 993, no. 1–3, pp. 219–224, 2011.

[403] M. Ristic and S. Music, "Nano / microstructure and optical properties of ZnO particles precipitated from zinc acetylacetonate," vol. 1090, no. 2015, pp. 121–128, 2014.

[404] M. Abdullah, T. Morimoto, and K. Okuyama, "Generating Blue and Red Luminescence from ZnO/Poly(ethylene glycol) Nanocomposites Prepared Using an In-Situ Method," *Adv. Funct. Mater.*, vol. 13, no. 10, pp. 800–804, 2003.

[405] R. Augustine, N. Kalarikkal, and S. Thomas, "Effect of zinc oxide nanoparticles on the in vitro degradation of electrospun polycaprolactone membranes in simulated body fluid," *Int. J. Polym. Mater. Polym. Biomater.*, vol. 65, no. 1, pp. 28–37, 2016.

[406] R. S. Andre, A. Pavinatto, L. A. Mercante, E. C. Paris, L. H. C. Mattoso, and D. S. Correa, “Improving the electrochemical properties of polyamide 6/polyaniline electrospun nanofibers by surface modification with ZnO nanoparticles,” *RSC Adv.*, vol. 5, no. 90, pp. 73875–73881, Sep. 2015.

[407] R. Augustine, E. A. Dominic, I. Reju, B. Kaimal, N. Kalarikkal, and S. Thomas, “Electrospun polycaprolactone membranes incorporated with ZnO nanoparticles as skin substitutes with enhanced fibroblast proliferation and wound healing,” *RSC Adv.*, vol. 4, no. 47, p. 24777, Jun. 2014.

[408] H. Hallaji, A. R. Keshtkar, and M. A. Moosavian, “A novel electrospun PVA/ZnO nanofiber adsorbent for U(VI), Cu(II) and Ni(II) removal from aqueous solution,” *J. Taiwan Inst. Chem. Eng.*, vol. 46, pp. 109–118, Jan. 2015.

[409] H. Rokbani and A. Ajji, “Rheological Properties of Poly(lactic acid) Solutions Added with Metal Oxide Nanoparticles for Electrospinning,” *J. Polym. Environ.*, vol. 26, no. 6, pp. 2555–2565, 2018.

[410] R. Augustine *et al.*, “Electrospun poly(vinylidene fluoride-trifluoroethylene)/zinc oxide nanocomposite tissue engineering scaffolds with enhanced cell adhesion and blood vessel formation,” *Nano Res.*, vol. 10, no. 10, pp. 3358–3376, 2017.

[411] R. Augustine *et al.*, “Electrospun polycaprolactone/ZnO nanocomposite membranes as biomaterials with antibacterial and cell adhesion properties,” *J. Polym. Res.*, vol. 21, no. 3, pp. 347–364, 2014.

[412] R. Augustine, E. A. Dominic, I. Reju, B. Kaimal, N. Kalarikkal, and S. Thomas, “Investigation of angiogenesis and its mechanism using zinc oxide nanoparticle-loaded electrospun tissue engineering scaffolds,” *RSC Adv.*, vol. 4, no. 93, pp. 51528–51536, 2014.

[413] M. Kancheva, A. Toncheva, D. Paneva, N. Manolova, I. Rashkov, and N. Markova, “Materials from Nanosized ZnO and Polyacrylonitrile: Properties Depending on the Design of Fibers (Electrospinning or Electrospinning/Electrospraying),” *J. Inorg. Organomet. Polym. Mater.*, vol. 27, no. 4, pp. 912–922, 2017.

[414] H. Rodríguez-Tobías, G. Morales, A. Ledezma, J. Romero, and D. Grande, “Novel antibacterial electrospun mats based on poly(D,L-lactide) nanofibers and zinc oxide nanoparticles,” *J. Mater. Sci.*, vol. 49, no. 24, pp. 8373–8385, 2014.

[415] J. H. Kim, M. K. Joshi, J. Lee, C. H. Park, and C. S. Kim, “Polydopamine-assisted immobilization of hierarchical zinc oxide nanostructures on electrospun nanofibrous membrane for photocatalysis and antimicrobial activity,” *J. Colloid Interface Sci.*, vol. 513, pp. 566–574, 2018.

[416] Ž. Petrović, M. Ristić, M. Marciuš, M. Ivanda, V. Đurina, and S. Musić, “Hydrothermal processing of electrospun fibers in the synthesis of 1D ZnO nanoparticles,” *Mater. Lett.*, vol. 176, pp. 278–281, Aug. 2016.

[417] P. Argos, K. Pedersen, M. D. Marks, and B. A. Larkins, “A structural model for maize zein proteins.,” *J. Biol. Chem.*, vol. 257, no. 17, pp. 9984–9990, 1982.

[418] a S. Tatham *et al.*, “Solution conformational analysis of the alpha-zein proteins of maize,” *J. Biol. Chem.*, vol. 268, no. 35, pp. 26253–26259, 1993.

[419] N. Matsushima, G.-I. Danno, H. Takezawa, and Y. Izumi, “Three-dimensional structure of maize a-zein proteins studied by small-angle X-ray scattering,” *Biochim. Biophys. Acta*, vol. 1339, pp. 14–22, 1997.

[420] L. A. Forato, A. C. Doriguetto, H. Fischer, Y. P. Mascarenhas, A. F. Craievich, and L. A. Colnago, “Conformation of the Z19 Prolamin by FTIR, NMR, and SAXS,” *J. Agric. Food Chem.*, vol. 52, no. 8, pp. 2382–2385, 2004.

[421] M. R. Bugs *et al.*, “Spectroscopic characterization and structural modeling of prolamin from maize and pearl millet,” *Eur. Biophys. J.*, vol. 33, no. 4, pp. 335–343, 2004.

[422] L. Di Gioia and S. Guilbert, “Corn protein-based thermoplastic resins: Effect of some polar and amphiphilic plasticizers,” *J. Agric. Food Chem.*, vol. 47, no. 3, pp. 1254–1261, 1999.

[423] M. Stading, D. M. R. Georget, S. A. Barker, T. Gillgren, and P. S. Belton, “Plasticization of Zein: A Thermomechanical, FTIR, and Dielectric Study,” *Biomacromolecules*, vol. 10, no. 5, pp. 1135–1139, 2009.

[424] H. Xu, Y. Chai, and G. Zhang, “Synergistic effect of oleic acid and glycerol on zein film plasticization,” *J. Agric. Food Chem.*, vol. 60, no. 40, pp. 10075–10081, 2012.

[425] D. P. Erickson, S. Renzetti, A. Jurgens, O. H. Campanella, and B. R. Hamaker, “Modulating state transition and mechanical properties of viscoelastic resins from maize zein through interactions with plasticizers and co-proteins,” *J. Cereal Sci.*, vol. 60, no. 3, pp. 576–583, 2014.

[426] W. Huo, D. Wei, W. Zhu, Z. Li, and Y. Jiang, “High-elongation zein films for flexible packaging by synergistic plasticization: Preparation, structure and properties,” *J. Cereal Sci.*, vol. 79, pp. 354–361, 2018.

[427] J. Liang, Q. Xia, S. Wang, J. Li, Q. Huang, and R. D. Ludescher, “Influence of glycerol on the molecular mobility, oxygen permeability and microstructure of amorphous zein films,” *Food Hydrocoll.*, vol. 44, pp. 94–100, 2015.

[428] Y. Luo and Q. Wang, “Zein-based micro- and nano-particles for drug and nutrient delivery: A review,” *J. Appl. Polym. Sci.*, vol. 131, no. 16, pp. 1–12, 2014.

[429] X. Liu, Q. Sun, H. Wang, L. Zhang, and J. Y. Wang, “Microspheres of corn protein, zein, for an ivermectin drug delivery system,” *Biomaterials*, vol. 26, no. 1, pp. 109–115, 2005.

[430] A. R. Patel and K. P. Velikov, “Zein as a source of functional colloidal nano- and microstructures,” *Curr. Opin. Colloid Interface Sci.*, vol. 19, no. 5, pp. 450–458, 2014.

[431] Y. Chen *et al.*, “Design, fabrication and biomedical applications of zein-based nano/micro-carrier systems,” *Int. J. Pharm.*, vol. 513, no. 1–2, pp. 191–210, 2016.

[432] H. Chen and Q. Zhong, “A novel method of preparing stable zein nanoparticle dispersions for encapsulation of peppermint oil,” *Food Hydrocoll.*, vol. 43, p. 593e602-602, 2015.

[433] H. Li *et al.*, “Fabrication of stable zein nanoparticles coated with soluble soybean polysaccharide for encapsulation of quercetin,” *Food Hydrocoll.*, vol.

87, no. August 2018, pp. 342–351, 2019.

[434] N. M. Barkoula, B. Alcock, N. O. Cabrera, and T. Peijs, “Fatigue properties of highly oriented polypropylene tapes and all-polypropylene composites,” *Polym. Polym. Compos.*, vol. 16, no. 2, pp. 101–113, 2008.

[435] Q. Zhong, M. Jin, D. Xiao, H. Tian, and W. Zhang, “Application of supercritical anti-solvent technologies for the synthesis of delivery systems of bioactive food components,” *Food Biophys.*, vol. 3, no. 2, pp. 186–190, 2008.

[436] Q. Zhong, M. Jin, P. M. Davidson, and S. Zivanovic, “Sustained release of lysozyme from zein microcapsules produced by a supercritical anti-solvent process,” *Food Chem.*, vol. 115, no. 2, pp. 697–700, 2009.

[437] D. Hu, C. Lin, L. Liu, S. Li, and Y. Zhao, “Preparation, characterization, and in vitro release investigation of lutein/zein nanoparticles via solution enhanced dispersion by supercritical fluids,” *J. Food Eng.*, vol. 109, no. 3, pp. 545–552, 2012.

[438] J. Gomez-Estaca, M. P. Balaguer, R. Gavara, and P. Hernandez-Munoz, “Formation of zein nanoparticles by electrohydrodynamic atomization: Effect of the main processing variables and suitability for encapsulating the food coloring and active ingredient curcumin,” *Food Hydrocoll.*, vol. 28, no. 1, pp. 82–91, 2012.

[439] Z. P. Liu, Y. Y. Zhang, D. G. Yu, D. Wu, and H. L. Li, “Fabrication of sustained-release zein nanoparticles via modified coaxial electrospraying,” *Chem. Eng. J.*, vol. 334, no. October 2017, pp. 807–816, 2018.

[440] S. Babitha and P. S. Korrapati, “Biodegradable zein-polydopamine polymeric scaffold impregnated with TiO2 nanoparticles for skin tissue engineering,” *Biomed. Mater.*, vol. 12, no. 5, p. 055008, 2017.

[441] M. Zhang, Y. Liu, Y. Jia, H. Han, and D. Sun, “Preparation and evaluation of electrospun Zein/HA fibers based on two methods of adding HA nanoparticles,” *J. Bionic Eng.*, vol. 11, no. 1, pp. 115–124, 2014.

[442] X. Chen *et al.*, “Facile fabrication of gold nanoparticle on zein ultrafine fibers and their application for catechol biosensor,” *Appl. Surf. Sci.*, vol. 328, pp.

444–452, 2015.

[443] D. Dippold, M. Tallawi, S. Tansaz, J. A. Roether, and A. R. Boccaccini, “Novel electrospun poly (glycerol sebacate)– zein fiber mats as candidate materials for cardiac tissue engineering,” *Eur. Polym. J.*, vol. 75, pp. 504–513, 2016.

[444] X. Hu, L. liang Yang, K. Wang, Y. Z. Wei, H. Deng, and J. Dong, “Studies of mechanical properties of electrospun zein/poly(ε-caprolactone) composites and antibacterial properties against *Listeria monocytogenes* strains of zein/poly(ε-caprolactone)/ poly(ε-lysine) films,” *Text. Res. J.*, p. 004051751773208, 2017.

[445] F. Yang, Y. Miao, Y. Wang, L.-M. Zhang, and X. Lin, “Electrospun Zein/Gelatin Scaffold-Enhanced Cell Attachment and Growth of Human Periodontal Ligament Stem Cells,” *Materials (Basel).*, vol. 10, no. 10, p. 1168, 2017.

[446] L. Deng, X. Kang, Y. Liu, F. Feng, and H. Zhang, “Characterization of gelatin/zein films fabricated by electrospinning vs solvent casting,” *Food Hydrocoll.*, vol. 74, pp. 324–332, 2018.

[447] L. Deng, Y. Li, F. Feng, and H. Zhang, “Study on wettability, mechanical property and biocompatibility of electrospun gelatin/zein nanofibers cross-linked by glucose,” *Food Hydrocoll.*, vol. 87, no. June 2018, pp. 1–10, 2019.

[448] S. Torres-Giner, M. J. Ocio, and J. M. Lagaron, “Novel antimicrobial ultrathin structures of zein/chitosan blends obtained by electrospinning,” *Carbohydr. Polym.*, vol. 77, no. 2, pp. 261–266, 2009.

[449] D. R. Figueira, S. P. Miguel, K. D. De Sá, and I. J. Correia, “International Journal of Biological Macromolecules Production and characterization of polycaprolactone- hyaluronic acid / chitosan- zein electrospun bilayer nanofibrous membrane for tissue regeneration,” vol. 93, pp. 1100–1110, 2016.

[450] H. Lee *et al.*, “Electrospun tri-layered zein/PVP-GO/zein nanofiber mats for providing biphasic drug release profiles,” *Int. J. Pharm.*, vol. 531, no. 1, pp. 101–107, 2017.

[451] N. Alhusein, I. S. Blagbrough, M. L. Beeton, A. Bolhuis, and P. A. De Bank, “Electrospun Zein/PCL Fibrous Matrices Release Tetracycline in a Controlled

Manner, Killing Staphylococcus aureus Both in Biofilms and Ex Vivo on Pig Skin, and are Compatible with Human Skin Cells," *Pharm. Res.*, vol. 33, no. 1, pp. 237–246, 2016.

[452] J. Feng, Y. Ju, J. Liu, H. Zhang, and X. Chen, "Polyethyleneimine-templated copper nanoclusters via ascorbic acid reduction approach as ferric ion sensor," *Anal. Chim. Acta*, vol. 854, pp. 153–160, 2015.

[453] D. Yan, C. Deng, Y. He, Y. Ge, and G. Song, "Sensitive Naked Eye and Autofluorescence Detection of Cu2+in Biological Fluids by Polyethyleneimine Microspheres," *J. Fluoresc.*, vol. 26, no. 5, pp. 1763–1772, 2016.

[454] H. Jin, R. Gui, Y. Wang, and J. Sun, "Carrot-derived carbon dots modified with polyethyleneimine and nile blue for ratiometric two-photon fluorescence turn-on sensing of sulfide anion in biological fluids," *Talanta*, vol. 169, pp. 141–148, 2017.

[455] H. B. Wu, D. H. Bremner, H. L. Nie, J. Quan, and L. M. Zhu, "Electrospun polyvinyl alcohol/carbon dioxide modified polyethyleneimine composite nanofiber scaffolds," *J. Biomater. Appl.*, vol. 29, no. 10, pp. 1407–1417, 2015.

[456] Y. Weng, B. Jiang, K. Yang, Z. Sui, L. Zhang, and Y. Zhang, "Polyethyleneimine-modified graphene oxide nanocomposites for effective protein functionalization," *Nanoscale*, vol. 7, no. 34, pp. 14284–14291, 2015.

[457] Z. yu Fan, Y. li Zhao, X. yue Zhu, Y. Luo, M. wu Shen, and X. yang Shi, "Folic acid modified electrospun poly(vinyl alcohol)/polyethyleneimine nanofibers for cancer cell capture applications," *Chinese J. Polym. Sci. (English Ed.*, vol. 34, no. 6, pp. 755–765, 2016.

[458] Y. Zhao, Z. Fan, M. Shen, and X. Shi, "Capturing hepatocellular carcinoma cells using lactobionic acid-functionalized electrospun polyvinyl alcohol/polyethyleneimine nanofibers," *RSC Adv.*, vol. 5, no. 86, pp. 70439–70447, 2015.

[459] K. Li, J. Jiang, S. Tian, F. Yan, and X. Chen, "Polyethyleneimine-nano silica composites: A low-cost and promising adsorbent for CO2 capture," *J. Mater. Chem. A*, vol. 3, no. 5, pp. 2166–2175, 2015.

[460] D. Hu, Y. Xiao, H. Liu, H. Wang, J. Li, and B. Zhou, “Loading of Au/Ag bimetallic nanoparticles within electrospun PVA/PEI nano fi bers for catalytic applications,” *Colloids Surfaces A Physicochem. Eng. Asp.*, vol. 552, no. May, pp. 9–15, 2018.

[461] M. Liu *et al.*, “Self-polymerization of dopamine and polyethyleneimine: Novel fluorescent organic nanoprobes for biological imaging applications,” *J. Mater. Chem. B*, vol. 3, no. 17, pp. 3476–3482, 2015.

[462] Y. Mo, R. Guo, Y. Zhang, W. Xue, B. Cheng, and Y. Zhang, “Controlled Dual Delivery of Angiogenin and Curcumin by Electrospun Nanofibers for Skin Regeneration,” *Tissue Eng. Part A*, vol. 23, no. 13–14, pp. 597–608, 2017.

[463] C. Du *et al.*, “Polyethyleneimine-capped silver nanoclusters for microRNA oligonucleotide delivery and bacterial inhibition,” *Int. J. Nanomedicine*, vol. 12, pp. 8599–8613, 2017.

[464] J. Park *et al.*, “Quantum Dots in an Amphiphilic Polyethyleneimine Derivative Platform for Cellular Labeling, Targeting, Gene Delivery, and Ratiometric Oxygen Sensing,” *ACS Nano*, vol. 9, no. 6, pp. 6511–6521, 2015.

[465] N. Uzal, N. Ates, S. Saki, Y. E. Bulbul, and Y. Chen, “Enhanced hydrophilicity and mechanical robustness of polysulfone nanofiber membranes by addition of polyethyleneimine and Al2O3 nanoparticles,” *Sep. Purif. Technol.*, vol. 187, pp. 118–126, 2017.

[466] X. Fang, S. Xiao, M. Shen, R. Guo, S. Wang, and X. Shi, “Fabrication and characterization of water-stable electrospun polyethyleneimine/polyvinyl alcohol nanofibers with super dye sorption capability,” *New J. Chem.*, vol. 35, no. 2, pp. 360–368, 2011.

[467] G. Katwal, M. Paulose, I. A. Rusakova, J. E. Martinez, and O. K. Varghese, “Rapid Growth of Zinc Oxide Nanotube-Nanowire Hybrid Architectures and Their Use in Breast Cancer-Related Volatile Organics Detection,” *Nano Lett.*, vol. 16, no. 5, pp. 3014–3021, 2016.

[468] N. Rashidi, V. L. Kuznetsov, J. R. Dilworth, M. Pepper, P. J. Dobson, and P. P. Edwards, “Highly conducting and optically transparent Si-doped ZnO thin films

prepared by spray pyrolysis," *J. Mater. Chem. C*, vol. 1, no. 42, pp. 6960–6969, 2013.

[469] D. Dippold, M. Tallawi, S. Tansaz, J. A. Roether, and A. R. Boccaccini, "Novel electrospun poly(glycerol sebacate)-zein fiber mats as candidate materials for cardiac tissue engineering," *Eur. Polym. J.*, vol. 75, pp. 504–513, 2016.

[470] F. Lionetto, L. Mascia, and M. Frigione, "Evolution of transient states and properties of an epoxy-silica hybrid cured at ambient temperature," *Eur. Polym. J.*, vol. 49, no. 6, pp. 1298–1313, 2013.

[471] Y. Chen, R. Ye, and J. Liu, "Effects of different concentrations of ethanol and isopropanol on physicochemical properties of zein-based films," *Ind. Crops Prod.*, vol. 53, pp. 140–147, 2014.